UNIVERSITEIT VAN PRETORIA
UNIVERSITY OF PRETORIA
YUNIBESITHI YA PRETORIA

Anti-ferroptotic properties of isolates from traditional South African medicinal plants in a 6-hydroxydopamine-induced SH-SY5Y cytotoxicity model

by

Andries Daniël de Beer

Thesis submitted in fulfilment of the requirements for the degree

Philosophiae Doctor

in the Department of

Pharmacology

in the

Faculty of Health Sciences

at the

University of Pretoria

Supervisor: Prof W Cordier
Co-supervisor(s): Dr M Balmith and Prof V Steenkamp
November 2024

Declaration of originality

I, Andries Daniël de Beer

Student number: 21775266

Declare that

1. I understand what plagiarism is and am aware of the University's policy in this regard.
2. I declare that this Thesis (e.g. essay, report, project, assignment, dissertation, thesis, etc) is my own original work. Where other people's work has been used (either from a printed source, Internet, or any other source), this has been properly acknowledged and referenced in accordance with departmental requirements.
3. I have not used work previously produced by another student or any other person to hand in as my own.
4. I have not allowed and will not allow anyone to copy my work with the intention of passing it off as his or her own work.

SIGNATURE OF STUDENT:

Date:

Author contributions:

Study conception, laboratory experiments, data collection, analysis, and interpretation were done by AD de Beer and W Cordier. The drafting of thesis was done by AD de Beer and review was done by W Cordier, M Balmith and V Steenkamp.

ABSTRACT

Introduction:

Parkinson's disease (PD), a progressive neurodegenerative disorder, lacks disease-modifying treatments, and thus relies on symptomatic relief only. A potential untapped disease-modifying pathway for PD is the iron-dependent cell death process ferroptosis, which promotes oxidative stress within cells. Medicinal plants in Sub-Saharan Africa are a potential source of new chemical entities or scaffolds for anti-ferroptotic pharmacotherapy. During the study, a series of semi-automated fractions from African herbal remedies with ethnomedicinal claims of central nervous system activities were investigated to protect against 6-hydroxydopamine (6-OHDA)-induced cytotoxicity in the SH-SY5Y neuroblastoma cell line as an *in vitro* model of PD.

Methods:

Twenty-four plants were extracted and fractionated to produce a crude extract and seven associated fractions. All samples were screened for both inherent cytotoxicity in the SH-SY5Y cell line, as well as cytoprotection against 6-OHDA-induced cytotoxicity. Acellular ferroptotic-associated assays were conducted, including the iron chelation and ferric reducing antioxidant power (FRAP) assays. Cytoprotective fractions of five plants were selected for further analyses to assess their ability to reduce reactive oxygen species (ROS; 2′,7′-dichlorodihydrofluorescein diacetate assay), modulate glutathione (GSH) levels (monochlorobimane fluorescence), inhibit lipid peroxidation (thiobarbituric acid reactive substances assay), and alter mitochondrial integrity (CytoPainter Red) in the SH-SY5Y cell line. For the fractions subjected to further analyses, compound identification was done using high-performance liquid chromatography mass spectrometry and the Dictionary of Natural Products, and the identified compounds' physicochemical properties were determined. These compounds were also investigated using *in silico* molecular docking against ferroptosis-relevant targets.

Results and discussion:

A total of 24 plants were screened, with only 15 selected fractions that were elucidated to assess their effects ferroptosis role-players. No correlation between FRAP or iron chelation and cytoprotection was present. Of the screened fractions, one fraction of *Acokanthera oppositifolia*, two fractions of *Bulbine latifolia* and *Aptosimum procumbens*, four fractions of *Schotia brachypetala* and five fractions of *Polygala virgata* increased cell density by 30% after 6-OHDA exposure and had little inherent cytotoxicity (≤ 10% reduction in cell density). The fractions of *P. virgata* exhibited significant ($p < 0.05$) reductions in intracellular ROS, with fraction 4 displaying

the largest reduction (2.09-fold). Additionally, *P. virgata* fractions 3, 5, 6, and 7 demonstrated similar ROS reductions (1.28- to 1.47-fold). *A. procumbens* fraction 3 increased GSH levels by 25.79%, followed by *A. procumbens* fraction 4 (22.98%, $p < 0.05$), *B. latifolia* fraction 3 (22.96%), and *P. virgata* fraction 6 (19.25%). These findings suggest that plant fractions from *P. virgata* and *A. procumbens* offer promising antioxidant and cytoprotective effects, with fraction 4 of *P. virgata* being particularly effective in reducing lipid peroxidation (0.284-fold reduction). In addition, several fractions enhanced mitochondrial integrity, with *B. latifolia* (fraction 5) and *S. brachypetala* (fraction 3) normalising the active mitochondrial ratio. Physicochemical elucidation via SwissADME shows that there are some compounds with theoretical blood-brain barrier penetration. Molecular docking of identified compounds also provided a base for the investigation of the compounds as potential leads for drug design, with xanthones (*P. virgata* fractions 5 to 7) and butanedioate (*A. procumbens* fraction 4) being identified as promising scaffolds.

Conclusion:

The semi-automated fractions of the selected plants offer a promising approach to mitigating the complex cellular processes involved in oxidative stress patterns and ferroptotic role-players (GSH, lipid peroxides and mitochondrial integrity), but whether the ferroptosis pathway is the underlying pathway modulated for cytoprotection remains unclear. While the results indicate that these compounds may protect cells and maintain mitochondrial function, further research is needed to optimise their pharmacological properties, including bioavailability and blood-brain barrier penetration. Fractions 5 to 7 from *P. virgata*, due to high ROS scrubbing, and fraction 4 from *A. procumbens*, due to GSH increases, are currently primed for further research. The research also shows the need to advocate for the systematic investigation and cataloguing of traditional plant medicines, aiming to provide a foundation for the development of novel therapeutic strategies for PD and other neurodegenerative diseases. These results highlight the therapeutic potential of multi-target plant-based therapies in managing PD, supporting the integration of traditional healing practices into modern medicine. Further studies are needed to optimise bioavailability and target specific neuroprotective pathways.

Keywords: 6-hydroxydopamine, ethnopharmacology, ferroptosis, molecular docking, oxidative stress, Parkinson's disease, plant fractionation

ACKNOWLEDGEMENTS

The following thesis represents 10 years of undergraduate and postgraduate studying, and is nothing short of a show of dedication, mindfulness, hard work, and an extreme stubbornness to not give up, to reach a goal only some can reach within a lifetime. I could not have done this alone, not without the support of several people:

To my Mom and Dad, both of you have shown me that hard work and a pursuit of something bigger than oneself is commendable, and to enact change you must be the bearer of said change. The amount of time, effort, money and talks that went into my education has culminated in this thesis and I love you so much.

To the rest of my family, Ronel, Lize, and Elbé, I cannot be the person I am today without you. The immense support through happiness and frustration has been invaluable, and I know that we always have each other's back no matter what.

To my supervisor, Prof. Werner Cordier, I owe a lot of my professional development to you. You took a chance on someone with no cell culture experience and has given me the skills to go further than I ever thought I could. Your steadfastness and support have made me a better researcher and person, and I will carry these lessons with me to wherever life may take me.

To my co-supervisors, Dr. Marissa Balmith and Prof. Vanessa Steenkamp, I will be forever grateful for the opportunities and support you have given me. The time you have set aside for me in these past years and the knowledge you have imparted has helped me immensely.

To my friends, Ethan, Brittany, Adele, Wikus, Phillip and Hafiza, we have been through the toughest of times, and the fact that we made it this far, is testament to the love and respect we have for each other. I will always be grateful for the years that we have been in each other's lives.

To the Department of Pharmacology, I value all the support and opportunities I have received over the years, and I will always be grateful.

And lastly, to myself: You have shown that with a grit of teeth and not losing yourself, you can do anything you set your mind to. This has been a labour of love, and you should always stay proud of what and who you are.

"All you have to decide is what to do with the time that is given to you."

- Gandalf The Grey, *The Lord of the Rings*, J.R.R Tolkien.

OUTPUTS FROM STUDY

Presentations:

AD de Beer, M Balmith, V Steenkamp, W Cordier. Affinity of phytochemicals from three traditional African herbal remedies towards ferroptosis-associated targets and dopamine receptors for potential use in Parkinson's disease**. South African Society for Basic and Clinical Pharmacology Conference. North-West University, Virtual, 12 - 13 October 2022.**

AD de Beer, E Alberts, W Rudolph, M Balmith, V Steenkamp, W Cordier. Extracts of herbal remedies offer cytoprotection and acellular anti-ferroptotic activity in the 6-hydroxydopamine-induced SH-SY5Y neuroblastoma cytotoxicity model. **South African Society for Basic and Clinical Pharmacology Conference. Rhodes University, Makhanda, 24 - 27 August 2023.**

AD de Beer, W Rudolph, M Balmith, V Steenkamp, W Cordier. Cytoprotective mechanisms of ethnomedicinally-relevant African herbal remedies against 6-hydrodopamine-induced SH-SY5Y cytotoxicity. **South African Society for Basic and Clinical Pharmacology Conference. Sefako Makgatho Health Sciences University, Pretoria, 15 - 17 September 2024.** Awarded Merit for achieving 80% and above for Oral Presentation.

AD de Beer, W Rudolph, M Balmith, V Steenkamp, W Cordier. Fractions of *Polygala virgata* reduces oxidative stress in a 6-hydrodopamine-induced SH-SY5Y cytotoxicity model. **ISE/APSS International Conference, Cape Town, 23 - 27 October 2024.**

Posters:

AD de Beer, M Balmith, V Steenkamp, W Cordier. Semi-automated extracts of herbal remedies offer acellular anti-ferroptotic activity and cytoprotection in the 6-hydroxydopamine-induced SH-SY5Y neuroblastoma cytotoxicity model. **International Federation of Clinical Chemistry and Laboratory Science Conference. Dubai, 26-30 May 2024.**

LIST OF ABBREVIATIONS

#	
ΔΨm	Mitochondrial membrane potential
µg	Microgram(s)
µm	Micrometre(s)
µmol	Micromole(s)
$-NH_2$	Amino group
3-OMD	3-Methyldopa
4-HNE	4-Hyroxynonenal
6-OHDA	6-Hydroxydopamine
A	
AADC	Aromatic amino acid decarboxylase
ABTS	2,2'-amino-bis(3-ethylbenzothiazoline)-6-sulfonic acid
AChE	Acetylcholine esterase
ACN	Acetonitrile
ADP	Adenosine diphosphate
ADME-Tox	Absorption, distribution, metabolism, excretion, toxicity
ATP	Adenosine triphosphate
ALA	Alanine
ARG	Arginine
ASN	Asparagine
ASP	Aspartic acid
B	
BBB	Blood brain barrier
C	
Cc	Cytochrome C
CA	Catecholamine
Ca^{2+}	Calcium ion(s)
CA	Catecholamine
CADD	Computer aided drug design
CAT	Catalase
CNS	Central nervous system
COMT	Catechol-*O*-methyltransferase
Com I	Complex I
CoQ	Co-enzyme Q
Cu	Copper
CYS	Cysteine
D	
DA-R	Dopamine receptor
DCM	Dichloromethane
DNA	Deoxyribonucleic acid
DMEM	Dulbecco's Modified Eagle's Medium
DMSO	Dimethyl sulfoxide
DPPH	1,1-Diphenyl-2-picryl-hydrazyl
DOPAL	3,4-Dihydroxyphenylacetaldehyde
E	
EDTA	Ethylenediaminetetraacetic acid
ETC	Electron transport chain
EtOAc	Ethyl acetate
EtOH	Ethanol

F	
FCS	Foetal calf serum
Fe^{3+}/Fe(III)	Ferric iron
Fe^{2+}/Fe(II)	Ferrous iron
FRAP	Ferric reducing antioxidant power
G	
GABA	γ-Amino-butyric acid
GPx	Glutathione peroxidase
GSH	Glutathione
GLN	Glutamine
GLU	Glutamic acid
GLY	Glycine
H	
h	Hour(s)
H	Hydrogen
HO●	Hydroxyl radical
H_2O_2	Hydrogen peroxide
HIS	Histidine
I	
IC_{50}	Half maximum inhibitory concentration
ILE	Isoleucine
L	
L●	Fatty acid radicals
L-dopa	Levodopa
LNAA	Large neutral amino acid group
LAT-1	Large neutral amino acid transporter
LIP	Labile iron pool
LO●	Lipid peroxyl radicals
LOO●	Alkoxyl radicals
LEU	Leucine
LYS	Lysine
M	
MAO	Monoamine oxidase
MDA	Malondialdehyde
MeOH	Methanol
MET	Methionine
Mg^{2+}	Magnesium ions
mg	Milligram(s)
Min	Minutes
mL	Milliliter(s)
Mn	Manganese
MnSOD	Manganese superoxide dismutase
MTBE	Methyl tert-butyl ether
MtDNA	Mitochondrial deoxyribonucleic acid
MPTP	1,2,3,6-Tetrahydropyridine
MPP^+	1-Methyl-4-phenylpyridium
N	
$NADH_2/NAD^+$	Nicotinamide adenine dinucleotide
NCE	New chemical entity
O	
O_2	Oxygen
$O_2^{\bullet-}$	Superoxide
P	

PBS	Phosphate-buffered saline
PD	Parkinson's disease
PHE	Phenylalanine
PK	Pharmacokinetics
PRO	Proline
PUFA	Polyunsaturated fatty acids
R	
RNS	Reactive nitrogen species
ROS	Reactive oxygen species
S	
SAR	Structure-activity relationships
SER	Serine
SNpC	Substantia nigra pars compacta
SOD	Superoxide dismutase
SSA	Sub-Saharan Africa
SRB	Sulforhodamine B
SPE	Solid phase extraction
T	
THR	Threonine
TPTZ	2,4,6-Tri(2-pyridyl)-1,3,5-triazine
TRP	Tryptophan
TYR	Tyrosine
U	
UV	Ultraviolet
V	
VAL	Valine
W	
w/v	Weight per volume
WHO	World Health Organization
Z	
Zn	Zinc

LIST OF TABLES

LIST OF FIGURES

TABLE OF CONTENTS

CHAPTER 1: INTRODUCTION

1.1 Life expectancy and health in Sub-Saharan Africa

The life expectancy of persons living in developing countries has increased due to several factors: modernisation of the countries, greater access to healthy food and clean water,[1] and improved healthcare infrastructure and availability of disease treatment.[2] Modernisation brings with it improvements to farming and food technology, as well as the mass production of medicines. These factors have led to an increase in life expectancy over the last 30 years.[3] The elderly population (>65 years) in sub-Saharan Africa (SSA) is expected to rise to 45 million people by 2030.[4] Furthermore, the World Health Organization (WHO) has projected that >300 000 people will be older than 90 years by 2030 in SSA.[5, 6] Life expectancy in SSA increased from 46 to 56 years between 1980 and 2000, and with an expected world average of life expectancy to reach 76 years by 2025, this is higher than the SSA region with an average life expectancy of 69.1 years by 2025 (**Figure 1-1**).[6] The increased life expectancy affords individuals the opportunity to reach an advanced age, however, old age is also the biggest risk factor for the development of neurodegenerative diseases.[7] Neurodegenerative diseases such as Alzheimer's, Huntington's, and Parkinson's disease (PD), are becoming the leading cause of disability in the modern world.[8] These diseases contributed to 16.8% of deaths worldwide between 1990 and 2005 and increased by a further 7.4% at the end of 2015.[9] In 2019, the death rate associated with neurodegenerative diseases increased to 5.67 per 100 000.[10] Data regarding the prevalence of neurodegenerative diseases in SSA is scarce, with most information reported from Central and Western Africa.[11-13] In 2018, a prevalence for neurodegenerative diseases of 2.3 to 7.6% was estimated in SSA.[14]

Neurodegenerative diseases comprise a myriad of pathologies incurred by the loss of neurophysiological properties which can be categorised according to specific characteristics.[15] These include diseases such as amyotrophic lateral sclerosis, tauopathies, age-related macular degeneration, age-related dementias, psychosis, and PD.[16] With over 8.5 million people in the world living with PD, it is the second most prevalent neurodegenerative disease.[17] Incidence rates of PD increase steadily in age groups over 65 years of age, with a notable rise between 70 and 79 years of age, with a higher incidence in males (**Figure 1-2**).[18] Population growth projections for SSA suggest that the overall population group above the age of 65 is projected to be more than 45 million people by 2030 (**Figure 1-3**).[5] The expected increase in neurodegenerative diseases in the population will thus cause an exceptional burden to the healthcare infrastructure. The SSA region is the fastest growing region in the world yet still struggles most with proper access to healthcare.[19] The WHO classifies proper access to healthcare as having one doctor per 1 000 population.[20,21]

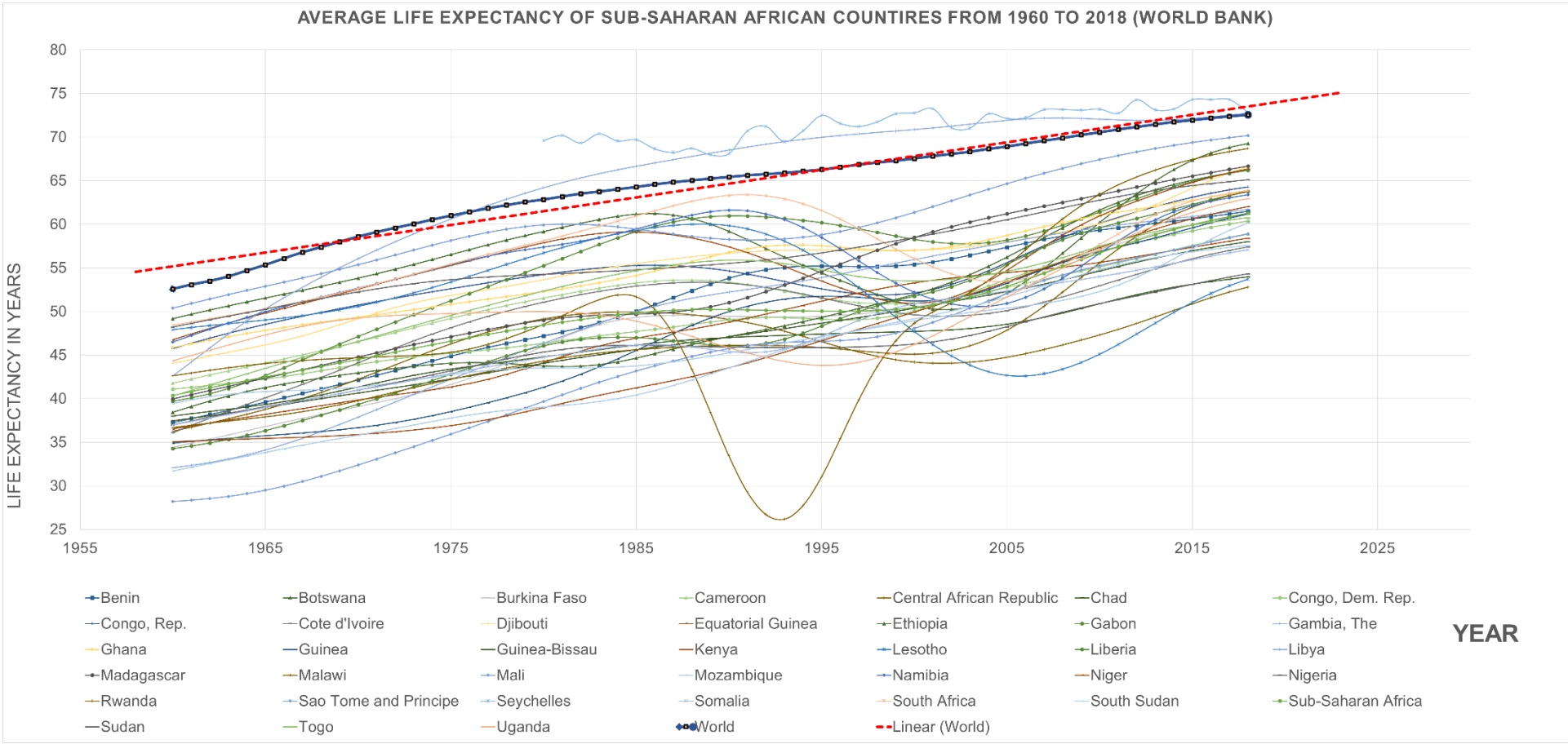

Figure 1-1: Change in life expectancy (in years) between 1955 and 2025 for sub-Saharan Africa countries in comparison to the world. Self-generated graph using data from The World Bank, under a Creative Commons Attribution 4.0 International License.

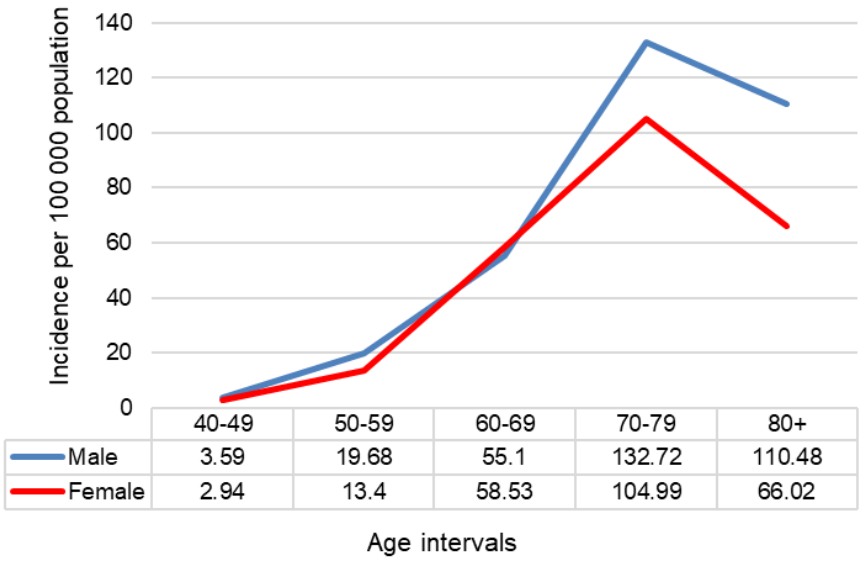

Figure 1-2: **Worldwide gender-specific incidence of Parkinson's disease stratified by age group. Self-generated graph from published data.[18]**

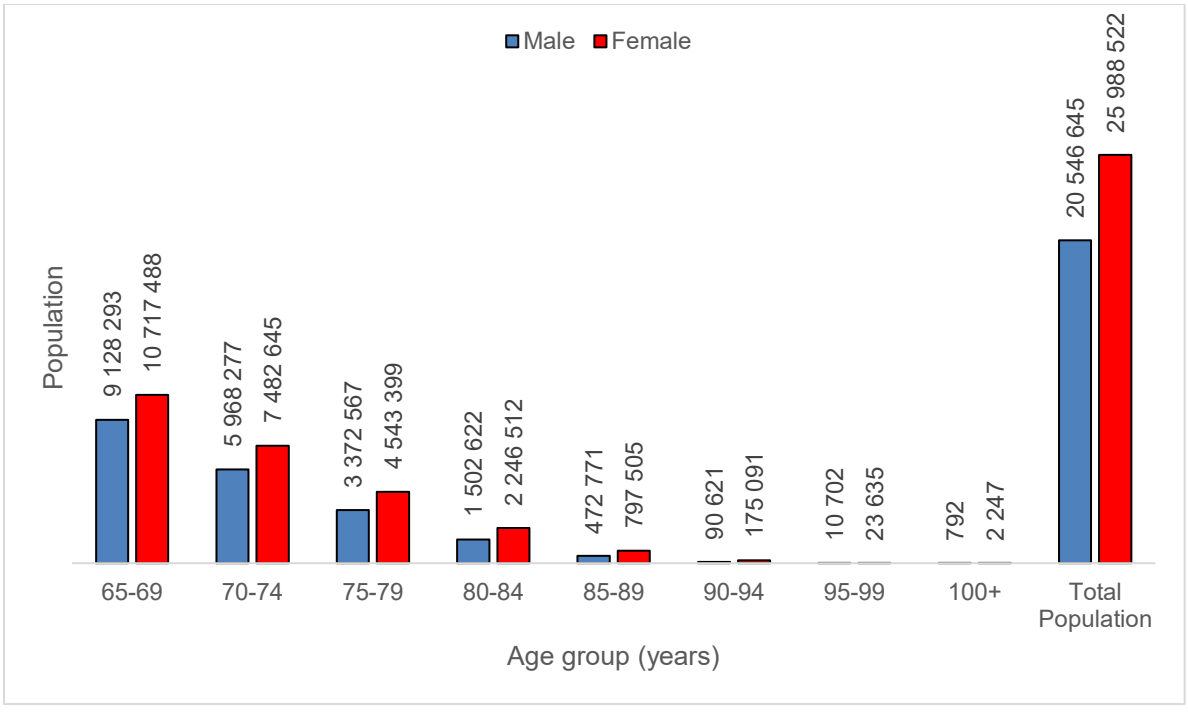

Figure 1-3: **Projected population size that will be older than over 65 years of age in sub-Saharan Africa in 2030.[5] Self-generated graph from published data.**

1.2 Neurodegeneration and access to healthcare

1.2.1 Current treatments for Parkinson's disease in South Africa

Characterised by a loss of dopaminergic neurons in the midbrain, the disease presents with tremors, bradykinesia, shuffling gait and other non-movement symptoms such as depression and loss of smell.[22] Treatment is complex and requires both human and financial resources from the healthcare system, however, SSA lacks access to such infrastructure.[23] Anti-Parkinson's disease drugs are only available in 3% of African countries on a primary care level, and in 22% of countries at a hospital level.[24]

Parkinson's disease has no known cure, and treatment remains symptomatic for both the motor and non-motor symptoms.[25] The current standard treatment, both worldwide and in South Africa, for tremors and bradykinesia is levodopa (L-dopa)/carbidopa (Sinemet®, Carbilev®, Teva Carbi-Levo®), which supplements dopamine stores in the brain due to the provision of the L-dopa pro-drug and inhibiting the breakdown down of L-dopa.[26] In addition to L-dopa-induced dyskinesia, "wearing-off" is a major limitation of its therapy.[27] "Wearing-off" is a common feature, where lowered efficacy due to reduced bioavailability of L-dopa to the brain is observed.[28-30] The increased release of dopamine into the brain can also increase the production of the cytotoxin, 6-hydroxydopamine (6-OHDA), which is why additional neuroprotective agents such as iron chelators (phase II trials) have been suggested for advanced PD therapies (due to the potential contribution of iron-related cell death mechanisms).[31, 32] More selective treatments for motor symptoms includes dopamine agonist therapy with either pramipexole (Pexola®) or bromocriptine (Parlodel®),[33] or the monoamine oxidase B (MAO-B) inhibitor, rasagiline (Azilect®), which inhibits the degradation of dopamine in the synaptic cleft resulting in a higher concentration of free dopamine.[34]

Treatment of PD is dynamic due to the progressive neurodegeneration observed and the need to manage the increased frequency of side-effects.[35] The dosage used to maintain therapeutic efficacy invariably increases as a response to the worsening of the disease, accompanied by additional adjunct therapies and adjustments to manage motor symptoms.[36] This large-dose regimen required to manage both motor and non-motor symptoms can lead to various complications of possible drug-drug interactions and side-effects, which includes fibrosis,[37] cardiac insufficiency,[38] and insulin resistance.[39] Modern research into therapies is currently focused on disease-modification of the illness[40] with the aim to reduce the side-effects associated

with conventional therapy. Direct or adjuvant therapies can also extend to natural remedies, such as traditional medicine.

1.3 Traditional medicines

The reduced access to Western medicine, resulting from, among others, infrastructure deficiencies or financial constraints, makes indigenous medicines a valuable treatment resource for healthcare.[41] In many cultures, traditional medicines are perceived as more effective, because of the interwovenness of both medicine and religion (seen as a holistic integration of herbal remedies, divination and spiritualism).[42-44] This form of healthcare is geographically more accessible to many patients, generally more affordable, and may be more acceptable due to the cultural beliefs and worldview of the patient.[45] Indigenous knowledge practitioners are normally less expensive than Western medicine practitioners and can treat patients in the comfort of the home or community, thus reducing expenses for travel and childcare.[46] The increased cost of medicines, long waiting times at healthcare facilities, and limited accessibility to medical practitioners[47] often leads to community members seeking guidance from traditional healers for their healthcare needs. Traditional healer knowledge is either passed down from or acquired from other healers with more experience.[48]

Some African cultures see illness or disease as not only the physical state of the body, but also the social standing, morality, and spiritual well-being.[49] Western medicines, on the other hand, are perceived as only focusing on physical or mental health, thus resulting in a targeted approach, with specialists for each niche field of medicine.[50] Due to the targeted nature of Western medicine approaches, side-effect profiles are better understood, but there are always risks associated with the usage of any medicine.[51]

Ethnomedicine broadly refers to traditional medical practices concerned with the cultural interpretation of health, diseases, and illness that addresses healthcare processes and healing practices.[52] Several ethnomedicines exist for the treatment of neurological disorders, such as seizures, convulsions and headaches.[53] Ethnomedicines are normally interwoven with both cultural and religious beliefs and is seen as holistic.[54] Each region has their own integration and belief as to how disease is caused, for example, by some lack of ancestral respect, or by breaking taboos set by the community, and some also do abide by germ theory.[55] Whilst a specific diagnosis is rarely given, seeing as the cultural context lacks the Western image of

pathophysiology, these concepts of disease are reflected in the treatment, and thus it extends into the ethnomedicinal rationale with certain plants or mixtures.[56]

1.4 Drug development

The drug development process is a long and cost-intensive process.[57] This process from pre-clinical research to market release consists of four phases; pre-clinical development, clinical development, data review and approval, and post-marketing surveillance (**Figure 1-4**).[58] It is during the initial stages of investigation; i.e. pre-clinical phase, where the majority of drug candidates fail. This may be due to inefficiency towards the specific disease state or toxicity towards *in vitro* targets, such as cell lines or animal models.[59] Pre-clinical investigations involve *in silico*, *in vitro* and *in vivo* models to test or predict outcomes. These can range from drug target binding studies, enzyme inhibition to basic cytotoxicity assessment.[58] Collation of this pre-clinical data can expose toxicity or efficacy when reviewed within a specific modality.[60] Given the potential of new chemical entities (NCE) to be identified from natural sources, herbal remedies, or purified fractions thereof, afford researchers the potential to investigate a diverse and potential multi-targeted phytochemical matrix for biological activity.

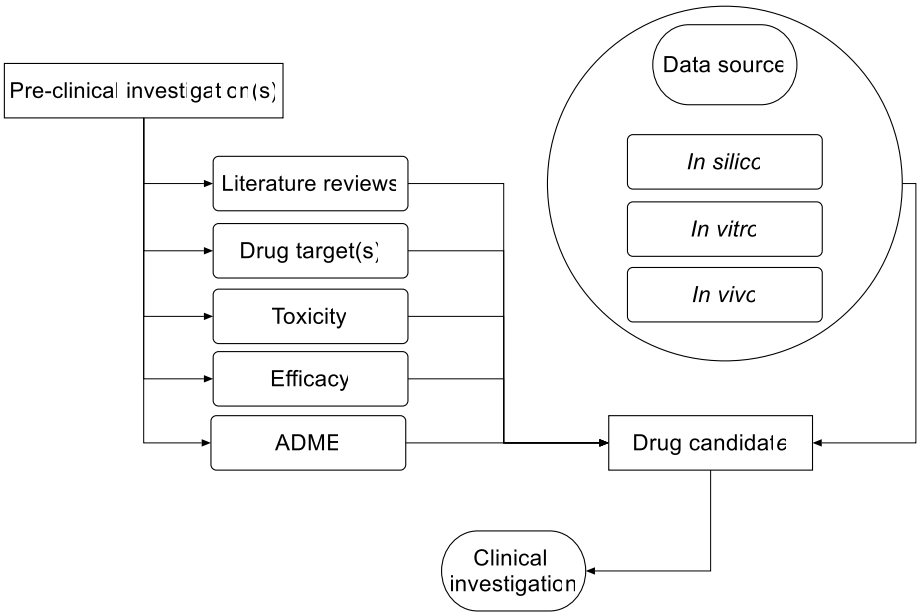

Figure 1-4: The flow diagram shows how the various drug discovery and pre-clinical investigations serve as the foundation for clinical investigations. Several aspects of drug properties (ADME, toxicity and efficacy) are needed for the drug candidate to move to clinical trials. Image is self-generated. ADME: absorption, distribution, metabolism, and excretion.

1.5 Aim and objectives

The aim of this study was to determine the cytoprotective and anti-ferroptotic properties of semi-automated fractions of selected African medicinal plants in a 6-OHDA-induced SH-SY5Y neuroblastoma neurodegenerative model.

The objectives of the study were to:

- determine the inherent cytotoxicity of the samples (i.e., the crude extract and semi-automated fractions of selected medicinal plants) in the SH-SY5Y cell line using the sulforhodamine B assay.
- determine the cytoprotective effects of samples against 6-OHDA-induced cytotoxicity using the sulforhodamine B assay.
- determine the involvement of anti-ferroptotic properties in the most cytoprotective samples by investigating acellular antioxidant and iron chelation properties, and alteration to the cellular redox status, mitochondrial membrane stability and glutathione concentration.
- elucidate the phytochemical constituents present in the samples with the highest cytoprotection using ultra performance liquid chromatography tandem mass spectrometry; *and*
- investigate the physiochemical properties and binding affinity of the identified phytochemical constituents using *in silico* approaches.

CHAPTER 2: PATHOPHYSIOLOGY OF PARKINSON'S DISEASE

2.1 Ageing as a risk factor

Ageing is one of the primary risk factors for the development of neurodegenerative diseases,[61] and contributes to the average increase in years lived with disability, as it increased by 15% between 1990 and 2015.[62, 63] With a predicted increase of up to 12 million new patients by 2030, PD is one of the fastest growing neurological diseases.[64]

Ageing is associated with several biochemical and physiological hallmarks (**Figure 2-1**).[65] The primary characteristics of these hallmarks are genomic instability, epigenetic alterations, telomere attrition and the loss of proteostasis.[66] These hallmarks cause certain compensatory or protective responses to mitigate cellular damage, such as mitochondrial dysfunction, cellular senescence, and deregulated nutrient sensing.[67] As the severity of these responses increase, the resulting damage become irreparable.[68] Age-related cellular dysfunction is ultimately attributed to stem cell exhaustion and altered cellular communication arising from cumulative damage from both primary and antagonistic responses and hallmarks.[69] Hallmarks of ageing are similar to those that characterise neurodegenerative diseases, such as PD (**Figure 2-1**).[70]

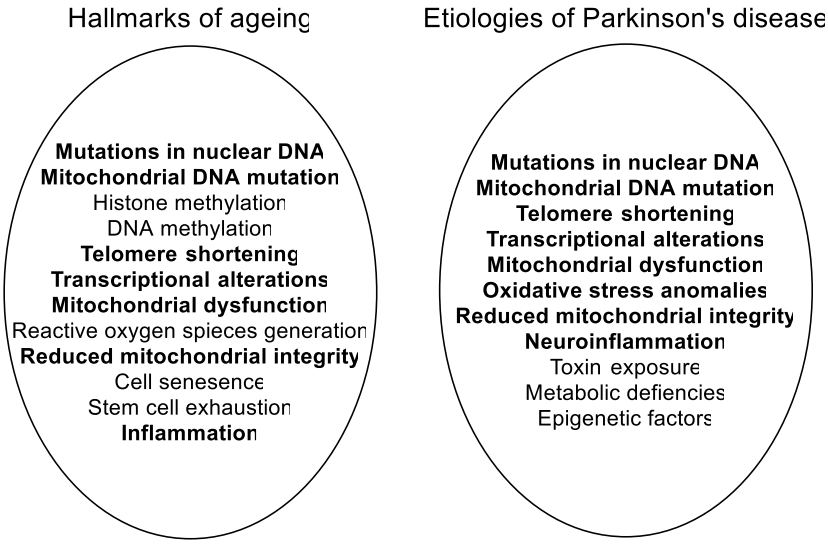

Figure 2-1: The hallmarks of ageing and Parkinson's disease. Bold text indicates overlapping detriments.[61, 65, 70] Self-generated figure from literature.

2.2 Neuropathology

Parkinson's disease is recognised as a multi-system disorder due to its extensive range of motor and non-motor symptoms.[25] The disease is attributed to the progressive and irreversible loss of dopaminergic neurons in the midbrain, especially the substantia nigra pars compacta (SNpC).[71] The SNpC is a pigmented area of the midbrain where a loss of pigmentation directly correlates to the loss of neuromelanin-containing dopaminergic neurons (as seen in PD).[71] These cells, namely A9 neurons, are posited to be the only cells undergoing cell death in PD, whereas other neuronal types and glial cells are spared.[72] Using cross-sectional, age-adjusted studies of brains sampled from the cadavers of individuals diagnosed with PD during post-mortem, clinical motor symptoms was perceived at approximately a 30% loss of dopaminergic neurons.[73] The loss of dopaminergic neurons reduces the concentration of dopamine in the striatum, which leads to the clinical movement symptoms (tremor, bradykinesia and shuffling gait) observed in PD.[74]

2.2.1 Dopamine as a neurotransmitter for movement

Dopamine is produced in the cytoplasm of dopaminergic neurons via a two-step process.[75] L-tyrosine is hydroxylated at the phenol ring by tyrosine hydroxylase to yield L-Dopa, which is then decarboxylated by aromatic amino acid decarboxylase (AADC) to dopamine **(Figure 2-2).** The binding of dopamine to dopamine receptors (DA-R) is beneficial to the normal functioning of the CNS, as a subset of cell-to-cell communications.[76] Five subtypes of DA-R exist, each with its own unique function and action **(Table 2-1).**

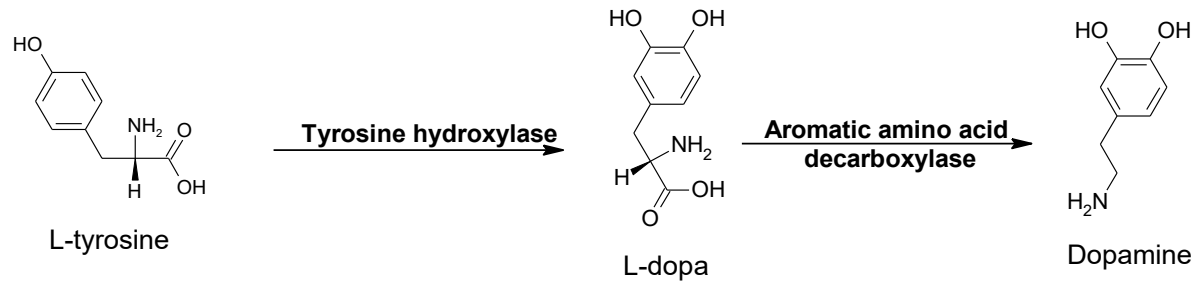

Figure 2-2: Synthesis of dopamine. Self-generated figure from literature.[75]

Table 2-1: Location and function of dopamine receptor sub-types.[76]

Dopamine receptor (DA-R) subtype	Function	Locations with highest expression
DA-R1	Memory, attention, impulse control, regulation of renal function, locomotion	Striatum, nucleus accumbens, olfactory bulb, and substantia nigra[76]
DA-R2	Locomotion, attention, sleep, memory, learning, reproduction behaviours, vomiting	Striatum, as well as the external globus pallidus, core of the nucleus accumbens, hippocampus, amygdala, and cerebral cortex[76]
DA-R3	Cognition, impulse control, attention, sleep	
DA-R4	Cognition, memory, fear, impulse control, attention, sleep	
DA-R5	Decision making, cognition, attention, renin secretion, reproduction behaviours	Striatum, nucleus accumbens, olfactory bulb, and substantia nigra[76]

The DA-R1 and DA-R5 are both G-protein coupled receptors with a stimulatory site that activates adenylyl cyclase, and share the same locations of higher density expression.[77] Simultaneously, phospholipase C is activated, resulting in intracellular calcium ion (Ca^{+}) release and protein kinase C activation.[78] Calcium also influences neurotransmitter release via exocytosis.[78]

The DA-R2, -R3 and -R4 all bind to G-coupled proteins with active sites that inhibit adenylyl cyclase and activate potassium channels.[79] These receptors also influence extrapyramidal activity mediated by postsynaptic receptors.[76] The DA-R2, DA-R3 and DA-R4 play a vital role in the survival and development of human dopaminergic neurons.[80] The DA-R1 is the most abundant DA-R within the central nervous system (CNS), hence loss of the neurons with this receptor expression has a profound effect on movement and locomotion in PD.[81]

2.2.2 Neuronal movement circuits in Parkinson's disease

Movement is a complex execution of processing brought on by correct sensory-motor information within the brain and complex neural networking associated with the cerebral cortex, motor thalamus and basal ganglia nuclei.[82] The basal ganglia are functionally interposed between both the thalamus and cortex with the main task of processing input signals from the cortex and facilitating output signals through the cortex to the thalamus to modulate movement.[83] The basal ganglia are associated with several interconnected nuclei; namely the caudate nucleus and

putamen (commonly referred to as the striatum or corpus striatum), globus pallidus, substantia nigra (split into the SNpC and substantia nigra pas reticulata [SNpR]), and the subthalamic nucleus.[84] Each of these nuclei has associated neural projections and neurotransmitters (**Table 2-2**).

Table 2-2: Nuclei associated with the basal ganglia and their projections.

Nuclei		**Neurotransmitters**	**Projects into**
Striatum	Caudate nucleus	γ-amino-butyric acid (GABA) with enkephalin and substance P[85, 86]	Globus pallidus[87]
	Putamen	Acetylcholine, somatostatin and GABA with parvalbumin and calretin[88]	SNpR [87]
Globus pallidus	Medial	GABA and glutamate[89]	Thalamus[87]
	Lateral	GABA with enkephalin[90]	Subthalamic nucleus, SNpC[87]
Substantia nigra	Pars compacta	Dopamine and neuromelanin[91]	Striatum, subthalamic nucleus and globus pallidus[87]
	Pars reticulata	GABA and glutamate[92]	Thalamus[87]
Subthalamic nucleus		Glutamate[93]	SNpR and lateral globus pallidus[87]

GABA: γ-amino-butyric acid; SNpC: substantia nigra pars compacta; SNpR: substantia nigra pas reticulata

Movement circuits (**Figure 2-3**) have been modelled to simplify the complex circuitry and structures used to facilitate both healthy and affected movement.[94] These models can explain the effects in movement in individuals living with PD and how the change in brain structures and chemistry can affect healthy movement.[95]

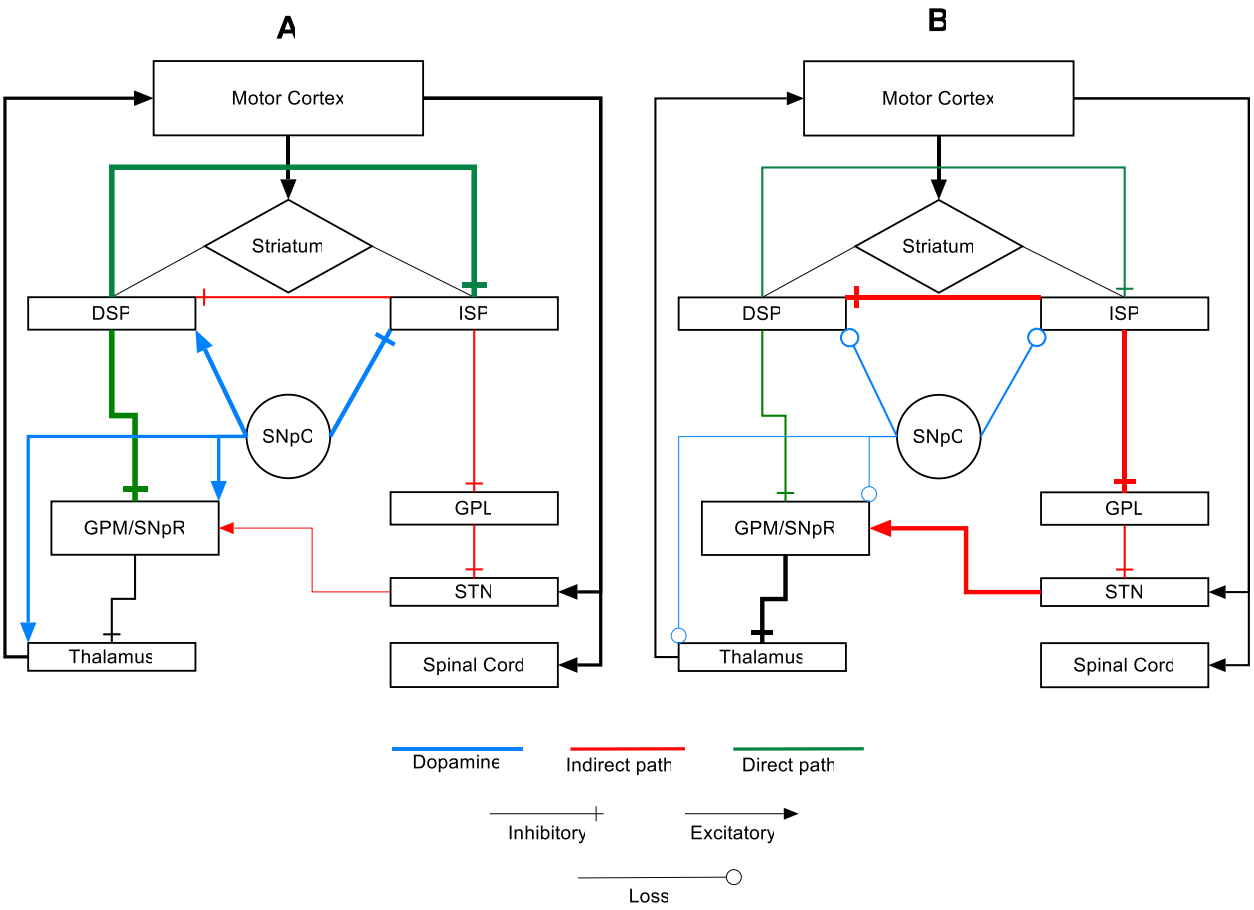

Figure 2-3: **Classical model of movement in a healthy brain (A) compared to a brain affected by Parkinson's disease (B).[96] Bolded lines show an excitement of the pathway from normal circuits (A) to Parkinsonian circuits (B). DSP: direct spiny projections; GPL: lateral globus pallidus; GPM: medial globus pallidus; SNpR: substantia nigra pars reticulata; STN: subthalamic nucleus.**

The classical model for movement (**Figure 2-3 A**) explains the influence of dopamine on motor output and how the loss of dopaminergic neurons within the midbrain affects movement in PD.[95] This model divides the spiny neuronal projections into two populations i.e., direct (DSP) and indirect (ISP).[97] The DSP projects directly into the main basal ganglia output centre, both the medial globus pallidus (GPM) and the SNpR expressing DA-1R.[98] The activation of the direct pathway is thought to disinhibit the thalamus by reducing total basal ganglia output and promoting movement to the spinal cord via the cortex.[99]

In PD, the reduced dopaminergic neurons and free dopamine within the SNpC results in less activation of the DSP and a net loss of activation to the direct pathway (**Figure 2-3 B**).[100] The loss of dopamine also decreases the inhibition of the indirect pathway.[96] This decrease in inhibition then increases basal ganglia output, inhibiting the thalamus and thus inhibiting movement.[96] The excessive activation of the indirect pathway further suppresses lateral globus pallidus (GPL) firing and in turn increases subthalamic nucleus (STN) activity.[101] This spike in activity through the STN suppresses the thalamus and subsequently movement.[102]

Suppression of the thalamus is translated into several clinical motor symptoms observed in PD, namely bradykinesia (slowness of movement), tremors, rigidity, and postural instability.[25, 72, 103] Several non-motor symptoms are also present and these may precede motor symptoms by some years.[104] This may be due to original degeneration in the autonomic nervous system and/or the olfactory bulb, which spreads to the SNpC in the CNS.[105] Non-motor symptoms, based on the proposed pathological changes, include hyposmia (loss of smell), constipation and rapid eye movement sleep behavior,[22, 25] as well as depression and anxiety in some cases.[62, 106, 107]

2.3 Disease aetiology

2.3.1 Mitochondrial function

Mitochondria are crucial for cellular function as the organelle is responsible for energy synthesis in the form of adenosine triphosphate (ATP).[108] These organelles are highly efficient and specialised, producers of energy from oxygen (O_2) and substrates such as glucose or pyruvate.[109] The organelle consists of two membranes (inner and outer), an intermembrane space and intracellular matrix. The electron transport chain (ETC) (**Figure 2-4**) is situated within the inner membrane, organised into a larger mega complex in a specific sequence to facilitate energy production ATP synthesis.[110] Mitochondria also contain and maintain a separate genome linked to function and, when damaged or impaired, leads to dysfunction.[111]

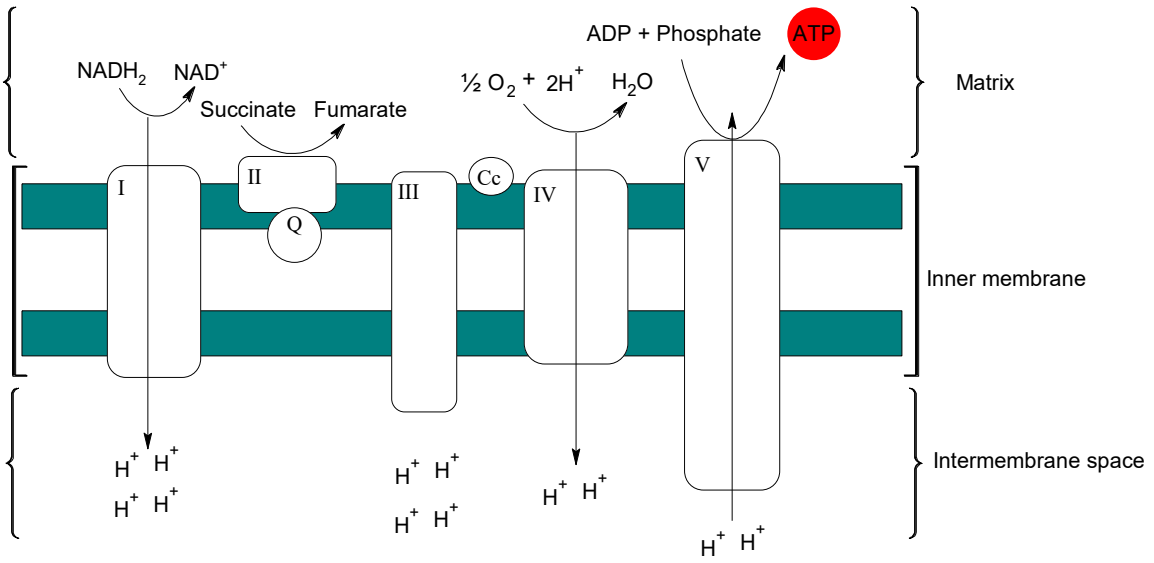

Figure 2-4: **Schematic representation of the electron transport megacomplex as situated within the inner mitochondrial membrane, where the flow of protons facilitates ATP generation.[112] Self-generated image from literature. $NADH_2$/NAD+: nicotinamide adenine dinucleotide (reduced/oxidised); ADP: adenosine diphosphate; ATP: adenosine triphosphate; O_2: oxygen; H: hydrogen; Q: coenzyme Q; Cc: cytochrome C.**

The ETC is composed of four enzymatic sub-unit complexes, where the oxidation of nicotinamide adenine dinucleotide ($NADH_2$) to NAD^+ takes place via complex I (Com I), and leads to a reduction of the lipid-soluble mobile electron carrier, coenzyme Q (CoQ).[113] Complex III oxidises the reduced CoQ and in turn reduces cytochrome C (C*c*).[114] This oxidation donates an electron to complex IV to reduce the molecular oxygen to water.[112] The increased proton flow into the intermembrane space drives the generation of ATP at complex V (also known as ATP synthase).[112] This proton flow is known as the mitochondrial membrane potential (ΔΨm).[115]

The ΔΨm serves as an intermediate storage of energy generated from the Krebs cycle.[116] Adenosine triphosphate synthase uses the ΔΨm to produce ATP[117] via the flow of electrons through the ETC and the accumulation of H^+ in the trans membrane space.[116] Normal cell activity is reported to depend on cells being able to maintain stable levels of intracellular ATP and Δψm.[118] Additionally, it implies that although these parameters may vary as a result of physiological activity, these modifications should only last a short time and that a sustained disturbance of any

one element may endanger the viability of the cells, having pathological repercussions.[119] It has been suggested that the ΔΨm can be employed to determine ATP generation as well as the viability of mitochondria.[118] A reduction in ATP production via depolarisation of the mitochondrial membrane may lead to the leakage of cations, C*c* and Ca^{+} into the intracellular space, which in turn may promote mitophagy (removal of non-functioning mitochondrial via lyases).[120] The ΔΨm serves as a catalyst for the transportation of charged substances, some of which are necessary for the survival of mitochondria.[121]

2.3.2 Mitochondrial dysfunction within Parkinson's disease

2.3.2.1 Complex I inhibition

Complex I serves as the entry point for both H^{+} and electrons into the ETC, facilitating the transfer of electrons from NADH generated in the tricarboxylic acid cycle. [122] A single electron can be transferred to oxygen to produce superoxide ($O_2^{\bullet-}$) at this site.[123] Manganese superoxide dismutase (MnSOD) converts $O_2^{\bullet-}$ to hydrogen peroxide (H_2O_2), and in the presence in ferrous iron (Fe^{2+}), is further converted to hydroxyl radicals via the Fenton reaction.[124] Inhibition of Com I increases the production of reactive oxygen species (ROS), the $O_2^{\bullet-}$ molecule, which in turn can form peroxynitrite with nitric oxide, or toxic hydroxyl radicals (HO●).[125] Under normal physiological conditions, only 0.2% to 2% of electrons leak from om I resulting in ROS production within the cytoplasm.[120]

There is a necessity for ROS and the oxidative modifications of proteins and kinases, such as the cysteine residue modification, are essential for altering protein structure and function between redox states.[126] These redox-derived changes in protein function can influence key processes, including transcription, phosphorylation, and other vital signalling events, as well as alter metabolic fluxes and reactions in the cell by modifying enzyme properties.[127] However, an overwhelming amount of ROS produced due to dysfunction may lead to protein aggregation and deoxyribonucleic acid (DNA) damage.[128]

When ROS is produced in excess, these radicals contribute to mitochondrial DNA (mtDNA) mutations and a loss of Δψm.[117] Mitochondrial membrane potential is directly proportionate to ROS production, where a reduction in ΔΨm is linked to a reduction in ROS.[129] An increase in ΔΨm has been linked to the inhibition of ATP synthase, where an increase in ROS production is observed.[130]

In 1983, patients with PD-like symptoms were admitted to hospital after intravenous drug use with a potent inhibitor of Com I known as 1,2,3,6-tetrahydropyridine (MPTP).[131] After oxidation via monoamine oxidase (MAO) in glial cells, MPTP is transformed into a toxic lipophilic form, 1-methyl-4-phenylpyridinium (MPP^+).[132] The MPP^+ molecule interferes with Com I in dopaminergic neurons, causing selective neurodegeneration in the SNpC.[133-135] Complex I inhibition causes a lack of electrons to be transferred to co-enzyme Q (CoQ) and Com II, leading to increased ROS production due to an accumulation of electrons within Com I.[136] Complex I inhibition is not considered to be an effect or cause of PD; however, this inhibition contributes to the oxidative damage seen in PD patients.[136] There is evidence to suggest that there is a Com I deficiency in PD patients, however, it is not known whether this deficiency is seen as a pre-symptomatic (indicative of bigger factors) or post-diagnoses (a downstream effect of other factors) characteristic.[137]

2.3.2.2 Mitochondrial deoxyribonucleic acid mutations

The mtDNA exists as circular chromosomes within the cytoplasm, making mtDNA vulnerable to mutations.[138] Observed mtDNA deletion within dopaminergic neurons located in the SNpC supports the idea that these mutations and mtDNA damage may cause functional defects.[139, 140] Mutations in mtDNA are generally attributed to the accumulation of damaged DNA in the neurons which compromise functioning[141] and precipitate early cell death.[142] The associated cell death can occur through apoptotic (intrinsic and extrinsic pathways[143]) and non-apoptotic means (such as ferroptosis and necrosis).[144, 145] Nuclear DNA and mtDNA replicate independently, thus damage to the mtDNA can occur sporadically due to the absence of DNA repair mechanisms[146] and protective histones in the mitochondria.[147, 148]

The HO● is especially toxic to DNA base pairs as it has been linked to oxidative damage of the heterocyclic and sugar moieties, which may result in mutagenesis, carcinogenesis, and ageing.[149, 150] This DNA damage can be traced back to mtDNA deletions, as most of the respiratory actions occur within the mitochondria, where ROS can easily reach the mtDNA.[151] Damage to mtDNA has been observed in dopaminergic neurons situated within the SNpC of individuals with PD, which indicates that the damage is more localised to the motor cortex.[140] Mutations in mtDNA result in mis encoding of essential proteins responsible for stabilising ROS and $\Delta\Psi m$, leading to impaired functionality of dopaminergic neurons.[152] As mtDNA programs metabolic functions, damage in lieu of mitochondrial repair mechanisms lead to the production of more ROS.[153]

2.3.2.3 Reduction in neuronal antioxidant systems

The cell has a variety of antioxidant systems that either prevent or inhibit excessive ROS production.[154] Cytosolic enzymes reduce the amount of lipid peroxides and H_2O_2 and are important in maintaining the structure of the cell membrane and its function through varying reactions (**Table 2-3**). Superoxide dismutase (SOD) is located within the cytosol and the mitochondria, and has several metals as co-factors, including manganese (Mn), Cu and zinc (Zn).[155] The reaction of SOD includes the conversion of $O_2^{\bullet-}$ into H_2O_2.[156] The MnSOD is the antioxidant enzyme within the mitochondrial matrix which is essential for survival for aerobic cells.[157] Catalase (CAT) is mainly present in peroxisomes where it converts H_2O_2 into oxygen and water.[158] It uses Fe^{2+} as a cofactor,[159] and although it cannot be saturated by H_2O_2, the inhibition of CAT leads to oxidative stress and cytotoxicity.[160] The glutathione peroxidase (GPx) family of antioxidative enzymes contribute to antioxidant systems of cells by focusing on lipid peroxides by using glutathione (GSH) as a co-factor, as well as having an affinity towards H_2O_2.[161]

Neural cells possess several mechanisms to reduce oxidative damage, as well as a complex antioxidant system consisting of different enzymes and non-enzymes.[162] Antioxidant defence systems prevent the generation of excess ROS and sequester the associated generated radicals.[163] Antioxidants work directly to remove oxidising radicals and restore oxidised molecules in cells.[164] Whilst the SnPC experiences a decrease in antioxidant defences with age, the SnPC of an individual with PD undergoes severe and widespread loss in antioxidants.[165] The overabundance of ROS can cause a state of oxidative stress, where the ratio of ROS to antioxidant defences are skewed in the favour of ROS.[166] Excessive ROS promotes cellular dysfunction. Oxidative stress and the role of ROS in the aetiologies of neurodegenerative illness are increasing and has been seen as a key component of dopaminergic neurons' degeneration in PD.[167]

2.3.3 Oxidative stress and cell death

Excessive ROS production can result in oxidative stress, a condition that arises when the antioxidative systems (**Table 2-3**) are unable to effectively neutralise ROS and maintain their levels below a toxic threshold.[168] In PD, the SNpC has been shown to exhibit early and significant depletion of the antioxidant protein GSH, reduced mitochondrial complex I activity, elevated oxidative damage to lipids, proteins, and DNA, increased SOD activity, and higher free iron levels.[169, 170]

Table 2-3: Enzymatic antioxidants and the associated antioxidative reactions.[154]

Enzyme	Substrate	Reaction
Manganese superoxide dismutase	$O_2^{\bullet-}$	$O_2^{\bullet-} \rightarrow H_2O_2$
Catalase	H_2O_2	$H_2O_2 \rightarrow O_2$ + water
Glutathione peroxidase(s)	H_2O_2	H_2O_2 + glutathione → reduced glutathione + water
	Lipid peroxides	Lipid peroxides + glutathione → reduced glutathione + associated aldehyde

H_2O_2: hydrogen peroxide, O_2: oxygen molecule, $O_2^{\bullet-}$: superoxide anion

This imbalance, coupled with several ROS-adjacent pathologies, forms a self-forming loop, where the abundance of ROS depletes intracellular GSH, which in turns increases the formation of lipid peroxides.[171] These lipid peroxides then alter lipid within the cellular and mitochondrial membrane, altering pores and increasing the permeability of the cell membrane.[172] If the permeability of the mitochondria is affected, this in turn changes the ΔΨm, which downstream produces more ROS.[118] The permeability is not just affected by lipid peroxides, but also protein aggregation **(Section 2.3.3.2),** which impairs not only the storage of neurotransmitters, as well as metals. The rise in metal levels, such as Fe^{2+}, triggers specific reactions with ROS and catalyses interactions not only with cellular organelles, but also with DNA.[173] These protein aggregates lead to permanent changes in the structure and function of certain enzymes, further hindering the activity of antioxidants within the cell.[174] This complex interplay of ROS-induced damage and mitochondrial dysfunction creates challenges in pinpointing the exact mechanisms of cell death in PD research.[175]

2.3.3.1 Reactive oxygen species

Reactive oxygen species are highly reactive chemical molecules derived from molecular oxygen via a series of four one-electron reduction reactions (**Figure 2-6**). These reactions frequently occur within the ETC and mitochondria, where intermediate O_2 species are generated.[176] The three primary ROS types; $O_2^{\bullet-}$, H_2O_2 and the HO●, are categorised based on their reactivity and oxygen content.[177] The $O_2^{\bullet-}$ and HO● radicals, commonly referred to as "free radicals," interact with organic molecules, forming intermediate species that can propagate the production of additional ROS.[178] For instance, when HO● abstracts a hydrogen atom from a C-H bond, it creates a carbon-centred radical that readily reacts with oxygen to form a peroxyl radical (RO_2●).[179]

Despite their reactivity, the basal ROS concentration is tightly regulated to prevent the harmful effects of excessive ROS levels.[180]

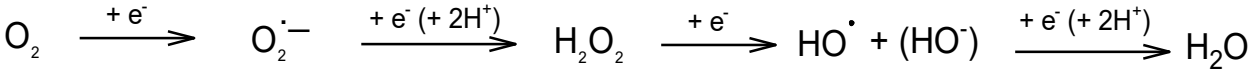

Figure 2-5: **The generation of reactive oxygen species (ROS) as byproducts of molecular oxygen within the electron transport chain. O_2: oxygen; O2•–: superoxide; H_2: hydrogen; HO•: hydroxyl ion; HO^-: hydroxide ion; H_2O_2: hydrogen peroxide; H_2O: water; e^-: electron. Self-generated image from reference.[176]**

The radicals formed during the synthesis of ATP, are metabolised and rendered non-toxic through various antioxidative enzymes such as GPx and SOD.[165] The ROS regulates certain cellular communications, processes and signalling, including autophagy (breakdown of intracellular proteins) and immunity.[181]

The toxicity of ROS is amplified by two key reactions: the Haber-Weiss[182] and Fenton reactions (**Figure 2-6**).[183] Both reactions ultimately generate HO●, which can further propagate damage through electron abstraction, hydrogen abstraction and double bond addition.[184] The Fenton reaction involves the formation of hydroxide (OH^-) and HO● radicals catalysed by Fe^{2+} and H_2O_2, in contrast to the Haber-Weiss reaction, where HO● radicals and hydroxide are generated by a reaction between H_2O_2 and $O_2^{\bullet-}$ catalysed by iron (**Figure 2-6**).[185] In the Haber-Weiss reaction, molecular oxygen reacts with electrons (e^-) that leak from the ETC to produce $O_2^{\bullet-}$. The latter is scrubbed by MnSOD into O_2^{2-}, which then decomposed into HO● radicals in the presence of Fe^{2+}.[182] The Fenton reaction is where molecular oxygen is produced from $O_2^{\bullet-}$ in the presence of iron(III) (Fe^{3+}) to produce Fe^{2+}.[186]

The HO● radical is electrophilic and has a strong affinity for electron-rich sites of molecules, in particular aromatic or sulphur-containing molecules.[187] Whilst ROS are short-lived, the subsequent reactions that are catalysed have lasting effects in the neuron and mitochondria, leading to DNA damage, lipid peroxidation and both protein and enzyme damage.[188]

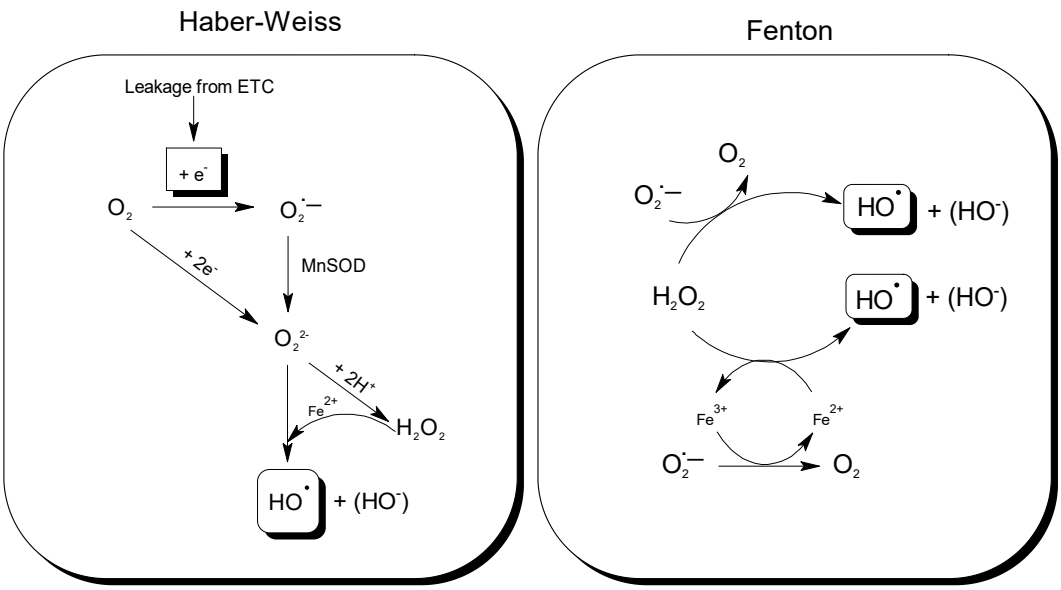

Figure 2-6: **Reaction schemes for the Haber-Weiss and Fenton reactions.[182, 186] . O_2: oxygen; O2•–: superoxide; H_2: hydrogen; HO•: hydroxyl ion; HO^-: hydroxide ion; H_2O_2: hydrogen peroxide; H_2O: water; e^-: electron; iron(III): Fe^{3+}; iron(II): Fe^{2+}.**

The breakdown of neurotransmitters within the synaptic cleft also leads to the production of ROS,[75] such as the MAO- and catechol-*O*-methyltransferase (COMT)-facilitated metabolism of dopamine via the Fenton reaction.[189] This reaction leads to the production of H_2O_2, which is a normal physiological by-product, however dysregulation can cause excess damage.[189] Dysregulation in the metabolic processes of neurotransmitters, i.e. the release and storage of neurotransmitters can cause physiological imbalance and clinical symptoms. Where in PD the synthesis of dopamine has been reduced, and the synaptic storage is affected by ROS and ROS by-products.[72]

2.3.3.2 Protein aggregation

A histological trademark of PD is the protein-aggregates (**Figure 2-7**) of alpha-synuclein (α-syn).[190] The α-syn protein is concentrated in the presynaptic compartment of the neurons and is thought to facilitate vesicle dynamics, and by extension, neurotransmitter release.[191] The α-syn pathology is now known to include aggregates as seen in Lewy bodies which are insoluble aggregates that cause, among others, mitochondrial infiltration,[183] subsequent mitochondrial dysfunction, and eventual cell death via mitophagy.[192] These aggregates also damage several other cell organelles including the Golgi apparatus[193] and endoplasmic reticulum.[194]

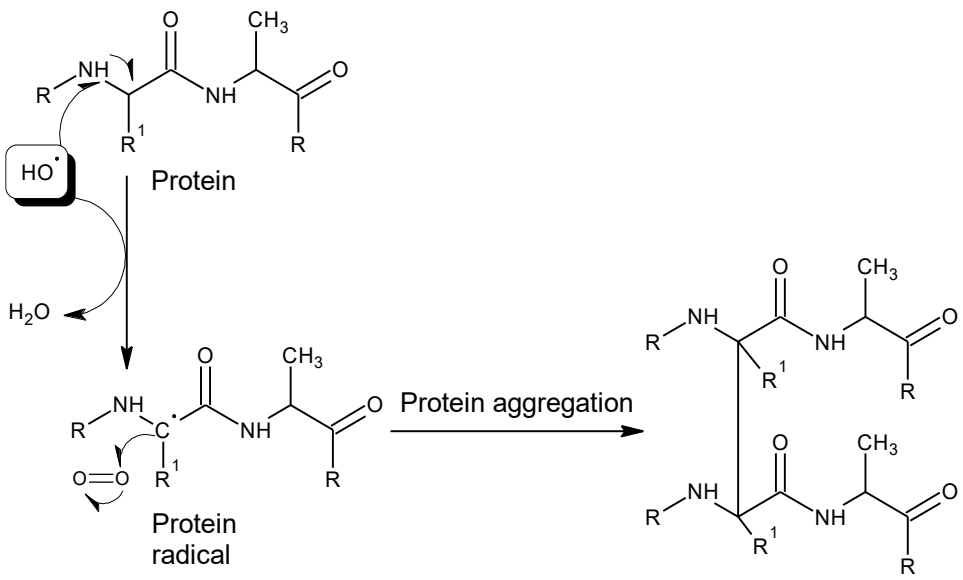

Figure 2-7: **A schematic representation of catalysis of aggregated proteins by hydroxyl radicals. HO•: hydroxyl ion; H_2O: water, O=O: oxygen. Figure is self-generated from reference.[195-197]**

2.3.3.3 Dopamine metabolism and associated effects

Dopamine, the key neurotransmitter involved in movement and motor circuits, has several degradation pathways, which produce ROS as by-product.[75, 189, 198] Dopamine is readily degraded by MOA-A and MAO-B to reactive 3,4-dihydroxyphenylacetaldehyde (DOPAL) and H_2O_2, which promotes further radical production downstream.[199] Glial cells absorb free dopamine in the synaptic cleft to facilitate the degradation by MAO and COMT.[200] Both MAO enzymes play a critical role in the metabolism of neurotransmitters within the brain and nervous system, with each isoform exhibiting substrate specificity.[201] MAO-A primarily degrades neurotransmitters such as serotonin, norepinephrine, and dopamine, whereas MAO-B metabolises dopamine, in addition to phenylethylamine, thereby contributing to the regulation of neurotransmitter levels.[202] The regional concentration of these enzymes within the brain can have profound implications for neurological function and the development of neuropsychiatric disorders.[203] Variations in the concentration of MAO-B across different brain regions may, influence individual susceptibility to neurodegenerative diseases, highlighting the potential therapeutic relevance of targeting MAO-B activity in the treatment of such conditions.[204]

As a non-mitochondrial enzyme, COMT plays an important role in both peripheral and central dopamine metabolism.[29, 75] The degradation of dopamine leads to the formation of dopaquinones

via tyrosinase, or in the presence of Fe^{2+}, 6-OHDA is formed as a downstream by-product of dopamine interacting with the HO● radical.[75] Under normal physiological conditions, dopaminergic breakdown products are cleared by neuronal vesicles in the post-synaptic neuron. However, when protein dysregulation occurs, such as protein aggregations, the formation of pore-forming α-syn aggregates can disrupt vesicular function and impair clearance[205]

Vesicles are intracellular bodies which stores and protects non-peptide neurotransmitters produced in the cytoplasm for exocytosis into the synaptic cleft.[206] Under physiological conditions, these vesicles are bound with α-syn which stabilises and groups the vesicles before exocytosis to prevent movement within the cytoplasm.[207] This grouping of vesicles is called the resting pool.[208] With influx of Ca^{2+}, the vesicles are removed from the α-syn grouping, and moved to the cell membrane where a complex fusion of the vesicle and cell membrane results in the release of the neurotransmitter into the synaptic cleft.[208] In certain pathophysiological conditions, α-syn may be modified through the binding of DOPAL, where the protein will then permeabilise the storage vesicles of dopamine, and results in an increased cytoplasmic dopamine concentration (**Figure 2-9**).[205] The binding of DOPAL to the protein occurs through two reactions: where DOPAL acts as a Schiff-base with lysine (**Figure 2-8 A**), or the other where DOPAL undergoes autoxidation in the presence of oxygen, forms covalent bonds with cysteine (**Figure 2-8 B**).[209]

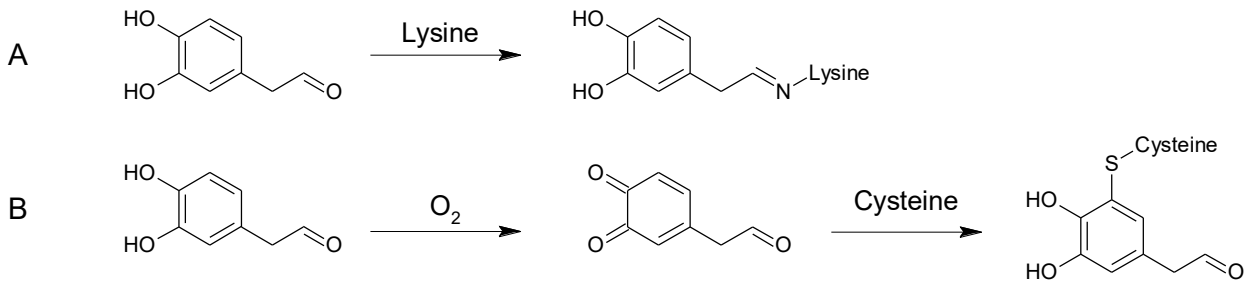

Figure 2-8: Schematic indicating the interactions of protein residues with 3,4-dihydroxyphenylacetaldehyde. A) 3,4-dihydroxyphenylacetaldehyde acts as a Schiff-base with lysine, B) 3,4-dihydroxyphenylacetaldehyde undergoes autoxidation in the presence of oxygen, forms covalent bonds with cysteine O_2: oxygen. Figure is self-generated from reference.[209]

An increased cytoplasmic dopamine concentration leads to a cyclic self-amplifying loop, where more DOPAL is formed via MAO, and more α-syn is modified with DOPAL.[210] The increase in

DOPAL can be seen as a downstream effect of aldehyde dehydrogenase (ALDH) under expression.[211] A reduction in messenger ribonucleic acid (mRNA) levels of ALDH transcription factors can result from inherited mutations in mtDNA or nuclear DNA, as well as age-related under expression.[212] A change in the enzyme expression could then be associated with an increase in DOPAL concentration, and several other possible influences on proteins, including those used in Fe^{2+} and Ca^{2+} storage and movement.[213]

Part of the formation of Fe^{2+}-sequestering neuromelanin, a dark polymer pigment found in certain catecholaminergic neurons, is oxidative polymerisation of dopamine.[214] Physiologically, neuromelanin is believed to bind, store, protect and release free dopamine and sequester metals (Zn, copper [Cu], Fe^{2+} and Mn) where it resembles a cytoprotective scaffold.[215] It exerts this cytoprotection by sequestering both reactive dopa-quinones and semiquinones,[216] and containing the by-products of dopamine metabolism in a lipid and protein shell made up of cholesterol, α-tocopherol and phospholipids.[217] Precise biosynthesis pathways have not yet been elucidated, however, the oligomerisation of phenolic structures within proteins (cysteine, histidine and lysine) mediated by both Fe^{3+} and Cu seems to be the most likely route.[218] However, with dopaminergic neurons undergoing cell death, neuromelanin is released into interstitial spaces, where Fe^{2+} is then released and can produce more HO●, which in turn increases the production of 6-OHDA (**Figure 2-9**).[215,219]

As a downstream metabolite of physiological dopamine breakdown, 6-OHDA is present in the brain, and does not cross the blood-brain barrier (BBB), thus its breakdown is localised within neurons.[220] The 6-OHDA has been seen to have several cytotoxic mechanisms, namely radical production during its breakdown, release of transition metals to form ROS via Fenton's reactions, protein interactions, thiol group modification and inhibition of mitochondrial function.[221] The release of transition metals (i.e., Fe and Cu), especially Fe^{2+} ions, is a main contributor to the pathology seen in ferroptosis and is a new way of studying non-apoptotic cell death within a neurodegenerative modality.[222] There is currently a chicken-and-egg debate on the pathophysiology of idiopathic PD, where the cycle of cell death makes sense when all attributes are combined, although the triggers are under researched. Some authors believe the trigger is age related,[61] others due to environmental or dietary factors,[223] or simply a genetic susceptibility.[224] Among the various theories, the most prominent suggest that neuromelanin loss [215] and age-related stem cell exhaustion [61] is believed to play a central role. This author is of the opinion that each patient has a unique set of pathologies that play a role, as disease modification

will be a more personalised manner of therapy, however, not a lot of research is poised on the oxidative state and the exploitation of the innate antioxidative enzymes.

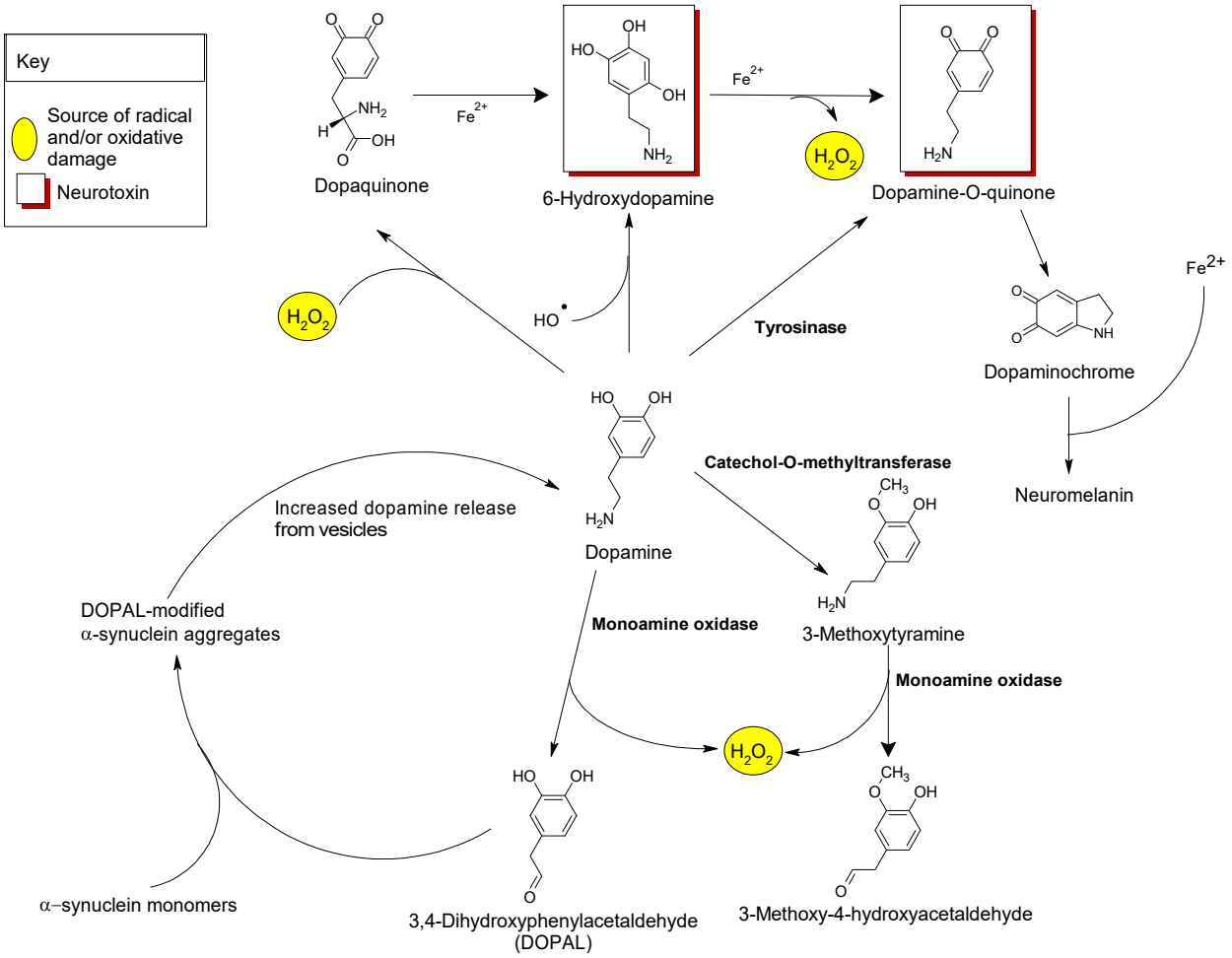

Figure 2-9: Schematic representation of the enzymes and reactions related to the synthesis of dopamine and metabolism, and the products involved in neuronal degradation.[75, 165, 215] Self-generated image from literature.

2.3.4 Cell death

Apoptosis is a coordinated and energy-dependant process than involves a cascade of events that link stimuli to the final demise of the cell. Three pathways are described: intrinsic (mitochondrial), extrinsic (death receptor), and perforin **(Figure 2-10).**[225] The intrinsic pathway, associated with discussed mitochondrial changes, is the most prevalent cell death in PD.[226] The intrinsic pathway is also categorised by the generation of ROS, cytochrome *c* release and ATP depletion.[226]

Apoptotic pathways converge into the energy-dependant activation of caspase-3, and results in DNA cleavage, degradation of cytoskeletal and nuclear proteins, protein cross-linkage, apoptotic body formation, increased phagocytic cell receptor expression and finally the uptake by phagocytic cells.[227] Caspases are widely expressed in an inactive proenzyme form, and once activated, amplifies the apoptotic signalling towards rapid cell death.[228, 229] Protein cross-linking is a characteristic of apoptosis and is activated by the expression of tissue transglutaminase.[230]

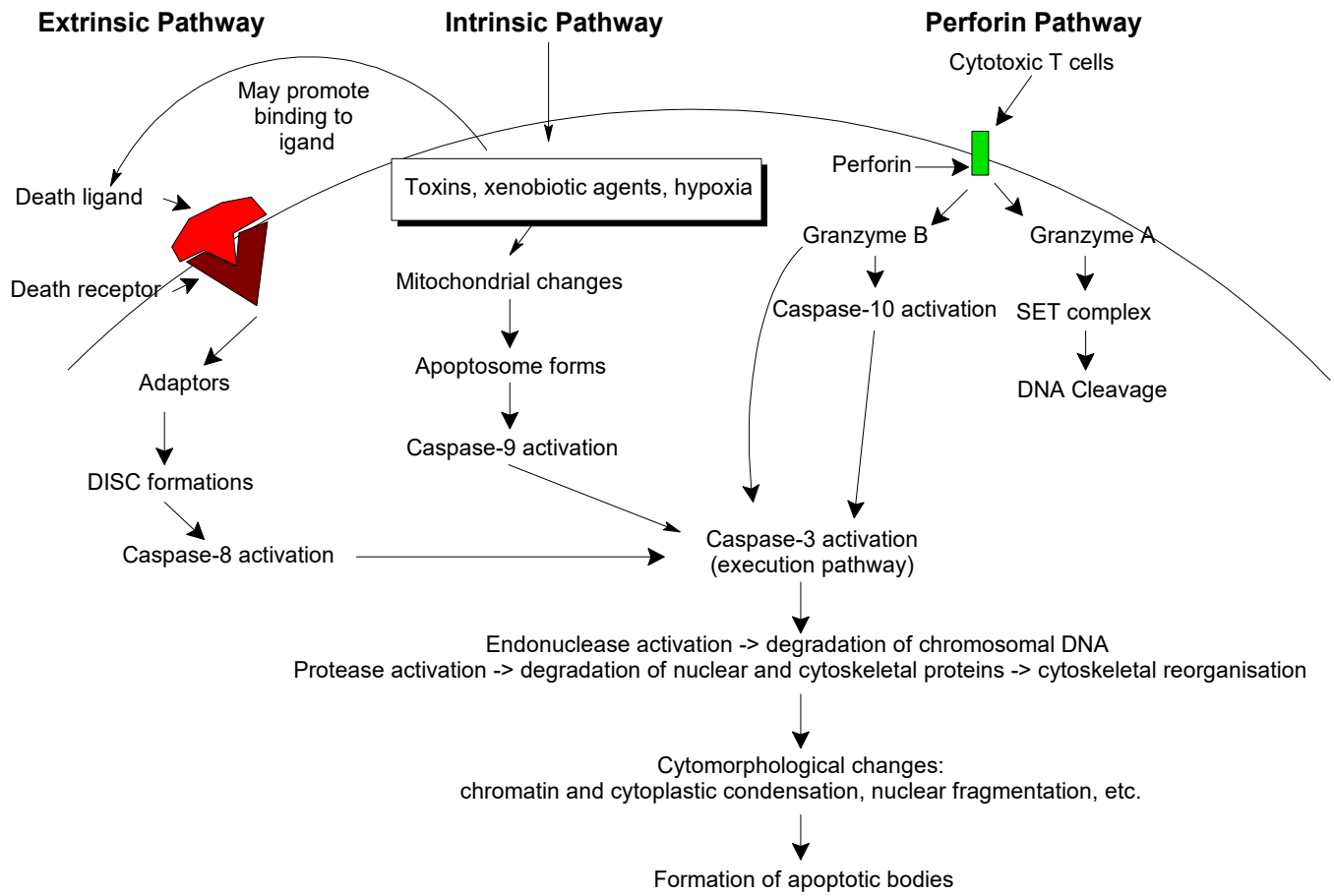

Figure 2-10: Representation of mechanisms (the intrinsic, extrinsic or perforin pathway) whereby apoptotic cell death takes place.[231, 232] DNA: deoxynucleic acid; SET complex: Endoplasmic reticulum-associated oxidative stress response complex; DISC: death-inducing signalling complex.

The degradation of DNA is caused by Ca^{2+} and magnesium (Mg^{2+})-dependant endonucleases, resulting in DNA cleavage from a double helix strand to 180 to 200 base pairs.[233] In PD pathology, Ca^{2+} efflux can be impaired via α-syn mutations.[234] These mutations lead to an increase in Ca^{2+} spikes within the mitochondria which produces both a hypercalcaemic (collecting of Ca^{2+} within vesicles) and a hypocalcaemic state (exocytosis of Ca^{2+}) within the cells.[235] These alternating states of both hyper- and hypocalcaemia interferes with the regulation of dopamine release and the firing of neurons within the midbrain.[236] The loss in Ca^{2+} homeostasis causes to either over- or under express several Ca^{2+}-dependant proteins (calpains, directly linked to caspase activation[237]), which in turn can trigger cell death.[238] Although multiple theories underlie cell death,

the loss of Ca^{2+} homeostasis and both cellular and molecular damage is considered an origin of early cell death.[239] An increase in free cytoplasmic Ca^{2+} may induce apoptotic cell death,[240] and this has been seen in several neurodegenerative diseases.[241] With Ca^{2+} affecting the extended release of dopamine into the synaptic space, the hypercalcaemic state increases ROS production, thus forming a self-replicating loop.[242]

Analysis of the brain tissues of people who died with PD during post-mortem has revealed several characteristics of apoptosis, such as DNA fragmentation, cell shrinkage (apoptotic bodies), and chromatin condensation.[243-245] Studies conducted using cell models have shown that cell death can be inhibited by the anti-apoptotic protein BCL-2[246] as well as caspase inhibitors.[247] However, given the known mtDNA mutations and the elevated ROS production in the brain of a patient with PD, many researchers suggest that the intrinsic pathway is the primary mechanism of regulated cell death.[226] However, given the known mtDNA mutations and the elevated ROS production in the PD brain, many researchers suggest that the intrinsic pathway is the primary mechanism of regulated cell death[226] The rise in Ca^{2+} disrupts $\Delta\Psi m$ and triggers a cascade of ROS-related effects, including the release of iron.

2.4 Ferroptosis and ferroptotic cell death

Ferroptosis, a non-apoptotic means of cell death, is a mode of regulated cell death.[222] It is characterised by the depletion of reduced GSH and unchecked lipid peroxidation, as well as an age-related or pathological accumulation of electron donating Fe^{2+}.[248] Morphological features of ferroptosis that are seen in mitochondrial shrinkage and membrane rupture.[222] This differs from apoptosis, where a total reduction in cellular and nuclear volume is seen with nuclear rupture.[249] The depletion of reduced GSH inhibits the functionality of GPx4, a key role player in preventing excessive lipid peroxidation.[250, 251] It serves as the primary regulator of the ferroptotic process as it halts the chain reaction of lipid peroxidation by scrubbing lipid peroxides.[252] Under normal physiological conditions GPx4 is the only selenoprotein in the GPx family capable of this reaction.[253] The reduced co-factor GSH is thiol-containing compound that can be used to repeatedly reduce the oxidised GPx4, and consists of three amino acids: cysteine, glutamic acid and glycine.[254] Cysteine depletion is particularly prominent in ferroptosis, where the free pool of cysteine is too low to allow for reduced GSH synthesis, leading to ferroptosis.[255]

The synthesis of GSH begins with the formation of the dipeptide γ-glutamylcysteine through the activation of glutamate cysteine ligase, utilizing ATP hydrolysis.[256] Cysteine is transported into the

cell via the antiporter system Xc^-, where one glutamate is exchanged for one cysteine residue.[257] Following this, the enzyme glutathione synthase (GSR) adds glycine to the dipeptide, also through ATP hydrolysis, to produce GSH.[258] The formation of GSH is reduced in systems with low ATP in the case with cells undergoing oxidative stress.[259, 260] In studies conducted using GPx4-knockout lines were used, it was proposed that cell death is associated with lipid peroxides in the absence or inhibition of GPx4.[261-263]

2.4.1 Lipid peroxide generation

Ferroptosis has been implicated in neurodegeneration[264] as a result of abhorrent lipid peroxidation seen in several neurodegenerative illnesses.[265-268] The CNS contains the highest content of polyunsaturated fatty acids (PUFA),[269] and is thus at the highest risk for ferroptotic cell death. The PUFAs that are located within cell membranes are the most susceptible to peroxidation due to the presence of multiple double bonds that can cause protons to be extracted from adjacent acyl chains.[270]

Intracellular Fe^{2+} catalyses the Fenton reaction to produce OH● ions, which in turn reacts with PUFA to fatty acid radicals (L●).[250, 271, 272] Subsequently, oxygen is then added to produce lipid peroxyl radicals (LOO●), which causes a chain reaction to produce more L●.[250, 271, 272] There is also a non-enzymatic reaction, which uses LOO● and PUFA to produce LOOH, that will convert to alkoxyl radicals (LO●) via a Fe^{2+} ion.[250, 271, 272] These LO● radicals form 4-hydroxynonenal (4-HNE), which is a known cytotoxin in excess,[273] and exerts physiologically beneficial effects at lower intracellular concentrations (<2 µM)[274] and cytotoxic effects at higher concentrations (>100 µM) **(Figure 2-11)**.[275]

Chemically, 4-HNE is known as a Michael acceptor, which forms adducts with certain biomolecules such as the amino acids cysteine, histidine and lysine.[276] These adducts lower the amount of unchanged amino acids that can participate in cell homeostasis and promotes cell death.[277] When 4-HNE encounters proteins, it reacts with the amino ($-NH_2$) groups to form a covalent bond.[278] Several proteins are affected by the addition of 4-HNE; ion channels, as well as glucose and glutamine transporters.[278] These proteins' functions are then impacted, and when in excess, total cellular function is compromised which could disrupt cell homeostasis.[278]

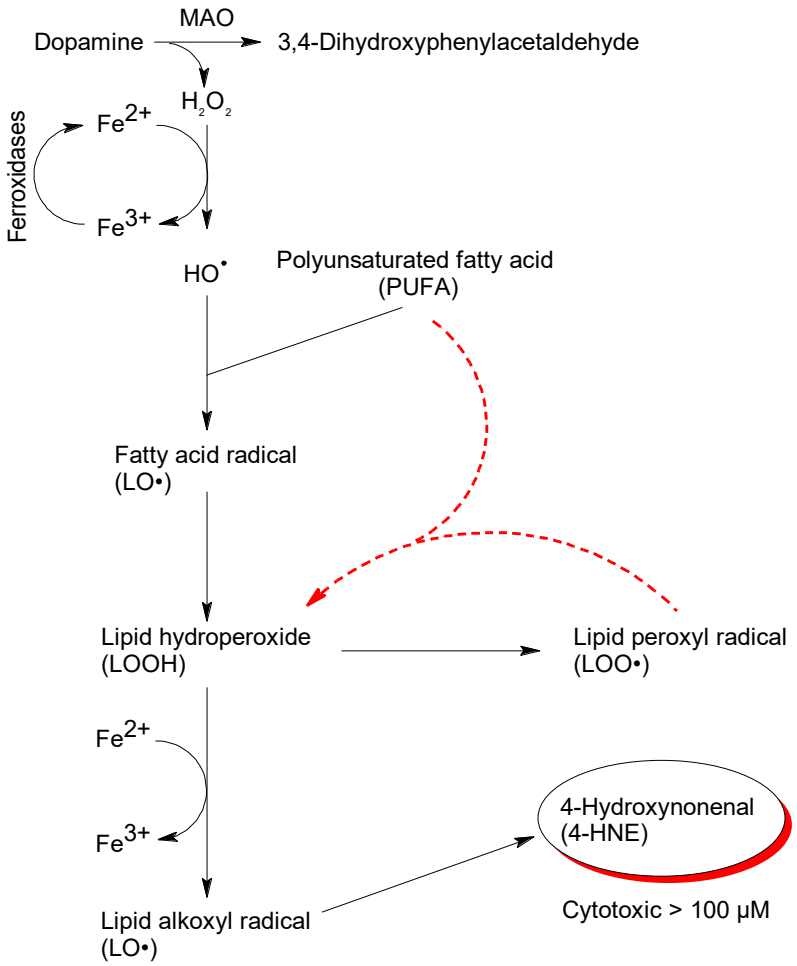

Figure 2-11: **Schematic presentation of the generation of 4-hydroxynonenal via Fenton reactions in the presence of iron ions (Fe). Red line indicates the self-proliferation of lipid hyperoxides.[279] Figure is self-generated. 4-HNE: 40hydroxynonenal; OH●: hydroxyl radical; H_2O_2: hydrogen peroxide; MAO: monoamine oxidase.**

2.4.1.1 Regulation of lipid peroxidases via glutathione peroxidase-4

In the presence of adequate GSH, oxidation of the reduced GPx4 active site by a hydroperoxide-type compound occurs.[280] During the initial step, selenocysteine or cysteine is converted to selenic or cysteine acids in the GPx4 catalytic site.[281] The harmful hydroperoxide is simultaneously converted into the corresponding safe alcohol (**Figure 2-12**).[281] The reduction phase involves two subsequent steps, the first producing a glutathionylated intermediate GPx4 enzyme where the oxidised GPx4 reacts with one equivalent of GSH.[281] In the subsequent step, a second equivalent of GSH reacts with the glutathionylated intermediate to form the stable

oxidised GSH product, and this allows for the release of the reduced selenium or cystine for the next catalytic cycle.[282]

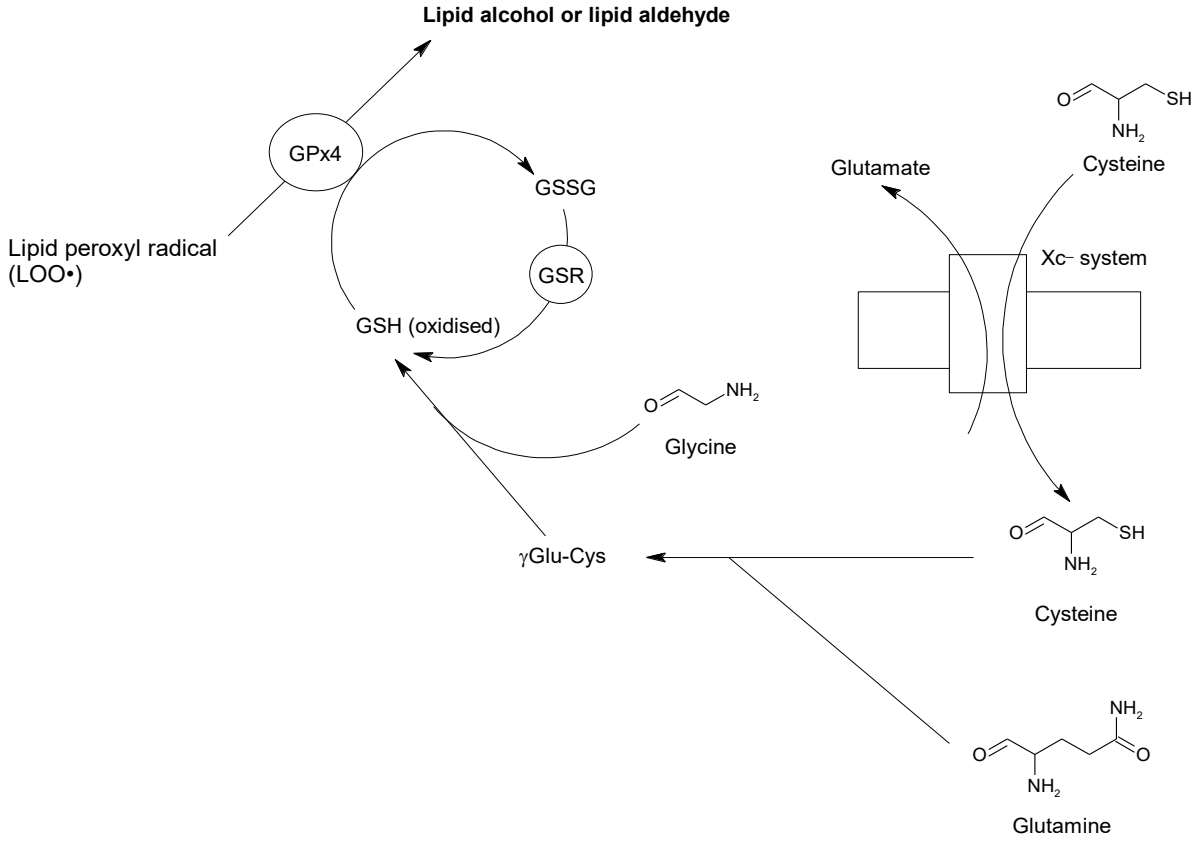

Figure 2-12: Schematic representation of the metabolism of lipid peroxyl radicals via glutathione peroxidase 4 (GPx4), and glutathione. The Xc⁻ system amino acid transporter is responsible for cysteine entry into the cell. GSH/GSSH: glutathione oxidised/reduced; GSSH: glutathione disulphate; GSR: glutathione-disulphate reductase; GPx4: glutathione peroxidase 4; LOO●: Lipid peroxyl radical. Figure is self-generated.

In recent years,[283] several small molecule inhibitors and agonists of GPx4 have been identified as potential treatment routes.[284] While targeting GPx4 pharmaceutically offers significant therapeutic benefits, the protein's unique structural characteristics make the creation of small molecule inducers and inhibitors challenging.[285] The enzyme has an allosteric binding pocket,[286] and the activation thereof may influence the enzyme's ability to metabolise LOO●.[283] Inhibition of the GPx4 enzyme allosteric pocket may lead to an accumulation of lipid peroxides, and downstream to cellular death.[261] The GPx4 relies on a nucleophilic selenocysteine residue for

proper enzymatic functioning, as it lacks a binding pocket resembling that of a drug, thus GSH selenocysteine residue can reactivate the enzyme.[281]

2.4.1.2 Iron homeostasis

Iron accumulation significantly increases with ageing, and in early-stage PD, this accumulation has been observed in the SNPc.[287, 288] Dysregulation in α-syn triggers redistribution of oligomers within the cytoplasm, which alters transferrin-mediated iron import, which in turn increases the amount of free iron in the cytosol.[289, 290] The increased free iron reacts with free dopamine and metabolic products of dopamine, thereby increasing cytoplasmic ROS.[291] Iron accumulation can also be precipitated by dysregulation of ferritin molecules, as these molecules hold and distribute free ferrous ions to and from the mitochondria.[292] Ferritin is found in both the cytosol and mitochondria, as well as in high oxygen-consuming areas such as the CNS.[293] It regulates iron concentrations by keeping iron reserves non-reactive but accessible for use in homeostasis.[294] When the iron is not contained in ferritin or neuromelanin, it forms part of the labile iron pool (LIP).[295] Within the CNS, iron plays an important role in respiration, protein formation and acts as a redox active metal to both donate and accept electrons.[296] These interactions between electrons, leads iron as a necessary co-factor for the formation of myelin, neurotransmitters and metabolism.[297]

Should 6-OHDA be present, ferritin proteins may release excess ferrous ions into the cytosol or mitochondria that can participate in Fenton's reactions to produce free radicals within the organelle.[298] Over expression of mitochondrial ferritin has been shown to reduce the effects of ROS by lowering the LIP.[299] With the known pathophysiology, the current treatments can be reviewed to establish known targets.

2.5 Treatments for Parkinson's disease

Parkinson's disease has no known cure, and treatment remains symptomatic for both the motor and non-motor symptoms.[25] Treatment of PD is dynamic due to the progressive neurodegeneration observed and the need to manage the increased frequency of side-effects.[300] As such, the patient is often subjected to dosage increases, adjunct therapies, and adjustments to manage motor symptoms.[301] Modern research is currently focused on disease-modification of the illness to lessen the side-effects together with conventional therapy.[40]

As mentioned earlier, PD is a neurodegenerative disease characterised by the lack or loss of dopamine-producing neurons in the mid-brain.[22, 302] The increase in endogenous dopamine can

be achieved by either mimicking the action of dopamine at the synaptic cleft[303] or by increasing the endogenous dopamine levels in the brain. [304]

Current treatment for tremors and bradykinesia in South Africa is L-dopa/carbidopa (Sinemet®, Carbilev®, Teva Carbi-Levo®), which supplements dopamine stores in the brain due to provision of the levodopa pro-drug.[26]

L-dopa is part of the large neutral amino acid (LNAA) group consisting of tyrosine, phenylalanine, tryptophan, leucine, isoleucine and valine.[305] The enzyme AADC metabolises the bulk of the L-dopa before reaching the systemic circulation. This is the reason why the decarboxylase inhibitors carbidopa or benserazide is co-formulated with L-dopa. This causes an increase in the concentration of unchanged L-dopa that reaches the BBB by inhibiting its peripheral metabolism.[306] A diet containing low protein meals is advised to prevent competition at the LNAA transporter-1 (LAT-1).[307] The half-life of L-dopa ranges from 0.7 to 1.4 h in chronically treated patients.[308] There are both age and biological sex differences[309] in the maintenance of the half-life of appropriate concentrations for absorption into the brain for conversion to dopamine.

An increase in L-dopa dosing leads to side-effects which includes nausea, dizziness and postural hypotension.[310] In addition to L-dopa-induced dyskinesia, “wearing-off” is a major limitation of L-dopa therapy.[27] “Wearing-off” is a common phenomenon, which is brought on by a reduction in efficacy of L-dopa therapy due to reduced bioavailability of L-dopa to the brain.[28-30] The increased release of dopamine into the brain, also allows for the production of 6-OHDA, which is why additional neuroprotective agents such as iron chelators are suggested in the treatment of advanced PD patients, to help combat ferroptotic processes.[31, 32] To combat the side-effects, a new class of treatment could be added to ensure more L-dopa reaches the BBB, by inhibiting the peripheral metabolism of L-dopa outside of known AADC inhibitors. This drug class is the catechol-*O*-methyltransferase (COMT) inhibitors.[311]

Catechol-*O*-methyltransferase is the enzyme that acts as the catalyst for the transfer of an activated methyl group to the catechol neurotransmitter substrate, rendering it inactive.[312] Clinically, COMT inhibitors are usually prescribed in conjunction with L-dopa therapy to limit its peripheral metabolism to 3-methyldopa (3-OMD) outside the CNS.[313] This therefore results in an increase in amount of L-dopa that reaches the BBB by inhibiting peripheral metabolism **(Figure 2-13)**.[314]

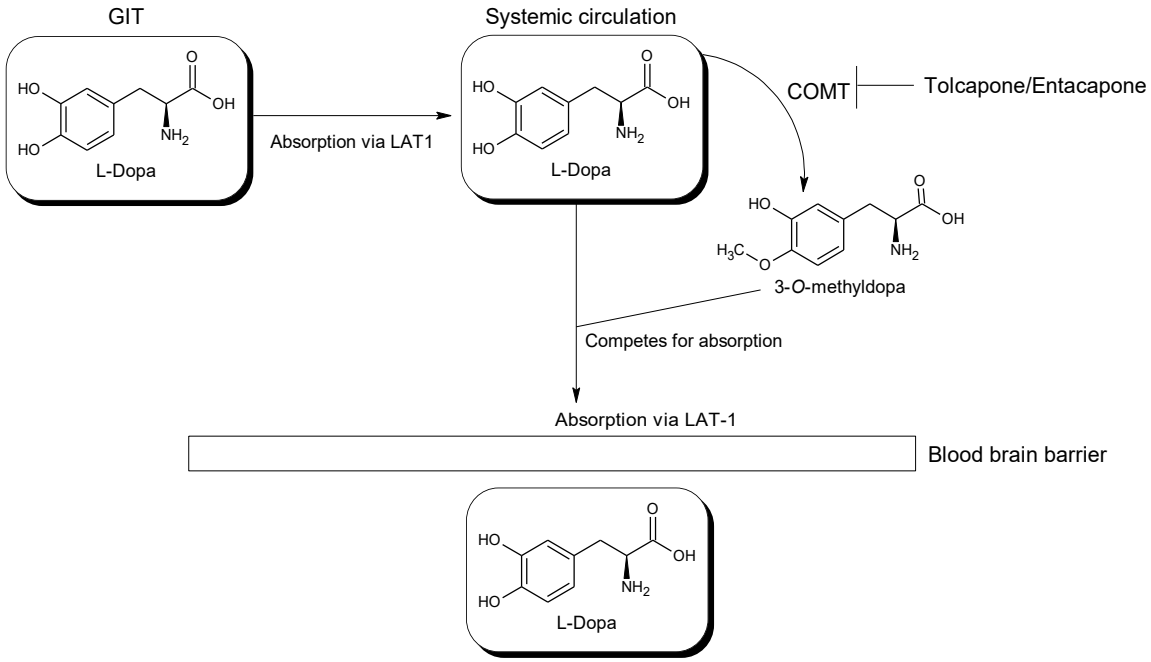

Figure 2-13: **Schematic representation of the catechol-O-methyltransferase dependant metabolism of L-dopa forms 3-*O*-methyldopa, that competes for absorption at the blood brain barrier with L-dopa. Lowering the concentration L-dopa to reach the brain.[315] GIT: gastrointestinal tract, LAT-1: large neutral amino acid transporter-1. Figure is self-generated.**

By reducing the amount of 3-OMD produced in the central circulation, the penetration of L-dopa into the CNS is enhanced.[316] Clinically used COMT inhibitors (entacapone and tolcapone) contain acidic nitrocatechol groups **(Figure 2-14)**.[317] Their mechanism of action has been described as tight, yet reversible, dose-dependent inhibition, with tolcapone being more potent than entacapone.[318]

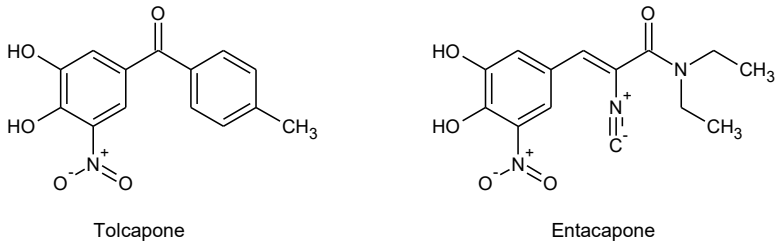

Figure 2-14: **The structures of catechol-*O*-methyltransferase inhibitors used commercially.[319] Figure is self-generated.**

Increasing the amount of L-dopa that penetrates the brain, allows for the conversion to dopamine, thereby replenishing the depleted dopamine levels and alleviating symptoms.[320] However, once the conversion to dopamine has taken place, its metabolism further depletes the brain's endogenous dopamine stores.[321] Consequently, inhibiting dopamine metabolism through MAO is also a key treatment strategy.[321]

Monoamine oxidase are found in two isoforms that primarily oxidise a variety of substrates including small-molecule amines, polyamines and modified amino acids within certain proteins.[322] The enzyme MAO is responsible for the oxidative deamination of many catecholamine (CA) compounds.[323, 324] MAO-A and MAO-B are located on the outer mitochondrial membrane, where they catalyse the oxidation of primary, secondary, and tertiary amines, as well as neurotransmitters, into their corresponding imines.[201]

During the process of oxidative deamination of CAs, radical species (H_2O_2) are produced, as exemplified by degradation of dopamine in the presence of MAO **(Figure 2-15)**. Two different clinical effects are obtained, depending on the enzyme inhibited. Inhibition of MAO-A has anti-depressive and anti-anxiolytic effects, whereas inhibition of MAO-B yields anti-parkinsonian effects.[199] The MAO-A isoform is more prevalent in the gut lining whereas MAO-B is concentrated in the basal ganglia.[323, 325] The preferred substrates of the MAO-A isoform are noradrenaline and serotonin,[323] with both isoforms metabolising dopamine and tyramine in equally.[326] This is the reason why MAO-B is used as the target for the treatment of advanced PD **(Figure 2-16)**.[327]

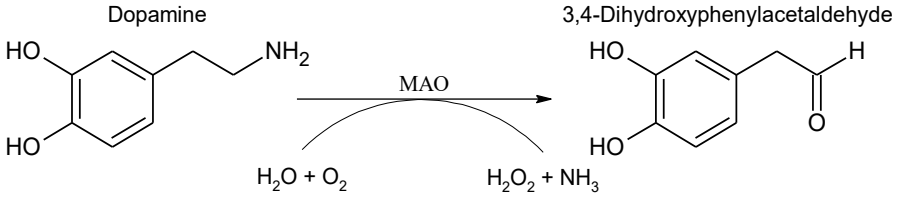

Figure 2-15: Chemical reaction indicating the degradation of dopamine by monoamine oxidase to produce 3,4-dihydroxyphenylacetaldehyde.[328]

Free radical species are known to cause oxidative stress,[329] therefore inhibition of MAO will result in lower radical production and hence less oxidative stress.[330] The inhibition of MAO-B induces both antiapoptotic [331, 332] and antioxidative effects.[333, 334] Whilst not the primary indication of MAO-B inhibitors, the class does offer a secondary benefit by design.

These MAO-B inhibitors may help mitigate neurodegeneration by reducing the production of ammonia, aldehyde, and H_2O_2, which are byproducts of amine oxidation.[335] Clinically used irreversible MAO-B inhibitors include (R)-deprenyl and rasagiline.[336] (R)-deprenyl, when combined with L-dopa therapy, can cause side effects such as dry mouth, orthostatic hypotension, and certain dyskinesias.[337] As a monotherapy, it may lead to side effects like anorexia and nausea, and in rare cases, cardiac arrhythmias.[338] Lazabemide and safinamide are multi-action drugs that combine MAO-B inhibition with mechanisms such as Ca^{2+} channel blocking and dopamine re-uptake inhibition.[339, 340]

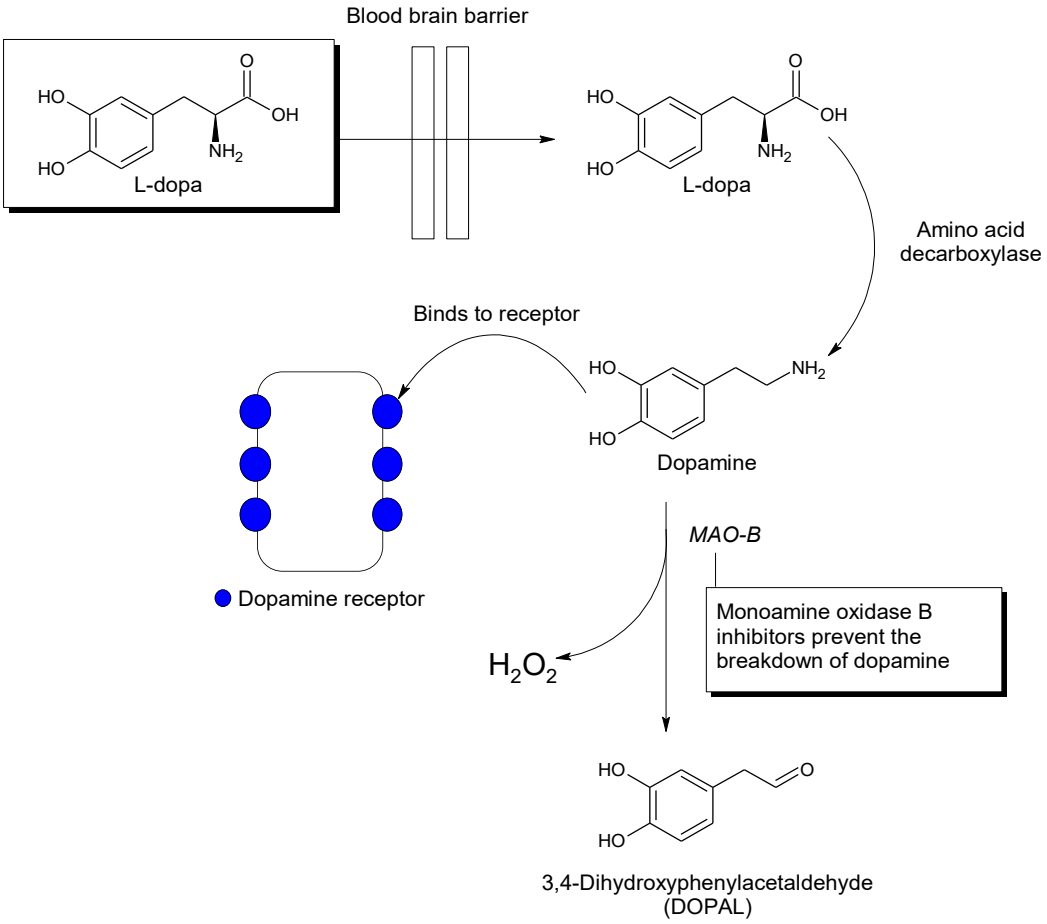

Figure 2-16: Scheme indicating the rationale for using monoamine oxidase-B inhibitors in conjunction with levodopa to improve conversion to dopamine. Figure is self-generated. [336]

Dopamine agonists have become a popular first line treatment, albeit there still is uncertainty concerning its long-term effects and cost effectiveness of this treatment.[341] The use of dopamine

agonists stem from the direct stimulation of the dopamine receptor to mimic the endogenous effects of dopamine.[342] When there is a reduced dopamine secretion in the synaptic cleft, dopamine agonists can have a very beneficial effect, if used properly.[343, 344]

Bromocriptine, cabergoline and pergolide, are mainstream ergot-derived dopamine agonists.[345] The use of ergot-derivatives is limited due to side-effects like vasospasm, fibrotic degeneration of cardiac valves and cardiac arrhythmias.[343, 346, 347] The concurrent use of these ergot alkaloids with L-dopa has been associated with greater dyskinesia and longer recovery periods after an "wearing-off" episode.[348] This is primarily due to the reduced dosage requirement for L-dopa to achieve the therapeutic effect.[349] In the case of ergot-derivatives, an average reduction of 20 to 30% in the L-dopa dosage is necessary to overcome L-dopa-induced dyskinesia and overdosing.[349] These ergot alkaloids can have a beneficial impact on brain chemistry as well, seeing as they are not oxidised via conventional dopaminergic pathways and thus mitigate additional ROS formation,[350] thereby preventing additional neuronal damage.[351, 352]

Current treatments for PD are symptomatic and none of the drugs address the need to modify the disease for a focus on neuronal death as to prevent symptoms.[353] New targets and drug therapies are needed, and *in silico* modelling and tools can assist in identifying promising candidates.

2.5.1 *In silico* approaches to drug design

Computer-aided drug discovery (CADD) accelerates the drug discovery and development process by utilising computational algorithms and predictive models to identify and optimise potential therapeutic molecules.[354] It facilitates tasks such as computational target identification, virtual screening of extensive chemical libraries for promising candidates, further refinement of these compounds, and *in silico* assessments of their potential toxicity.[355] Once these computational processes are complete, selected compounds undergo in vitro and in vivo validation.[356]

During the early phases of drug development, conventional predictive methods like quantitative structure-activity relationship (QSAR) models are used to prioritise drug candidates based on their pharmacological properties and possible side effects.[357] QSAR models also help elucidate the various substituent and functional groups on the molecular scaffold, shedding light on interactions within the target's active site.[358]

In response to the growing availability of open-source software, a number of machine learning-based prediction methods have emerged, aimed at the prediction of the BBB permeability of compounds,[359] drug-target interactions,[360] and absorption, distribution, metabolism, excretion and toxicity (ADME-Tox)[361] characteristics of therapeutic candidates.[362] The identification of small molecule inhibitors or inducers are fundamental in disease treatment and requires minimal toxicity and an efficient pharmacokinetic (PK) profile.[363] These parameters are referred to as “drug-like properties”.[364]

Drug-like properties play a pivotal role in drug research, where they serve as key criteria for identifying novel clinical candidates.[364] These parameters help to streamline drug development efforts into chemical space, where success rates for improved PK and safety are better.[365] Following the discovery of new drugs, the known PK values exert significant influence on various aspects, including the development of predictive models for human PK and its relationship to pharmacodynamics, understanding structure-property and structure-activity relationships, directing structure modifications to optimise physicochemical properties, identifying underlying reasons for undesirable PK and toxicity, and optimising and interpreting bioassays.[364]

Drug design has different starting points, either with the known endogenous ligand or with certain plant secondary metabolites.[366] Plants have been integral to medicine discovery for centuries, and investigating ethnopharmacologically significant plants allows for the evaluation of their potential as sources for future therapies and drug development.[367] With many herbal medicines being used, and the multi-targeted approaches and effects, a disease like PD with multiple aetiologies can be investigated to produce active therapies *in vitro*.[368] With several targets that can be used to promote cell health and stave off cell death, the investigation into some CNS relevant plants can yield results into the pathophysiological attributed of the disease.

CHAPTER 3: PLANT SELECTION, EXTRACTION, FRACTIONATION AND SCREENING

3.1 Introduction to phytomedicine

Ethnomedicine has been practised since before the start of written records, with methods and knowledge passed down generations through oral tradition.[50, 369] Several traditional medicine disciplines exist, such as Chinese traditional medicine, Indian traditional medicine (Ayurveda), African traditional medicine (Muti) and Arabian/Islamic medicine (Unani).[367] Traditional medicines are used to promote "healing from within" from a holistic perspective (mentally, spiritually and emotionally combined with the associated physical ailments and symptoms) and involves practices such as acupuncture, yoga, tai chi and breathing exercises.[370]

Humans are dependent on plant material for housing, clothing, and food, and for their organoleptic properties including smell, tastes and colours; although this dependency has reduced in the modern era.[371] Refining of plant material for the use in medicine, hunting, hallucinogens, rituals, stimulants and inebriants has shaped both history and cultures throughout the centuries.[372] Medicinal plants have long been a source of phytochemicals and a starting point of drug discovery for disease treatment.[373] Almost 25% of modern medicines have originated in some way from plants, for example, as a direct isolation or derivatisation of a phytochemical, or even the extract itself.[374-376] The use of herbal medicines has since been a global market leader, with total estimated sales in the United States of America exceeding 11 million USD in 2020.[377] The use of medicinal plants and the generation of medically important drugs and drug scaffolds from them has branched into a science known as "phytochemistry".[378] The use of plant-based remedies to heal human illnesses has a long-standing history. Several plant species, including opium (*Papaver somniferum* L.), myrrh (*Commiphora* species), and liquorice (*Glycyrrhiza glabra* L.), were mentioned on clay tablets from Mesopotamia in 2600 BC.[379, 380] These examples are still used, either alone or as one of the ingredients in other herbal formulations, to treat a variety of diseases.[381]

Quinine, extracted from the quina-quina tree (*Cinchona pubescens* L., Family: Rubiaceae) is regarded as the first extracted pure phytochemical to treat malaria and its associated symptoms.[382] The legend follows a hunter lost in the forest with a high fever due to insect bites, and when he drank water, he thought was contaminated by the trees in the vicinity (due to the bitter taste), the fever subsided, and his symptoms got better with subsequent use of the water.[383]

Other popular phytochemicals used in modern times are caffeine, morphine, digoxin, and salicylic acid.[384] With the increasing use of traditional and complementary medicines, regulations have been implemented to ensure the safety of these medicines for the use by the public, with the advent of several pharmacopoeias and international guidelines.[385] This is to ensure that the sole and combinational use of these remedies are known and are safe and effective.[386]

Plants are a priceless source for developing new drugs using methods such as derivatisation. Plant and plant-adjacent (i.e. certain fungus strains that are endemic to specific plants, like taxol production from the *Taxomyces andreanae* found on the yew tree[387]) structures contain a vast range of physiologically relevant chemical space. This chemical space that cannot be effectively investigated using synthetic compounds, due to complexity in the structures found endemically in plants. Commercially available screening libraries is not sufficient, due to the fact that secondary metabolites have evolved over thousands of years to acquire particular ligand-protein binding patterns.[388] To understand the effect plant extracts have on *in vitro* systems, the identification of molecules is needed to elucidate pathways that are affected by the inclusion of the compounds into biological systems.[389] Identification can lead to an understanding of underlying synergistic or antagonistic interactions between the compounds, as multiple compounds may be needed to elucidate an effect.[390]

Plants are a crucial source of potential lead compounds for the development of new and more effective medications. Structural modification of plant-derived compounds, along with the discovery of NCEs, holds promise for therapeutic applications.[391] Secondary metabolites from plants are believed to exhibit greater biological compatibility and drug-like properties compared to compounds derived solely from synthetic sources.[392] The environment in which the plant grows also affects the concentration and complexity of these metabolites.[392] The complex nature of these secondary metabolites is due to evolution as plants have developed these compounds to protect themselves from pests or viruses.[393] These compounds are synthesized in response to various biotic stresses and also perform essential physiological functions.[392, 394]

3.2 Plants investigated in this study

3.2.1 Plants used for central nervous system pathologies in South Africa

Several plants have been investigated for their use in several CNS pathologies.[395] For use in Alzheimer's disease, the main treatment option is currently the use of acetylcholinesterase inhibitors such as galantamine, which was extracted and purified from the genus *Galanthus*, and

reversibly inhibits acetylcholinesterase.[396] Although there are a lot of plants that have effects against PD-related pathologies, not many endemic African plants have been studied for this purpose.[397] Other CNS-related pathologies have been investigated more thoroughly, such as Alzheimer's disease, anxiety and depression.[398-400] Several different pathologies originating in or involving the CNS are treated with traditional medicine, including epilepsy, convulsions, depression, age-related dementia and debilitative mental disorders (**Table 3-1**).[399-401] Whilst some of these plants are known to be toxic, the drug discovery aspect should not be hindered in an *in vitro* setting.

Plant selection for the study was based on documented CNS effects from ethnomedicinal sources from SSA countries (i.e. use for headaches, sedation, hallucinatory properties, epilepsy, or insomnia), or from *in vitro* or *in vivo* studies that focused on exploration of the ethnomedical uses noted (i.e. GABA-binding studies, MAO-B inhibition, anti-depressive effects, and epilepsy). The uses combined with the availability of samples led to the selection of plants (**Table 3-1**). The repository (basement storage of plants in the dark in polyurethane bags) is catalogued per plant and then split into the parts of the plant available (e.g., stems, leaves, flowers). Where it was possible, the plant part that was reported to have activity was used, however, in the case of insufficient sample or misplacement of the sample, the leaves of the plants were used, as recommended by the WHO's guideline on good agricultural and collection practises.[402] Even though there is wisdom on the part of the plant used traditionally, the constraints of the repository were considered.

Table 3-1: Plants selected for extraction and investigation for the current study.

Family	Plant name, Authority, voucher number	Vernacular name*		Plant part available in repository	Traditional preparation	Traditional uses
Amaryllidaceae	*Boophone disticha* (L.f) Herb.[403] NB221a	English	"Century plant", "poison bulb"	Bulb	Weak decoctions of bulb scales	Sedation of violent and psychotic patients[404]
		Afrikaans	"Gifbol", "kopseerblom" and "Boesmangif"		Bulb infusions	Induction of hallucinations[403] and undisclosed mental illnesses[405]
		isiXhosa, isiZulu	"Incontho"		Bulb extracts	Stress-related[406] anxiety, depression and memory loss[407]
		South Sotho	"Kxutsana-yanaha"			
Anacardiaceae	*Lannea discolor* (Sond.) Engl [408] P25668	English	"Tree grape" or "live-long"	Leaves	Root infusions and powdered inner bark used as a wash[409]	Wash with infusion for convulsions[410]
		Afrikaans	"Dikbas"			
		Sepedi	"Mokgôkgôthwane"			
		Venda	"Muvhumbu"			
	Mangifera indica L.[411] P23552	English	"Mango tree"	Leaves	Leaves, either as pulp or burned in fire	Anti-inflammatory, smoke from leaves inhaled for throat illnesses, stomach aches. Anticholinergic effects[412]
Apocyneceae	*Acokanthera oppositifolia* (Lam.) Codd.[399] NC211c	English	"Bushman's poison"	Roots	Dried leaves ground into a snuff	Headaches
		isiZulu	"inHlugunyembe"		Infusions	Convulsions and septicaemia
		Afrikaans	"Boesmansgif"		Powdered roots either as a tea or snuff	Orally active painkiller

Family	Plant name, Authority, voucher number	Vernacular name*		Plant part available in repository	Traditional preparation	Traditional uses
Apocyneceae	*Gomphocarpus physocarpus* E.Mey[413] P22303	English	"Balloon milkweed" or "bindweed"	Leaves	Flowers steeped in water[414]	Body pains, heart palpitations
		Afrikaans	"Balmelkbossie" or "wilde kapok"		Leaves dried to be used as snuff	Powered leaves are used as sedative[404]
	Xysmalobium undulatum (L.) Aiton f. var. *undulatum*[398] NB211b	English	"Milk bush", "milkwort" or "wild cotton"	Roots	Roots dried and crushed	Headaches, depression, and hysteria[398, 415]
		Afrikaans	"Bitterhoutwortel" or "melkbos"			
		isiXhosa	"iShongwane"			
		isiZulu	"iShinga"			
		South Sotho	"Leshokoa"			
Asphodelaceae	*Bulbine latifolia* (L.f) Roem. Et Schult.[416] P13826	English	Broad-leaved bulbine"	Whole plants	Root infusions	Convulsions, vomiting and rheumatism[417]
		Afrikaans	"Rooiwortel", "Geelkopieva"			
		isiKhosa	"Incelwane"			
		isiZulu	"Ibhucu"			
Asteraceae	*Arctotis arctotoides* (L.f.) O. Hoffman.[418] P19442	isiXhosa	"Ubushwa"	Leaves	Root and leaves ground and filtered	Juice applied directly to skin to treat ringworm and acne[419] Juice is used as a treatment for epilepsy[418]
		Afrikaans	"Botterblom"			
		South Sotho	"Putswa-pududu"			
	Vernonia myriantha Hook.f. [229] Recently reclassified as *Gymnanthemum myrianthum* (Hook.f.) P17959	English	"Blue bittertea" or "wild lilac"	Leaves	Leaf extract	Undisclosed mental illnesses[420]
		Afrikaans	"Bosbloutee"			
		isiZulu	"Umhlwazi"		Roots decoction	Used as contraceptive[421]
		Zulu	"Uhluhlunga" or "umhlungahlunga"			
Combretaceae	*Combretum molle* R.Br. ex G.Don.[422] P12551	English	"Velvet bush willow"	Leaves	Leaves and powered bark extracts	Used as a pain reliver and anti-inflammatory gargle.[423]
		Afrikaans	"Basterrooibos" and "Fluweelboswilg"			
		Tsonga	"Xikhuktsane"			
		North Sotho	"Mokgwethe"			

Family	Plant name, Authority, voucher number	Vernacular name*		Plant part available in repository	Traditional preparation	Traditional uses
Crassulaceae	*Cotyledon orbiculata* L.[409] P22270	English	"Pig's ears" or "cotyledon"	Leaves	Leaf infusion	Epilepsy[424, 425]
		Afrikaans	"Skilpadknol		Leaf juice and water	Toothache and earache[418]
		Swazi	"Lunyawo-lwendlovu"			
Dioscoreeaceae	*Dioscorea sylvatica* Eckl.[426] P12310	English	"(Forest) Elephant's foot"	Seeds	Fresh bulbs are dried and powered to produce a tonic	Skin irritation and blood pressure
		Afrikaans	"Kouterie"		Bulbs and tubers made as water infusions	Epilepsy[427], "Histeria"[428]
		isiXhosa	"Imphewula "			
Euphorbiacea	*Acalypha villicaulis* Hochst. Ex. A. Rich.[429] P21955	Zulu	"Umpendulo"	Roots	Leaf made into a tea[430]	Epilepsy
	Croton sylvaticus Hochst.[431] P17959	English	"Forest fever-berry"	Roots	Leaves are dried and ground and fumes are inhaled over hot coals[404, 432]	Insomnia[433]
		Afrikaans	"Boskoorsbessie"			
		isiXhosa	"UmFeze" or "uMagwaqane"			
		Venda	"Mula-thoho" or "muima-vanda"			
	Euphorbia milii Des Moul.[434] P20871	English	"Crown of thorns" or "Christ's thorns"	Stems	Smoke of aerial parts	Relief from a stroke[435]
		Afrikaans	"Christusdoring"			
		isiZulu	"Umbababa" or "Umbemiso"			

Family	Plant name, Authority, voucher number	Vernacular name*		Plant part available in repository	Traditional preparation	Traditional uses
Fabaceae	*Schotia brachypetala* Sond.[405] P12940	English	"Weeping boer-bean"	Leaves	Leaves and bark as infusions	For undisclosed nervous conditions[405]
		isiXhosa	"Umfofofo" or "umgxam"			
		isiZulu	"Ihluze" or "uvovovo"			
		Tsonga	"Nwavilombe			
Lamiaceae	*Leonotis leonurus* (L.) R.Br.[436] P23764	English	"Wild dagga", "Lion's ear" or "Leonotis"	Flowers	Smoked and made into a medicinal tea	Relief of epilepsy, hypnotic effect[437]
		Afrikaans	"Wildedagga" or "Duiwelstabak"			
		isiKhosa	"Imvovo" or "umunyamyna"			
		isiZulu	"Umcwili" or "imunyane"			
	Mentha longifolia polydena L.[438] P22317	English	"Wild mint"	Leaves	Leaves and aerial parts steeped as tea or made into infusion[439]	General analgesic, antipyretic, sedative[438, 440]
		Afrikaans	"Kruisement" or "balderjan"			
		South Sotho	"Koena-ya-thaba" or "bohatsu"			
		isiZulu	"Ufuthana lomhlanga"			
Oleaceae	*Jasminum abyssinicum* Hochst. ex DC. P18826	English	"Forest jasmine"	Leaves	Leaves used as wraps	Wounds[441]
Polygalaceae	*Polygala virgata* Thunb.[442] P22085	English	"Purple broom"	Roots	Leaves and stem are prepared in unnamed method[405]	Used as a pain reliver and anti-inflammatory gargle[423]
		Afrikaans	"Persboom" or "Bloukappie"			
		Sotho	"Hlokoa leleue"			
		Zulu	"Ithethe"			

Family	Plant name, Authority, voucher number	Vernacular name*		Plant part available in repository	Traditional preparation	Traditional uses
Scrophulariaceae	*Aptosimum procumbens* (Lehm.) Burch. Ex Steud[400] P22024	English	"Carpet flower	Whole plant	Used in a multi-plant mixture as an enema	Epilepsy
		Afrikaans	"Kankerbos"			
Solanaceae	*Datura stramonium* L.[443] P12600	English	"Jimsonweed", "Apple of Peru" and "Devil's trumpet"	Leaves	Seeds are smoked for narcotic and euphoric properties[444]	Headaches, euphoria. Relieving of indigestion[445] Asthma[446] Insomnia[447]
		Afrikaans	"Malpitte" and "Doringappel"			
		isiXhosa	"Umhlavuthwa" and "Umvumbangwe"			
		isiZulu	"Ijoye"			
	Withania somnifera (L.) Dunal[448] P19215	English	"Winter cherry"	Roots	Roots are steeped into a tea	Aphrodisiac,[449] hepatoprotective, anti-inflammatory[450, 451] Neuronal regenerator[452]
		Afrikaans	"Bitterappelliefie", "geneesblaasbossie" or "koorshout"			
		Sotho	"Bofepha"			
		Hindi	"Aswagandha"			
Verbenaceae	*Lippia javanica* (Burm.f.) Spreng[453] P24086	English	"Fever tea" or "Lemon bush"	Leaves	Leaves steeped as tea, or crushed and rubbed on face and gums	Convulsions,[454] fatigue and tiredness[455]
		Afrikaans	*"Koorsbossie" or "beukesbossie"*			
		Swati	*"Mutswane" or "umsutane"*			
		Tswana	*"Musukudu"*			

3.2.2 Evaluation of plant extracts being investigated for neurodegeneration

Plant extracts are complex matrixes of different classes of phytochemicals, starches, sugars and proteins.[372] Each of these components has the potential to elicit a physiological response, which may be either beneficial or harmful. Therefore, it is crucial to identify the phytochemicals and understand their biological effects.[456] Thus, isolation and fractionation practises are commonplace in phytopharmacological investigations.[457]

3.2.2.1 Antioxidant assays

Various assays are used to evaluate antioxidant capabilities, each targeting distinct mechanisms to provide insight into the nature and efficiency of the antioxidative properties of a compound or extract.

The 1,1-diphenyl-2-picryl-hydrazyl (DPPH) assay is a colorimetric assay that measures the ability of a sample to scrub free radicals commonly associated with reactive nitrogen species (RNS) and ROS.[458] Initially, the DPPH solution exhibits a distinctive deep violet colour, when an antioxidant is introduced into the solution, it can cause a pronounced change in colour from violet to colourless.[459] The extent of this colour change is directly proportional to the antioxidant activity of the compound under investigation. A more significant reduction in absorbance indicates a stronger antioxidant capacity.[460]

The 2,2'-azino-bis(3-ethylbenzothiazoline)-6-sulfonic acid (ABTS) assay is a second colorimetric assay used to determine the inhibition of the production of ABTS radical by the associated sample.[461] Initially, the ABTS solution is deep blue or green due to the presence of the ABTS radical cation. When an antioxidant is introduced into the solution, it reduces the ABTS radical cation, leading to a colour change from green or blue to a lighter colour or colourless, depending on the strength of the antioxidant.[462]

The ferric reducing antioxidant power (FRAP) assay is used to determine a sample's ability to donate an electron to reduce Fe^{3+} to Fe^{2+}.[463] While many components within plant extracts can produce this effect, it essentially provides the stoichiometry for the associated antioxidants for the mechanism with the Fe^{2+}/2,4,6-tripyridyl-s-triazine complex.[464] The use of this assay is important in pathologies with a known iron component, such is the case in ferroptosis.

3.2.2.2 Cytotoxicity or cytoprotection assays

Cytotoxicity refers to the harmful or destructive effects of a substance or condition on living cells, particularly when it results in cell damage, dysfunction, or death.[465] Cytotoxicity can be quantified through various assays and tests, and plays a crucial role in assessing the safety and potential harm of substances, as well as in the development of pharmaceuticals and understanding the mechanisms underlying cell damage.[466] In cytotoxicity assays, a higher concentration needed to cause cell death suggests a beneficial result when the context is safety assessment. Consequently, cytotoxicity data should be assessed at levels relevant to the physiological

response under study. As this dose-response relationship is seen as the crux to the pharmacodynamics and PK, where a lower concentration could be beneficial, and the higher concentration could precipitate possible side-effects when investigated from a clinical aspect. This is considered a therapeutic window, representing a concentration range that produces the desired physiological response without causing harmful effects.[467] Thus, a wide therapeutic window makes for a drug that can have maximum efficiency with low side-effects.[468] The cytotoxicity of an extract or sample at low doses suggests the presence of a compound that disrupts normal cellular function, thereby narrowing the therapeutic window.[469] This means that while the drug may still exhibit a physiological effect, it could only do so at potentially cytotoxic concentrations.[468] This is normally a first-line assay to determine an extract or sample is going to undergo further investigation or be rejected due to toxicity.[470]

Cytoprotection in *in vitro* assays refers to the ability of a substance or treatment to protect or preserve the structural and functional integrity of cultured cells when they are exposed to various harmful agents or conditions.[471] These harmful agents can include toxins, chemicals, oxidative stress, or other factors that would typically cause damage or cell death.[472] Cytoprotection is assessed by measuring the extent to which the substance or treatment prevents or reduces cell damage, maintains cell viability, or supports normal cellular function under the adverse conditions being tested.[471] It is an essential concept in cell biology and pharmacology, often used to evaluate the potential therapeutic or protective effects of compounds, drugs, or natural products on cell health and survival. Several assays are available to determine cell survival, including the sulforhodamine B (SRB) assay. The SRB assay is based on the binding of the SRB dye under acidic conditions to intact cell membranes (*i.e*. basic amino acids) where if read under 530 nm and the absorbance measured.[473] The amount of bound SRB is reflective of the amount of protein present and is used as a proxy for cell density.[473] The advantage of using the SRB assay is that it is indefinitely stable after protein precipitation and before the solubilising of the dye, and it is inexpensive and provides a rapid way to determine cytotoxicity, with a full assay runtime of normally under an hour.[474] As it stands, it is currently approved for high-throughput screening as it can be handled by automation.[475]

3.3 Materials and methods

3.3.1 Extraction of dried plant material

The identification and elucidation of phytochemicals can be achieved using chromatographic methods, where the compounds can be isolated from an extract via solubility in different solvents.[476] The difference in polarity of certain solvents produces fractions, each with a unique mixture of phytochemicals to be identified via techniques such as high-performance liquid chromatography (HPLC) and mass spectrometry (MS). The use of HPLC is a method of separating substances based on how they interact with the solvent of the mobile phase (the solvent the compounds are dissolved in) and the solid particles in a densely packed column. A polar liquid phase, typically a combination of water and another solvent, and a non-polar solid phase, such as C18, are used in modern HPLC.[477]

The dried plant material (**Table 3-1**) was obtained from the Council for Scientific and Industrial Research (CSIR; Pretoria, South Africa) and donated to the Biodiscovery Centre within the Department of Chemistry (University of Pretoria, herbarium samples were deposited and identified by the South African National Biodiversity Institute (SANBI), whilst *A. oppositifolia*, B. *disticha* and *X. undulatum* were sourced from the in-house Department of Pharmacology repository. Dried plant material was stored in polyurethane zip-lock bags and kept in cardboard boxes in the dark. The bags were marked with the database code (P-number) (**Table 3-1**). Apart from *L. javanica* and *W. somnifera,* all other plant samples were subjected to the full extraction process described below. *L. javanica* and *W. somnifera* were previously extracted using the same method stipulated below for an unrelated project by the Department of Chemistry and were stored at -80°C in their phytomedicine library.

Extraction was undertaken in sintered glass funnels fitted with stopcocks and labelled with the sample code. Dried plant material (7.0 to 7.3 g) was added to the funnel. A volume of 50 mL dichloromethane:methanol (DCM:MeOH; 1:1) was added to the funnels, which were partially submerged in an ultrasonic bath containing water at room temperature for 1 h. The water temperature was maintained below 28°C to ensure the DCM did not evaporate. After the first extraction, the solvent mixture was decanted into round-bottom flasks and temporarily stored at room temperature in a cupboard. The marc was extracted with 50 mL 100% MeOH and the same procedure followed as for the DCM:MeOH solvent**.**

The DCM:MeOH and MeOH extracts where combined in round bottom flasks and dried under reduced pressure using a rotational evaporator (Buchi Rotavapor R-300, with a Buchi B-300 Heating Bath and a Buchi V-300 Vacuum Pump; Labotec, Midrand, South Africa). After the extracts where dried, crystals were reconstituted with MeOH, decanted into pre-weighed 10 mL glass polytops, and dried down at 35°C for 6 h using a Genevac® EZ-2 Plus Mk III centrifugal evaporator (United Scientific, Ipswich, United Kingdom).

3.3.2 Fractionation of crude extracts

After drying, a portion of the crude extract (> 200 mg) was transferred into pre-weighed 10 mL plastic tubes for fractionation. The crude extract was reconstituted in a calculated amount (to ensure full solubility or suspension of crude extract) of a 6:3:1 mixture of HPLC-grade (>98%) methanol:ethyl acetate:methyl tert-butyl ether (MeOH:EtOAc:MTBE) as determined by the Hamilton® Microlab® STARLET™ M automated liquid handler (Hamilton Robotics, Inc; Nevada, United States of America) and vortex-mixed until solubilised.

The solubilised crude extract was decanted onto dental cotton wool inserted into 10 mL glass polytops and dried via centrifugal reduced pressure. Once dried, the crude extract-saturated cotton wool was inserted into empty 6 cc polypropylene Strata® (Phenomenex®) solid-phase extraction (SPE) cartridges containing a single frit (Separations, Phenomenex; Torrance, California, USA) and stored at 4°C until use.

Fractionation was carried out using a Gilson® GX-241 ASPEC® liquid handler (Gilson Scientific via LASEC SA (Pty) Ltd, Gilson Inc.; Middleton, Wisconsin, USA) and C8 HyperSep® 2 g/6 mL cartridges (Anatech Instruments (Pty) Ltd, ThermoFisher Scientific Inc.; Waltham, USA). The absorbent of the cartridges was activated with 11 mL 100% MeOH, and thereafter with 5:95 MeOH:H_2O via a Gilson® Verity® 4060 solvent pump (Gilson Scientific via LASEC (Pty) Ltd, Gilson Inc.; Middleton, Wisconsin, USA). The cotton wool-loaded cartridges were fitted onto C8 HyperSep® cartridges and fractionated at a flow rate of 10 mL/min with a washout step for the needle between each solvent system. This equates to a fractionation time of ~1 h per three plants. Fractions were labelled with the suffix –F1 to –F7 to indicate the gradient solvent system used. An aqueous solvent system was used for F1 - F6 with an increasing gradient of MeOH, after which F7 was created using 50:50 MeOH:acetonitrile (ACN) (**Table 3-2**). After eluting out the fraction using pressurised air, each fraction was stored in a barcoded plastic tube at -40°C until use.

Table 3-2: Gradient solvent system used for the preparation of different fractions (F).

Fraction (F) suffix	MeOH	H_2O	Acetonitrile
F1	5	95	0
F2	20	80	0
F3	40	60	0
F4	80	20	0
F5	90	10	0
F6	100	0	0
F7	50	0	50

Once fractionation was completed, the fractions were pipetted into a BioPointe Scientific® 96 deep-well plate (BioPointe Scientific Inc. via Separations (Pty.) Ltd., BioPointe Scientific Inc.; Claremont, California, USA), and mapped into a spreadsheet via the MicroLab® system. The deep-well plates were then dried under centrifugal reduced pressure for 14 h using the Genevac® HT-6 Series 3i centrifugal evaporator (United Scientific, SP Scientific; Ipswich, UK). Once dry, the tubes were placed into polyurethane bags and stored at 4°C for future use. The dried samples in the deep well plate were reconstituted in biological grade dimethyl sulfoxide (DMSO) and transferred to a FluidX® 1.0 mL EXT Co-Mold Jacket Tube pre-packed 96 position rack (FluidX Ltd. Via Separations (Pty.) Ltd., FluidX Ltd.; Cheshire, UK) at 5 mg/mL as determined by the MicroLab® system, apart from those fractions that could not be concentrated more. Samples were pipetted into a deep well plate in 40 µL DMSO aliquots and heat-sealed with an aluminium heat seal using the BIOBASE® PS-2 Semi Automated Plate Sealer (BIOBASE Group; Shandong, China). Plates were stored at -80°C to ensure no phytochemical breakdown until use. The samples in the FluidX® tubes are kept in the Department of Chemistry under -80°C in a Hamilton® Verso® Q20 (Hamilton Company via Separations (Pty) Ltd, Hamilton Storage GmbH, Switzerland) for future studies. After both rounds of extractions were combined and dried, the final weight was recorded, and extraction yield was calculated using the following equation:

$$Extraction\ yield\ (\%) = \frac{Final\ weight\ of\ dried\ extract\ (g)}{Starting\ weight\ of\ plant\ material\ (g)} \times 100$$

Fractionation commenced once the sample of the dried crude extract was completely dried, weighed and redissolved onto dental cotton wool. The solvent system used to capture the fractions are recorded in **Table 3-2**. Each fraction was collected into tubes over a period of 1 h (for all solvent systems) and marked with the fraction name and bar code for ease of sample identification. After drying the fractions, the tubes were weighed, and fraction yield was calculated using the following equation:

$$Fraction\ yield\ (\%) = \frac{Weight\ of\ tube\ after\ drying\ (g) - weight\ of\ tube\ before\ fraction\ (g)}{Original\ sample\ weight\ prefractionation\ (g)} \times 100$$

The fractions were dried and then reconstituted in DMSO at a standardised concentration of 5 mg/mL and transferred to FluidX Tubes for long term storage at -80°C.

3.3.3 Cell maintenance and assays

3.3.3.1 Maintenance of SH-5YSY neuroblastoma cells

The SH-SY5Y neuroblastoma cell line (ATCC CRL-2266) was gifted by the North-West University (Potchefstroom, South Africa), Department of Pharmacology. Cells were cultured in a 1:1 mixture of Ham's F12 medium and Dulbecco's Modified Eagle's Medium (DMEM) (Sigma Aldrich, St Louis, USA). Complete medium was created by supplementing the mixture with 1% non-essential amino acids, penicillin (100 IU/mL), streptomycin (100 IU/mL) and 10% foetal calf serum (FCS) (Sigma Aldrich, St Louis, USA). The cells were maintained at 37°C in a humidified environment of 5% CO_2. Confluent cells (80%) were washed three times with 1 mL sterile phosphate-buffered saline (PBS) and chemically detached using 3 mL TrypLE™ Express Enzyme (~5 min). Cells were harvested using centrifugation (5 min, 200 *g*), and the pellet was resuspended in 1 mL complete medium.

3.3.3.2 Preparing cells for assays

The trypan blue assay is a dye exclusion test used to determine the number of viable cells present in a cell suspension.[478] Trypan blue is excluded from live, intact cell membranes, however, is included in dead cell membranes. An aliquot of the re-suspended cells (20 µL) was diluted in 180 µL trypan blue solution (0.1 % w/v) (Sigma Aldrich, St Louis, USA) and counted after ~3 min. The viable cell percentage was calculated using the following formula:

$$Viable\ cells\ (\%) = \frac{total\ number\ of\ viable\ cells\ of\ aliqout}{total\ number\ of\ cells\ of\ aliqout} \times 100$$

Cell stock was calculated using the following calculation:

$$Cell\ concentration\ (cells.mL^{-1}) = counted\ cells \times 10^4 \times dilution\ factor$$

After counting viable cells via the trypan blue assay, the cells were re-suspended at 1 x 10^5 cells/mL for 96 well-plates.

3.3.3.3 Cytotoxicity determination for 6-hydroxydopamine

A volume-adjusted SRB assay was used to determine the cytotoxicity of 6-hydroxydopamine (6-OHDA).[479] Cells (100 µL, 1 x 10^5 cells/mL) were seeded into 96-well plates and incubated overnight for cellular attachment. Cells were exposed to either 100 µL medium (negative control), 0.05% ascorbic acid (vehicle control), 1% saponin (positive control) (Sigma Aldrich, St Louis, USA) and a range of 6-OHDA concentrations made up from a 25 mM aliquot in 1% ascorbic acid solution (0.25, 2.5, 10, 50, 150, 250, 300, and 500 µM) prepared in FCS-free medium for 48 h. Blanks (200 µL) consisting of 5% FCS-supplemented medium were used as sterility and background noise control. Following exposure, the cells were fixed with 50 µL of a 50% (v/v) trichloroacetic acid solution overnight at 4°C. The fixed cells were washed twice with tap water, dried, and stained for 30 min with 100 µL SRB solution (0.057% w/v in 1% acetic acid). After staining, cells were washed three times with 150 µL 1% acetic acid solution and allowed to dry. Bound dye was dissolved using 200 µL Tris-base (10 mM; pH 10.5) for 30 min using a shaker. Plates were then read spectrophotometrically using an EL-X 800 microplate reader at 510 nm with a reference wavelength of 630 nm. Cell density (relative to the negative control) was calculated using the following equation:

$$Cell\ density\ (\%\ of\ negative\ control) = \left(\frac{Absorbance\ of\ sample}{Average\ \ absorbance\ of\ negative\ control}\right) \times 100$$

A volume-adjusted SRB assay was used to determine the cytotoxicity of both the fractions and crude extracts.[479] Cells (100 µL, 1 x 10^5 cells/mL) were seeded into 96-well plates and incubated overnight for cellular attachment. Cells were exposed to either 100 µL medium (negative control), 0.05% ascorbic acid (vehicle control), 0.5% DMSO (vehicle control), 35 µM 6-OHDA and the fractions or crude extracts (10 µg/mL in-well concentration) constituted in into FCS-free medium for 48 h. The concentration was based on the National Cancer Institute's Natural Products Discovery (NCI-NPNPD, Maryland, USA) one-dose screening concentration, as this concentration is more achievable with plant extracts.[480] Blanks consisting of cells with 5% FCS-supplemented medium were used as sterility and background noise control.

3.3.3.4 Evaluation of cytoprotection of fractions and crude extracts against 6-hydroxydopamine-induced cytotoxicity

Cells were seeded as per Section 3.3.3.2 after which it was treated with 50 µL 6-OHDA (35 µM) for 2 h. After treatment, cells were either treated with 50 µL fractions or crude extract (40 µg/mL) or medium (negative control), 0.05% ascorbic acid (vehicle control), 0.5% DMSO (vehicle control) for 48 h. The SRB assay (Section 3.3.3.3) was used to assess cytoprotection. Fractions or crude extracts showing promising cytoprotection (≥60% protection) and minimal cytotoxicity (>90% cell density) was used to investigate further acellular and cellular mechanisms.

3.3.3.5 Ferric reduction antioxidant power assay

The FRAP assay measures the antioxidant capacity of a sample relative to its iron reduction activity. This reduction is indicated by the formation of a blue colour as ferric ions bind to 2,4,6-tri(2-pyridyl)-1,3,5-triazine (TPTZ), which can be measured spectrophotometrically at 593 nm.[481] The increase in antioxidative power is directly correlated to the intensity of the blue colour produced, as the Fe^{3+}-TPTZ complex is reduced to a Fe^{2+}-TPTZ complex.[481]

Using a 96-well plate, each well had 150 µL acetic acid buffer (0.30 M, pH 3.5), 15 µL TPTZ solution (10 mM, with 0.006% hydrochloric acid in 100 mL) and 15 µL iron chloride ($FeCl_3$) solution (20 mM). The reaction was initiated by the addition of 5 µL of crude extract or fraction (370 µg/mL to achieve 10 µg/mL in-well), or the iron sulphate ($FeSO_4$) standard (0 to 1,000 µM), and was incubated at 37°C for 20 min. The absorbance was measured at 593 nm (Synergy 2, BioTek, South Africa). The FRAP value was interpolated from the standard curve and the antioxidant capacity is calculated using the following formula:

$$FRAP\ value\ (\text{mmol}\ FeSO_4\ equivalanece\ .\text{g}^{-1}\ \text{sample}) = \frac{\text{mM eq}\ FeSO_4}{final\ in-well\ weight\ of\ sample\ (g)}$$

3.3.3.6 Chelation ability

Chelation refers to the bonding of ions and molecules with metal ions.[482] It involves the formation or presence of two or more bonds with distinct coordinates between a multi-aliased (multiple bond) ligand and a central metal atom.[483] It is used to remove or deactivate metal ions to a less reactive state, in the case for iron, from a reactive Fe^{2+} to a less reactive Fe^{3+}.[483] Ferrozine reacts with Fe^{2+} to form a stable pink/magenta colour, thus, the principle of the assay is to pretreat the iron (II) sulphate ($Fe(II)SO_4$) and then measure the change in baseline absorbance, with

absorbance correlating with the percentage change of Fe^{2+} when compared to the negative control.

Chelation ability was measured using Fe(II)SO_4 (2 mM, 10 µL) shaken with 200 µL of either plant fraction/extract sample, water (vehicle control), iron sulphate (2 mM, Fe(II)SO_4) or EDTA (400 mg/mL) within a 96-well plate for 20 min. Ferrozine (5 mM, 40 µL) was added to the mixture to achieve a final sample concentration of 10 µg/mL, and read at 562 nm on a Synergy II spectrometer after 10 min incubation at room temperature.[484, 485] Chelation ability is expressed as percentage chelation ability (% chelation) at 10 µg/mL fraction/crude extract was determined with the following formula:

$$\%\ Chelation = \frac{Average\ absorbance\ (sample)}{Average\ absorbance\ (negative\ control)} \times 100$$

3.3.4 Statistics

Raw data was captured using Microsoft Excel (Microsoft Office Suite) and statistical analyses were performed using GraphPad Prism 8.0.2. At least three biological and technical repeats were performed (n ≥ 9), expect for lipid peroxides where an n = 8 was used due to the change in plate size. Linear regressions were done using the ordinary least squares method to fit the best-fit line. All data was expressed as the mean ± standard error of the mean (SEM). Changes in protein content was calculated using the Kruskal-Wallis analysis of variance test with a Dunn's multiple comparison post-test. Outliers were identified and removed using GraphPad Robust regression and the outlier removal (ROUT) method. The indicator of significance was $p \leq 0.05$.

3.4 Results and discussion

3.4.1 Plant extraction and fractionation

Apart from *C. orbiculata*, all plants were only extracted once from dried plant material. *C. orbiculata* did not provide enough crude extract to be fractionated, thus a second extraction was performed, and the extracts were combined to ensure that enough crude material was available for the fractionation process (**Table 3-3**).

Table 3-3: Extraction yields for the crude extracts of the plants investigated in the study.

Plant name	Raw material weight (g)	Extract weight (mg)	Crude extraction yield (%)	Weight used for fractionation (mg)
A. villicaulis	7.33	486.58	6.63	217.45
A. oppositifolia	7.29	609.94	8.36	251.87
A. procumbens	7.26	395.19	5.44	218.31
A. arctotoides	7.30	606.83	8.31	204.91
B. disticha	7.17	980.35	13.67	342.66
B. latifolia	7.31	619.58	8.48	200.80
C. molle	7.24	797.57	11.02	347.95
C. orbiculata (two extractions)	7.33	193.22	2.64	298.25
	7.18	187.37	2.61	
C. sylvaticus	7.30	812.91	11.14	202.40
D. stramonium	7.29	279.46	3.83	210.95
D. sylvatica	7.23	297.34	4.11	200.09
E. milli	7.25	515.58	7.11	283.05
G. physocarpus	7.14	945.77	13.25	232.19
J. abyssinicum	7.34	531.33	7.24	215.36
L. discolor	7.22	379.62	5.26	203.51
L. leonurus	7.13	329.34	4.62	213.30
*L. javanica**	~ 7.00	N/D	N/D	372.92
M. indica	7.32	1,115.82	15.24	251.89
M. longifolia polydena	7.29	234.00	3.21	234.82
P. virgata	7.24	922.40	12.74	311.30
S. brachypetala	7.26	1944.70	26.78	274.45
V. myriantha	7.34	374.49	5.10	201.90
*W. somnifera**	~ 7.00	N/D	N/D	529.45
X. undulatum	7.15	1476.80	20.65	346.19

* Previously extracted by the Department of Chemistry (University of Pretoria, South Africa) (samples in biorepository).

The fractionation process yielded seven fractions, with F1 – F3 being more aqueous in nature (water % > 50%, isolating more hydrophilic compounds), and F4 – F7 being more organic in nature (water % < 50 %, isolating more lipophilic compounds).

Table 3-4: Extraction yields for the fractions of each plant investigated in this study.

Plant name	Fraction #	Fraction weight (mg)	Yield (%)
A. villicaulis	1	31.52	14.50
	2	20.13	9.26
	3	1.70	0.78
	4	3.01	1.38
	5	4.35	2.00
	6	14.85	6.83
	7	11.39	5.24
A. oppositifolia	1	55.33	21.97
	2	36.65	14.55
	3	20.70	8.22
	4	19.55	7.76
	5	17.06	6.77
	6	10.79	4.28
	7	15.93	6.32
A. procumbens	1	40.21	18.42
	2	21.21	9.72
	3	26.09	11.95
	4	17.07	7.82
	5	16.51	7.56
	6	10.92	5.00
	7	18.04	8.26
A. arctotoides	1	12.29	6.00
	2	27.27	13.31
	3	3.15	1.54
	4	9.64	4.70
	5	37.59	18.34
	6	31.95	15.59
	7	15.38	7.51
B. disticha	1	45.80	16.54
	2	25.30	9.14
	3	20.56	7.42
	4	6.95	2.51
	5	7.08	2.56
	6	8.82	3.18
	7	7.16	2.59
B. latifolia	1	16.23	8.08
	2	8.94	4.45
	3	6.01	2.99
	4	10.48	5.22
	5	11.03	5.49

Plant name	Fraction #	Fraction weight (mg)	Yield (%)
	6	5.39	2.68
	7	5.09	2.53
C. molle	1	38.44	14.20
	2	23.59	8.72
	3	22.48	8.31
	4	19.28	7.12
	5	13.62	5.03
	6	28.78	10.63
	7	17.40	6.43
C. orbiculata	1	79.45	26.64
	2	31.16	10.45
	3	25.93	8.69
	4	15.43	5.17
	5	17.86	5.99
	6	14.15	4.74
	7	19.25	6.45
C. sylvaticus	1	29.59	14.62
	2	52.06	25.72
	3	14.68	7.25
	4	11.43	5.65
	5	7.32	3.62
	6	11.43	5.65
	7	5.98	2.95
D. stramonium	1	26.37	12.50
	2	6.50	3.08
	3	3.73	1.77
	4	9.95	4.72
	5	24.99	11.85
	6	21.08	9.99
	7	14.65	6.94
D. sylvatica	1	22.63	11.31
	2	14.89	7.44
	3	1.23	0.61
	4	2.04	1.02
	5	6.91	3.45
	6	28.78	14.38
	7	17.03	8.51
E. milli	1	83.11	29.36
	2	0.25	0.09
	3	6.30	2.23

Plant name	Fraction #	Fraction weight (mg)	Yield (%)
	4	9.06	3.20
	5	13.45	4.75
	6	23.69	8.37
	7	35.17	12.43
G. physocarpus	1	34.42	11.81
	2	11.26	3.86
	3	5.52	1.89
	4	15.38	5.28
	5	9.87	3.39
	6	10.59	3.63
	7	34.58	11.86
J. abyssinicum	1	60.93	28.29
	2	40.25	18.69
	3	1.21	0.56
	4	3.92	1.82
	5	6.41	2.98
	6	9.24	4.29
	7	11.63	5.40
L. discolor	1	26.90	13.22
	2	11.63	5.71
	3	11.85	5.82
	4	19.05	9.36
	5	12.03	5.91
	6	7.81	3.84
	7	13.86	6.81
L. leonurus	1	15.14	7.10
	2	7.38	3.46
	3	5.10	2.39
	4	9.22	4.32
	5	30.10	14.11
	6	96.39	45.19
	7	14.26	6.69
M. indica	1	28.68	11.39
	2	20.27	8.05
	3	25.24	10.02
	4	65.95	26.18
	5	16.74	6.65
	6	11.40	4.53
	7	14.26	5.66
M. longfolia polydena	1	26.35	11.22

Plant name	Fraction #	Fraction weight (mg)	Yield (%)
	2	12.11	5.16
	3	2.47	1.05
	4	3.16	1.35
	5	5.44	2.32
	6	19.41	8.27
	7	22.98	9.79
P. virgata	1	45.74	15.38
	2	38.22	12.85
	3	13.45	4.52
	4	13.77	4.63
	5	33.64	11.31
	6	47.00	15.80
	7	30.51	10.26
S. brachypetala	1	21.79	7.94
	2	27.05	9.86
	3	3.90	1.42
	4	9.80	3.57
	5	11.35	4.14
	6	88.16	32.12
	7	53.08	19.34
V. myriantha	1	37.17	18.41
	2	15.23	7.54
	3	7.20	3.57
	4	12.59	6.24
	5	8.86	4.39
	6	9.74	4.82
	7	16.36	8.10
X. undulatum	1	39.8	14.56
	2	16.84	6.16
	3	6.16	2.25
	4	88.71	32.44
	5	50.63	18.52
	6	8.38	3.06
	7	8.54	3.12
	Crude	273.43	80.12

3.4.2 Cytotoxicity of 6-hydroxydopamine

By using the SRB assay, a half-maximal inhibitory concentration (IC_{50}) was calculated using non-linear regression and was determined to be 35 µM for subsequent studies **(Figure 3-1)**, where a dose-dependent cytotoxicity was observed. After screening, the previously calculated IC_{50} 6-OHDA did not yield any cytotoxicity, possibly due a phenotypic shift in the cells used, it was decided to use 70 µM (2 x IC_{50}) as exposure with a response elucidated like the original IC_{50}.

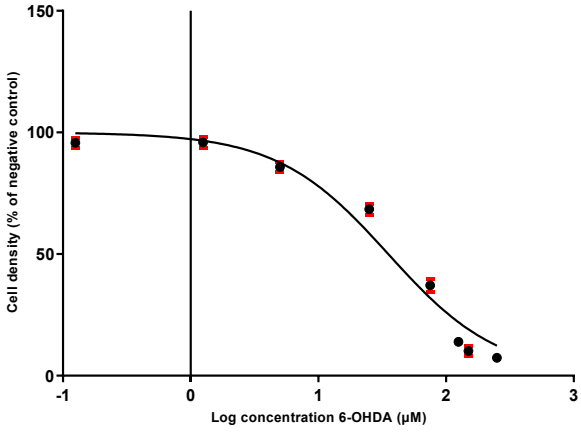

Figure 3-1: The cytotoxicity of 6-hydroxydopamine in the SH-SY5Y cell line after 48 h exposure, as a log[concentration] against percentage cell density ± SEM.

3.4.3 Cytotoxicity and cytoprotection of crude extracts and fractions

Boophone disticha, family Amaryllidaceae, displayed significant ($p < 0.005$). cytotoxicity after exposure to F2 to F5. Fractions 3 to 5 (organic fractions) reduced cell density the most by 51.6%, 49.4% and 51.5%, respectively. The aqueous F2 had significantly ($p < 0.05$), reduced cell density (31.26%), which was comparable to the crude extract (26.4%). Aqueous F1 and organic F6 and F7 did not reduce cell density **(Figure 3-2 A)**. When exposed to 6-OHDA, only the organic F6 and F7 presented with notable, but non-significant, cytoprotection (20.94% and 17.49%) **(Figure 3-2 B)**. Methanol crude extracts of *B. disticha* have been reported to be non-toxic at 10 µg/mL,[486] with IC_{50} values of 22.4 µg/mL and 11.5 µg/mL in MeOH and acetone crude extracts respectively (**Table 3-5**).[487, 488]

Lannea discolor (family Anacardiaceae) did not affect the density of SH-SY5Y cells **(Figure 3-3 A)**. Aqueous F1 displayed cytoprotection as seen by an increase in cell density of 25%, although this was not statistically significant **(Figure 3-3 B)**. Toxicity has been noted for the crude extracts

with LC_{50} values of 0.408 mg/mL in hepatoma cell lines (**Table 3-5**), with no information available on neuroblastoma cell lines.[425] Fraction 1 of *M. indica* (family Anacardiaceae) indicated cytotoxicity (22.6%), whilst F4 to F7 had no effect on cell density. The crude fraction showed no effect on cell density **(Figure 3-4 A)**. Fractions 5 to 7 showed no significant increase in cell density after 6-OHDA exposure **(Figure 3-4 B)**. Studies done on MeOH, chloroform and water extracts all show a cell density increase of 25% after H_2O_2 exposure, and only a reduction between 18 – 20% out of the water and MeOH extracts at 100 µg/mL (**Table 3-5**).[489]

Table 3-5: Pre-clinical data, case reports and associated assay conditions for selected plants with a focus on antioxidant capacity, cytotoxicity and cytoprotection where available.

Plant species	Activity	Extraction process	Cell line studied and/or assay performed	Result(s)	Important phytochemicals previously identified
A. villicaulis	Antioxidant	*Not stated*	DPPH assay	IC_{50} 92 µg/mL[490]	N/D
A. oppositifolia	Antioxidant	Stems airdried and ground Methanol (MeOH) extraction over 48 h at RT	FRAP assay	301.21 ± 12.96 µmol Fe(II)/g[491]	3-Caffeoylquinic acid 4-Caffeoylquinic acid 5-Caffeoylquinic acid Acobioside A Acolongifloroside K Acovenoside A and B Opposide Ouabain[492, 493]
			ABTS assay	99% at 0.08 mg/mL 90.5% at 0.01 mg/mL[491]	
			DPPH assay	70% at 0.1 mg/mL[491]	
	Cytotoxicity	Ground roots were dried and extracted mid-polarity solvents	SH-SY5Y neuroblastoma cell line[488] via SRB assay	IC_{50}: 30.5 µg/mL (Acetone) 41.4 µg/mL (MeOH)	
			MCF-7 breast cancer cell line[494] via SRB assay	IC_{50}: 12.50 µg/mL (Dichloromethane [DCM])	
			Human drug-sensitive CCRF-CEM leukaemia[495] via resazurin assay	IC_{50}: 2.5 µg/mL (MeOH)	
			Multi-drug resistant CEM/ADR5000 leukaemia[495] via resazurin assay	IC_{50}: 2.83 µg/mL (MeOH)	
			HepG2 hepatocarcinoma via SRB assay[496]	IC_{50}: 26.63 µg/mL (MeOH) 13.86 µg/mL (hot water)	
A. procumbens	Anticonvulsant	Dried aerial parts extracted in ethanol (EtOH) via sonication over 1 h	$GABA_A$-benzodiazepine binding assay	± 90% binding at 10 µg/mL[404]	Sesamin Spinescin Piperitol Pinoresinol

Plant species	Activity	Extraction process	Cell line studied and/or assay performed	Result(s)	Important phytochemicals previously identified
					Pinoresinol dimethyl ether Aptosimone Aptosimol Iridoid shanziside ester Verbascoside Pinocembrinin-7-neohesperidoside[497]
A. arctotoides	Antioxidant[498]	Roots in acetone, MeOH and water at RT	FRAP assay	15.28 – 82.87 µmol Fe(II)/g[498]	3-O-[β-D-(6´-nonadeanoate) glucopyranosyl]-β-sitosterol Daucosterol Stigmasterol Nepetin Pedalitin β-Farnesene [499]
			ABTS assay at 100 µg/mL	96.7% (Acetone) 95.5% (MeOH) 91.1% (Water) [498]	
			DPPH assay at 100 µg/mL	68.2% (MeOH at 0.1 mg/mL) 61.8 % (acetone) 7.5% (water) [498]	
B. disticha	Anti-depressant (selective serotonin reuptake inhibition)[398]	Leaves, roots, and bulbs in 70% EtOH/Water or 100% water	[^{3}H]citalopram binding assay at 0.001 mg/mL	85% binding (water) 74% binding (70% EtOH/water)	Buphanisne Buphanidrine Galanthamine Undulatine Vittatine Trisphaeridine[500]
	Rat model for depression[399]	Undisclosed plant material dried and extracted three times in 1:10 w/v ethanol for 60 min via sonication	^{3}[H]citalopram binding assay	IC_{50} 0.5 mg dry extract/mL	
			Serotonin uptake assay	IC_{50} 423.8 µg/mL	
			Adrenaline uptake assay	IC_{50} 77.3 µg/mL	
			Dopamine uptake assay	IC_{50} 93.5 µg/mL	
	Acetylcholinesterase (AChE) inhibition[501]	Bulb powder sonicated in water or EtOH	AChE inhibition assay	30% inhibition at 0.1 mg/mL (EtOH 2% inhibition at 0.1 mg/mL (water)	
	Cytoprotection in SH-SY5Y neuroblastoma cells[488]	Bulb powder extracted into MeOH and acetone via sonication	Cell viability (% of control)	IC_{50} 22.4 µg/mL (MeOH) 11.5 µg/mL (acetone)	

Plant species	Activity	Extraction process	Cell line studied and/or assay performed	Result(s)	Important phytochemicals previously identified
B. latifolia* synonym*: B. natalensis	Cytotoxicity	Water and MeOH extracts of root, leaves, and bulb	Leukaemia K562 cell line[502] via MTT cytotoxicity assay (% cell density compared to control)	(all MeOH extracts) Leaf extract: 1.8% (100 µg/mL) 2.1 % (1000 µg/mL) Root: 5.3 % (100 µg/mL) 8.7 % (1000 µg/mL) Bulb: 6.1 % (100 µg/mL) 7.8 % (1000 µg/mL)	Chrysophanol Asphodeline 10,7'-bichrysophanol Chryslandicin Knipholone anthrone Knipholone Isoknipholone Aloe-emodin 8-hydroxy-1-methylnaphtho[2,3-c] furan- 4,9-dione 5,8-dihydroxy-1-methylnaphtho[2,3-c] furan-4,9-dione[503] Bulbnatalonoside A-E[504]
C. molle	Antioxidant	Chloroform, MeOH, acetone and water/EtOH extracts of leaves	DPPH assay	IC_{50} MeOH: 46.83 mg/mL Chloroform: 82.12 mg/mL Acetone: 57.21 mg/mL Water/EtOH: 43.99 mg/mL[505]	Combretene A Combretene B Combregenin 4,7-Dihydroxy-2,3,6-trimethoxyphenanthrene 3,4'-dihydroxy-4,5-dimethoxybibenzyl[506]
C. orbiculata	Anti-epileptic in mouse model[424]	Refluxed in water for aqueous fraction Extracted via Soxhlet in MeOH	Hind limb extension in induced seizures	Aqueous extract (100 - 200 mg/kg) reduced onset by 25%. MeOH extract (100 - 200 mg/kg) reduced onset by 50%	Cotyledoside C Orbicusides A-C[507]
	Antioxidant[508]	Hexane, acetone, EtOH, MeOH, water.	ABTS assay	IC_{50} Hexane: >100 µg/mL Acetone: 6.86 µg/mL EtOH: 1.96 µg/mL MeOH: 3.35 µg/mL Water: >100 µg/mL	
			DPPH assay	IC_{50} Hexane: >100 µg/mL Acetone: 23.52 µg/mL Ethanol: 16.2 µg/mL MeOH: 3.76 µg/mL Water: >100 µg/mL	

Plant species	Activity	Extraction process	Cell line studied and/or assay performed	Result(s)	Important phytochemicals previously identified
C. sylvaticus	Antioxidant[509, 510]	Roots extracted with MeOH, water	DPPH assay	IC_{50} MeOH: 9.51 µg/mL[509] IC_{50} MeOH: 11.28 µg/mL Water: 11.28 µg/mL[510]	Julocrotine 15,1 –Dihydroxy-trans-entcleroda-3,13-diene 15-Acetoxy-2-oxo-trans-ent-cleroda-3,13- diene Transannonene 15-Acetoxy-trans-cleroda-3,13-diene 5-Hydroxy-trans-cleroda-3,13-dien-15-ol Sylvaticinol Lupenone 3β acetoxylup-20(29)-ene β-amyrin [5R, 6S, 9R]-4,5–dihydroblumenol A Lignoceryl trans–ferulate (+)–syringaresinol[509] Quercetin Kaempherol[511]
	AChE inhibition[511]	Leaves extracted with 20% MeOH:water, EtOAc	AChE inhibition assay	IC_{50} 4.695 mg/mL (crude) EtOAC: 235.0 µg/mL	
	Anticonvulsant[404]	Bark extracted out of ethanol	$GABA_A$-benzodiazepine binding site assay	97.5% binding at 5 µg/mL	
D. stramonium	Epilepsy[443]	Water extracts containing *Scutellaria lateriflora, Gelsemium sempervirens,* and *Datura stramonium*	Visual confirmation on Wistar rats	> 95% reduced epilepsy episodes in mixed herbal tonic	Hygrine Tropinone Tropine Aposcoploamine Hyoscyamine 3.6-Dihydroxytropane[512, 513]
	Anticholinergic properties[514]	Leaves and seeds ingestion	Toxicology reports in human cases	Signs of cholinergic inhibition including dry mouth, loss of vision, flushing and urinary retention[515]	
	Antioxidant[516]	Dried leaves extracted into MeOH	DPPH assay	IC_{50}: 6.7 µg/mL	
D. sylvatica	AChE inhibition[517]	Fresh bulbs extracted into DCM, ethyl acetate (EtOAc)	AChE inhibition assay via TLC plates	Weak activity at 40 µg/mL after visual inspection	Diosgenin Dioscin Dioscorine Dihydrodioscorine Dumetorine Batatasine I – V[517]

Plant species	Activity	Extraction process	Cell line studied and/or assay performed	Result(s)	Important phytochemicals previously identified
E. milii	Antioxidant	Aerial and root parts macerated in DCM and MeOH[518]	ABTS assay	Aerial MeOH: 28.36 TE/g Aerial DCM: 22.71 mg TE/g Root MeOH: 89.14 TE/g Root DCM: 36.79 TE/g	Eremopetasitenin A1 Lusitanicoside Fraxetin Megastachine Peruvoside[518]
			FRAP assay (as Trolox equivalents/gram of extract)	Aerial MeOH: 40.38 TE/g Aerial DCM: 24.47 mg TE/g Root MeOH: 87.73 TE/g Root DCM: 41.61 TE/g	
			Cupric ion reducing antioxidant capacity assay (CUPRAC)	Aerial MeOH: 88.94 TE/g Aerial DCM: 46.93 TE/g Root MeOH: 136.44 TE/g Root DCM: 82.02 TE/g	
	Metal chelating capacity[518]	Aerial and root extracts in MeOH and DCM	Iron ion chelating (as mg EDTA equivalence [EE])	Aerial MeOH: 23.51 mg EE/g Aerial DCM: 49.92 mg EE/g Root MeOH: 23.36 mg EE/g Root DCM: N/D	
	AChE inhibition[518]	Aerial and root extracts in MeOH and DCM	AChE inhibition assay (as mg galathamine equivalents [GE]/g)	Aerial MeOH: 3.98 GE/g Aerial DCM: 5.37 GE/g Root MeOH: 3.63 GE/g Root DCM: 4.59 GE/g	
	Cytotoxicity[519]	Dried aerial parts, powdered and extracted using MeOH, partitioned using hexane, diethyl ether chloroform, EtOAc, butanol and water	MTT cell viability assay on HeLa and HepG2 cell lines	HeLa: IC_{50} (MeOH): 27.9 µg/mL IC_{50} (chloroform): 22.1 µg/mL HepG2: IC_{50} (MeOH): 15.9 µg/mL IC_{50} (chloroform): 11.2 µg/mL	

Plant species	Activity	Extraction process	Cell line studied and/or assay performed	Result(s)	Important phytochemicals previously identified
				IC_{50} (EtOAc): 63.80 µg/mL Butanol, diethyl ether and water partitions presented with non-significant results	
G. physocarpus	Cytotoxicity	Unnamed plant parts, dried and extracted using DCM, and then DCM/MeOH (1:1)	SRB assay on TK10 [human kidney adenocarcinoma], MCF7 [breast adenocarcinoma], UACC62 [melanoma] cell lines)	IC_{50} TK10 – 6.43 µg/mL MCF7 – 20.80 µg/mL UACC62 – 15.00 µg/mL	No isolation has been performed
	Anticonvulsant	Leaves extracted with EtOH	$GABA_A$-benzodiazepine binding site assay	67.7% binding at 0.005 mg/mL[404]	
J. abssynicum	Antioxidant	Leaves extracted in 80% EtOH[520]	DPPH assay	IC_{50} 26.3 µg/mL	Craigosides A - C[521] Saponins, terpenoids, triterpenes, glycosides and flavonoids[522]
			Oxygen radical absorbance capacity (ORAC) assay (as Trolox equivalents/mg of extract)	1023.7 µg TE/mg extract	
L. discolor	Antioxidant	Dried and powered root and bark samples, extracted with 50% MeOH [523]	DPPH assay	Root showed higher inhibition activity than the bark at unknown concentration at same time interval	Catechin Rutin Vanillic acid Sinapic acid Ferulic acid Quercetin[524]
		Leaves were powered, extracted with 80% v/v MeOH[408]	DPPH assay	89.09 % inhibition at 0.5 mg/mL	
		Leaves were dried and powered, extracted with 80% v/v MeOH[408]	FRAP assay (as mg Trolox equivalent antioxidant capacity per g dry weight (TEAC/g DW))	166.3 mg TEAC/g DW	
	Cytotoxicity[525]	Leaves were extracted in acetone	MTT viability assay on C3A liver cells, Vero kidney cells, RAW 264.7 [murine macrophage cells]	IC_{50} C3A – 0.408 mg/mL RAW 264.7 – >1 mg/mL Vero - >1 mg/mL	

Plant species	Activity	Extraction process	Cell line studied and/or assay performed	Result(s)	Important phytochemicals previously identified
L. javanica	Antioxidant	Water extracts of leaves	DPPH assay as TEAC/g DW	EC_{50}: 358 µg/mL[526] TEAC: 1,462.54 mmol/100 g[527]	Coumarin Tricin Xanthine Eucaluptol Carene Geranlol Nerolidol Icterogenin[528]
		Various extracts of leaves	DPPH assay	IC_{50} Water: 0.059 g/mL 50% MeOH: 0.04 g/mL EtOH: 0.025 g/mL 50% EtOH: 0.027 g/mL Acetone: 0.057 g/mL 50% Acetone: 0.022 g/mL EtOAc: 0.066 g/mL[529, 530]	
	Cytotoxicity[531, 532]	MeOH extract of leaves	Brine shrimp lethality assays	40% mortality after 48 h exposure	
L. leonurus	Anticonvulsant	Water extraction	Hind limb extension in induced seizures	400 mg/kg plant material prevented seizures in 50% of animals[436]	Leonurenone A and B Leonurine Leoleorin C[533]
			$GABA_A$-benzodiazepine binding site assay	81% binding at 1 mg/mL[534]	
M. indica	Antioxidant	Leaves extracted out of water and 1:1-water:EtOH[535]	DPPH assay (as IC_{50})	IC_{50} Water 0.49 mg/mL Water:EtOH: 0.17 mg/mL	β-Selinene Cyperene (*E*)-Caryophyllene α-Humalene Terpinolene α-Selinene Mangiferin Gallic acid Quercetin[536]
			ABTS assay (as IC_{50})	IC_{50} Water: 0.049 mg/mL Water:EtOH: 0.13 mg/mL	
			Lipid peroxidation assay	IC_{50} Water: 0.321 mg/mL Water:EtOH: 1.36 mg/mL	
		Leaves washed and extracted using 80% MeOH [537]	DPPH (as % inhibitory activity)	60% at 0.025 mg/mL	
			ABTS assay	IC_{50} MeOH: 1.33 µg/mL	

Plant species	Activity	Extraction process	Cell line studied and/or assay performed	Result(s)	Important phytochemicals previously identified
		Leaves; MeOH, water and chloroform extracts[489]		Water: 2.96 µg/mL Chloroform: 6.56 µg/mL	
			DPPH assay	IC_{50} MeOH: 6.18 µg/mL Water: 5.57 µg/mL Chloroform: 72.40 µg/mL	
			FRAP assay	IC_{50} MeOH: 202.92 µg/mL Water: 298.55 µg/mL Chloroform: N/A	
			Superoxide scavenging assay	IC_{50} MeOH: 0.07 µg/mL Water: 0.06 µg/mL Chloroform: N/A	
	Cytotoxicity	Leaves extracted out of water and 1:1-water:EtOH[535]	Sandwich-enzyme-immunoassay[538] at 500 µg/mL of extract (directed against histone DNA fragments)	NIH/3T3 (normal mouse fibroblast cell line): Water: reduced cell concentration by a factor of 0.25 Water:EtOH: Reduced cell concentration by a factor of 0.75 4TI (mouse mammary cancer cell line): Water: Reduced cell concentration by a factor of 0.4. Water:EtOH: Reduced cell concentration by a factor of 0.6	
		Leaves; MeOH, water and chloroform extracts[489]	NG108-15 neuroblastoma cells with MTT assay	80% cell viability at 100 µg/mL MeOH extract 82% cell viability at 100 µg/mLwater extracts Chloroform results not published	

Plant species	Activity	Extraction process	Cell line studied and/or assay performed	Result(s)	Important phytochemicals previously identified
	Cytoprotection	Leaves MeOH, water and chloroform extracts[489]	NG108-15 neuroblastoma cells treated with hydrogen peroxide (H_2O_2) at 100 µM	25% cell viability increase at 100 µg/mL MeOH extract from ~50% cell density. 10% cell viability increase at 100 µg/mL H_2O extract from ~50% cell density	
M. longifolia* subsp, *polydena	Antioxidant	Leaves in MeOH and essential oils[539]	DPPH assay	IC_{50} MeOH: 57.4 µg/mL Essential oil: 10 700 µg/mL	Piperitone oxide Piperitone Piperitenone β-caryophyllene D-limonene Carvone Menthone Pulegone1,8-cineole Menthol[439]
			β-carotene/linoleic acid assay at 2 mg/mL	MeOH: 24% inhibition Essential oil: 36% inhibition	
		Leaves extracted with MeOH (80%)[540]	DPPH assay	93.68% inhibition at unknown concentration	
	Neuroprotectivity[541]	Leaves extracted in EtOH	Evans blue extravasation in male Wistar rat excised brain matter after induction of stroke using nylon thread via the external carotid artery via FRAP assay	Brain antioxidant power increased as measured in µmol Fe^{2+} reduction	
			Malondialdehyde (MDA) assay	Reduced concentration of MDA in brain tissue	
	Cytoprotection[542]	Leaves extracted with DCM, MeOH, EtOAC and water and combined	PC12 pheochromocytoma cells under H_2O_2 250 µM treatment with MTT assay	55.9% cell viability (5% lower than H_2O_2 control at 60.5%)	
P. virgata	Antioxidant	Leaves and stem in 97% MeOH [543]	DPPH assay	14% inhibition at 2,5 mg/mL	5,7-dihydroxy-8,4'-dimethoxyisoflavone 5,7,4'-trihydroxy-6,8-dimethoxyisoflavone[544] Various isoflavonones[545]
			H_2O_2 scavenging	51% inhibition at IC_{50} of 74 µg/mL	
S. brachypetala	Antioxidant		DPPH assay	Root: IC_{50}	Methyl-5,11,14,17-eicosatetraenoate

Plant species	Activity	Extraction process	Cell line studied and/or assay performed	Result(s)	Important phytochemicals previously identified
		Root and bark in DCM:MeOH (1:1) and water[546]		DCM:MeOH: 0.05 mg/mL Water: 0.05 mg/mL Bark: IC_{50} DCM:MeOH: 1.90 mg/mL Water 0.13 mg/mL	9,12,15-octadecatrienoic (δ-linolenic acid)[547-548]
			ABTS assay	Root: IC_{50} DCM:MeOH: 3.26 x 10^{-7} mg/mL Water: 3.7 x 10^{-7} mg/mL Bark: IC_{50} DCM:MeOH: N/D Water: 0.15 mg/mL	
		Leaves in water and EtOH[548]	DPPH assay	IC_{50}: 9 µg/mL	
			FRAP (Fe^{2+} equivalents/mg of sample (FE/mg))	5 000 FE/mg	
			ABTS (Trolox equivalents/mg of sample [TE/mg])	1054 TE/mg	
	Monoamine oxidase (MAO) inhibition[549]	Bark extracted using EtOH and water	Non-selective MAO inhibition	IC_{50} EtOH: 44 µg/mL Water: 5 µg/mL	
	Alzheimer's disease induced into Swiss albino male mice[550]	Aerial parts extracted using EtOH and H_2O	Various tests in memory and *ex vivo* amyloid-beta quantification	Amyloid-beta production reduced by 44.8% Increased object recognition when compared to control	
V. myriantha **Recently reclassified as *G. myrianthum***	No relevant biological data (cytotoxicity/cytoprotection) or antioxidant studies found				Flavonoids Terpenoids Alkaloids Saponins Glycosides[551]

Plant species	Activity	Extraction process	Cell line studied and/or assay performed	Result(s)	Important phytochemicals previously identified
W. somnifera	Neurotic regeneration	Roots MeOH extracts [452]	Neurite growth after amyloid-beta introduction	Neurite extensions length increased by ~50 µm	Somniferine Somnine Somniferinine Withamine Withanmine Pseudowithamine Withanaminine Withanolides D – F Withaferin A Viscosalactone A and B [450]
	Growth inhibition in SF-268 (Central Nervous System, CNS) cells[552]	Extract bought commercially	MTT cell viability assay	Withaferin A IC_{50}: 0.36 µg/mL Viscosalactone B IC_{50}: 0.45 µg/mL	
	Neuroprotective effects in 6-OHDA lesioned rats[553]	EtOH crude commercial extract	Light-dark movement test Glutathione concentration (via sulfosalicylic acid colour change) Glutathionone-peroxidase-4 expression (via ELISA)	Increased distance moved in 6-OHDA lesioned rats in treatment groups with > 100 mg/kg extract Increased glutathione concentration with increased extract concentrations > 100 mg/kg (up to 15 mmol/g brain homogenate protein increase) Increased glutathione peroxidase-4 expression with increased extract concentrations > 100 mg/kg (up to a 5 nmol/g brain homogenate protein increased)	
	Neuroprotection[554]	Chloroform:MeOH root extractions	6-OHDA in SH-SY5Y neuroblastoma cells via Annexin V conjugated to Alexa-Fluor 488 assay for apoptosis	4 µg/mL extract: 1.9-fold increase of Annexin staining relative to negative control. 20 µg/mL extract: no increase in Annexin staining, thus prevented cell death after mechanical injury.	
			Lactate dehydrogenase activity	Viability of cells increased by 20% with 20 µg/mL extract	

Plant species	Activity	Extraction process	Cell line studied and/or assay performed	Result(s)	Important phytochemicals previously identified
	Anti-Alzheimer's disease activity[555]	EtOH:water root extract	PC-12 cell line via ELISA monoclonal conjugates on peripheral blood samples co-cultures	Reduced pro-inflammatory mediators in a dose dependent manner showing inhibition TNF-α, IL-1β, IL-6 and MCP-1 parameters at higher dose levels of oral 10 and 20 mg/kg.	
X. undulatum	Anti-anxiolytic activity[556]	DCM, MeOH, EtOAc and water extractions	Zebrafish larvae model	Fractions killed off zebrafish larvae 5 days post-fertilisation, after confirmation of death between 12.5 to 500 mg/L	
	AChE inhibition[410]	EtOAc extract[546]	AChE inhibition assay	IC_{50} 0.5 µg/mL	
	Cytoprotection[487, 488]	Root powder extracted into MeOH and acetone via sonication	Cell viability of SH-SY5Y neuroblastoma cells via SRB assay (% of control)	50% at30 µg/mL (MeOH) ~ 50 % at 30 µg/mL (Acetone)	
	ROS scrubbing induced by 6-OHDA[488]	Root powder extracted into MeOH and acetone via sonication	ROS quantification using dihydrodichlorofluorescein diacetate (H_2-DCF-DA)	Reduced ROS with almost ~200% (from induced 300%) at 15 µg/mL	

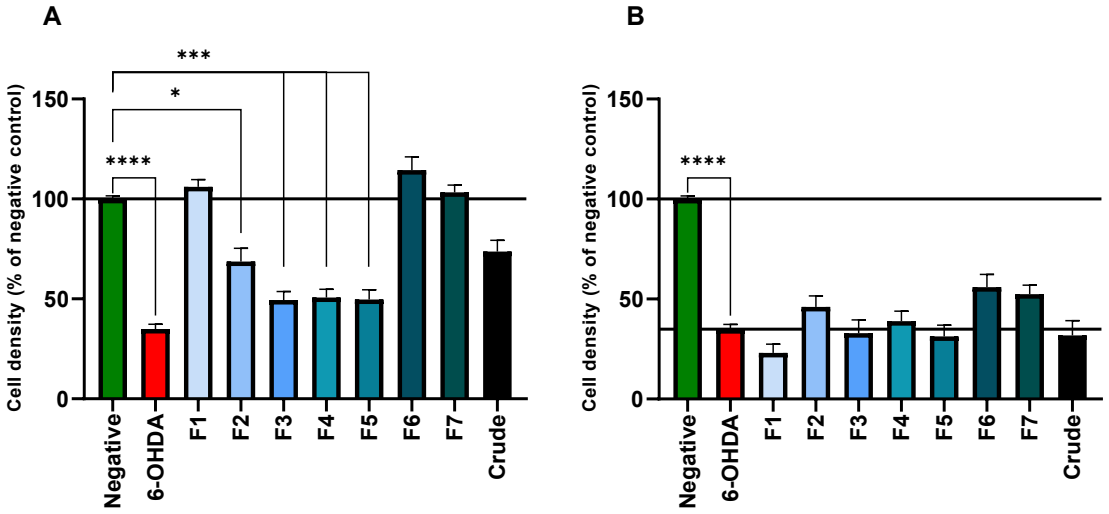

Figure 3-2: The effect of *Boophone disticha* crude extract and fractions on SH-SY5Y cell density alone after 48 h exposure (A) or after induction of 6-hydroxydopamine (6-OHDA)-mediated cytotoxicity (B). Significance was determined using a Kruskal-Wallis with post-hoc Dunn's test between the crude extract or fraction relative to the negative control (A) or 6-OHDA (B). *: p <0.05, *** p < 0.001 ****: p < 0.0001

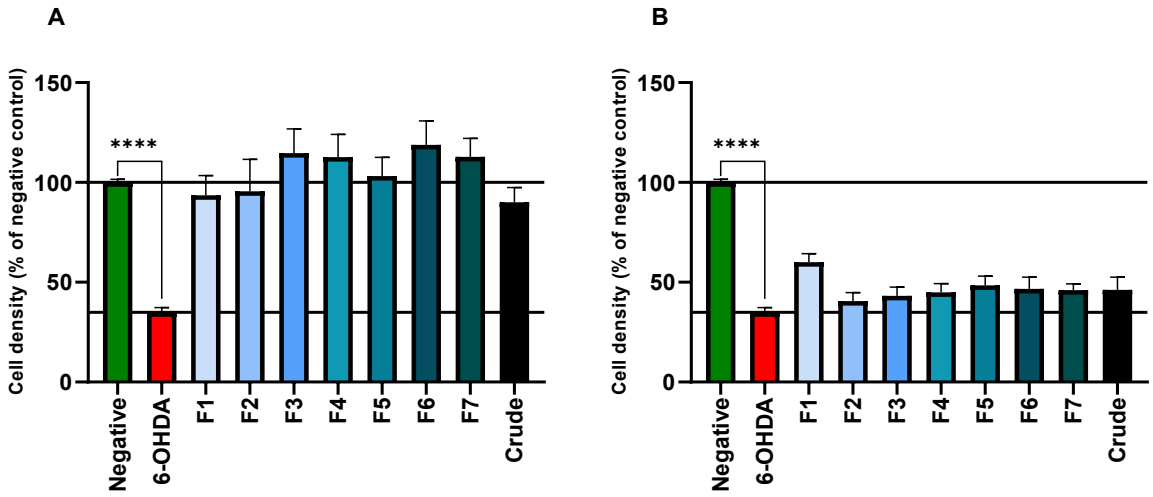

Figure 3-3: The effect of *Lannea discolor* crude extract and fractions on SH-SY5Y cell density alone after 48 h exposure (A) or after induction of 6-hydroxydopamine (6-OHDA)-mediated cytotoxicity (B). Significance was determined using a Kruskal-Wallis with post-hoc Dunn's test between the crude extract or fraction relative to the negative control (A) or 6-OHDA (B). ****: p < 0.0001

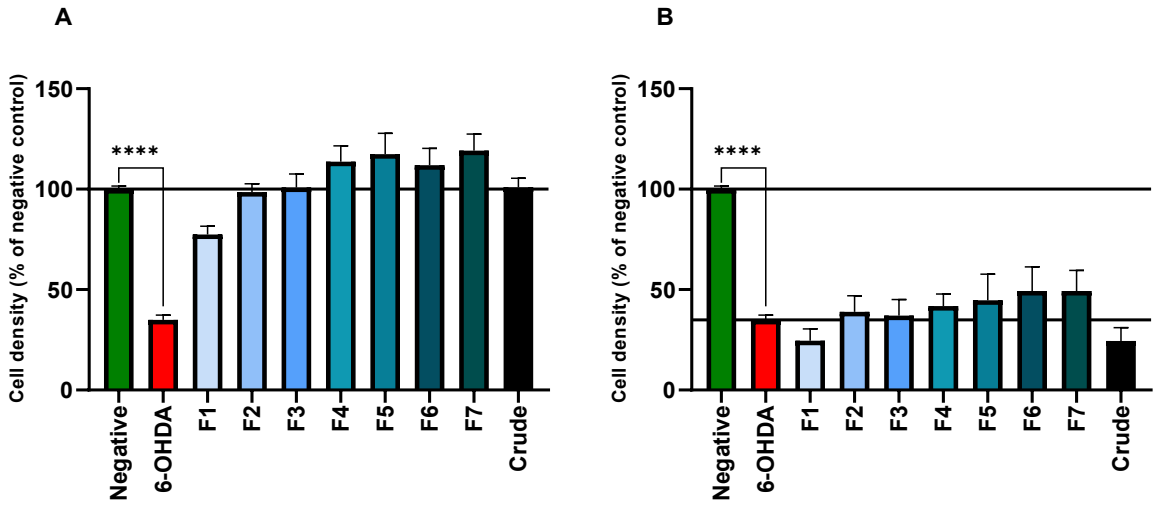

Figure 3-4: The effect of *Mangifera indica* crude extract and fractions on SH-SY5Y cell density after 48 h exposure alone (A) or after induction of 6-hydroxydopamine (6-OHDA)-mediated cytotoxicity (B). Significance was determined using a Kruskal-Wallis with post-hoc Dunn's test between the crude extract or fraction relative to the negative control (A) or 6-OHDA (B). ****: $p < 0.0001$

Fraction 5 of *A. oppositifolia* (family Apocynaceae) reduced cell density significantly ($p < 0.05$) to 56% **(Figure 3-5 A)**, whilst F3 increased cell density non-significantly after 6-OHDA exposure by 23.42% **(Figure 3-5 B)**. Previous cytotoxicity studies on MeOH extracts have indicated IC_{50} values of 2.5, 2.83, 12.50, 26.63 and 41.4 µg/mL for the CCRF-Cem leukaemia,[495] CEM/ADR 5000 leukaemia,[495] MCF-7,[494] HepG2[496] and SH-SY5Y cell line, respectively (**Table 3-5**).[488] The wide range of IC_{50} values from MeOH showcases the diverse phytochemical mixtures from these plants based on place of origin, and the cell line tested on.[492, 493]

Gomphocarpus physocarpus (family Apocynaceae) crude extract significantly reduced cell density by 35% ($p < 0.05$), whilst F4 and F5 exhibited significant cell density reductions of 55% ($p < 0.005$) and 68% ($p < 0.0001$), respectively **(Figure 3-6 A)**. Combined extracts of DCM and DCM/MeOH extractions has shown IC_{50} values between 6.43 – 20.8 µg/mL on TK10, MCF-7 and UACC62 cell lines (**Table 3-5**).[557] No significant cytoprotection was exhibited by any fraction or the crude extract **(Figure 3-6 B)**.

Xysmalobium undulatum (family Apocynaceae) presented with significant cell density reductions of ~48% ($p < 0.05$) for both fractions 4 and 5. The crude fraction reduced cell density by 64% (p

< 0.0001) **(Figure 3-7 A)**. No significant cytoprotection was seen at the screening concentration **(Figure 3-7 B)**. Cytoprotection was seen in the SH-SY5Y cell line after induction by 6-OHDA, with an increase of ~35% in cell density after exposure to 30 µg/mL MeOH extract (**Table 3-5**).[487, 488]

Of all the three plants in the family Apocyneceae (*A. oppositifolia, G. physocarpus* and *X. undulatum*), each plant's F5 showed a statistically relevant reduction. For *G. physocarpus* and *X. undulatum*, a significant reduction in cell density was evident for F4 of both plants, thus leading to the conclusion to the possibility of the presence of the same class of secondary metabolites with cytotoxic activities.

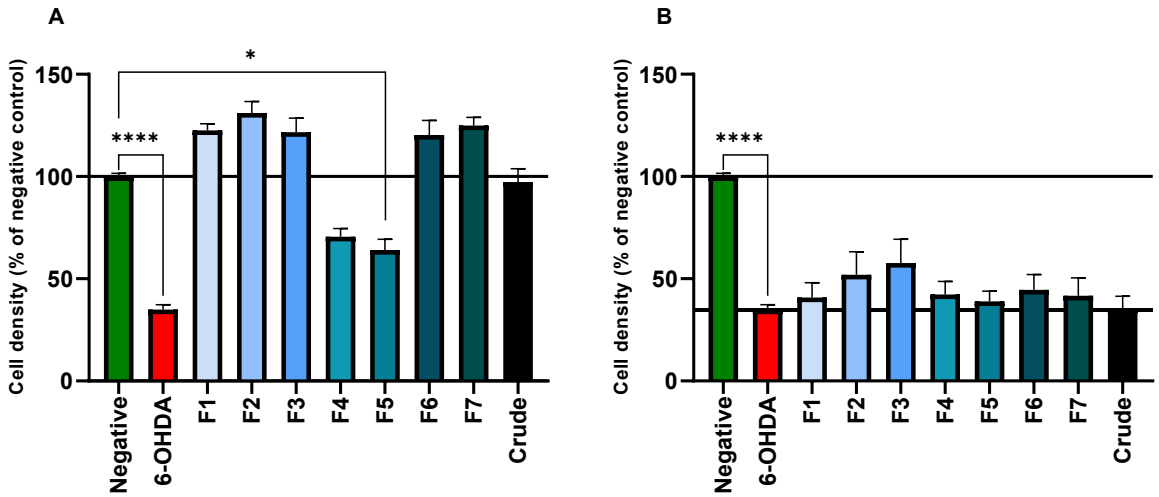

Figure 3-5: The effect of the crude extract and fractions of *Acokanthera oppositifolia* on SH-SY5Y cell density alone (A) or induction of 6-hydroxydopamine (6-OHDA)-mediated cytotoxicity (B) after 48 h exposure. Significance was determined using a Kruskal-Wallis with post-hoc Dunn's test between the crude extract or fraction relative to the negative control (A) or 6-OHDA (B). *: p <0.05; ****: p < 0.0001

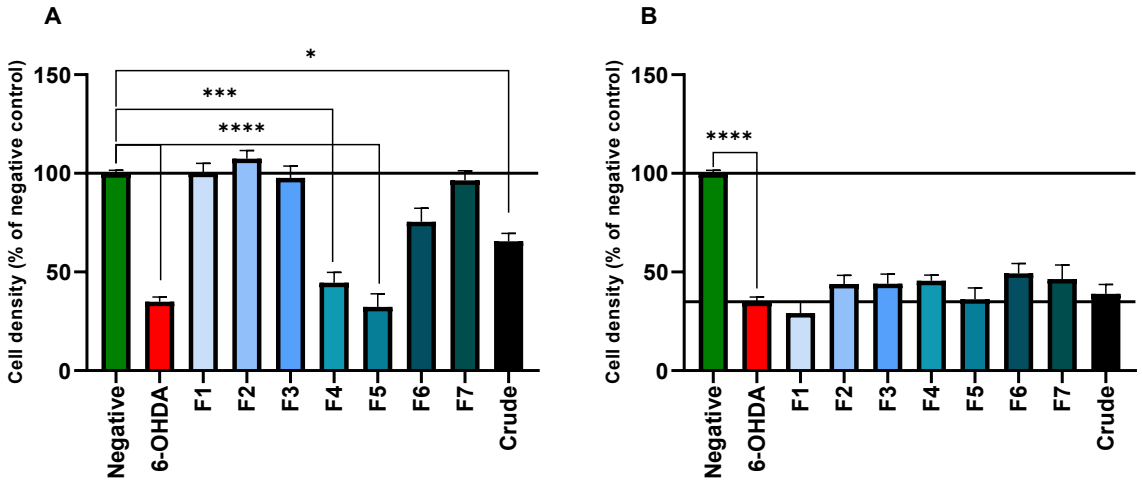

Figure 3-6: The effect of the crude extract and fractions of *Gomphocarpus physocarpus* on SH-SY5Y cell density alone (A) or induction of 6-hydroxydopamine (6-OHDA)-mediated cytotoxicity (B) after 48 h exposure. Significance was determined using a Kruskal-Wallis with post-hoc Dunn's test between the crude extract or fraction relative to the negative control (A) or 6-OHDA (B). *: p <0.05, *** p < 0.001, ****: p < 0.0001

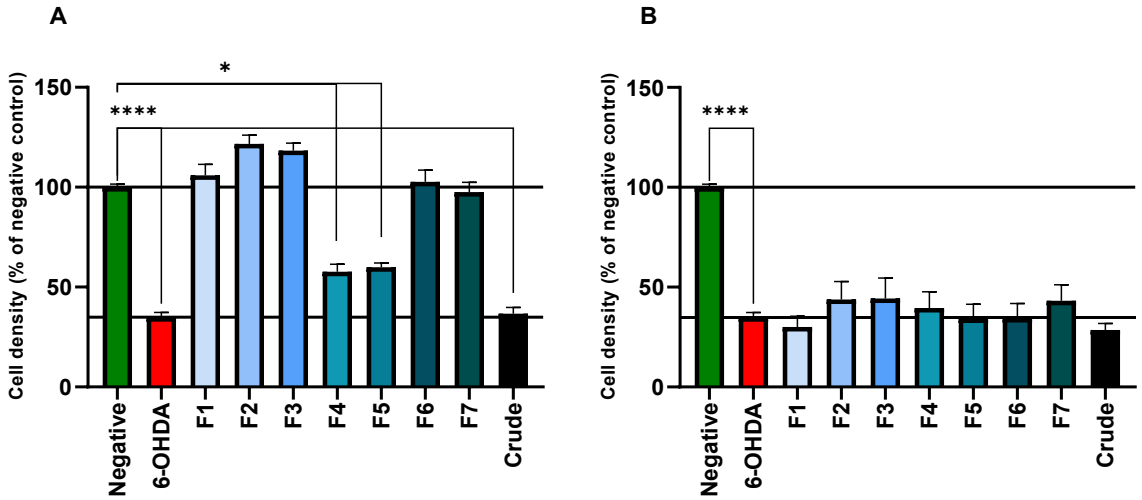

Figure 3-7: The effect of the crude extract and fractions of *Xysmalobium undulatum* on SH-SY5Y cell density alone (A) or induction of 6-hydroxydopamine (6-OHDA)-mediated cytotoxicity (B) after 48 h exposure. Significance was determined using a Kruskal-Wallis with post-hoc Dunn's test between the crude extract or fraction relative to the negative control (A) or 6-OHDA (B). *: p <0.05, ****: p < 0.0001

No significant cytotoxicity was noted when cells were treated with the fractions of *B. latifolia* (family Asphodelaceae). Rather, F1 - F5 increased cell density, albeit non-significantly **(Figure 3-8 A)**. This coincides with the high concentrations needed to reduce cell density, with both 100 and 1000 µg/mL EtOH leaf extracts only reducing K562 leukaemia cell line density to 1.8%[502] and root extracts reducing cell density in the CaCo colorectal adenocarcinoma cell line by 8.45% (**Table 3-5**).[558] Fraction 3 showed significant cytoprotection with an increase in cell density of 34% ($p < 0.05$). Fraction 5 also showed a non-significant increase of 25% after 6-OHDA induced-cytotoxicity **(Figure 3-8 B)**. Fraction 5 of *A. arctotoides* showed a significant level ($p < 0.0001$). of cytotoxicity comparable to 6-OHDA with cell density reduced by 63%. The crude extract diminished cell density non-significantly by ~20% **(Figure 3-9 A)**. No significant cytoprotection was seen after 6-OHDA exposure **(Figure 3-9 B)**. *V. myriantha* did not induce any significant alteration on SH-SY5Y cell density, though increased cell density non-significantly **(Figure 3-10 A)**. Fraction 5 showed a non-significant cell density increase after 6-OHDA exposure (15.1%) **(Figure 3-10 B)**. Both *A. arctotoides* and *V. myriantha* are from the family Asteraceae.

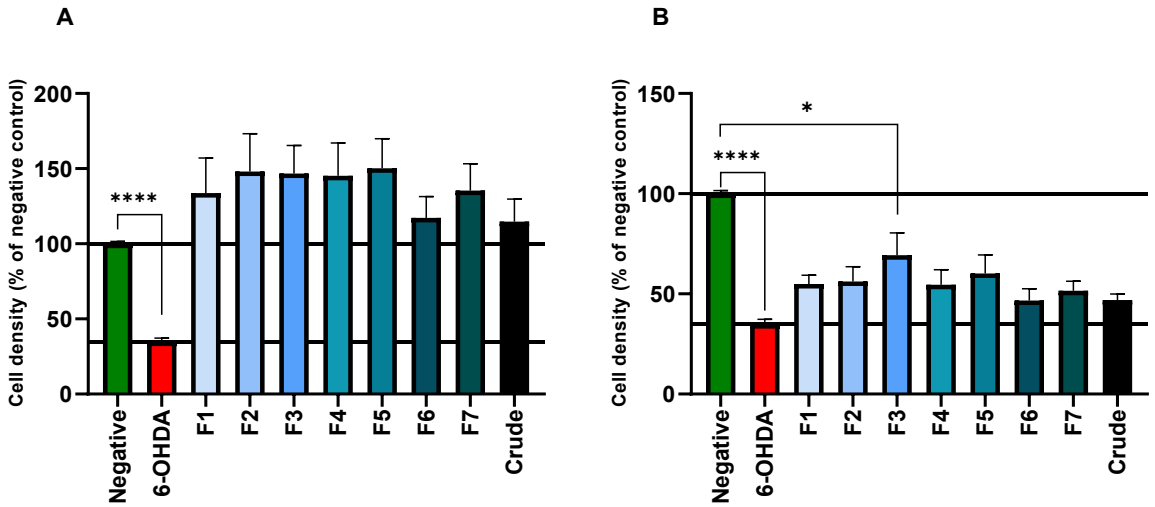

Figure 3-8: The effect of the crude extract and fractions of *Bulbine latifolia* on SH-SY5Y cell density alone (A) or induction of 6-hydroxydopamine (6-OHDA)-mediated cytotoxicity (B) after 48 h exposure. Significance was determined using a Kruskal-Wallis with post-hoc Dunn's test between the crude extract or fraction relative to the negative control (A) or 6-OHDA (B). *: $p < 0.05$, ****: $p < 0.0001$

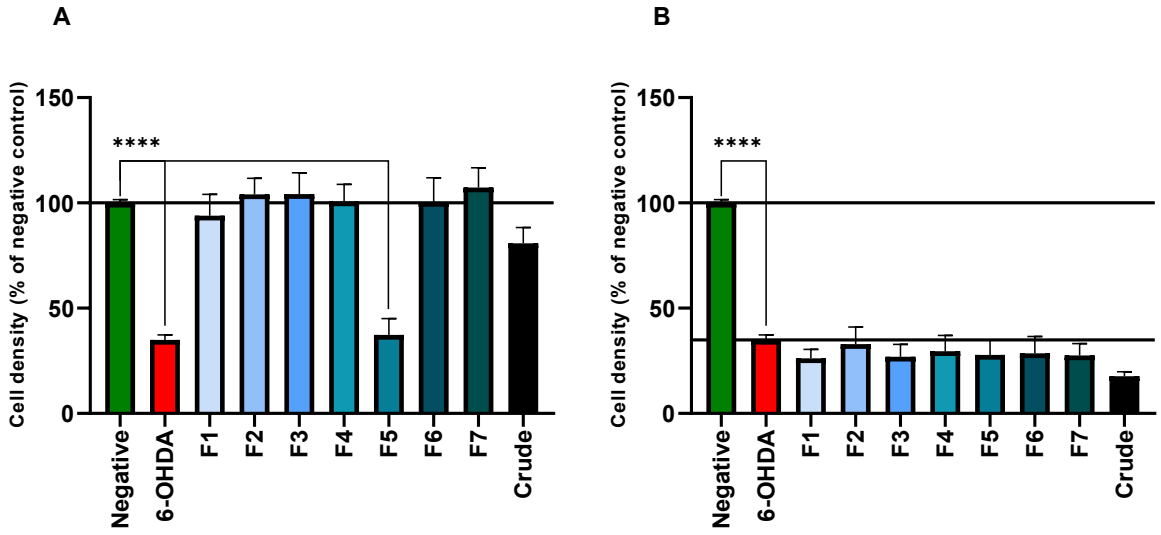

Figure 3-9: The effect of the crude extract and fractions of *Arctotis arctotoides* on SH-SY5Y cell density alone (A) or induction of 6-hydroxydopamine (6-OHDA)-mediated cytotoxicity (B) after 48 h exposure. Significance was determined using a Kruskal-Wallis with post-hoc Dunn's test between the crude extract or fraction relative to the negative control (A) or 6-OHDA (B). ****: $p < 0.0001$

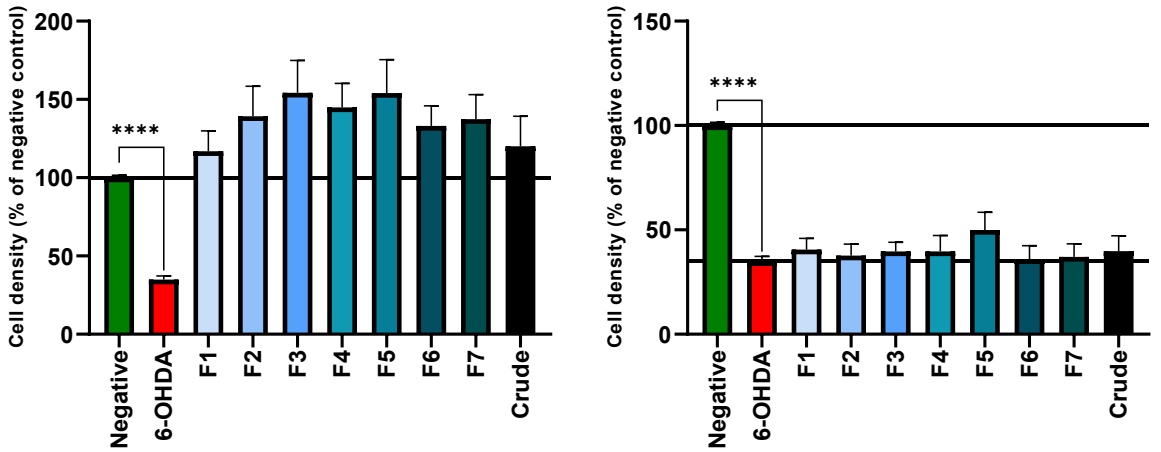

Figure 3-10: The effect of the crude extract and fractions of *Vernonia myriantha* on SH-SY5Y cell density alone (A) or induction of 6-hydroxydopamine (6-OHDA)-mediated cytotoxicity (B) after 48 h exposure. Significance was determined using a Kruskal-Wallis with post-hoc Dunn's test between the crude extract or fraction relative to the negative control (A) or 6-OHDA (B). ****: $p < 0.0001$

Jasminum abyssinicum, the only plant from the Oleaceae family, presented with only the crude extract showing a larger amount of cytotoxicity (~12% reduction), with minimal to no cytotoxicity exhibited by the fractions (**Figure 3-11 A**). Increasing cytoprotection was seen through F2 – F5, with F5 displaying the highest cytoprotection at 24% (**Figure 3-11 B**). *C. molle* (Combretaceae) F5 produced a significant reduction in cell density (42.93%, $p < 0.005$) (**Figure 3-12 A**). No significant cytoprotection was seen after 6-OHDA induced cell death (**Figure 3-12 B**). No fractions of *C. orbiculata* (Crassulaceae) improved cell density after exposure to 6-OHDA (**Figure 3-13 A)** or altered cell density after naïve exposure (**Figure 3-13 B**).

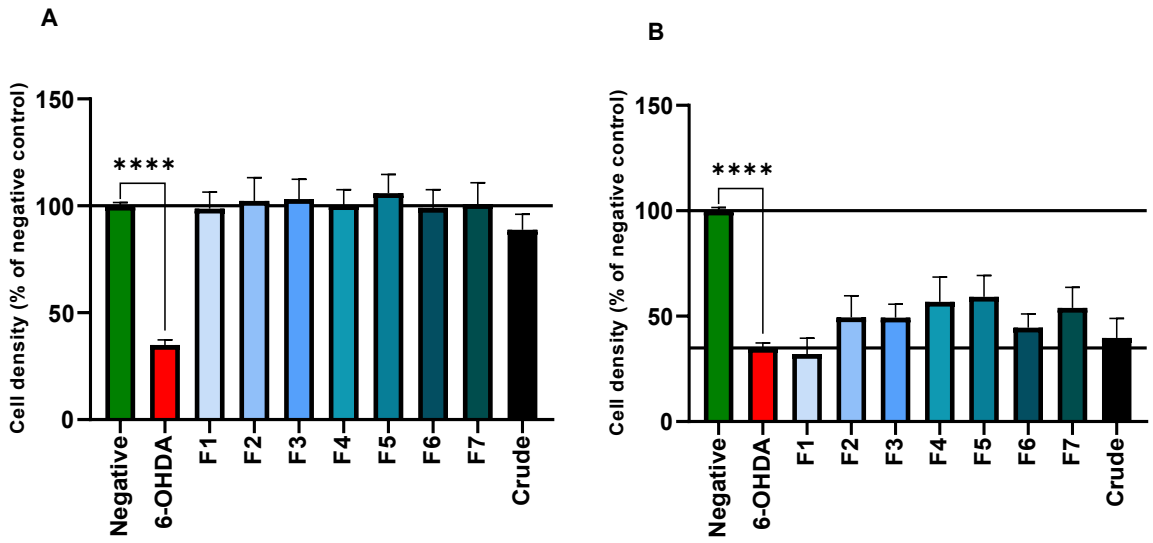

Figure 3-11: The effect of the crude extract and fractions of *Jasminum abyssinicum* on SH-SY5Y cell density alone (A) or induction of 6-hydroxydopamine (6-OHDA)-mediated cytotoxicity (B) after 48 h exposure. Significance was determined using a Kruskal-Wallis with post-hoc Dunn's test between the crude extract or fraction relative to the negative control (A) or 6-OHDA (B). ****: $p < 0.0001$

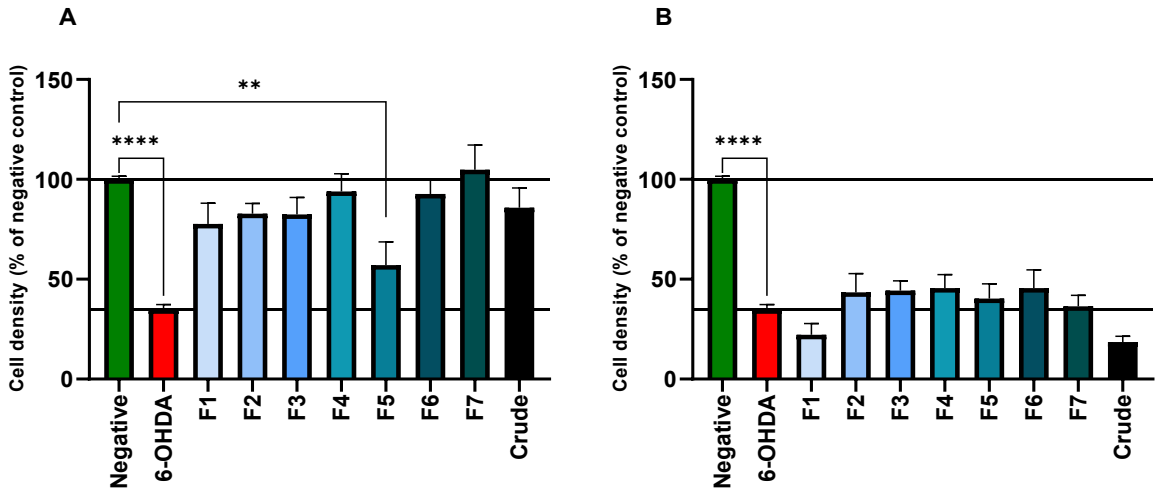

Figure 3-12: The effect of the crude extract and fractions of *Combretum molle* on SH-SY5Y cell density alone (A) or induction of 6-hydroxydopamine (6-OHDA)-mediated cytotoxicity (B) after 48 h exposure. Significance was determined using a Kruskal-Wallis with post-hoc Dunn's test between the crude extract or fraction relative to the negative control (A) or 6-OHDA (B). ** $p < 0.01$; ****: $p < 0.0001$

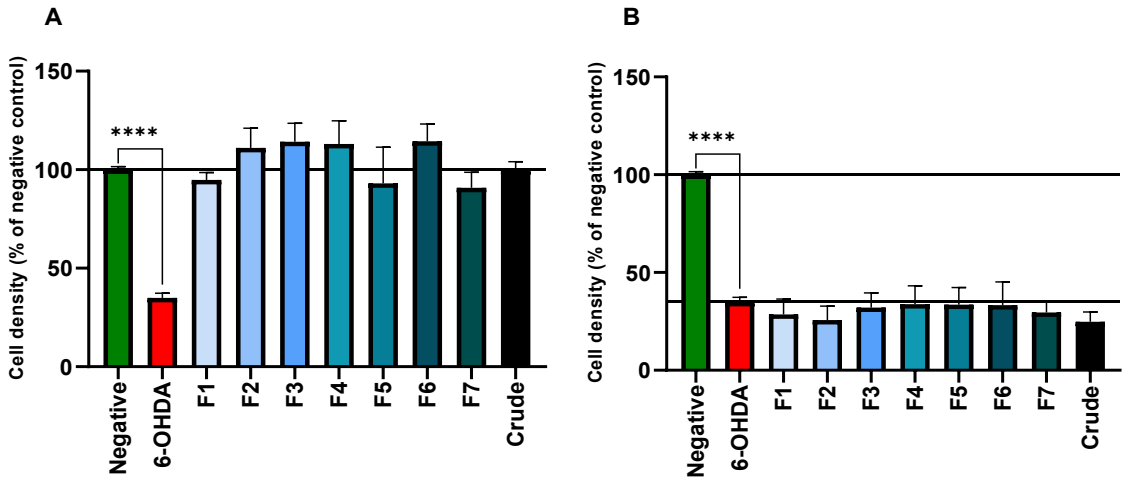

Figure 3-13: The effect of the crude extract and fractions of *Cotyledon orbiculata* on SH-SY5Y cell density alone (A) or induction of 6-hydroxydopamine (6-OHDA)-mediated cytotoxicity (B) after 48 h exposure. Significance was determined using a Kruskal-Wallis with post-hoc Dunn's test between the crude extract or fraction relative to the negative control (A) or 6-OHDA (B). ****: $p < 0.0001$

Dioscorea sylvatica (family Dioscoreaceae) fractions did not alter cell density significantly after exposure to 6-OHDA **(Figure 3-14 B)** or altered cell density after naïve exposure **(Figure 3-14 A)**. The IC_{50} from literature supports the lack of activity, with values of 27.9 and 22.1 µg/mL in the HeLa cell line form MeOH and chloroform crude extracts, respectively (**Table 3-5**).[519]

Acalypha villicaulis, *C. sylvaticus* and *E. milli* are from the Euphorbiaceae family. *Acalypha villicaulis* presented negligible cytotoxicity after 48 h **(Figure 3-15 A)**. An increase in cell density was seen in F3 – F5, possibly corresponding with the polarity changes, with F5 presenting non-significant cytoprotection at 23.35% increase in cell density after 6-OHDA exposure **(Figure 3-15 B)**. Fractions of *C. sylvaticus* did not present with significant cytotoxicity but presented with a non-significant increase of cell densities after naïve exposure **(Figure 3-16 A)**. No significant cytoprotection was seen after 6-OHDA exposure for 48 h after for all fractions of *C. sylvaticus* **(Figure 3-16 B)**.

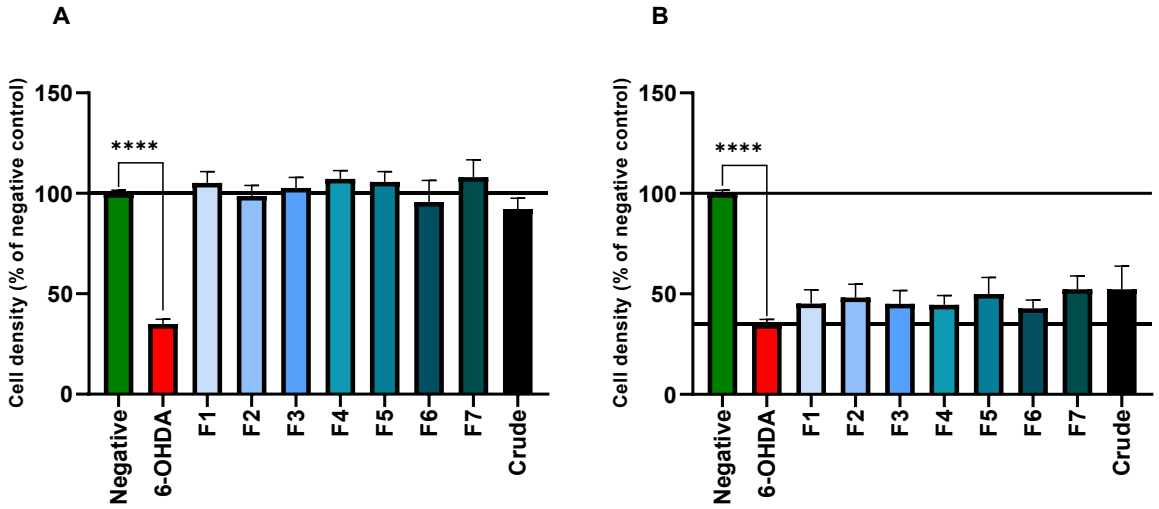

Figure 3-14: The effect of the crude extract and fractions of *Dioscorea sylvatica* on SH-SY5Y cell density alone (A) or induction of 6-hydroxydopamine (6-OHDA)-mediated cytotoxicity (B) after 48 h exposure. Significance was determined using a Kruskal-Wallis with post-hoc Dunn's test between the crude extract or fraction relative to the negative control (A) or 6-OHDA (B). ****: $p < 0.0001$

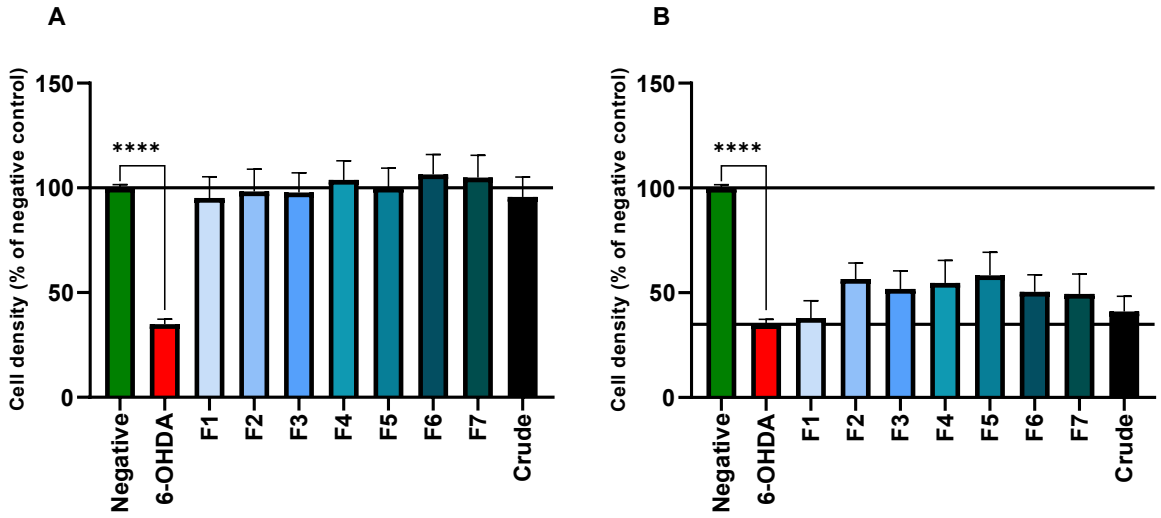

Figure 3-15: The effect of the crude extract and fractions of *Acalypha villicaulis* on SH-SY5Y cell density alone (A) or induction of 6-hydroxydopamine (6-OHDA)-mediated cytotoxicity (B) after 48 h exposure. Significance was determined using a Kruskal-Wallis with post-hoc Dunn's test between the crude extract or fraction relative to the negative control (A) or 6-OHDA (B). ****: $p < 0.0001$

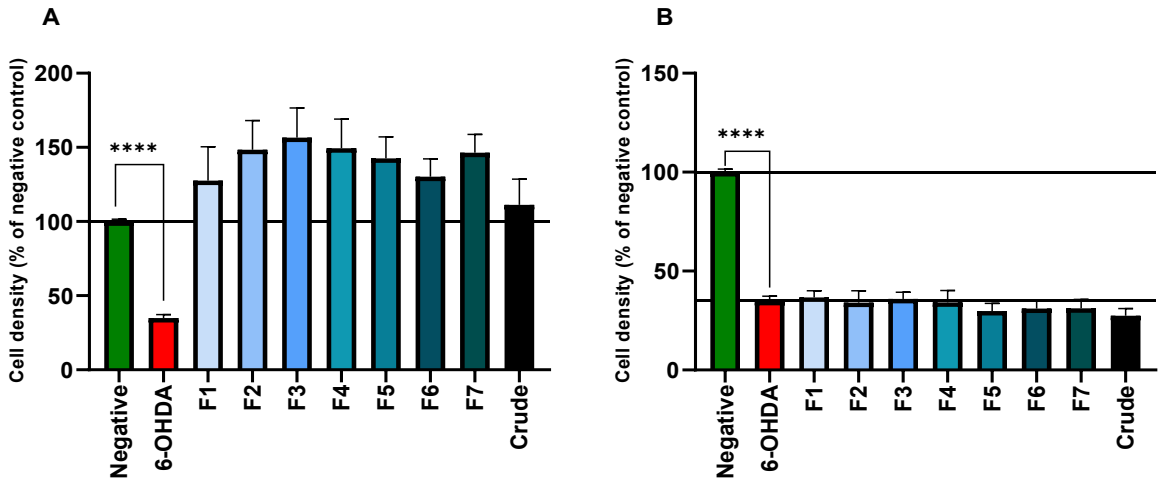

Figure 3-16: The effect of the crude extract and fractions of *Croton sylvaticus* on SH-SY5Y cell density alone (A) or induction of 6-hydroxydopamine (6-OHDA)-mediated cytotoxicity (B) after 48 h exposure. Significance was determined using a Kruskal-Wallis with post-hoc Dunn's test between the crude extract or fraction relative to the negative control (A) or 6-OHDA (B). ****: $p < 0.0001$

Like *C. sylvaticus*, *E. milii* showed no significant cell density increases after 6-OHDA exposure **(Figure 3-17 B)**. Cytotoxicity was also negligible as no significant decreases in cell density was observed. All fractions, however, resulted in increase in cell density over all fractions **(Figure 3-17 A)**. The fractions of *S. brachypetala* (family Fabaceae) did not present with any significant decrease in SH-SY5Y cell density after 48h, but all fractions, except F7, increased cell density **(Figure 3-18 A)**. Fractions 1, 2 and 4 improved cell density after 6-OHDA exposure by 25%, 29%, and 32%, respectively. Fraction 3 significantly increased cell density after 6-OHDA exposure by 27% ($p < 0.05$) **(Figure 3-18 B)**. Both *L. leonurus* and *M. longifolia* subsp. *polydena* are from the Lamiaceae family. The fractions of *L. leonurus* did not present with any significant changes in cell densities after naïve exposure, with an increase in cell density seen after 48 h **(Figure 3-19 A)**. None of the fractions presented any cytoprotection, with the cytotoxicity from 6-OHDA being compounded after 48 h **(Figure 3-19 B)**. *M. longifolia polydena* F1 – F6 showcased negligible cytotoxicity, but F7 and the crude extracts did reduce cell density by 51% and 14% respectively **(Figure 3-20 A)**. All fractions did not present with any cytoprotection after 48 h **(Figure 3-20 B)**. This coincides with literature, where an EtOH extract did not protect PC12 cells after H_2O_2 exposure (**Table 3-5**).[542]

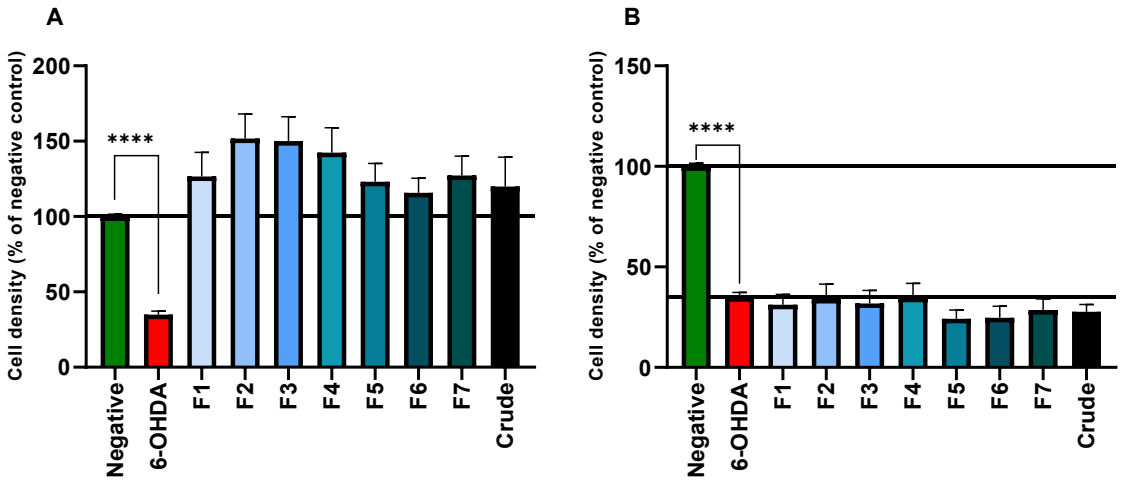

Figure 3-17: The effect of the crude extract and fractions of *Euphorbia milii* on SH-SY5Y cell density alone (A) or induction of 6-hydroxydopamine (6-OHDA)-mediated cytotoxicity (B) after 48 h exposure. Significance was determined using a Kruskal-Wallis with post-hoc Dunn's test between the crude extract or fraction relative to the negative control (A) or 6-OHDA (B). ****: $p < 0.0001$

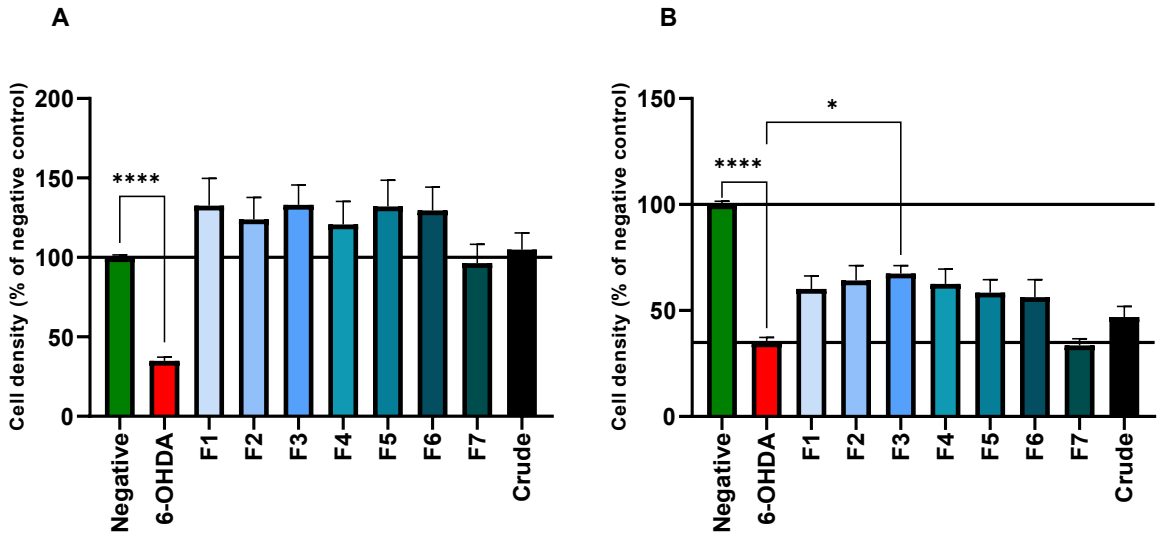

Figure 3-18: The effect of the crude extract and fractions of *Schotia brachypetala* on SH-SY5Y cell density alone (A) or induction of 6-hydroxydopamine (6-OHDA)-mediated cytotoxicity (B) after 48 h exposure. Significance was determined using a Kruskal-Wallis with post-hoc Dunn's test between the crude extract or fraction relative to the negative control (A) or 6-OHDA (B). *: p <0.05, ****: p < 0.0001

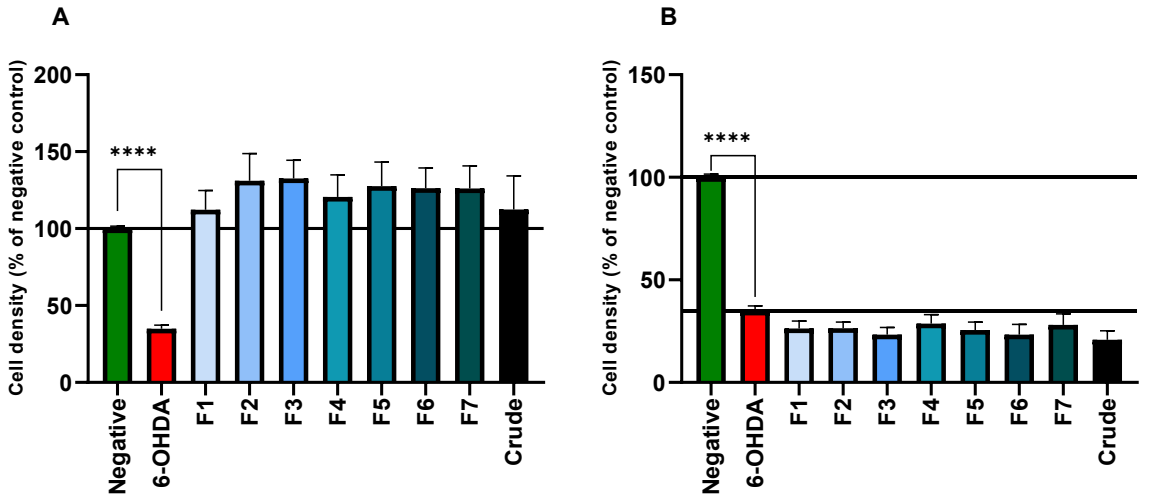

Figure 3-19: The effect of the crude extract and fractions of *Leonotis leonurus* on SH-SY5Y cell density alone (A) or induction of 6-hydroxydopamine (6-OHDA)-mediated cytotoxicity (B) after 48 h exposure. Significance was determined using a Kruskal-Wallis with post-hoc Dunn's test between the crude extract or fraction relative to the negative control (A) or 6-OHDA (B). ****: p < 0.0001

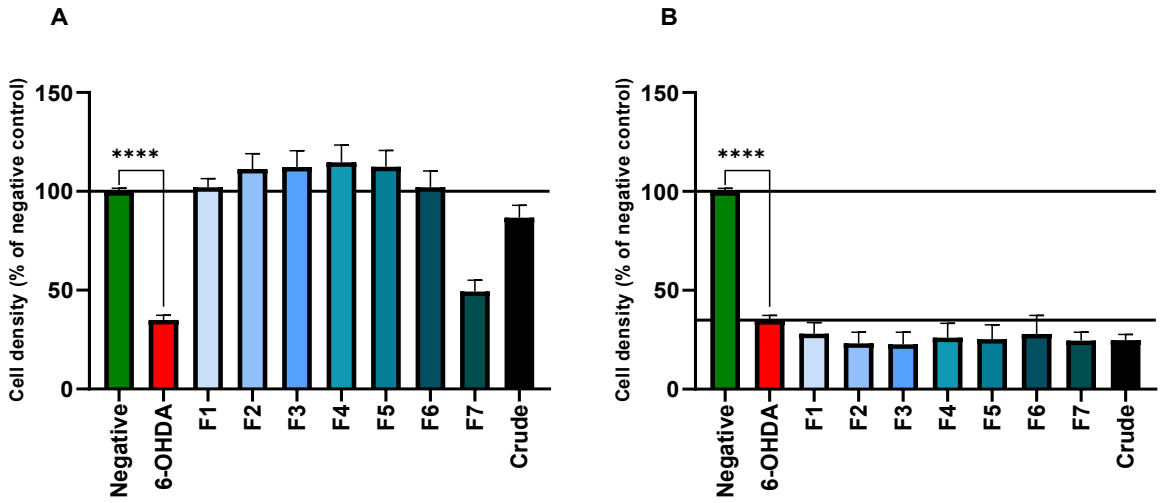

Figure 3-20: The effect of the crude extract and fractions of Mentha longifolia subsp. polydena on SH-SY5Y cell density alone (A) or induction of 6-hydroxydopamine (6-OHDA)-mediated cytotoxicity (B) after 48 h exposure. Significance was determined using a Kruskal-Wallis with post-hoc Dunn's test between the crude extract or fraction relative to the negative control (A) or 6-OHDA (B). ****: $p < 0.0001$

All fractions of *P. virgata* (family Polygalaceae) exhibited minimal cytotoxicity while promoting an increase in cell density. **(Figure 3-21 A)**. *P. virgata* has shown the largest increases in cell densities after 6-OHDA exposure over 48 h. Fractions 3 to 6 have increased cell densities by 31.14%, 28.08%, 30.72% ($p < 0.05$), 40.58% ($p < 0.005$) and 28.86%, respectively. Whilst all fractions do show cytoprotection, but the more organic F3 - F6 proved the most impactful on cytoprotection **(Figure 3-21 B)**. *A. procumbens* (family Scrophulariaceae) presented with a mixed cytotoxic response, whilst F1 – F6 exhibited no cytotoxic response, F6 – F7 and the crude extract lowered cell density by 72% ($p < 0.0001$), 19% and 44% ($p < 0.05$) respectively **(Figure 3-22 A)**. The change in response between the fractions does indicate some cytotoxic compounds were removed from the aqueous fractions during the fractionation process. The response after 6-OHDA shows an increase in cell density throughout F1 – F4, with F4 presenting with a significant increase in cell density (32%, $p < 0.05$). As seen with the cytotoxic response, F6 – F7 and the crude extract shows minimal to no cytoprotection after 48 h **(Figure 3-22 B)**.

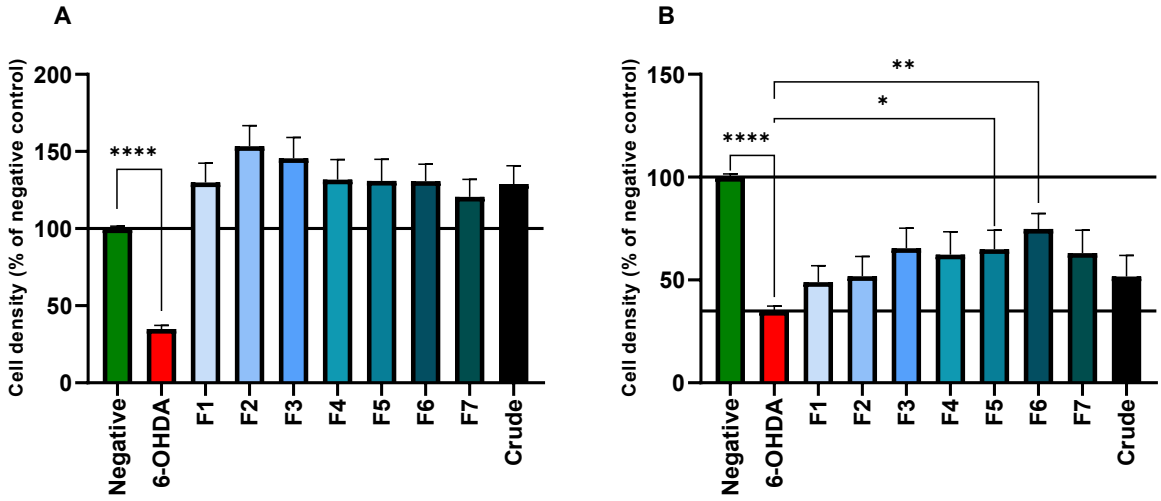

Figure 3-21: The effect of the crude extract and fractions of *Polygala virgata* on SH-SY5Y cell density alone (A or induction of 6-hydroxydopamine (6-OHDA)-mediated cytotoxicity (B) after 48 h exposure. Significance was determined using a Kruskal-Wallis with post-hoc Dunn's test between the crude extract or fraction relative to the negative control (A) or 6-OHDA (B). *: p <0.05, ** p < 0.01, ****: p < 0.0001

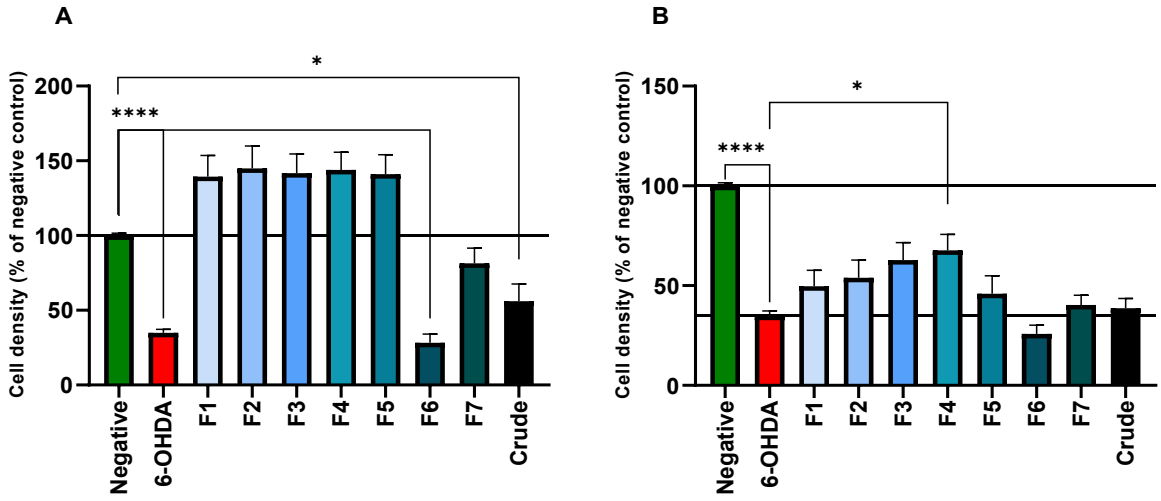

Figure 3-22: The effect of the crude extract and fractions of *Aptosimum procumbens* on SH-SY5Y cell density alone (A) or induction of 6-hydroxydopamine (6-OHDA)-mediated cytotoxicity (B) after 48 h exposure. Significance was determined using a Kruskal-Wallis with post-hoc Dunn's test between the crude extract or fraction relative to the negative control (A) or 6-OHDA (B). *: p <0.05, ****: p < 0.0001

D. stramonium, from the Solanaceae family, showcased negligible cytotoxicity thought all fractions and the crude extract, with cell density increases seen in F2 – F7 **(Figure 3-23 A)**. No cytoprotection is seen in any fraction or the crude extract after 48 h exposure to 6-OHDA **(Figure 3-23 B)**. All fractions and the crude extract of *W. somnifera* (family Solanaceae) presented with no reduction in cell density after naïve exposure, with an increase in cell density seen in all fractions **(Figure 3-24 A)**. Fraction 3 presents with the highest cytoprotection, with a non-significant increase in cell density of ~ 16% after 6-OHDA exposure **(Figure 3-24 B)**. Studies with the chloroform and MeOH combined extract did show neuroprotection in the 6-OHDA SH-SY5Y cell line, where at 20 µg/mL did show a total reduction in apoptotic body formation (**Table 3-5**).[554] *L. javanica* F5 – F6 and the crude fraction completely decimated cell density by more than 90% ($p < 0.0001$) after 48 h **(Figure 3-25 A)** and after 6-OHDA exposure **(Figure 3-25 B)**. Minimal to no cytoprotection was offered, with only F2 and F3 presenting with a non-significant cell density increase of 15% and 11% respectively **(Figure 3-25 B)**. *L. javanica* is the only plant from the Verbenaceae family.

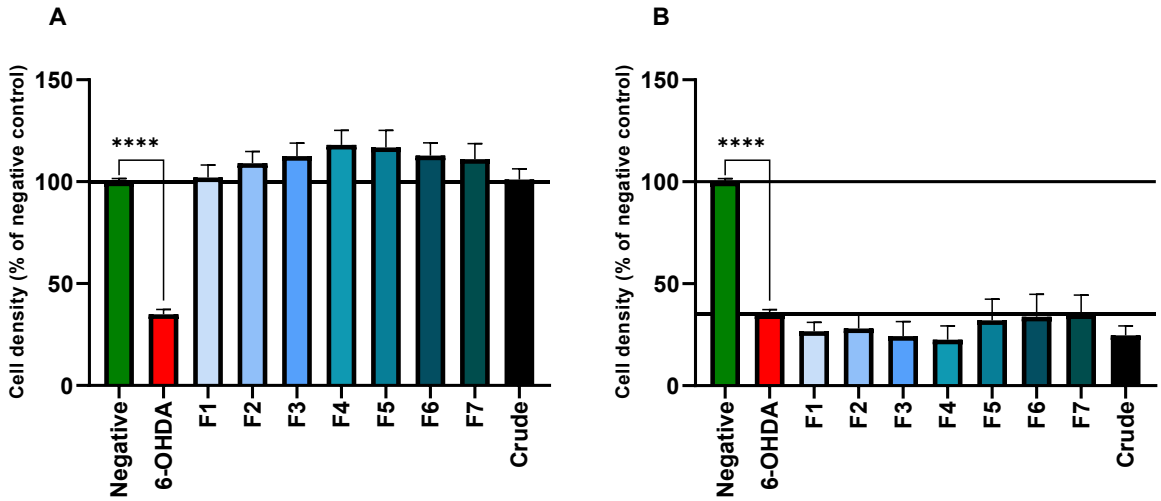

Figure 3-23: The effect of the crude extract and fractions of *Datura stramonium* on SH-SY5Y cell density alone (A) or induction of 6-hydroxydopamine (6-OHDA)-mediated cytotoxicity (B) after 48 h exposure. Significance was determined using a Kruskal-Wallis with post-hoc Dunn's test between the crude extract or fraction relative to the negative control (A) or 6-OHDA (B). ****: $p < 0.0001$

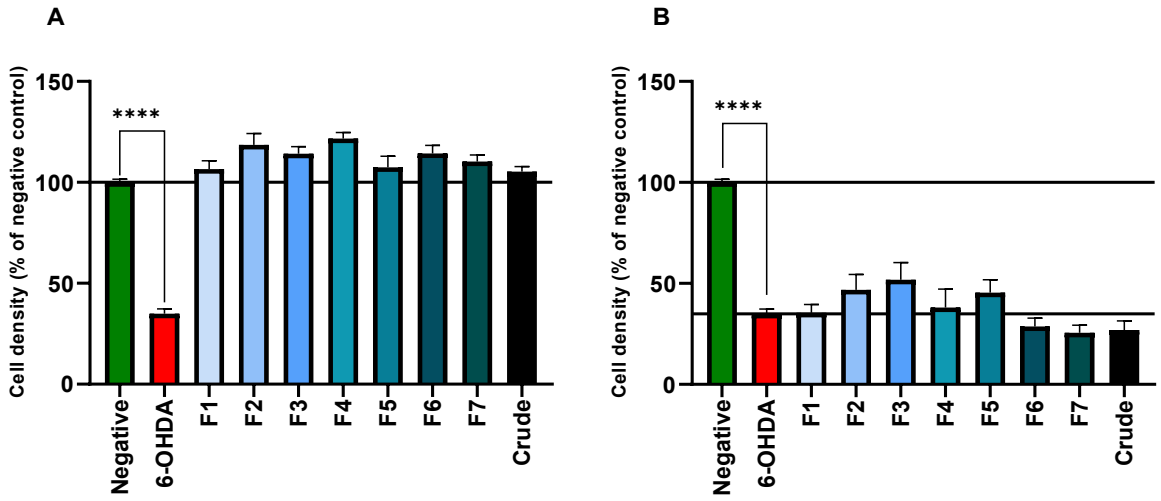

Figure 3-24: The effect of the crude extract and fractions of *Withania somnifera* on SH-SY5Y cell density alone (A) or induction of 6-hydroxydopamine (6-OHDA)-mediated cytotoxicity (B) after 48 h exposure. Significance was determined using a Kruskal-Wallis with post-hoc Dunn's test between the crude extract or fraction relative to the negative control (A) or 6-OHDA (B). ****: $p < 0.0001$

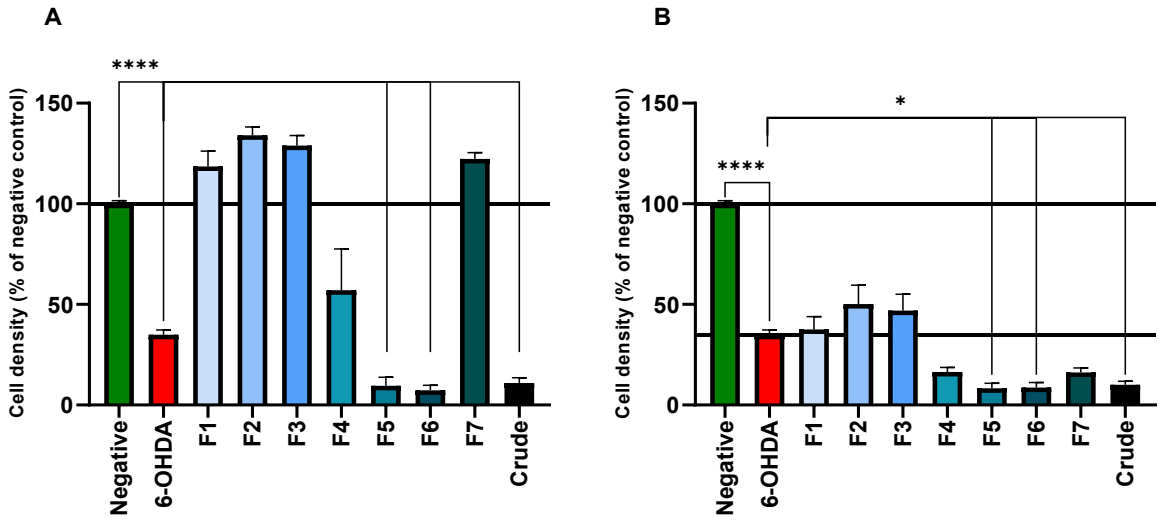

Figure 3-25: The effect of the crude extract and fractions of *Lippia. javanica* on SH-SY5Y cell density alone (A or induction of 6-hydroxydopamine (6-OHDA)-mediated cytotoxicity (B) after 48 h exposure. Significance was determined using a Kruskal-Wallis with post-hoc Dunn's test between the crude extract or fraction relative to the negative control (A) or 6-OHDA (B). *: $p < 0.05$, ****: $p < 0.0001$

Table 3-6: The effect of the fractions and crude extract on cell density on 6-hydroxydopamine (6-OHDA)-naïve and 6-OHDA-exposed cells after 48 h treatment. The negative control and 6-OHDA (35 µM) expressed a cell density of 100% ± 1.62 (n = 66) and 35% ± 2.27 (n = 66) respectively. Statistical significance was determined relative to the negative (for naïve cells) or 6-OHDA (for exposed cells) controls.

Plants		**Cell density (% relative to negative control) ± SEM**							
		F1	**F2**	**F3**	**F4**	**F5**	**F6**	**F7**	**Crude**
Amaryllidaceae									
B. disticha	Exposed	23.1 ± 4.36	46.04 ± 5.55	32.9 ± 6.69	38.89 ± 5.02	31.28 ± 5.61	55.94 ± 6.41	52.49 ± 4.42	31.76 ± 7.38
	Naïve	106 ± 3.62	68.74 ± 6.60	49.43 ± 4.27	50.67 ± 4.14	49.66 ± 4.90	114.50 ± 6.65	103.3 ± 3.71	73.64 ± 5.65
Anacardiaceae									
L. discolor	Exposed	60.00 ± 4.33	40.54 ± 4.25	43.24 ± 4.33	44.92 ± 4.44	48.4 ± 4.62	46.66 ± 5.85	46.05 ± 3.01	46.16 ± 6.46
	Naïve	93.50 ± 9.93	95.56 ± 15.98	114.70 ± 12.07	112.70 ± 11.37	103.20 ± 9.42	118.90 ± 11.90	112.80 ± 9.29	90.11 ± 7.35
M. indica	Exposed	24.57 ± 5.89	38.88 ± 7.99	37.05 ± 8.04	41.76 ± 6.00	44.75 ± 12.91	49.26 ± 12.10	49.35 ± 10.22	24.38 ± 6.69
	Naïve	77.40 ± 4.22	98.56 ± 4.06	100.80 ± 6.87	113.60 ± 7.97	117.5 ± 10.33	112.00 ± 8.39	119.20 ± 8.16	101.00 ± 4.48
Apocyneceae									
A. oppositifolia	Exposed	40.77 ± 7.25	51.92 ± 11.23	57.66 ± 11.69	42.31 ± 6.43	38.92 ± 4.99	44.58 ± 7.66	41.68 ± 8.71	35.48 ± 5.99
	Naïve	122.60 ± 3.26	131.00 ± 5.62	121.70 ± 6.91	70.62 ± 3.88	64.06 ± 5.28	120.30 ± 7.17	124.90 ± 3.99	97.32 ± 6.54
G. physocarpus	Exposed	29.19 ± 5.58	43.98 ± 4.34	44.1 ± 4.81	45.51 ± 2.97	36.21 ± 5.77	49.26 ± 5.12	46.45 ± 7.11	38.96 ± 4.69
	Naïve	100.30 ± 4.84	107.40 ± 4.19	97.63 ± 6.02	44.51 ± 5.35	32.27 ± 6.68	75.44 ± 6.92	96.41 ± 4.86	65.56 ± 3.96
X. undulatum	Exposed	30.01 ± 5.42	43.83 ± 48.97	44.33 ± 10.25	39.56 ± 8.15	34.33 ± 7.15	34.53 ± 7.26	43.25 ± 7.89	28.59 ± 3.23
	Naïve	105.90 ± 5.55	121.70 ± 4.35	118.30 ± 3.82	57.66 ± 3.81	59.88 ± 2.19	102.70 ± 5.85	97.55 ± 4.93	36.65 ± 3.11
Asphodelaceae									
B. latifolia	Exposed	54.9 ± 4.38	56.22 ± 7.30	69.34 ± 11.11	54.61 ± 7.48	60.21 ± 9.27	46.71 ± 5.87	51.56 ± 4.81	46.97 ± 2.93
	Naïve	133.7 ± 23.32	148.00 ± 25.28	146.70 ± 18.77	145.20 ± 21.83	150.2 ± 19.80	117.3 ± 14.19	135.30 ± 17.83	114.70 ± 14.94
Asteraceae									
A. arctotoides	Exposed	26.23 ± 4.26	32.95 ± 8.17	26.98 ± 5.82	29.55 ± 7.48	27.76 ± 7.07	28.52 ± 8.09	27.62 ± 5.52	17.67 ± 2.14
	Naïve	93.99 ± 10.01	104.10 ± 7.60	104.20 ± 10.04	100.70 ± 8.10	37.28 ± 7.81	100.40 ± 11.54	107.30 ± 9.39	80.82 ± 7.50

V. myriantha	Exposed	40.58 ± 5.34	37.65 ± 5.54	39.64 ± 4.45	39.74 ± 7.56	49.99 ± 8.49	35.88 ± 6.59	37.09 ± 6.28	39.75 ± 7.43
	Naïve	116.90 ± 13.08	139.30 ± 19.06	154.30 ± 20.66	144.90 ± 15.42	154.00 ± 21.34	133.10 ± 12.83	137.30 ± 15.76	120.10 ± 19.19
Oleaceae									
J. abyssinicum	Exposed	32.11 ± 7.39	49.49 ± 10.22	49.33 ± 6.37	56.82 ± 11.69	59.23 ± 10.05	44.59 ± 6.52	53.97 ± 9.70	39.68 ± 9.26
	Naïve	98.65 ± 7.74	102.30 ± 10.95	103.10 ± 9.29	100.40 ± 7.15	105.90 ± 8.80	99.04 ± 8.52	100.80 ± 9.93	88.75 ± 7.28
Combretaceae									
C. molle	Exposed	22.22 ± 5.62	43.45 ± 9.35	44.30 ± 4.83	45.60 ± 6.69	40.37 ± 7.29	45.56 ± 9.18	36.39 ± 5.58	18.52 ± 2.93
	Naïve	77.63 ± 10.48	82.87 ± 5.00	82.38 ± 8.51	93.93 ± 8.92	57.07 ± 11.60	92.70 ± 6.95	104.80 ± 12.35	85.85 ± 9.86
Crassulaceae									
C. orbiculata	Exposed	28.53 ± 7.85	25.66 ± 7.09	32.02 ± 7.53	33.77 ± 9.46	33.59 ± 8.73	33.32 ± 11.91	29.53 ± 5.25	24.86 ± 4.98
	Naïve	94.87 ± 3.75	111.10 ± 10.01	114.20 ± 9.44	113.10 ± 11.65	93.11 ± 18.40	114.5 ± 8.65	90.78 ± 7.94	99.81 ± 4.31
Dioscoreaceae									
D. sylvatica	Exposed	45.16 ± 6.90	48.13 ± 6.66	45.10 ± 6.54	44.53 ± 4.61	49.97 ± 8.25	42.87 ± 4.05	52.34 ± 6.57	52.29 ± 11.48
	Naïve	105.20 ± 5.64	98.65 ± 5.30	102.70 ± 5.22	107.10 ± 4.15	105.70 ± 5.11	95.67 ± 10.75	108.00 ± 8.66	92.24 ± 5.35
Euphorbiaceae									
A. villicaulis	Exposed	37.91 ± 8.31	56.54 ± 7.62	51.76 ± 8.65	54.68 ± 10.80	58.36 ± 10.98	50.41 ± 8.19	49.39 ± 9.51	41.06 ± 7.22
	Naïve	95.21 ± 10.05	98.29 ± 10.63	97.80 ± 9.44	103.80 ± 9.08	100.10 ± 9.36	106.40 ± 9.58	104.90 ± 10.72	95.74 ± 9.41
C. sylvaticus	Exposed	36.65 ± 3.39	34.06 ± 5.99	35.95 ± 3.34	34.24 ± 5.96	29.85 ± 3.89	31.03 ± 4.34	31.23 ± 4.47	27.43 ± 3.62
	Naïve	127.60 ± 22.84	148.40 ± 19.65	156.50 ± 20.07	149.50 ± 19.57	142.60 ± 14.46	130.30 ± 11.93	146.40 ± 12.46	111.20 ± 17.38
E. milii	Exposed	31.19 ± 5.16	34.01 ± 7.42	31.84 ± 6.47	34.72 ± 7.08	24.21 ± 4.42	24.71 ± 5.69	28.51 ± 5.58	27.69 ± 3.58
	Naïve	126.60 ± 16.10	151.80 ± 16.32	150.10 ± 16.13	142.30 ± 16.58	123.10 ± 12.19	115.70 ± 9.69	127.20 ± 12.80	120.00 ± 19.43
Fabaceae									
S. brachypetala	Exposed	60.14 ± 6.13	64.22 ± 6.92	67.42 ± 3.74	62.50 ± 7.11	58.38 ± 6.23	56.33 ± 8.19	33.51 ± 3.19	46.98 ± 4.98
	Naïve	132.60 ± 17.17	124.00 ± 13.74	133.00 ± 12.62	120.70 ± 14.55	132.10 ± 16.48	129.60 ± 14.64	96.46 ± 11.81	104.90 ± 10.47
Lamiaceae									
L. leonurus	Exposed	26.33 ± 3.67	26.43 ± 2.98	23.34 ± 3.50	28.68 ± 4.43	25.52 ± 3.85	23.26 ± 5.06	28.04 ± 5.45	20.81 ± 4.37
	Naïve	112.3 ± 12.37	131.00 ± 17.69	132.60 ± 11.73	120.60 ± 14.32	127.60 ± 15.64	126.30 ± 13.06	126.10 ± 14.65	112.50 ± 21.68
	Exposed	28.05 ± 5.69	23.20 ± 5.57	22.73 ± 6.05	26.10 ± 7.24	25.25 ± 7.26	27.95 ± 9.32	24.54 ± 4.28	24.75 ± 2.97

M. longifolia subsp. polydena	Naïve	102.10 ± 4.38	111.30 ± 7.75	112.30 ± 8.20	114.70 ± 8.67	112.40 ± 8.28	102.10 ± 8.18	49.33 ± 5.70	86.64 ± 6.24
Polygalaceae									
P. virgata	Exposed	48.98 ± 7.98	51.80 ± 9.68	65.38 ± 9.86	62.32 ± 11.13	64.96 ± 9.23	74.82 ± 7.45	63.10 ± 11.10	51.71 ± 10.26
	Naïve	129.90 ± 12.50	153.40 ± 13.40	145.60 ± 13.44	131.80 ± 13.07	130.80 ± 14.06	130.80 ± 10.90	120.60 ± 11.34	129.00 ± 11.78
Scrophulariaceae									
A. procumbens	Exposed	49.68 ± 8.06	53.97 ± 8.78	62.82 ± 8.71	67.64 ± 8.07	45.88 ± 9.09	25.79 ± 4.38	40.26 ± 4.87	38.67 ± 4.88
	Naïve	139.40 ± 14.17	144.90 ± 15.09	141.70 ± 12.89	143.90 ± 11.86	141.10 ± 13.02	28.19 ± 5.95	81.43 ± 10.17	56.03 ± 11.57
Solanaceae									
D. stramonium	Exposed	26.63 ± 4.41	28.10 ± 7.26	24.34 ± 7.08	22.51 ± 6.83	32.08 ± 10.37	33.78 ± 11.07	34.94 ± 9.51	24.69 ± 4.67
	Naïve	102.00 ± 6.18	109.10 ± 5.69	112.50 ± 6.39	118.10 ± 7.10	116.90 ± 8.28	112.90 ± 6.15	111.10 ± 7.59	101.10 ± 5.22
W. somnifera	Exposed	35.38 ± 4.21	46.80 ± 7.67	51.76 ± 8.59	38.05 ± 9.14	45.47 ± 6.34	28.64 ± 4.20	25.62 ± 3.71	26.89 ± 4.55
	Naïve	106.60 ± 4.15	118.60 ± 5.59	114.20 ± 3.57	121.70 ± 2.99	107.40 ± 5.48	114.30 ± 3.97	110.30 ± 3.24	105.30 ± 2.56
Verbenaceae									
L. javanica	Exposed	37.53 ± 6.38	50.14 ± 9.40	46.88 ± 8.14	16.49 ± 2.23	8.34 ± 2.46	8.74 ± 2.42	16.18 ± 2.28	10.07 ± 1.73
	Naïve	118.50 ± 7.68	134.10 ± 4.11	128.90 ± 5.03	57.08 ± 20.52	9.62 ± 4.21	7.34 ± 2.46	122.40 ± 3.13	10.99 ± 2.62

3.4.4 Selection of plant fractions for cellular mechanistic assays

Fractions of the plants were selected for further study based on two criteria; < 10% reduction in cell density after naïve exposure to the fraction or crude extract, and > 60% final cell density after exposure to 6-OHDA with cytoprotection observed. Fourteen fractions from five plant species that met the criteria, except for *A. oppositifolia* F3, which was chosen based of previous studies conducted on the same plant sample **(Table 3-7)**.

Table 3-7: Plant fractions selected*** for subjection to mechanistic cell-based assays.

Format	Plant	Cell densities as per treatment group (% cell density compared to negative control)						
		F1	F2	F3	F4	F5	F6	F7
Exposed to 6-OHDA	*A. oppositifolia***			57.66				
Reduction in 6-OHDA-induced cytotoxicity				23.42				
Naïve*				121.70				
Exposed to 6-OHDA	*A. procumbens*			62.82	67.64			
Reduction in 6-OHDA-induced cytotoxicity				28.58	33.4			
Naïve*				141.70	143.90			
Exposed to 6-OHDA	*B. latifolia*			69.34		60.21		
Reduction in 6-OHDA-induced cytotoxicity				35.10		25.97		
Naïve*				146.70		150.20		
Exposed to 6-OHDA	*P. virgata*			65.38	62.32	64.96	74.82	63.10
Reduction in 6-OHDA-induced cytotoxicity				31.14	28.08	30.72	40.58	28.86
Naïve*				145.60	131.80	130.80	130.80	120.60
Exposed to 6-OHDA	*S. brachypetala*	60.14	64.22	67.42	62.5			
Reduction in 6-OHDA-induced cytotoxicity		25.90	29.98	33.18	28.26			
Naïve*		132.6	124.00	133.00	120.70			

*Naïve cells were not exposed to 6-OHDA
** Selected based of previous studies on same plant material
***Selected for further study based on two criteria; < 10% reduction in cell density after naïve exposure to the fraction or crude extract, and > 60% final cell density after exposure to 6-OHDA with cytoprotection observed

3.4.5 Acellular assays

3.4.5.1 Antioxidant activity

A standard curve was constructed for $FeSO_4$ between 0 and 1,000 µM, and the absorbance plotted against the concentration **(Figure 3-26).** The $FeSO_4$ standard curve indicated high linearity (r^2 = 0.9925) as was used to interpolate the equivalence of activity for all plant fractions at 10 µg/mL.

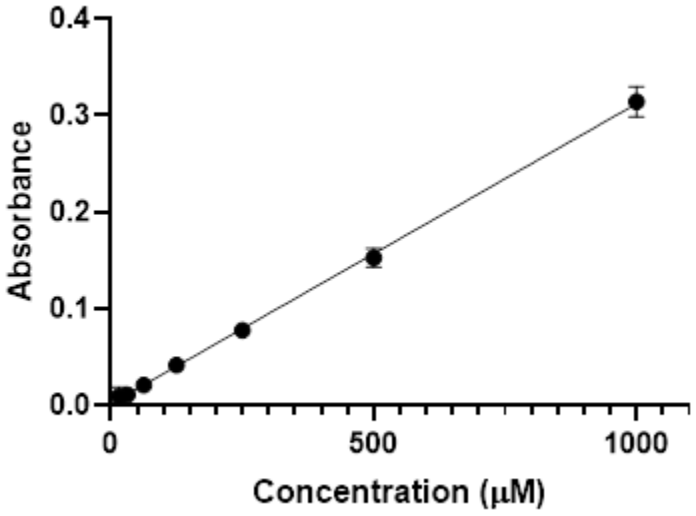

Figure 3-26: Standard curve of ferrous sulphate as measured by the ferric reduction antioxidant power (FRAP) assay. Each value represents absorbance ± SEM, n = 9.

Twenty-seven of the 192 fractions and extracts presented with FRAP values >100 µmol $FeSO_4$ equivalence/g extract **(Table 3-8)**. The fractions with the highest activity included *L. discolor* F2, F4, F5 and F3 between (384.95, 283.76, 233.05 and 217.73 µmol $FeSO_4$ equivalence/g extract, respectively). *L. discolor* was previously found to also precipitate hight FRAP values attributed to high polyphenolic contents of the bark of the plant (**Table 3-5**).[408] *A. oppositifolia* F3 and F4 displayed 255.08 and 182.87 µmol $FeSO_4$ equivalence/g extract, respectively. Previous studies on the antioxidant properties of *A. oppositifolia* methanol stem extract yielded a FRAP value of 301.21 µmol Fe(II)/g.[491] Fractions 1, 3, 4, and 5 (127.68, 195.25, 144.23, and 109.55 µmol $FeSO_4$ equivalence/g, respectively) of *M. indica* presented with high activity. This could possibly be due to high counts of flavonoids typically found in the plant.[489] None of the crude extracts showed the

highest value of the plants, indicating the fractionation process did concentrate the phytochemical ratio to produce more potent fractions.

The increase in activity noted between the crude extracts and certain fractions, could be ascribed to the fact that fractions are isolated and concentrated, as seen in the difference between *A. oppositifolia* F3 (255.08 µmol $FeSO_4$ equivalence/g) and crude (79.59 µmol $FeSO_4$ equivalence/g), and *C. molle* F3 and F4 (230.13 and 211.56 µmol $FeSO_4$ equivalence/g) and the crude extract (59.03 µmol $FeSO_4$ equivalence/g). The change in ratio can then affect the antioxidant potency of the fractions or extract, as different ratios of antioxidant compounds can exert different responses.[559] The fractionation process appears to have extracted more water-soluble phytochemicals, which contain polyphenolics, flavonoids, and other known potent antioxidants. The use of a water/MeOH system can elucidate thus more water-soluble in the earlier fractions, and more lipid soluble antioxidants in the more organic fractions. Structural studies have shown that an increase in hydroxyl groups (-OH) on flavonoid structures improves antioxidant activity.[560] It can thus be postulated that these polar antioxidants have been concentrated in the more aqueous fractions of the crude extract. Fractionation has been demonstrated to enhance the concentration of total phenolics in a sample.[561]

No correlation between FRAP values and cytoprotection was found (r^2 = 0.0051). The aqueous solution in which the assay is performed is not comparable to a biological system,[562] thus complex interactions between the compounds and proteins, amino acids and cell structures are not taken into account.[563, 564] Amino acids like cysteine, methionine and alanine have been shown to possess antioxidant effects, and these effects might prove to act synergistically with phytochemicals.[565, 566]

The single electron transfer mechanism measured by ferrozine is typically observed in ionizing solvents (water, EtOH, and MeOH), where the antioxidant donates a proton, stabilising the radical within its molecular structure.[567] Electrophilic antioxidants (electron-rich) such as polyphenolics, flavonoids and multi-hydroxylated compounds will have a better reaction centre to quench ROS.[568] Within the mechanism of ferroptosis, lipid peroxidation plays a major role in cell death, and whilst the quenching of ROS can prohibit the initial formation of lipid peroxides, there is evidence of self-propagation of new ROS from peroxyl radicals.[569] The lipid, while electron rich due to unsaturated double bonds, temporarily stabilises the radical via addition to a carbon-carbon double bond, and after a reaction with oxygen, the double bond reforms and the radical is fragmented off after an intramolecular hydrogen atom abstraction.[570] This temporary stabilisation

could be enough for toxic byproducts to start forming, such as 4-HNE, which is downstream toxic to cells.[188] The testing of the fractions in a biological system will be more beneficial to prove a true antioxidant effect, when the multiple pathways that generate ROS is in play to establish not only a reduction is more biologically relevant oxidant species, but a synergism with different cellular bodies.

3.4.5.2 Chelation ability

A highly linear standard curve (r^2 = 0.9946) **(Figure 3-27)** was produced using EDTA concentrations ranging from 0 mg/mL to 400 mg/mL.

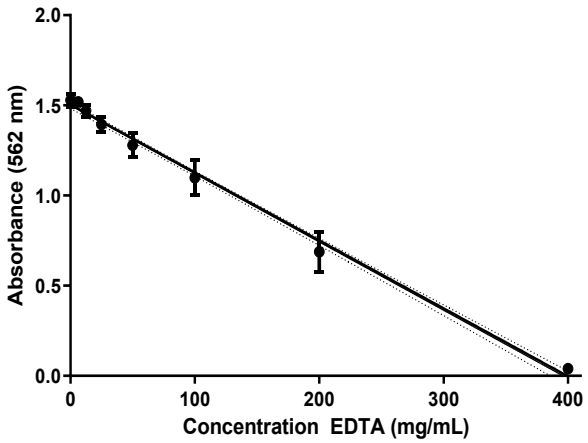

Figure 3-27: Ethylenediaminetetraacetic acid (EDTA) standard curve obtained by using ferrozine. Absorbance value ± SEM, n = 9.

None of the fractions or extracts presented with a chelation ability above 15% at 10 µg/mL **(Table 3-9)**. *D. sylvatica* F6 presented with the highest chelation ability at 15% reduction in total Fe^{2+}. The only plants with chelation ability in all fractions were *D. sylvatica* and *A. procumbens*. The more organic fractions (F4 – F7) of *D. stramonium* also presented with chelation ability above 10%. There was no correlation between chelation ability and cytoprotection (r^2 = 0.001979). Whilst the cytoprotection screening did not add additional iron into the media mixture, the lack of chelation implies that if Fe^{2+} was formed, it would not have been scrubbed. Thus, any reactions in the presence of Fe^{2+} would've been free to propagate. Literature on iron chelation reports very high IC_{50} values (> 1 mg/mL).[571, 572] With iron metabolism being complex and proteins used as storage mechanisms, reduction in Fe^{2+} within the biological system could be altered by phytochemical interactions with these storage vesicles and systems.[573]

As previously stated, acellular assays are not a true proxy for a biological system, with protein interactions contributing to cellular protection in the means of vesicles, enzymes, and other cellular bodies. Whilst the plants do show protection in a cellular model, the mechanism of these protections cannot be explained by a single point non-cellular assay. By focusing on the compounds that can be identified in the fractions, as well as the interaction of these compounds in a more complex system, a better picture of the mechanism of protection can be obtained.

Table 3-8: Antioxidant values of fractions and crude extracts as FRAP value (µmol $FeSO_4$ equivalence/g extract) ± SEM. n = 9.

FRAP activity (µmol $FeSO_4$ equivalence/g extract)								
Plants	**F1**	**F2**	**F3**	**F4**	**F5**	**F6**	**F7**	**Crude**
Amaryllidaceae								
B. disticha	ND	8.41 ± 1.31	7.35 ± 1.39	2.87 ± 1.62	17.89 ± 1.69	1.61 ± 1.21	1.89 ± 1.32	0.003 ± 1.29
Anacardiaceae								
L. discolor	28.49 ± 2.36	384.95 ± 13.2	217.73 ± 13.52	283.76 ± 9.42	233.05 ± 4.86	69.33 ± 7.99	11.67 ± 6.86	119.42 ± 13.02
M. indica	127.68 ± 14.22	24.60 ± 2.81	195.22 ± 16.42	144.21 ± 16.83	109.55 ± 8.81	28.933 ± 2.00	15.51 ± 1.55	154.62 ± 14.62
Apocyneceae								
A. oppositifolia	1.31 ± 1.21	126.95 ± 6.16	255.08 ± 14.00	182.87 ± 6.50	50.86 ± 2.82	7.39 ± 0.80	3.69 ± 1.40	79.59 ± 4.72
G. physocarpus	ND	4.768± 1.30	76.63 ± 1.85	75.61 ± 3.22	57.18 ± 2.23	10.55 ± 1.10	0.39 ± 1.28	10.55 ± 1.24
X. undulatum	ND	0.87 ± 1.26	12.54 ± 0.85	0.97 ± 1.38	1.80 ± 1.37	0.87 ± 1.61	0.14 ± 1.43	2.48 ± 1.73
Asphodelaceae								
B. latifolia	ND	38.65 ± 4.5	67.978± 3.92	101.67 ± 3.53	31.07 ± 5.86	7.92 ± 1.01	ND	13.52 ± 1.27
Asteraceae								
A. arctotoides	ND	10.84 ± 0.50	76.63 ± 3.89	101.43 ± 3.02	90.63 ± 12.84	50.47 ± 19.44	0.53 ± 0.45	31.31 ± 1.30
V. myriantha	12.30 ± 0.81	31.21 ± 1.61	85.72 ± 8.26	150.97 ± 4.03	83.14 ± 2.83	4.81 ± 0.71	1.21 ± 0.428	32.19 ± 1.42
Oleaceae								
J. abyssinicum	24.60 ± 2.09	51.64 ± 3.19	23.24 ± 0.78	52.22 ± 3.27	26.64 ± 1.09	2.14 ± 0.73	ND	47.60 ± 3.02
Combretaceae								
C. molle	19.79 ± 3.14	138.14 ± 14.65	230.13 ± 16.15	211.56 ± 12.05	106.87 ± 6.82	26.94 ± 2.00	13.32 ± 1.41	59.03 ± 3.38
Crassulaceae								
C. orbiculata	ND	12.40 ± 1.72	33.65 ± 4.15	109.50 ± 16.53	76.63 ± 9.78	11.57 ± 2.46	0.1 ± 0.32	35.01 ± 4.17
Dioscoreaceae								
D. sylvatica	ND	10.84 ± 0.50	76.63 ± 3.89	101.43 ± 3.02	90.63 ± 12.84	50.47 ± 19.44	0.53 ± 0.45	31.31 ± 1.30
Euphorbiaceae								
A. villicaulis	ND	2.82 ± 0.40	ND	10.11 ± 0.52	1.46 ± 0.65	ND	ND	ND
C. sylvaticus	ND	ND	5.98 ± 0.20	35.69 ± 1.42	7.68 ± 0.36	ND	ND	1.02 ± 0.28
E. milii	ND	ND	80.08 ± 3.42	90.92 ± 3.88	62.28 ± 1.34	15.85 ± 0.87	0.051 ± 0.30	17.31 ± 0.72

Fabaceae								
S. brachypetala	ND	1.02 ± 1.23	5.35 ± 2.61	10.40 ± 2.26	17.87 ± 3.99	6.42 ± 3.06	8.99 ± 3.29	4.57 ± 2.65
Lamiaceae								
L. leonurus	ND	0.97 ± 0.23	20.03 ± 0.58	24.46 ± 0.90	27.76 ± 3.59	ND	ND	6.51 ± 0.43
M. longifolia	ND	ND	5.06± 0.50	13.08 ± 0.97	7.88 ± 0.56	ND	2.19 ± 0.73	ND
Polygalaceae								
P. virgata	ND	ND	13.13 ± 1.52	61.51 ± 5.12	146.40 ± 11.51	23.14 ± 4.61	50.23 ± 5.99	34.03 ± 8.35
Scrophulariaceae								
A. procumbens	ND	27.66 ± 3.57	38.99 ± 0.74	134.14 ± 17.04	50.13 ± 6.08	24.84 ± 3.57	12.45 ± 4.33	37.34 ± 3.42
Solanaceae								
D. stramonium	ND	5.74 ± 2.80	23.82 ± 1.46	135.66 ± 4.64	65.30 ± 1.89	5.01 ± 0.63	ND	23.34 ± 0.63
W. somnifera	ND	8.94 ± 1.18	52.32 ± 7.62	92.43 ± 3.71	141.25 ± 20.29	52.32 ± 8.11	4.91 ± 1.43	34.03 ± 4.89
Verbenaceae								
L. javanica	2.23 ± 1.24	12.353± 1.49	65.98 ± 3.23	213.45 ± 14.69	121.22 ± 7.26	17.06 ± 1.59	3.35 ± 1.40	65.59 ± 2.89

ND: not detected

Table 3-9: The chelation ability of fractions and crude extracts at 10 µg/mL ± SEM (as % chelation as compared to negative control; n = 9).

Chelation ability (as % chelation as compared to negative control)								
Plants	**F1**	**F2**	**F3**	**F4**	**F5**	**F6**	**F7**	**Crude**
Amaryllidaceae								
B. disticha	ND	ND	ND	0.3 ± 0.63	8.63 ± 0.71	8.54 ± 0.59	3.29 ± 0.28	2.75 ± 0.34
Anacardiaceae								
L. discolor	ND	ND	ND	3.37 ± 5.33	3.52 ± 0.27	1.02 ± 0.31	4.51 ± 0.55	ND
M. indica	ND	ND	ND	ND	ND	ND	ND	ND
Apocyneceae								
A. oppositifolia	ND	ND	ND	ND	ND	ND	ND	ND
G. physocarpus	ND	ND	ND	ND	0.94 ± 0.98	1.68 ± 0.30	ND	ND
X. undulatum	ND	ND	ND	ND	ND	ND	ND	ND
Asphodelaceae								
B. latifolia	ND	ND	ND	0.83 ± 0.58	3.91 ± 0.36	2.94 ± 0.52	4.85 ± 0.62	0.78 ± 0.44
Asteraceae								
A. arctotoides	ND	ND	ND	0.3 ± 0.63	8.63 ± 0.71	8.54 ± 0.59	3.29 ± 0.28	2.75 ± 0.34
V. myriantha	ND	ND	ND	ND	2.59 ± 0.43	3.08 ± 0.38	0.77 ± 0.55	0.68 ± 0.73
Oleaceae								
J. abyssinicum	ND	1.79 ± 0.33	3.01 ± 0.22	2.35 ± 0.45	2.66 ± 0.66	5.5 ± 0.43	4.32 ± 0.21	2.33 ± 0.43
Combretaceae								
C. molle	ND	ND	ND	ND	ND	6.32 ± 0.86	ND	ND
Crassulaceae								
C. orbiculata	ND	ND	ND	ND	0.17 ± 0.87	ND	ND	ND
Dioscoreaceae								
D. sylvatica	10.76 ± 1.2	2.45 ± 0.21	1.87 ± 0.28	4.4 ± 0.34	4.83 ± 0.42	15.09 ± 0.57	2.94 ± 0.97	2.3 ± 0.55
Euphorbiaceae								
A. villicaulis	ND	ND	ND	ND	ND	ND	ND	ND
C. sylvaticus	ND	ND	ND	ND	1.95 ± 0.33	5.67 ± 0.34	5.91 ± 0.36	2.81 ± 0.32

E. milii	ND	ND	ND	0.12 ± 0.26	0.67 ± 0.29	6.87 ± 0.35	7.24 ± 0.36	1.69 ± 0.37
Fabaceae								
S. brachypetala	ND	ND	6.03 ± 11.44	ND	2.22 ± 0.81	ND	6.81 ± 0.53	0.64 ± 0.56
Lamiaceae								
L. leonurus	ND	ND	ND	ND	1.18 ± 0.39	ND	2.29 ± 0.72	2.79 ± 0.21
M. longifolia	ND	ND	0.64 ± 1.33	2.54 ± 2.39	9.51 ± 1.64	5.84 ± 1.83	6.27 ± 1.78	2.22 ± 2.99
Polygalaceae								
P. virgata	ND	ND	ND	ND	ND	ND	ND	ND
Scrophulariaceae								
A. procumbens	0.38 ± 0.71	2.24 ± 0.33	1.74 ± 0.19	3.72 ± 0.44	0.85 ± 0.71	2.41 ± 0.3	2.83 ± 0.3	1.79 ± 0.31
Solanaceae								
D. stramonium	ND	1.79 ± 0.33	3.00 ± 0.22	2.35 ± 0.45	2.66 ± 0.66	5.5 ± 0.43	4.32 ± 0.21	2.33 ± 0.43
W. somnifera	ND	ND	ND	ND	ND	ND	ND	ND
Verbenaceae								
L. javanica	ND	ND	8.48 ± 11.13	ND	ND	0.05 ± 0.37	ND	ND

ND = not detected.

CHAPTER 4: MASS SPECTROMETRY AND TARGET-SPECIFIC ASSAYS

4.1 Plants as sources of drugs

Organic substances derived from natural sources have been used and continue to be used to treat a variety of diseases.[574] These substances have been employed in both their unaltered state (as polyherbal or phytomedicine) and as building blocks for the creation of synthetic and semi-synthetic analogues with enhanced drugability.[575] Such active ingredients include naturally occurring phytochemicals (morphine, codeine, noscapine, papaverine, artemisinin and paclitaxel) or synthetic analogues or derivatives (chloroquine, lovastatin, reserpine) which are all used in therapeutic settings.[575]

Mass spectrometry is an effective analytical method for determining the structure and chemical characteristics of molecules as well as for identifying and quantifying known and unknown chemicals.[576] The molecular weight of the sample can be ascertained using the MS spectrum.[457] This technique, which simultaneously defines the molecular weight and a diagnostic fragment of the molecule, is primarily used for the structural elucidation of organic compounds, peptide or oligonucleotide sequencing, and high-specificity monitoring of the presence of previously characterized compounds in complex mixtures.[577] These parameters could be used to identify the phytochemicals through the Dictionary of Natural Products (Taylor & Francis, accessed 2023).[578]

4.2 Materials and method

4.2.1 Ultra-performance liquid chromatography-high resolution mass spectrometry tentative identification of phytochemicals

The selected fractions (*A. oppositifolia* fraction 3, *A. procumbens* F3 and F5, *P. virgata* F3 – F7, and *S. brachypetala* F1 – F4) were subjected to LC-MS/MS analysis. Ultra-performance liquid chromatography-high resolution mass spectrometry (UPLC-HRMS) analysis was conducted using a Waters Acquity UPLC system (Waters Corp., MA, USA), equipped with a binary solvent delivery system and an auto-sampler. The crude extract was prepared by dissolving the dried sample in a methanol (MeOH):H_2O (1:1) solution before filtering it through a 0.22 µm nylon syringe filter to remove particulate matter. Compound separation was performed on an ACQUITY UPLC® BEH (2.1 × 100 mm, 1.7 µm) column (Waters Inc., Milford, MA, USA). A gradient elution method was employed using H_2O (0.1% formic acid) and MeOH (0.1% formic acid) (Romil-SpS™, Microsep, South Africa) as solvent A and solvent B, respectively. The elution method was optimised as

follows: 97% solvent A, held for 0.1 min, followed by a linear gradient increase to 100% solvent B at 14 min. A 3-min washing hold was used (14–17 min) before reconditioning the column with the starting conditions (17.5–20 min). The column temperature was held constant at 40°C to ensure repeatable results with a fixed flow rate of 0.3 mL/min and an injection volume of 5 µL.

The system consisted of a Waters ACQUITY UPLC® connected to a quadrupole mass filter with a high-resolution time-of-flight (TOF) mass analyser. A Waters® Xevo G2 high-definition mass spectrometer (HDMS) system (Waters Inc., Milford, MA, USA) was used for compound separation and detection. The instrument was operated using MassLynx™ v. 4.1 (Waters Inc., Milford, MA, USA) software. Sodium iodide clusters were used to calibrate the MS using the Intellistart software function over a mass range of 50 –1 200 Da. The MS source parameters were optimised for electrospray ionisation (ESI) positive mode and were set as follows: source temperature of 120°C, extraction cone voltage of 4.0 V, sampling cone of 30.0 V, cone gas flow of 20.0 L/h, desolvation temperature of 350°C, desolvation gas flow of 600.0 L/h, and a capillary voltage of 2.8 kV for the positive mode. An internal lock mass control standard comprised a 2 ng/µL solution of leucine enkephalin (m/z 555.2693). To account for experimental drift in mass, a lock mass solution was infused directly into the source at a rate of 3 µL/min. The lock mass infusion was done intermittently every 10 s. The system is also equipped with a Waters photodiode array (PDA) detector. The PDA detector settings were optimised as follows: a sampling rate of 10 points/sec, an ultraviolet (UV) scan range of 210-700 nm and a resolution of 4.8 nm.

4.2.2 Preliminary identification of compounds

After injection, chromatograms were generated, and major peaks were identified and characterised per selected fractions. Information generated from these chromatograms were used in conjunction with the online database known as the Dictionary of Natural Products (CRC Press. Francis & Taylor, 2023). The database uses the molecular weight and the corresponding UV emission to match existing compounds with similar parameters. The use of this database should not be seen in a vacuum, as research into the existence of these compounds either within the plant itself, or at least the genus and family is necessary to elucidate and characterise the compounds found in full. Some products with overlapping molecular weights need to be scrutinised based on its probability of being found within the genus or family, as well as which solvents these molecules were extracted into. The database only lists the original plant and/or species it was identified from, thus the hits gathered from the database should be investigated independently to establish the relationship with the plant or species being investigated. In this study, if the compounds were found in the same or a different species of the same genus, or if an overarching chemotaxonomic marker within the family, the compounds were considered accurate.

4.2.3 Lipid peroxidation

Lipid peroxidation assessment was conducted by employing the thiobarbituric acid reactive substances (TBARS) assay.[579] In this assay, thiobarbituric acid (TBA) and lipid peroxidation products, mostly malondialdehyde (MDA), react to create MDA-TBARS adducts, also known as TBARS **(Figure 4-1)**.[580] Cells were seeded and exposed as per Section 3.4.4, upscaled to a 12-well plate format, with cell density being 35 000 cells/well. The oxidant 2,2'-azobis(2-amidinopropane) (AAPH, 500 µM in-reaction) served as a positive control. A 400 µL aliquot of the culture medium was extracted and transferred to 5 mL tubes, while the cells were detached using 100 µL of TrypLE and combined with the culture medium. The cellular suspension was then mixed with 100 µL of trichloroacetic acid (16.5%) and 100 µL of TBA (2.5% in 0.1 M sodium hydroxide and containing 50 µM ethylenediaminetetraacetic acid [EDTA]). The mixture was incubated for 20-minute in a water bath at 95 °C. After the heating step, 250 µL of butanol was added, and the resulting mixture was vortex mixed. Subsequently, the organic layer (100 µL) was carefully transferred into a black-walled, clear bottom 96-well plate following separation from the aqueous phase. The fluorescence intensity was quantified at an excitation wavelength of 508 nm and an emission wavelength of 590 nm (Synergy II, Biotek Instruments, Inc., Winooski, USA). Data was expressed as a fold increase compared to the negative control.

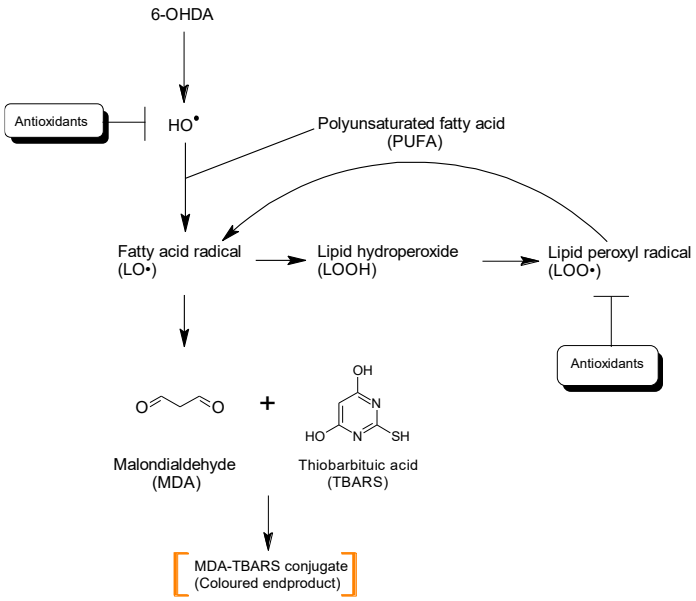

Figure 4-1: **Schematic representation of the induction of malondialdehyde (MDA) production via 6-hydroxydopamine (6-OHDA) and assay principle of thiobarbituric acid (TBARS), where the TBARS-MDA conjugate is measured fluorometrically at λex = 508 nm and λem = 590 nm, and inhibited by antioxidants. Self-generated image.**

4.2.4 Reactive oxygen species

2,7-Dihydrochlorofluorescein (H_2DCFDA) is used as a probe to determine the intracellular ROS concentration. The enzymatic cleavage and subsequent interaction with ROS produces the highly fluorescent dicholorofluorescein diacetate (**Figure 4-2**).[581] Cells were exposed as described in Section 3.4.4.. Potassium persulphate (500 µM in-reaction) was used as a positive control. After 48 h exposure to the 2 x IC_{50} 6-OHDA (70 µM, due to non-reactivity on the previously established IC_{50}), the media was replaced with 100 µL of a 10 µM H_2DCFDA in FCS-free media and incubated for 2 h at 37°C. The fluorescence intensity was measured at excitation wavelength of 480 nm and emission wavelength 590 nm (Synergy II, Biotek Instruments, Inc., Winooski, USA). The FI was blank-adjusted and was normalised according to cell density to account for treatment-induced cell-death. Cell density was determined using the SRB assay. Data is expressed as a fold increase compared to negative control.

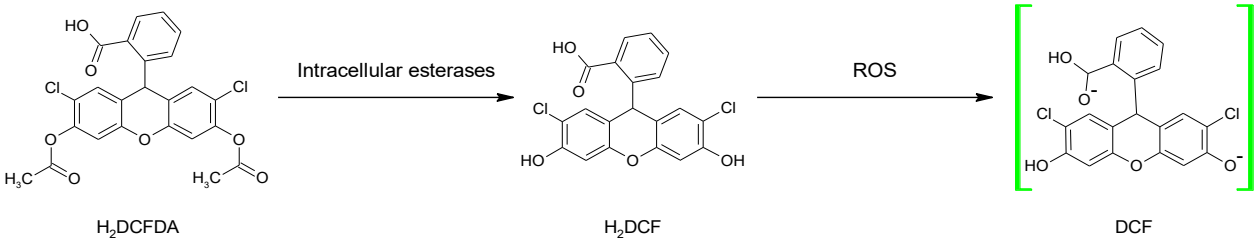

Figure 4-2: Scheme indicating the mechanism by which the 2,7-dihydrochlorofluorescein (H_2DCFDA) probe measures intracellular reactive oxygen species (ROS). H_2DCF: 2,7'-dicholorodihydrofluorescein, DCF: dicholorofluorescein. Self-generated image.

4.2.5 Mitochondrial integrity

Cells were seeded and exposed as per Section 3.4.4. Potassium persulphate (500 µM in-reaction) was used as a positive control. After exposure, the media was removed from the cells and replaced with 100 µL of a 0.3X solution of the CytoPainter Red (6 µL of 500X dye to a total of 10 mL FCS-free media) (Abcam via Biocom Africa Pretoria, South Africa, catalogue number AB112145). The cells were then incubated for 30 min in a humidified incubator at 37°C. After incubation the dye was replaced with 100 µL FCS-free media and read at excitation wavelength of 544 nm and emission wavelength of 620 nm (FLUOstar Optima plate reader, BMG Labtech, Offenburg, Germany). Results are expressed as the ratio of active mitochondria to normalised cell density compared to the negative control, as determined by the SRB assay.

4.2.6 Glutathione depletion

The conjugation of monochlorobimane to GSH (and the consequent formation of a fluorescent adduct, **Figure 4-3**) was used to determine intracellular GSH concentration.[582] n-Ethylmaleimide (10 µM in-reaction) was used as a positive control. After exposure as per Section 3.4.4, the medium was replaced with 100 µL monochlorobimane (16 µM in FCS-free media) and was incubated for 2 h. After incubation the fluorescence was measured at an excitation wavelength of 340 nm and an emission wavelength of 450 nm (Synergy II, Biotek Instruments Inc., Winooski, USA). Fluoresce intensity was blank adjusted and expressed as relative fluorescent units (RFU) compared to negative control.

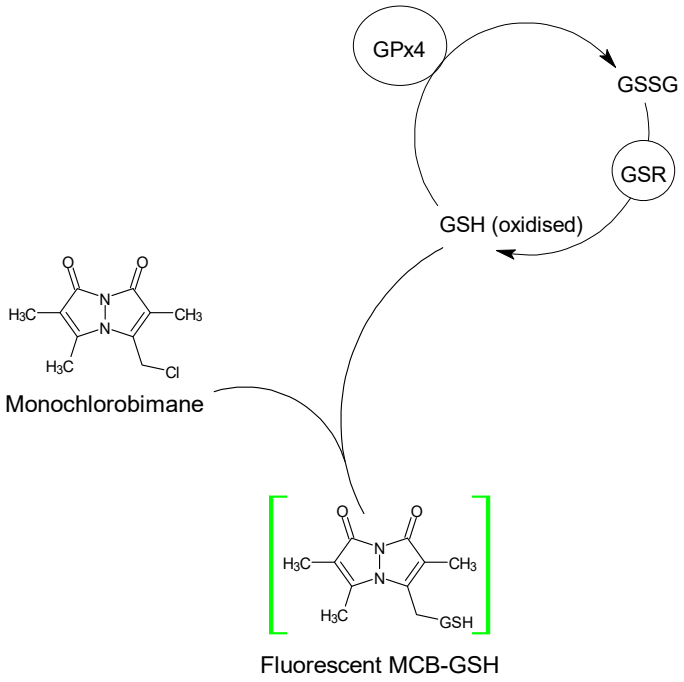

Figure 4-3: Scheme indicating the mechanism by which the monochlorobimane (MCB) probe measures intracellular glutathione (GSH). Figure is self-generated.

4.3 Results and discussion

4.3.1 Mass spectrometry compound identification

4.3.1.1 Compounds identified in *Acokanthera oppositifolia.*

Fraction 3 of *A. oppositifolia* presented with three major peaks **(Table 4-1, Figure 4-4).** At 4.213 min, the major constituents identified could be 2-*O*-caffeoylglucose (UV value of 298) or 1-*O*-*trans*-caffeoyl-β-D-allopyranoside **(Figure 4-5)** (UV value of 325). Derivatives of *myo*-inositol could also fall into the peak identified. The peaks identified at both 4.533 and 4.731 min (UV values 230 and

243), could be several forms of 4-*O*-caffeoylquinic acids, including 3-*O*-caffeoyl-muco-quinic acid or 4-(3,4-dihydroxycinnamoyl)quinic acid. When investigated at a UV value of 297, structures could be isobiflorin, however, no studies indicated its presence in the *Acokanthera* genus. Known phytochemicals acovenoside, ouabain, acobioside A and opposide was not detected in this fraction, which could explain the lack in toxicity, even though they have been identified from this same plant sample in previous studies.[492, 493]

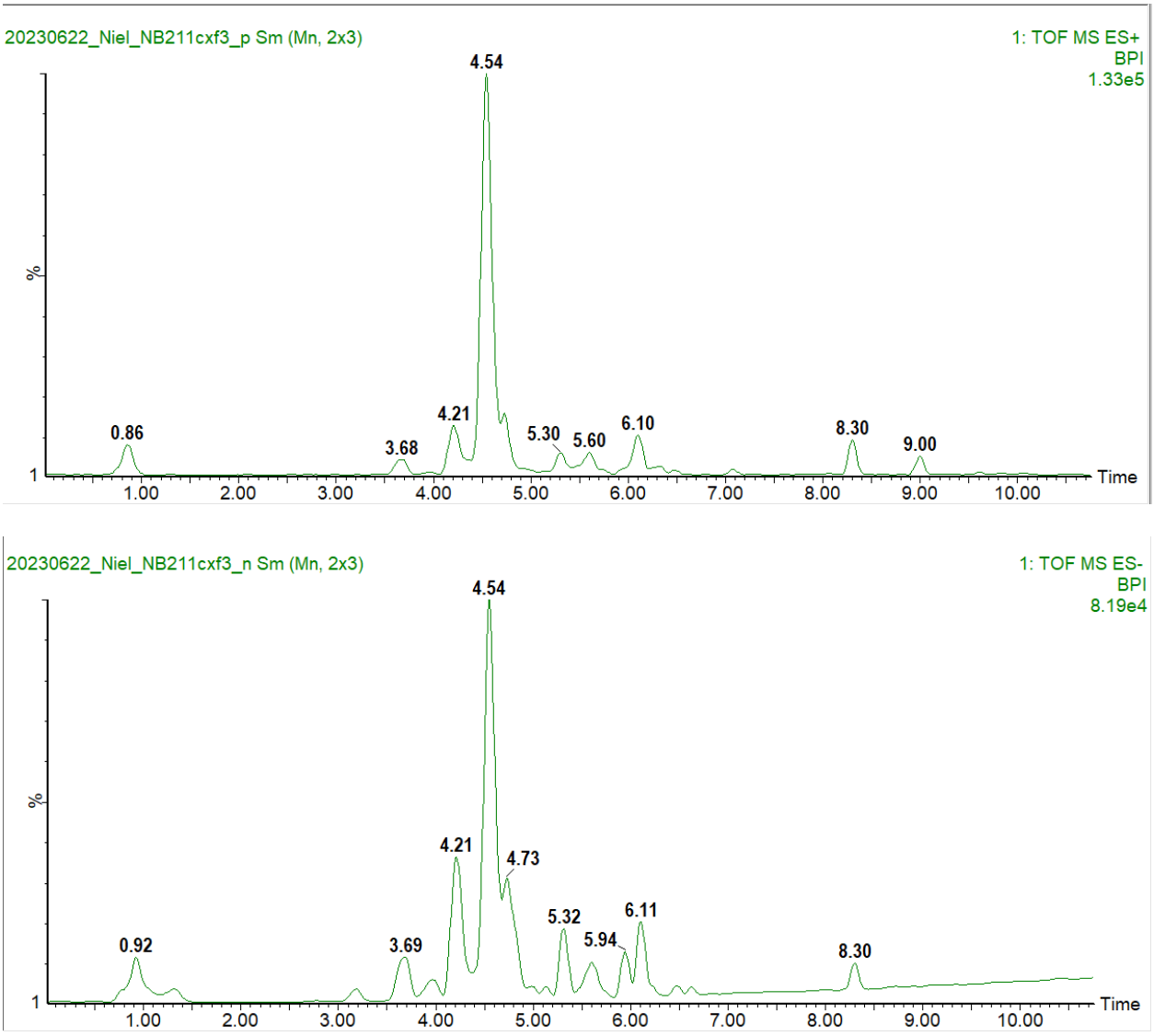

Figure 4-4: Electrospray ionisation chromatograms in both positive (+) and negative (-) mode for *A. oppositifolia* fraction 3.

Table 4-1: Peaks identified in the chromatographs of *Acokanthera oppositifolia* fraction 3.

Retention time (min)	m/z	M (Da) Experimental	Ion	Chemical formula	M (Da) Theoretical	UV
4.213	343.1013	342.0940	M+H	$C_{15}H_{18}O_9$	342.0951	240;298;324
	341.0871	342.0944	M-H	$C_{15}H_{18}O_9$	342.0951	240;298;325
4.533	355.1028	354.0955	M+H	$C_{16}H_{18}O_9$	354.0951	243;296
	353.0871	354.0944	M-H	$C_{16}H_{18}O_9$	354.0951	243;297
4.731	355.1028	354.0955	M+H	$C_{16}H_{18}O_9$	354.0951	230;297;325
	353.0868	354.0941	M-H	$C_{16}H_{18}O_9$	354.0951	

Da: Dalton, M: molecular mass; m/z: experimental mass without ion amendment; UV: ultraviolet absorption.

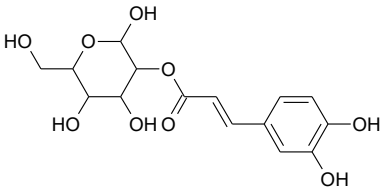

2-*O*-caffeoylglucose (*E*-form)

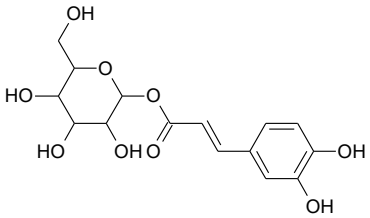

1-*O*-trans-caffeoyl-ß-D-allopyranoside

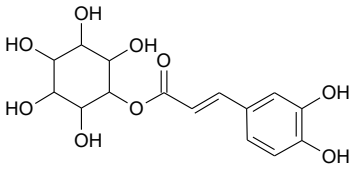

5-*O*-trans-caffeoyl-myo-inositol

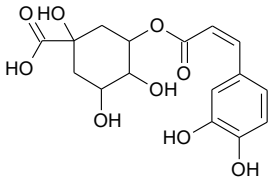

3-*O*-Caffeoyl-muco-quinic acid

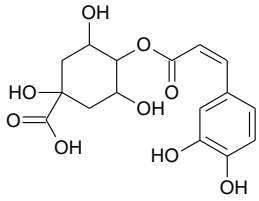

4-(3,4-Dihydroxycinnamoyl)quinic acid

Figure 4-5: Compounds and their associated chemical structures identified from chromatographs of *Acokanthera oppositifolia*. Figure is self-generated.

4.3.1.2 Compounds identified in *Aptosimum procumbens*

Iridoid glycosides as well triterpenoid saponins are commonly found in the family Scrophulariaceae under which *A. procumbens* is classified.[583] The peak identified at 5.081 min, could represent two different iridoid-based compounds, either gouwenoside A or 5-deoxypulchelloside I **(Figure 4-4)**. No evidence indicates the existence of this molecule as dimers, as observed in the 813.3042 Dalton peak (as a 2M+H), where "2M" signifies a dimer of the molecule **(Table 4-2)**.

A peak was observed at 6.052 min **(Figure 4-6)**; however, no match could be made with the databases used. The peak at 6.6 min was identified as a malic acid-derivative, dimethyl 2-[(2E)-3-(3,4-dihydroxyphenyl)prop-2-enoyl]oxy butanedioate, **(Figure 4-7)** which may be a possible upstream metabolite for the formation hydroxycinnamic acids[584] or phenylpropanoid derivatives as seen in the lateral *A. elongatum* species.[585]

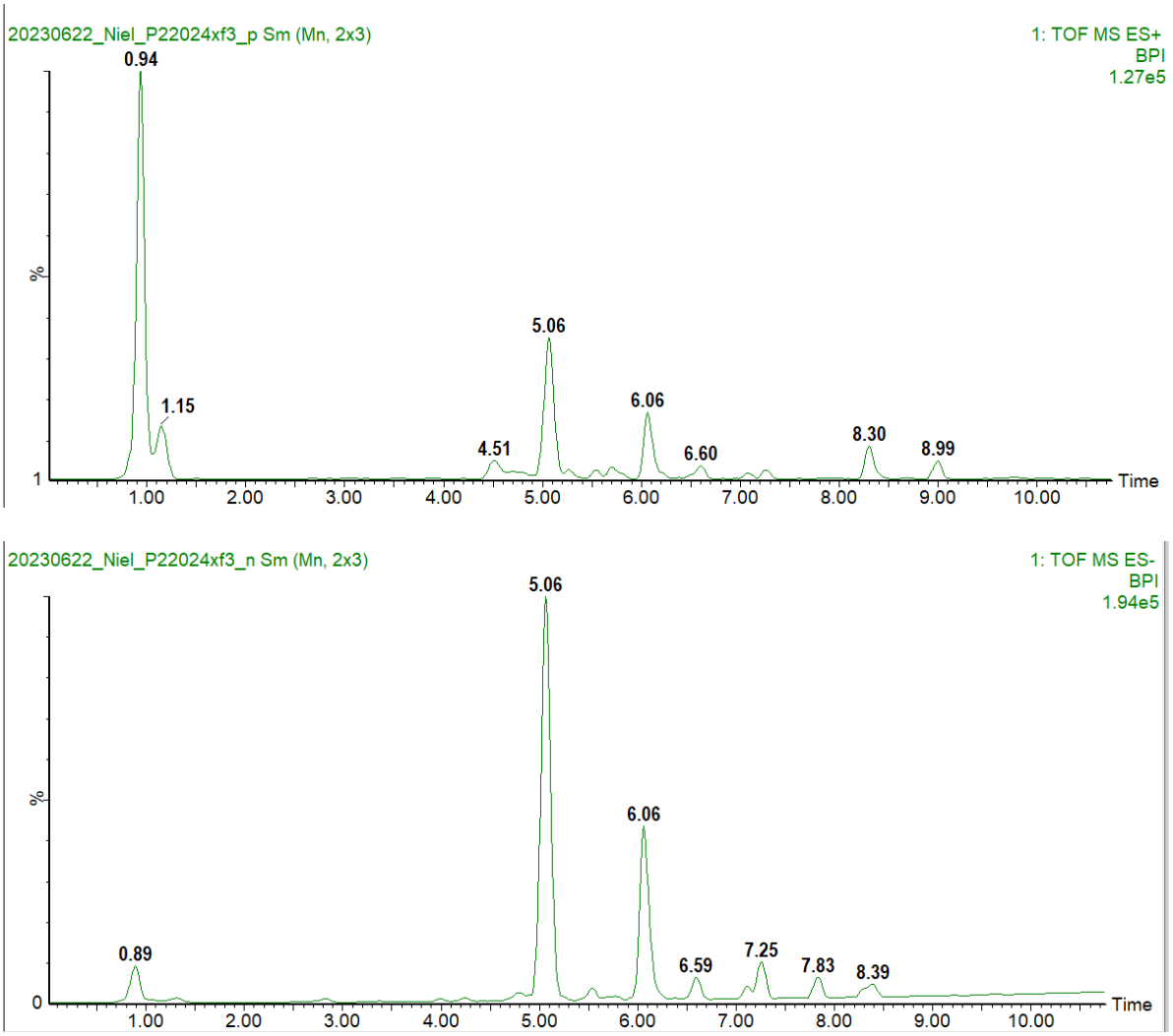

Figure 4-6: **Electrospray ionisation chromatograms in both positive (+) and negative (-) mode for *A. procumbens* fraction 3.**

Table 4-2: Peaks identified in the chromatographs for *Aptosimum procumbens* fraction 3

Retention time (min)	m/z	M (Da) Experimental	Ion	Chemical formula	M (Da) Theoretical	UV
5.081	407.1551	406.1478	M+H	$C_{17}H_{26}O_{11}$	406.38	238
	813.3042	406.1485	2M+H	$C_{17}H_{26}O_{11}$	406.38	N/D
6.052	413.1424	412.1351	M+H	$C_{14}H_{24}N_2O_{12}$	412.35	239
6.6	325.0927	324.0854	M+H	$C_{15}H_{16}O_8$	324.28	329 ;324

Da: Dalton, M: molecular mass; m/z: experimental mass without ion amendment; UV: ultraviolet absorption.

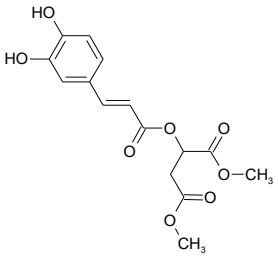

dimethyl 2-{[(2*E*)-3-(3,4-dihydroxyphenyl)prop-2-enoyl]oxy}butanedioate

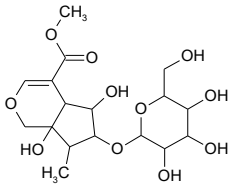

Gouwenoside A

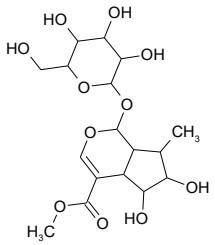

5-Deoxypulchelloside I

Figure 4-7: Compounds and their associated chemical structures identified from chromatographs of *Aptosimum procumbens* fraction 3. Figure is self-generated.

Fraction 4 produced peaks at 6.601, 7.023 and 8.521 min **(Table 4-3)**. The peaks at 6.601 and 7.023 min **(Figure 4-8)** coincides with the same peak on fraction 3, thus resulting in dimethyl 2-[(2E)-3-(3,4-dihydroxy-phenyl)prop-2-enoyl]oxy butanedioate being identified. The co-eluting under two retention times might suggests an enantiomer of the compound. These enantiomerically opposite metabolites can be produced within various genera or species, with one enantiomer isolated from one species and the other isolated from a different species or genera; or both enantiomers can be produced and isolated from a single species as a racemic mixture (with one enantiomer predominating).[586] There are multiple molecular formulas identified at the retention time of 8.521 min, with $C_{27}H_{40}O_{13}$ providing the closest to molecules found with the family Scrophulariaceae, with a derivative of hastatoside **(Figure 4-9)** (6-*O*-(8-hydroxy-2,6-dimethyl-2E,6E-octadienoyl). Hastatoside follows the same iridoid scaffold as seen in the family *Scrophulariaceae*.[583]

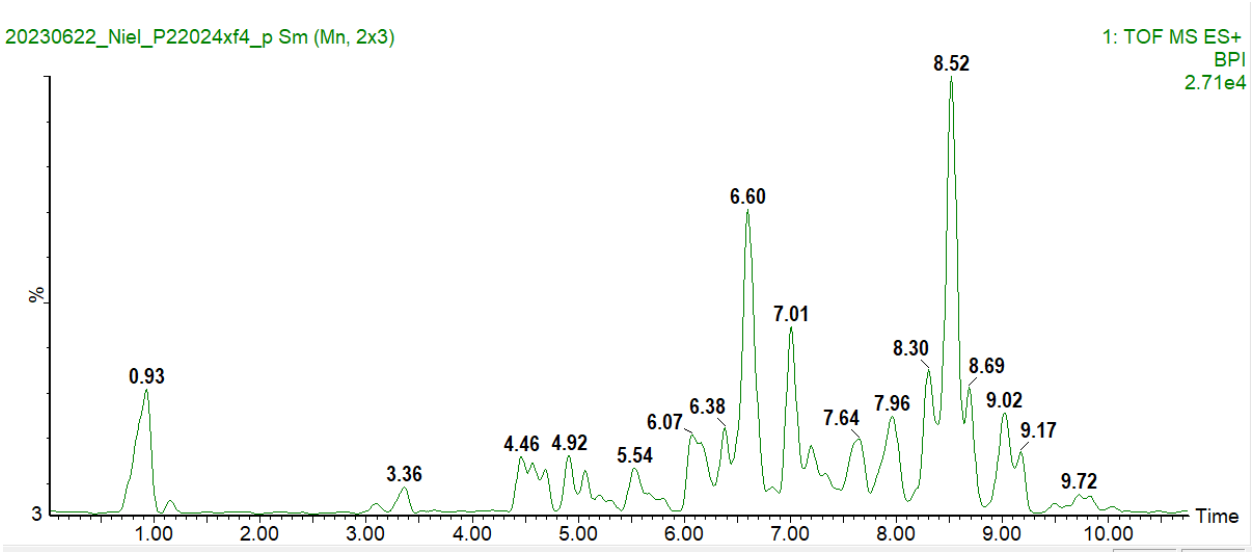

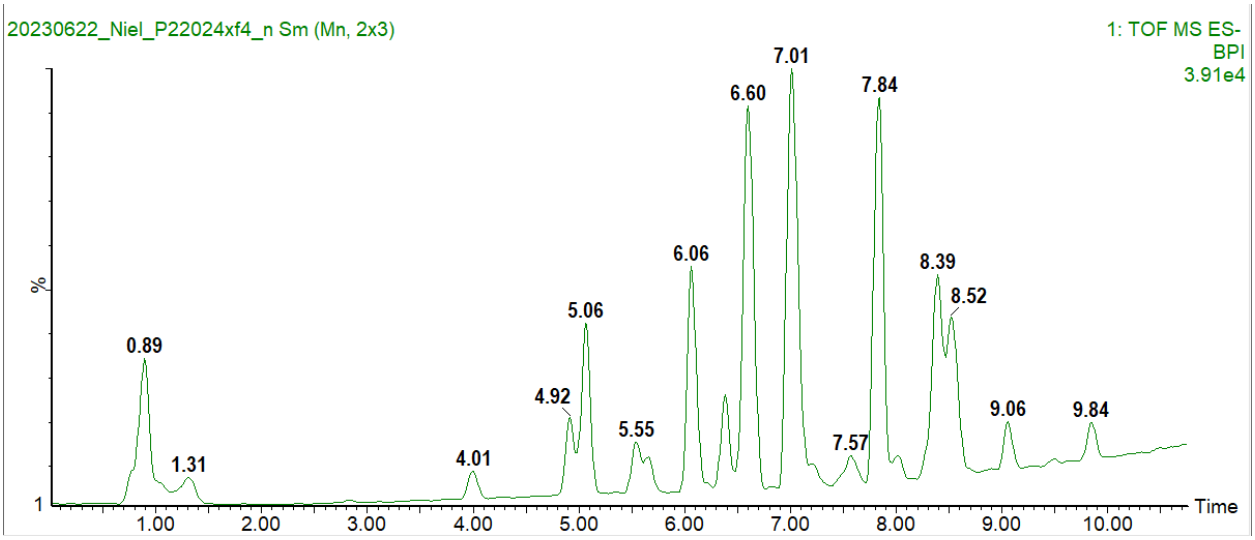

Figure 4-8: **Electrospray ionisation chromatograms in both positive (+) and negative (-) mode for *Aptosimum procumbens* fraction 4.**

Table 4-3: Peaks identified in the chromatographs for *Aptosimum procumbens* fraction 4.

Retention time (min)	m/z	M (Da) Experimental	Ion	Chemical formula	M (Da) Theoretical	UV
6.601	325.0925	324.084	M+H	$C_{15}H_{16}O_8$	324.28	329
7.023	325.0925	324.084	M+H	$C_{15}H_{16}O_8$	324.28	329
8.521	573.2571	271.875	M+H	$C_{28}H_{36}N_4O_9$	572.61	286;329
				$C_{27}H_{40}O_{13}$	572.60	
				$C_{35}H_{40}O_7$	572.69	N/D

Da: Dalton, M: molecular mass; m/z: experimental mass without ion amendment; UV: ultraviolet absorption.

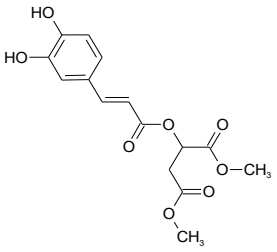

Dimethyl 2-{[(2*E*)-3-(3,4-dihydroxyphenyl)prop-2-enoyl]oxy}butanedioate

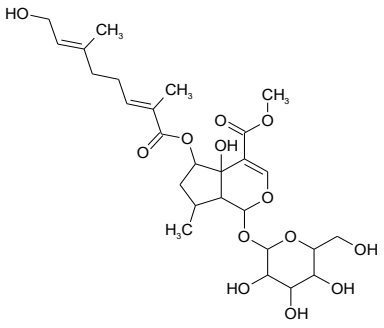

6-*O*-(8-hdydroxy-2,6-dimethyl-2*E*,6*E*-octadienoyl)hastatoside

Figure 4-9: **Compounds and their associated chemical structures identified from chromatographs of *Aptosimum procumbens* fraction 4. Figure is self-generated.**

4.3.1.3 Compounds identified in *Bulbine latifolia*

Fraction 3 of *B. latifolia* presented with three distinct major peaks at retention times of 3.201, 5,908 and 5.258 mins, respectively **(Table 4-4).** Even though a strong peak could be seen at a retention time of 3.201 min and a UV value of 292, the compound patulin is not known to exist within the species or genus. At the UV value of 258, the compound longianone was identified, an isomer of patulin. However, both products are seen as secondary metabolites within certain plant endemic fungi species.[587] At the retention time of 5.258 min, in both negative mode and positive mode, found a peak with the molecular weight of 184.07. This molecular weight at the UV value of 277, suggests the possible structure to be a pyran-2-one derivative, 6-(3-hydroxypropyl)-4-methoxy-2H-pyran-2-one. The peak 5.908 mins could be a possible monoterpenoid, as carvone has been seen in *B. abyssinica*,[588] or a lignan monomer. Both compounds identified at 10.908 and 11.073 mins are both highly lipophilic N-lauryl diethanolamine and 2-amino-1,3-hexadecanediol, respectively.

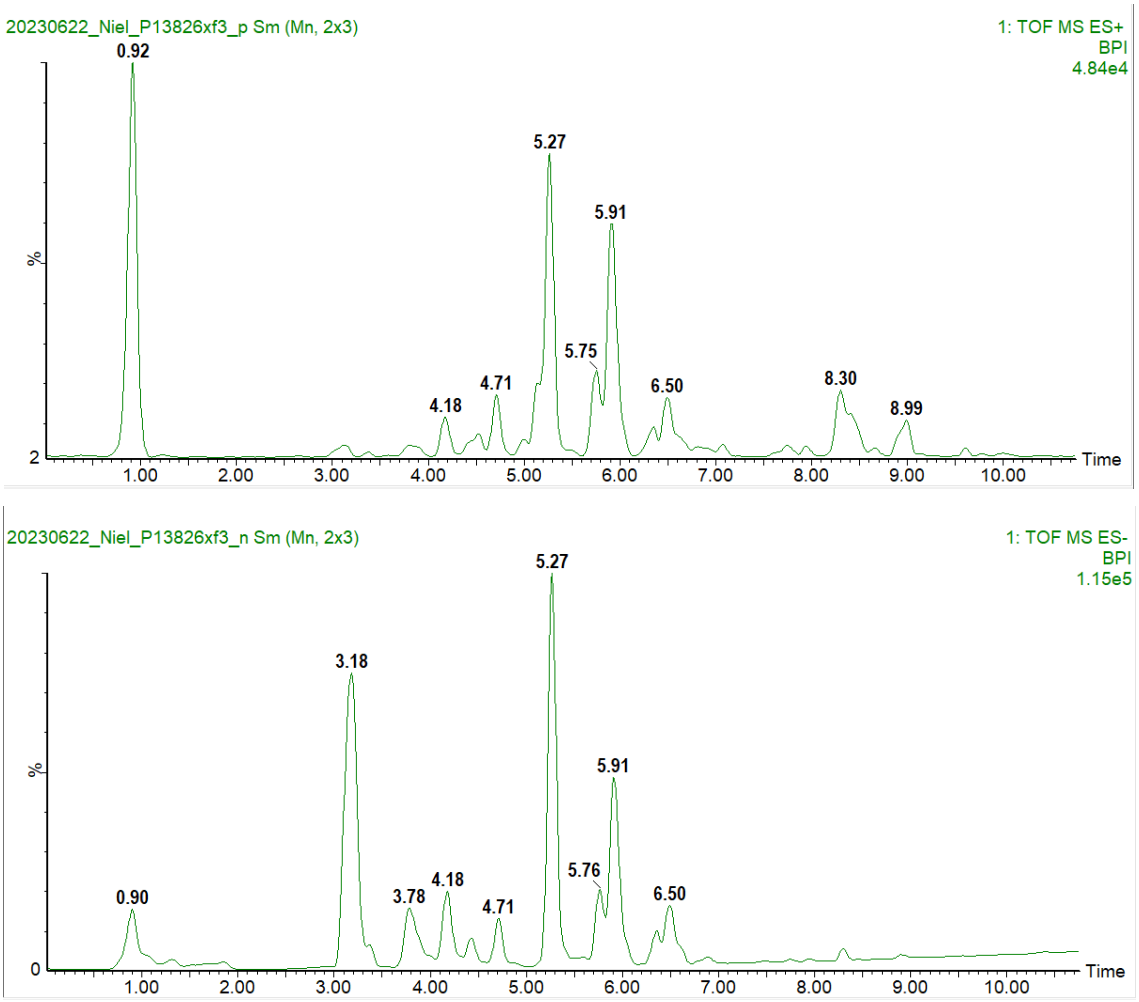

Figure 4-10: Electrospray ionisation chromatograms in both positive (+) and negative (-) mode for *Bulbine latifolia* fraction 3.

Table 4-4: Peaks identified in the chromatographs for *Bulbine latifolia* fraction 3.

Retention time (min)	m/z	M (Da) Experimental	Ion	Chemical formula	M (Da) Theoretical	UV
3.201	153.0183	154.0255	M-H	$C_7H_6O_4$	154.0266	258, 292
5.258	183.0651	184.0723	M-H	$C_9H_{12}O_4$	184.0736	277
	367.1386	184.0729	2M-H			N/D
	185.0813	184.0740	M+H			N/D
5.908	451.1441	406.1458	M-H+FA	$C_{17}H_{26}O_{11}$	406.1475	N/D
	405.1383	406.1456	M-H			N/D
10.908	274.2744	273.2671	M+H	$C_{16}H_{35}NO_2$	273.2668	N/D
11.073	290.2693	289.2620	M+H	$C_{16}H_{35}NO_3$	289.2617	N/D

Da: Dalton, M: molecular mass; m/z: experimental mass without ion amendment; UV: ultraviolet absorption.

Elucidation from fraction 5 presents with five distinct peaks **(Table 4-5)**. The peak at 6.249 min correlates with a molecular weight of 610.154 Daltons, tentatively identified as luteolin 7-sophoroside, with luteolin being a chemotaxonomic flavonoid found in the *Bulbine* species **(Figures 4-11 and 4-12)**.[589] This flavonoid is seen with the 7-sophoroside moiety in this fraction. The identified compounds at 7.272 min, currently without any further elucidation, are ambiguous. There is a possibility of several flavonoids, all falling under 6-C-β-D-glucopyranosyl-3',4',5-trihydroxy-7-methoxyflavone or 6-C-β-D-glucopyranosyl-3',4',5-trihydroxy-7-methoxyflavone, with the derivatives either being tri- or pentahydroxy substitutes. Although the chemical formula is stated as being $C_{17}H_{22}N_2O_{13}$, the more relevant structures based on compounds found in the *Bulbine* species is $C_{22}H_{22}O_{11}$.[590]

The peaks identified at 7.828 min presents with no specific molecules form the *Bulbine* genus on the database used. The molecules within the parameters are either isoflavone derivatives or glucopyranoside moieties. The peak of 7.828 also present with no matches specific to *Bulbine*.

The tentative identification at the peak of 8.54 min, is seen as a 1,8-Di-O-β-D-glucopyranoside derivative of 2-decene-4,6-diyne-1,8-diol. The peak identified at 8.93 min may be a possible monoterpene, as seen in *B. abyssinica* where carvone was isolated.[588]

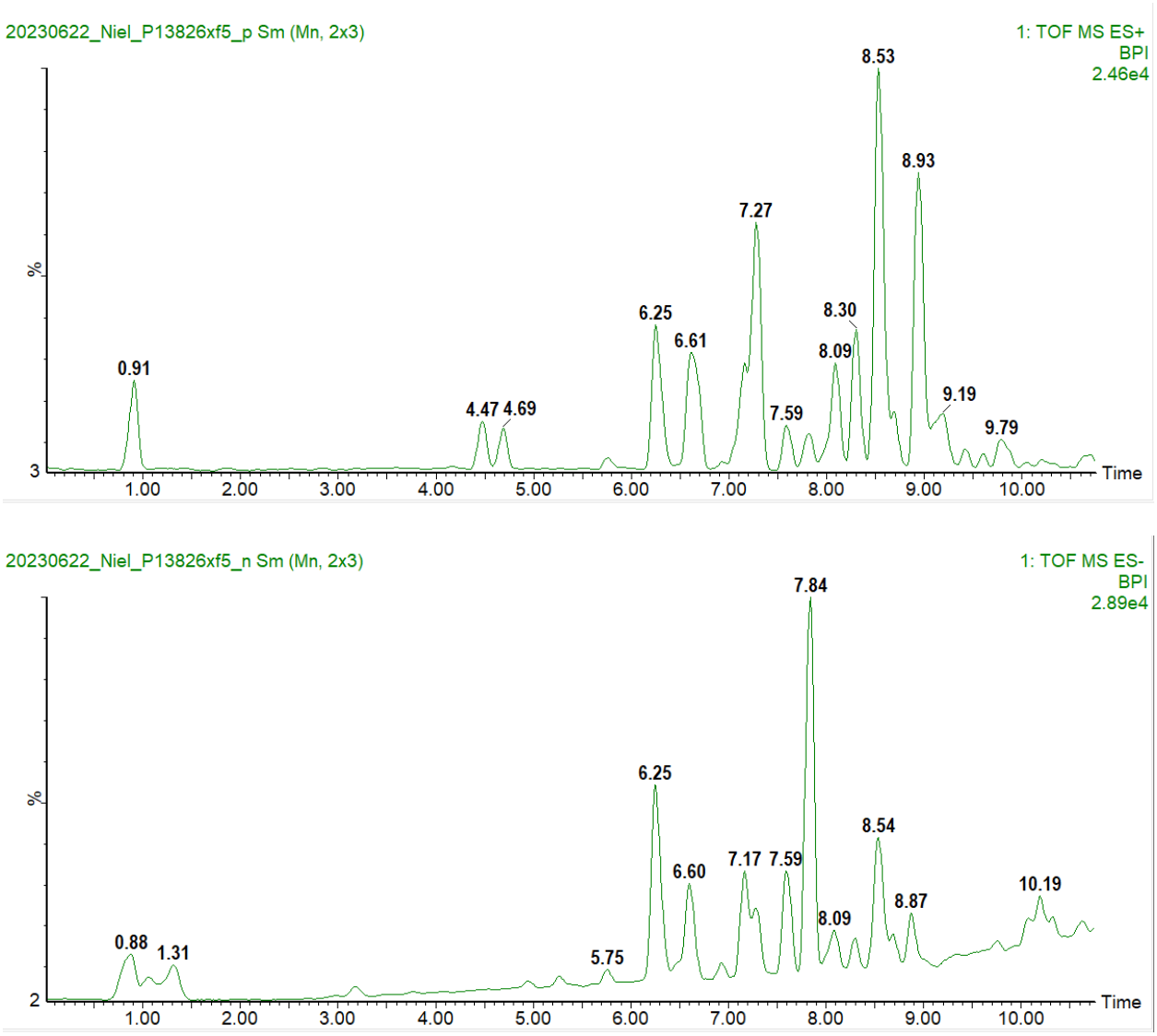

Figure 4-11: **Electrospray ionisation chromatograms in both positive (+) and negative (-) mode for *Bulbine latifolia* fraction 5.**

Table 4-5: Peaks identified in the chromatographs for *Bulbine latifolia* fraction 5.

Retention time (min)	m/z	M (Da) Experimental	Ion	Chemical formula	M (Da) Theoretical	UV
6.249	609.1457	610.1529	M-H	$C_{27}H_{30}O_{16}$	610.153	263;347
	611.1619	610.1546	M+H	$C_{27}H_{31}O_{16}$		N/D
	633.1417	610.1524	M+Na	$C_{27}H_{31}O_{16}$		N/D
7.272	463.1237	462.1164	M+H	$C_{17}H_{22}N_2O_{13}$	462.112	244;343
	461.1081	462.1153	M-H	$C_{17}H_{22}N_2O_{13}$	462.112	N/D
7.828	379.1646	378.1573	M+H	N/D		
	621.2562	620.2489	M+H	$C_{32}H_{36}N_4O_9$	620.242	239;329
8.54	975.3738	488.1905	2M-H	$C_{22}H_{32}O_{12}$	488.189	239

	1021.379	488.1904	2M-H+FA	$C_{22}H_{32}O_{12}$		N/D
8.93	181.1225	180.1152	M+H	$C_{11}H_{16}O_2$	180.115	243
	203.1049	180.1156	M+Na	$C_{11}H_{16}O_2$		N/D

Da: Dalton, M: molecular mass; m/z: experimental mass without ion amendment; UV: ultraviolet absorption.

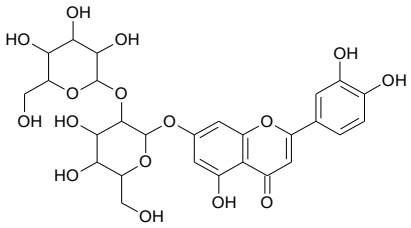

Luteolin 7-sophoroside

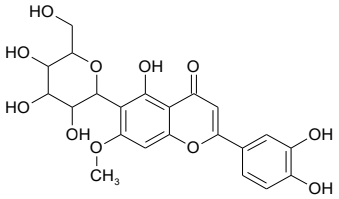

6-C-ß-D-Glucopyranosyl-3',4',5-trihydroxy-7-methoxyflavone

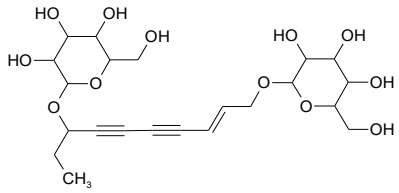

1,8-Di-O-ß-D-glucopyranoside derivative of
2-decene-4,6-diyne-1,8-diol

Figure 4-12: Compounds and their associated chemical structures identified from chromatographs of *Bulbine latifolia* fraction 5.

4.3.1.4 Compounds from *Polygala virgata*

Fraction 3 of *P. virgata* presented with three distinct peaks, at 4.69, 5.22 and 8.293 min, respectively. The initial peak observed at 4.69 min may correspond to one of three potential compounds: 6-*O*-(4-hydroxy-3-methoxy-E-cinnamoyl), 3'-*O*-(4-hydroxyhydroxy-3-methoxy-E-cinnamoyl), or 1'-*O*-(4-hydroxy-3-methoxy-E-cinnamoyl) **(Figures 4-13, 4-14)**. These compounds have been identified in both *P. arillate* roots and *P. tenuifolia* roots. Similar derivatives have also been isolated from *P. virgata*.[591] Both peaks 5.22 and 8.293 min remains unidentified.

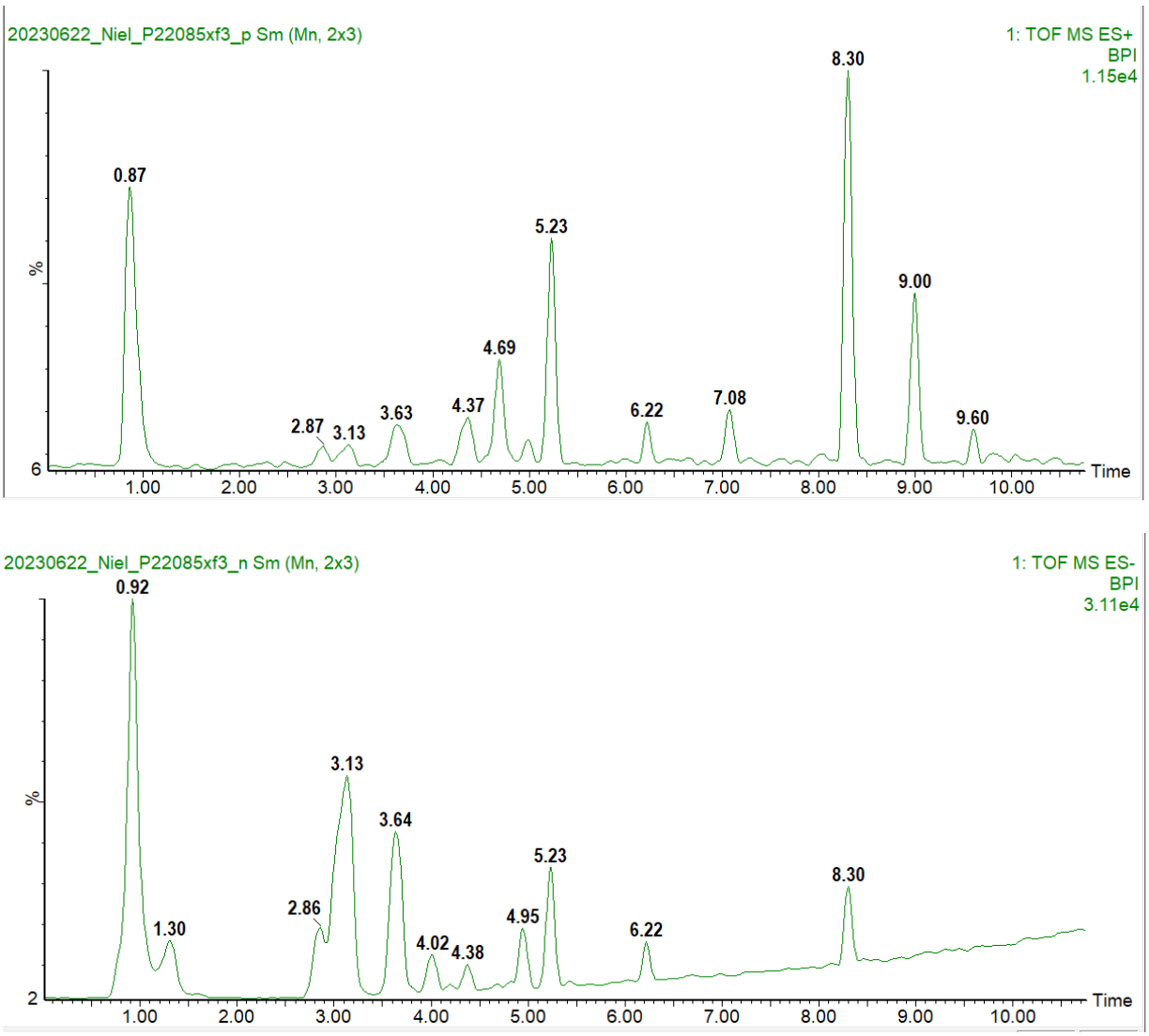

Figure 4-13: **Electrospray ionisation chromatograms in both positive (+) and negative (-) mode for *Polygala virgata* fraction 3.**

Table 4-6: Peaks identified in the chromatographs for *Polygala virgata* fraction 3.

Retention time (min)	m/z	M (Da) Experimental	Ion	Chemical formula	M (Da) Theoretical	UV
4.699	517.15	518.1626	M-H	$C_{22}H_{30}O_{14}$	518.1636	244; 282; 324
5.226	433.13	432.1262	M+H	$C_{18}H_{24}O_{12}$	432.1268	258
	455.11	432.1275	M+Na	$C_{18}H_{24}O_{12}$	432.1268	N/D
	431.11	432.1257	M-H	$C_{18}H_{23}O_{12}$	432.1268	N/D
8.293	340.26	339.2529	M+H	$C_{18}H_{33}N_3O_3$	339.2522	N/D

Da: Dalton, M: molecular mass; m/z: experimental mass without ion amendment; UV: ultraviolet absorption.

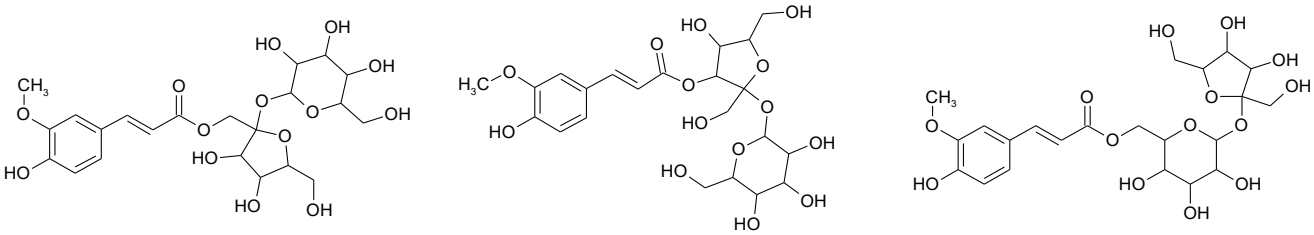

1'-O-(4-Hydroxy-3-methoxy-*E*-cinnamoyl) 3'-O-(4-Hydroxy-3-methoxy-*E*-cinnamoyl) 6-O-(4-Hydroxy-3-methoxy-*E*-cinnamoyl)

Figure 4-14: Compounds and their associated chemical structures identified from chromatographs of *Polygala virgata* fraction 3. Figure is self-generated.

Fraction 4 exhibits several peaks presenting a diverse mix of compounds (**Table 4-7)**. Although the peak at 4.68 min may resemble an alkaloid due to the presence of a single nitrogen atom in its chemical formula, a definitive identification could not be established. A potential compound resembling a 2,7'-cyclo-8,8'-lignan (2-[[6-hydroxy-8-(4-hydroxy-3-methoxyphenyl)-6,7-bis(hydroxymethyl)-1,3-dimethoxy-7,8-dihydro-5H-naphthalen-2-yl]oxy]-6-(hydroxymethyl) oxane-3,4,5-triol) is possibly observed at 6.538 mins (with a UV value of 234), as similar compounds have been documented in *P. chinensis*.[592] When examined at a UV value of 281, the same structure could be discerned, whereas at a UV value of 324 , no corresponding structures could be identified through the database utilised. Possible glycated protoberbine alkaloids could be present at 6.805 min at all three UV values, however, no evidence exists of these alkaloids being isolated out of the *Polygala* species. Using both UV value and chemical formula, no tentative identification could be made for the peak at 7.272 and 7.539 min. Several derivatives of chromones and coumarins, including glycated and sucrose-bound forms, as well as derivatives of benzo-pyran-4-one, may be observed based solely on the molecular formula and weight (at 7.539 minutes). However, this approach lacks precision, and further purification is necessary to determine which specific derivative scaffold can be identified. Two structures can be found at 7.539 mins using the UV value of 239. Haworforbin B and a glycated derivative of saccharonol A (6-O-β-D-glucopyranoside derivative of 6,8-dihydroxy-3,7-dimethylisocoumarin or 6-O-(4-O-methyl-β-D-glucopyranoside) derivative of 6,8-dihydroxy-3-methylisocoumarin) were also identified **(Figure 4-16)**. Coumarins have been found in both *P. boliviensis*[593] and *P. altomontana*.[594] The peak observed at 7.849 mins could potentially be a derivative of either butanedioic or pentanedioic acid. However, tentative identification is challenging because none of the compounds share any of the UV values.

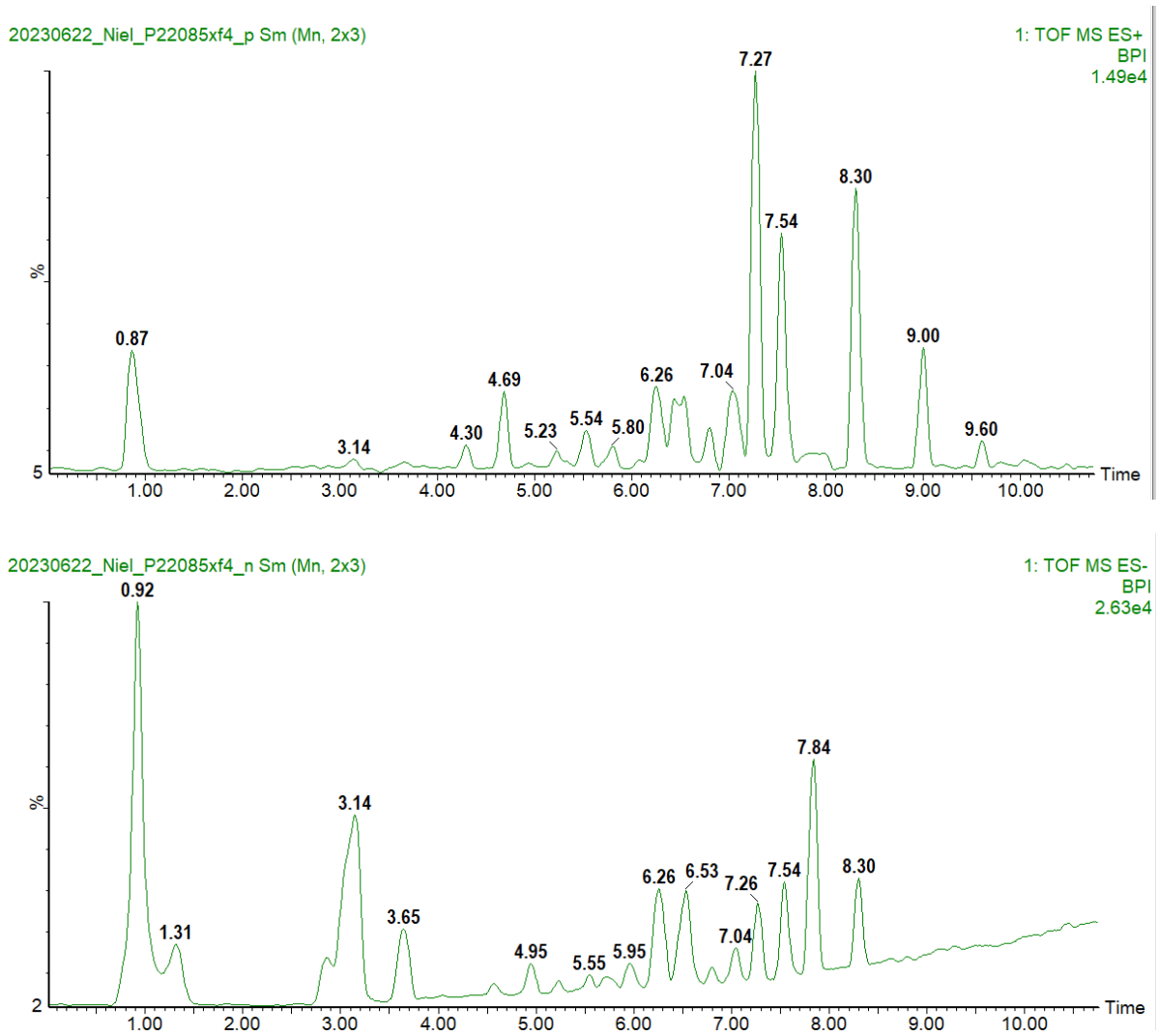

Figure 4-15: **Electrospray ionisation chromatograms in both positive (+) and negative (-) mode for *Polygala virgata* fraction 4.**

Table 4-7: Peaks identified in the chromatographs for *Polygala virgata* fraction 3.

Retention time (min)	m/z	M (Da) Experimental	Ion	Chemical formula	M (Da) Theoretical	UV
4.689	320.15	319.14	M+H	$C_{17}H_{21}NO_5$	319.142	N/D
6.538	567.20	568.21	M-H	$C_{27}H_{36}O_{13}$	568.2156	234;281;324
6.805	597.21	598.22	M-H	$C_{28}H_{38}O_{14}$	598.2262	239;277;324
7.272	605.18	582.19	M+Na	$C_{27}H_{34}O_{14}$	582.1949	249;300
	583.20		M+H	$C_{27}H_{34}O_{14}$		249;301
7.529	547.24	548.24	M-H	$C_{25}H_{40}O_{13}$	548.2469	239;330
7.539	369.11	368.11	M+H	$C_{17}H_{20}O_9$	368.1107	239;330
7.849	187.09	188.10	M-H	$C_9H_{16}O_4$	188.1049	234;281;324

Da: Dalton, M: molecular mass; m/z: experimental mass without ion amendment; UV: ultraviolet absorption.

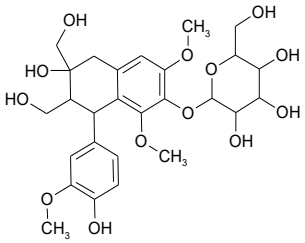

2-[[6-hydroxy-8-(4-hydroxy-3-methoxyphenyl)-6,7-bis(hydroxymethyl)-1,3-dimethoxy-7,8-dihydro-5H-naphthalen-2-yl]oxy]-6-(hydroxymethyl)oxane-3,4,5-triol

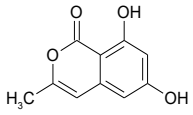

Saccharonol A

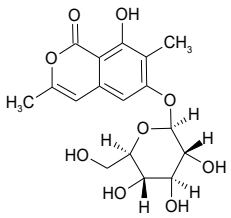

Haworforbin B

Figure 4-16: Compounds and their associated chemical structures identified from chromatographs of *Polygala virgata* fraction 3. Figure is self-generated.

The potential co-elution observed in fractions 5 and 6 also occurs in fraction 7 at 10.018 and 10.162 minutes, with identical structures being detected (**Figure 4-17**). Fraction 5 of *P. virgata* has shown several chemotaxonomic markers for the *Polygala* species, namely xanthones. Xanthones accumulate in *Polygala* and is used to identify and characterise several P*olygala* species.[595] The peak seen in 7.481 min **(Table 4-8)** can be interpreted as either 6,8-dihydroxy-3,7-dimethyl-1H-2-benzopyran-1-one (6-O-β-D-glucopyranoside derivative) or 7-hydroxy-6-(2-hydroxyethyl)-2H-1-benzopyran-2-one (2'-O-β-D-glucopyranoside derivative). The same base scaffold is seen in fraction 4 at 7.593 mins, hence possible co-elution could be taking place. Xanthones have been identified in both peaks at 9.179 and 10.162 mins, with a plethora of structures. Positive identification of the specific xanthone structure cannot be seen without further elucidation and fractionation. Possible xanthones seen at 9.179 mins can be 1,2,8-trihydroxy-5-methoxy-3-methylxanthone, 3,5-dihydroxy-1,2-dimethoxyxanthone, 1,5-dihydroxy-2,3-dimethoxyxanthone, 3,7-dihydroxy-1,2-dimethoxyxanthone, 1,5-dihydroxy-2,7-dimethoxyxanthone or 1,5-dihydroxy-2,3-dimethoxyxanthone. Xanthone structures have been seen at all UV values. For 10.162 mins, the following xanthones can be seen at all UV values; 1,3-dihydroxy-2,4,7-trimethoxyxanthone, 3,8-dihydroxy-1,2,7-trimethoxyxanthone, 7,8-dihydroxy-1,2,3-trimethoxyxanthone, or 1,8-dihydroxy-2,3,5-trimethoxyxanthone.

The same co-elution can be seen at 10.017 min, with several flavan and isoflavone derivatives that may be present, with the structures being isolated and identified from *P. virgata* in a different study.[544] 4',7-Dihydroxy-3'-methoxyflavan, 3',4'-dihydroxy-7-methoxyflavan, 2',7-dihydroxy-4'-methoxyisoflavan or 2',4'-dihydroxy-7-methoxyisoflavan are all possible structures for all UV values.

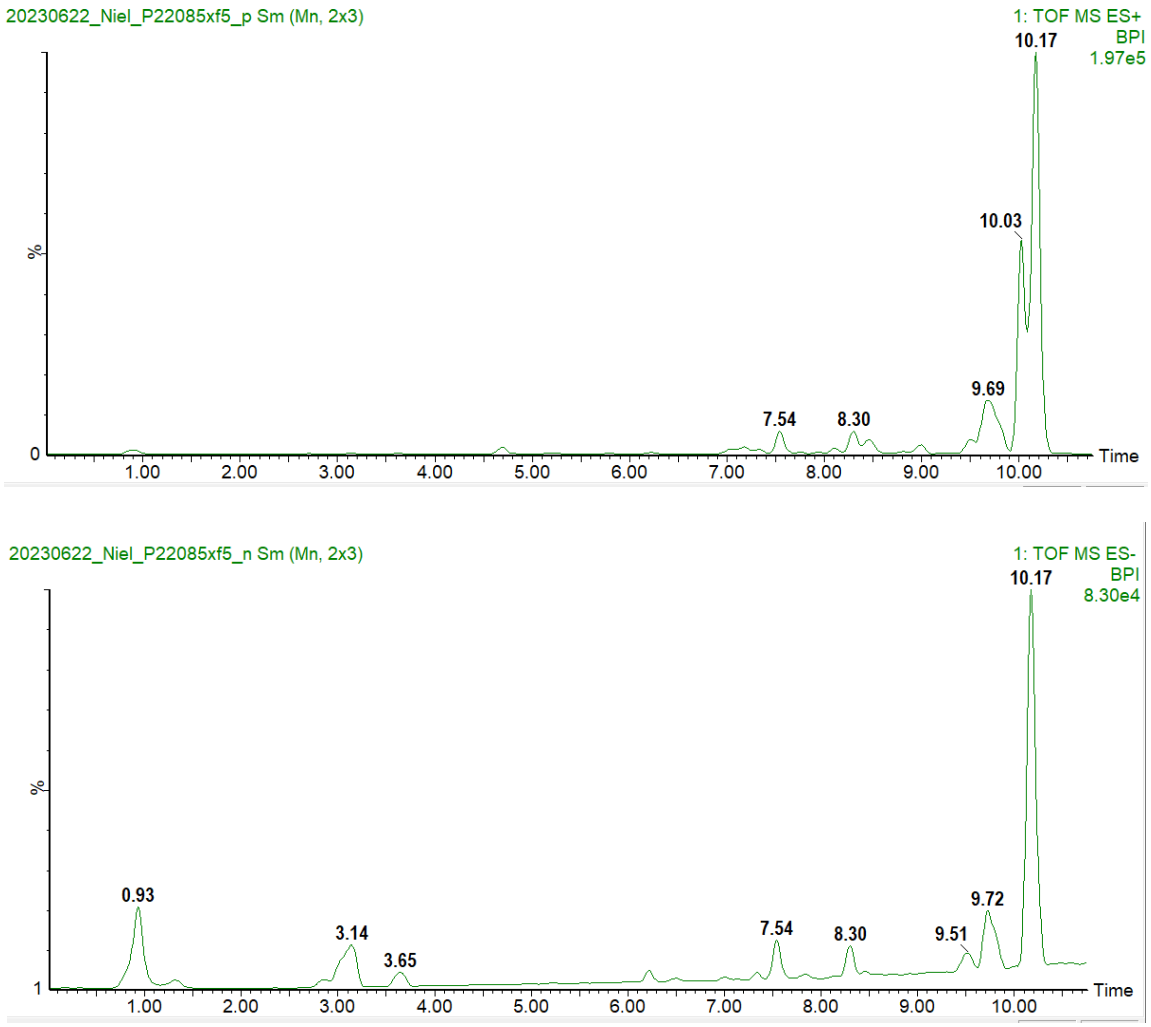

Figure 4-17: Electrospray ionisation chromatograms in both positive (+) and negative (-) mode for *Polygala virgata* fraction 5.

Table 4-8: Peaks identified in the chromatographs for *Polygala virgata* fraction 5.

Retention time (min)	m/z	M (Da) Experimental	Ion	Chemical formula	M (Da) Theoretical	UV
7.481	369.1178	368.1105	M+H	$C_{17}H_{20}O_9$	368.1107	239; 330
9.179	287.0547	288.062	M-H	$C_{15}H_{12}O_6$	288.0634	243; 262; 305; 376
	575.1175	288.0624	2M-H		288.0634	N/D
10.017	273.1124	272.1051	M+H	$C_{16}H_{16}O_4$	272.1049	249;289
	295.0946	272.1054	M+Na			N/D
10.162	319.0814	318.0741	M+H	$C_{16}H_{14}O_7$	318.074	235; 267; 305; 392
	341.0634	318.0742	M+Na	$C_{16}H_{14}O_7$		N/D
	317.0656	318.0729	M-H	$C_{16}H_{14}O_7$		N/D
	635.1406	318.0739	2M-H	$C_{16}H_{14}O_7$		N/D

Da: Dalton, M: molecular mass; m/z: experimental mass without ion amendment; UV: ultraviolet absorption.

Fraction 6 shows the same elucidation as fractions 5, indicating a co-elution throughout the fractionation process **(Table 4-9, Figure 4-18)**. At 10.162 min (UV values of 244, 267 and 391) the following xanthones can be seen; 3,6-dihydroxy-1,2,7-trimethoxyxanthone, 3,8-dihydroxy-1,2,6-trimethoxyxanthone, 1,3-dihydroxy-2,4,7-trimethoxyxanthone and 1,8-dihydroxy-2,3,5-trimethoxyxanthone. At the UV value of 305; the compound 2',3',4,4'-Tetrahydroxy-6,7-methylenedioxyisoflavan could be identified. The compound 2,3-dihydro-2-(2-hydroxy-3,5-dimethoxyphenyl)benzofuran (UV value of 288) can be identified at 10.017 mins for fraction 6, as well as 4',7-dihydroxy-3'-methoxyflavan, 3',4'-dihydroxy-7-methoxyflavan, which was also seen in fraction 5.

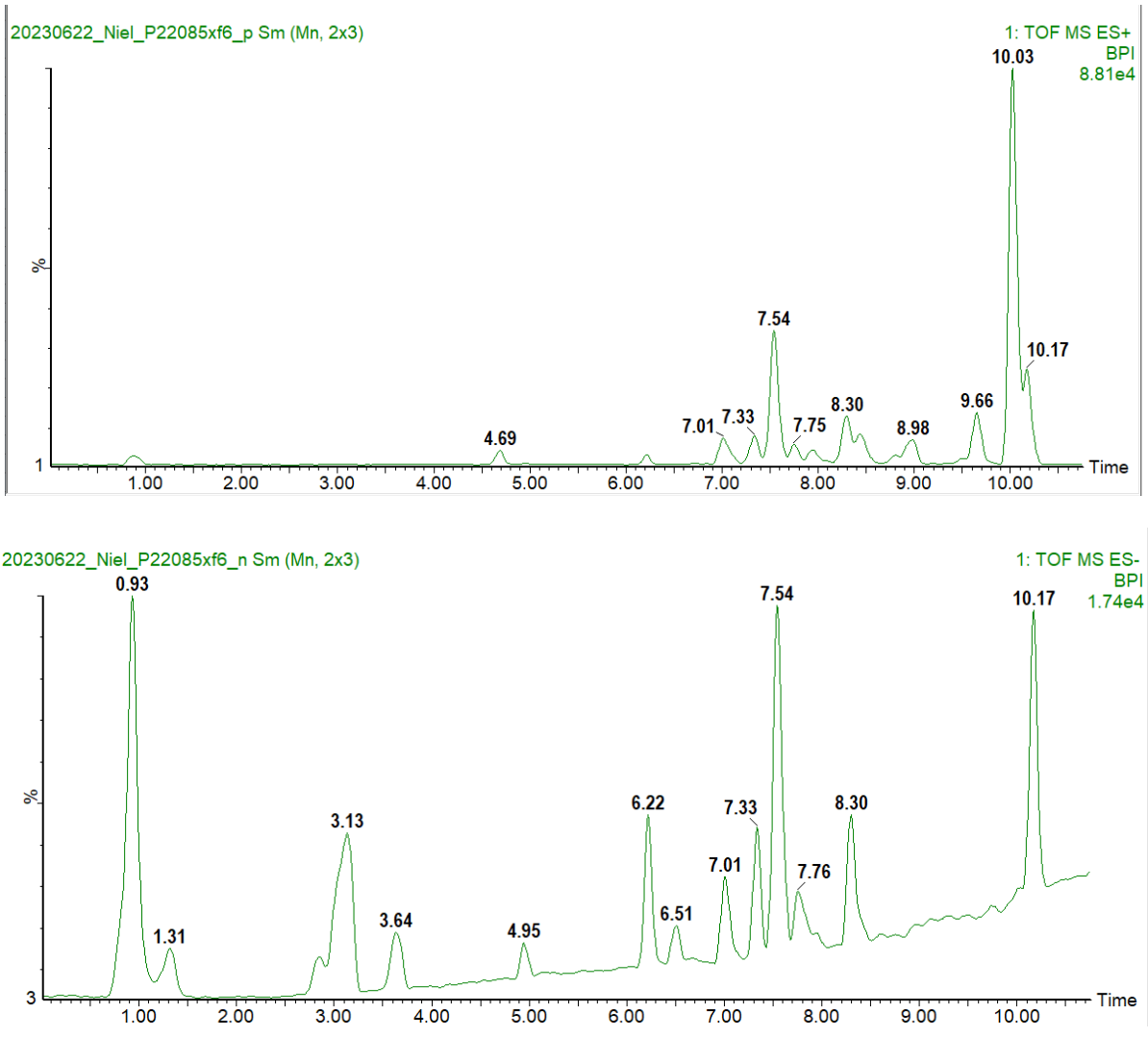

Figure 4-18: Electrospray ionisation chromatograms in both positive (+) and negative (-) mode for *Polygala virgata* fraction 6.

Table 4-9: Peaks identified in the chromatographs for *Polygala virgata* fraction 6.

Retention time (min)	m/z	M (Da) Experimental	Ion	Chemical formula	M (Da) Theoretical	UV
10.017	273.1124	272.1051	M+H	$C_{16}H_{16}O_4$	272.1049	249;288
10.162	319.0809	318.0736	M+H	$C_{16}H_{14}O_7$	318.074	244;267;305;391

Da: Dalton, M: molecular mass; m/z: experimental mass without ion amendment; UV: ultraviolet absorption.

Possible co-elution from fraction 4 could be seen at 7.529 min, with haworforbin B and a glycated derivative of saccharonol A (6-O-β-D-glucopyranoside derivative of 6,8-dihydroxy-3,7-dimethylisocoumarin and 6-O-(4-O-methyl-β-D-glucopyranoside) derivative of 6,8-dihydroxy-3-methylisocoumarin) being detected once more in fraction 7 (**Figure 4-19**).

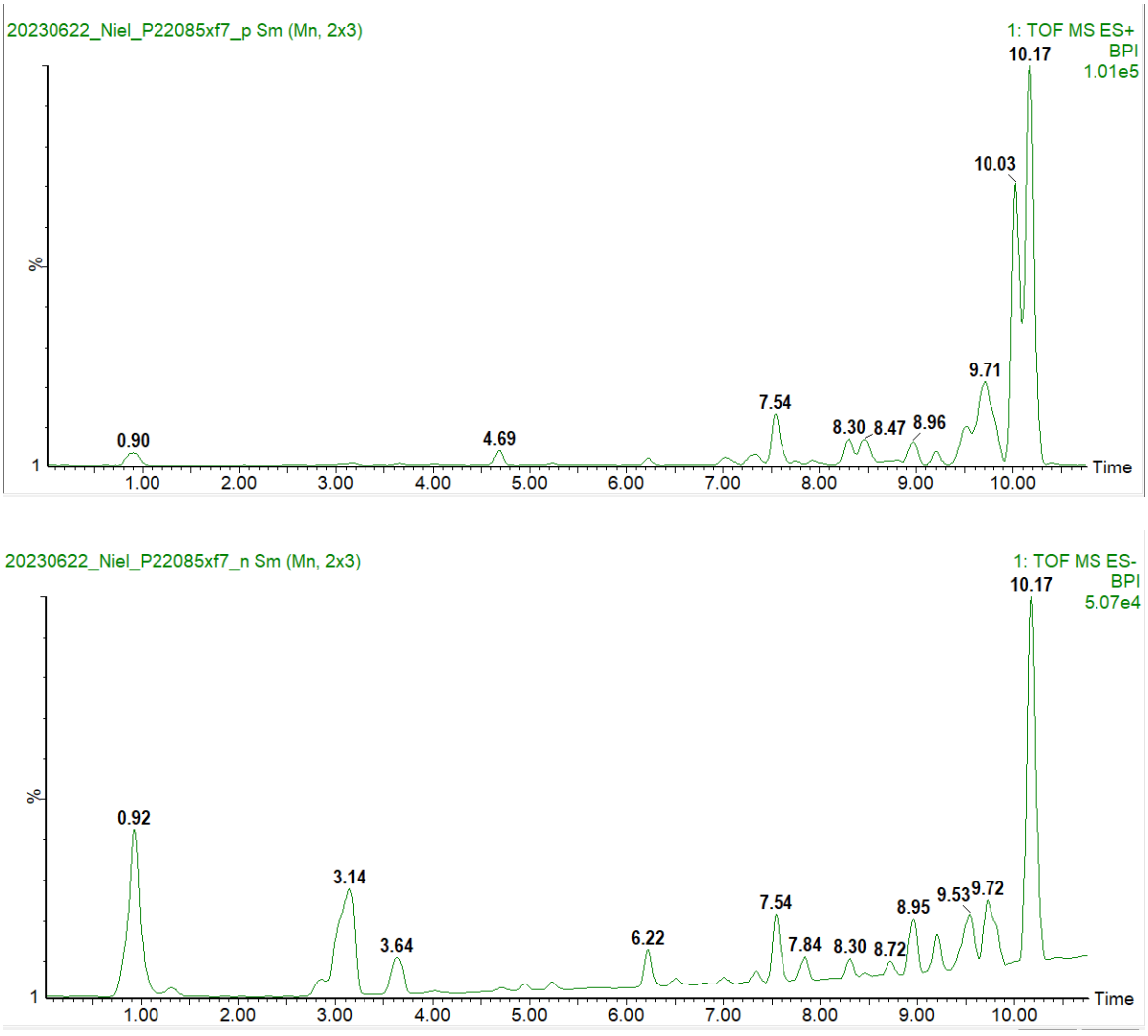

Figure 4-19: Electrospray ionisation chromatograms in both positive (+) and negative (-) mode for *Polygala virgata* fraction 7.

Table 4-10: Peaks identified in the chromatographs for *Polygala virgata* fraction 7.

Retention time (min)	m/z	M (Da) Experimental	Ion	Chemical formula	M (Da) Theoretical	UV
7.529	369.1177	368.1104	M+H	$C_{17}H_{20}O_9$	368.1107	239;330
10.018	273.1125	272.1052	M+H	$C_{16}H_{16}O_4$	272.1049	249;287
	295.0945	272.1053	M+Na	$C_{16}H_{16}O_4$		N/D
	567.2006	272.1057	2M+Na	$C_{16}H_{16}O_4$		N/D
10.163	319.0815	318.0742	M+H	$C_{16}H_{14}O_7$	318.074	238;267;305;392
	341.0638	318.0746	M+Na	$C_{16}H_{14}O_7$	318.074	N/D

Da: Dalton, M: molecular mass; m/z: experimental mass without ion amendment; UV: ultraviolet absorption.

The co-eluting peaks between fractions 5, 6 and 7 at 10.017 min where further investigated using the area calculated from the smooth peak over means and presented with ratio of the areas for fraction 5, fraction 6, and fraction 7 is approximately: 1.64: 1.41: 1.00. This represents the relative proportions of the areas, normalized by the smallest area (Fraction 7). The co-eluting is possible of similar structures at the same retention time as previously stated. The same can be seen in 10.162 minutes, with the ratio moving towards 9.42:1:4.78, normalized by the smallest area (fraction 6). This ratio change in the same compound could be what is driving the change in activity seen across the fractions in antioxidant power (146.40, 23.14, 50.23 mmol $FeSO_4$ equivalence/g, respectively).

4.3.1.5 Compounds identified in *Schotia brachypetala*

Fraction 1 presents with three peaks (**Table 4-11, Figure 4-20**), with the peak at 0.94 min being identified as a possible 2,7-naphthyride derivative, with not enough unique identifiers for a unique match on the database used.[596] These derivatives have been seen in the *Sophora* genus, also under the Fabaceae family.[597] At 4.628 min, the peak corresponds to 1-(3-propylphenyl)-β-carboline, a derivative from the β-carboline alkaloid scaffold. This group of alkaloids has been found in different species of Fabaceae.[598] Isocylexin A, a cyanide-containing phytoalexin, is seen at 4.762 min (**Figure 4-21**). Isocylexin A has been seen in other Fabaceae species and is presumed to play a role in antimicrobial defence.[599]

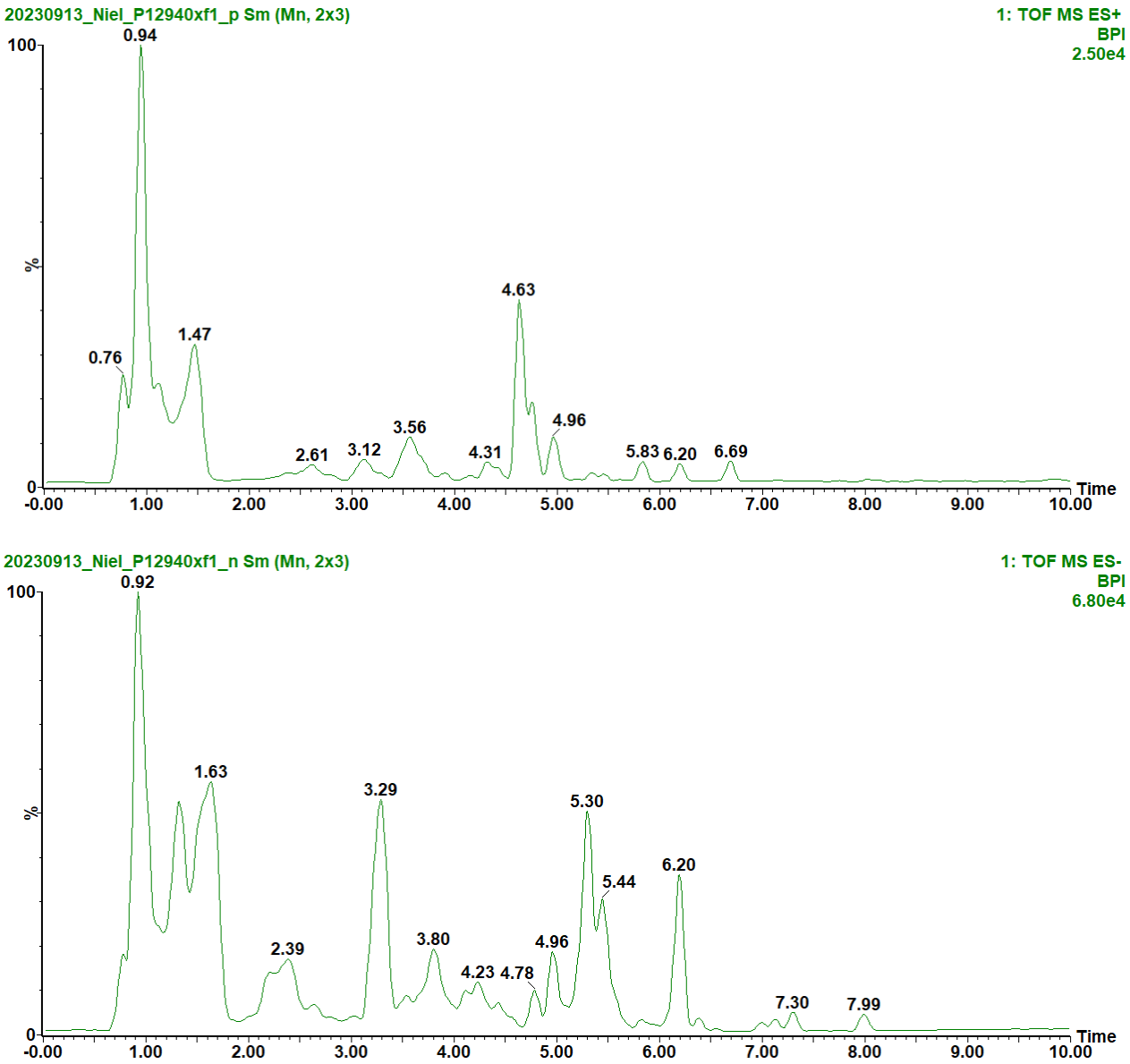

Figure 4-20: **Electrospray ionisation chromatograms in both positive (+) and negative (-) mode for *Schotia brachypetala* fraction 1.**

Table 4-11: Peaks identified in the chromatographs for *Schotia brachypetala* fraction 1.

Retention time (min)	m/z	M (Da) Experimental	Ion	Chemical formula	M (Da) Theoretical	UV
0.94	144.107	143.099	M+H	$C_{10}H_{14}O_6$	143.122	260
4.628	287.158	286.1502	M+H	$C_{20}H_{18}N_2$	286.370	N/D
4.762	173.081	172.0733	M+H	$C_8H_{12}O_4$	172.183	~220
	195.062	172.073	M+Na	$C_8H_{12}O_4Na$		~220

Da: Dalton, M: molecular mass; m/z: experimental mass without ion amendment; UV: ultraviolet absorption.

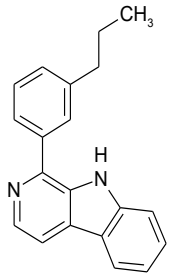

1-(3-Propylphenyl)-β-carboline

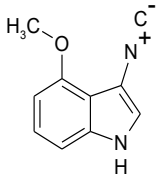

Isocylexin A

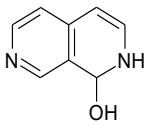

2,6-naphthyride scaffold

Figure 4-21: Compounds and their associated chemical structures identified from chromatographs of *Schotia brachypetala* fraction 1. Figure is self-generated.

Fraction 2 displays two peaks (**Table 4-12, Figure 4-22**), both of which exhibit some degree of co-elution, making it difficult to ascertain the absorbance values corresponding to each compound present. At both UVs for the peak at 4.73 min, they both can be attributed to a naphthoquinone derivative, 2-amino-5-hydroxy-1,4-naphthoquinone, with derivatives of the scaffold identified from *S. brachypetala* in water extractions (**Figure 4-23**).[548] The other compound, identified as nonylamine (or nonan-1-amine), is part of the n-alkyl aliphatic amine group of compounds. These compounds are linked to germination and insect attraction.[600] These amines are found in many families of plants, and is confirmed in the genus *Arachis* (Fabaceae), but given its properties in plant survival,[601] it could still be present.

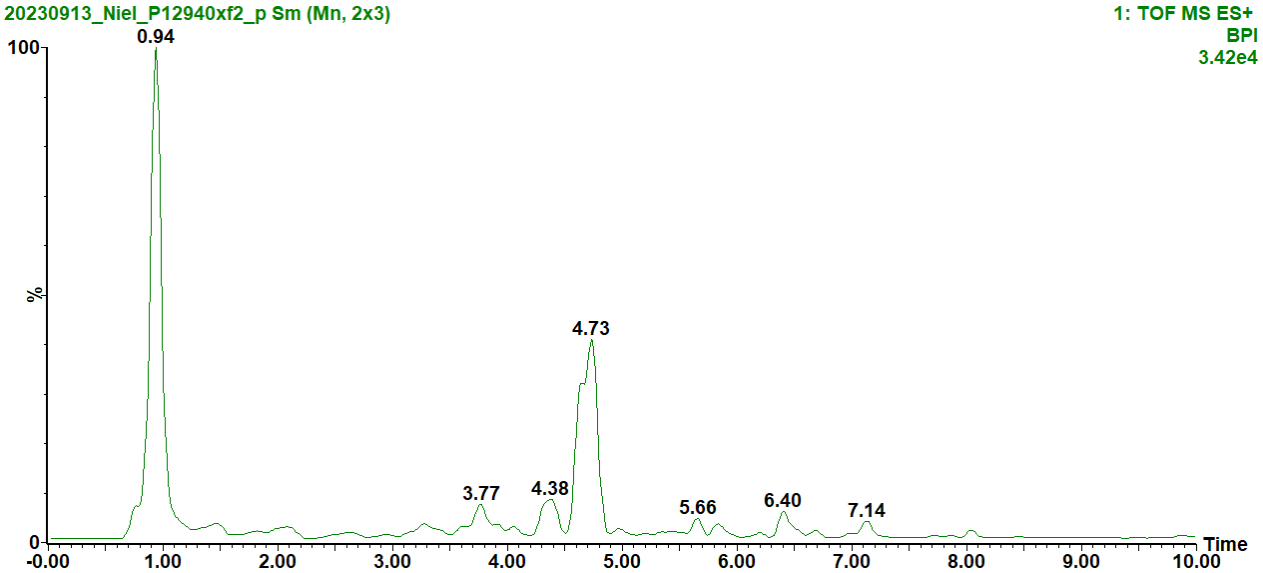

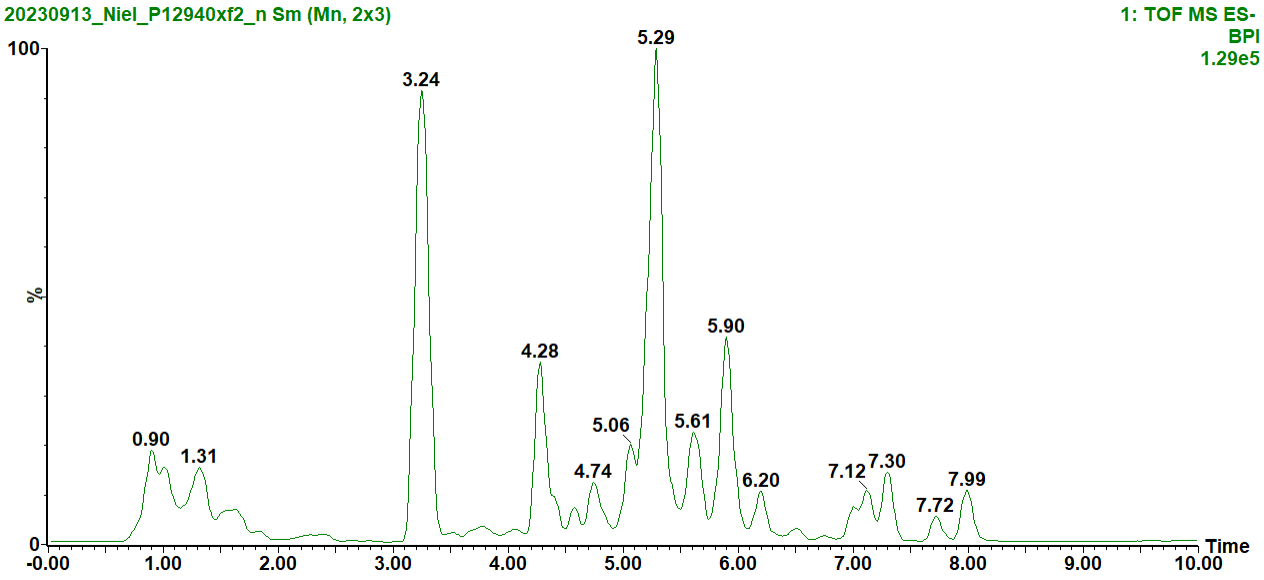

Figure 4-22: **Electrospray ionisation chromatograms in both positive (+) and negative (-) mode for *Schotia brachypetala* fraction 2.**

Table 4-12: Peaks identified in the chromatographs for *Schotia brachypetala* fraction 2.

Retention time (min)	m/z	M (Da) Experimental	Ion	Chemical formula	M (Da) Theoretical	UV
4.73	190.05	189.0424	M+H	$C_{10}H_7NO_3$		240, 330
4.75	144.175	143.1674	M+H	C9H21N		240, 330

Da: Dalton, M: molecular mass; m/z: experimental mass without ion amendment; UV: ultraviolet absorption.

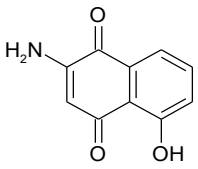

2-Amino-5-hydroxy-1,4-naphthioquinone

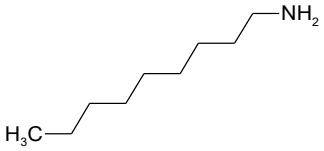

1-Nonylamine

Figure 4-23: **Compounds and their associated chemical structures identified from chromatographs of *Schotia brachypetala* fraction 2. Figure is self-generated.**

Fraction 3 of *S. brachypetala* showcases more phytochemicals, possibly due a more efficacious fractionation step **(Table 4-13, Figure 4-24)**. The peaks 1.271 and 1.995 min are both identified as pangamic acid, an amino sugar originally identified in the species *Cicer* from the *Fabaceae* family.[602] The difference in retention time could be attributed to the ionic status of the carboxylic acid moiety. The peak at 4.513 min has been seen to be ningopgenin, an iridoid monoterpene. At 6.25 min, the peak is seen as either isoferuylcholine or feruloylcholine, with not enough distinction

to say which isomer it is. It is a hydroxycinnamic acid derivative, with the class being one of the most naturally occurrent phytochemical classes.[603] This polyphenolic class has been abundantly seen in Fabaceae.[604] The peaks seen at both 6.393 and 6.714 mins is too broad a scope without any UV absorbance to identify at this time. Loliolide, a derivative of benzofuran, is identified at 7.002 min, as seen in the *Desmodium* species of the Fabaceae family.[605]

Two unique weights are seen at 7.107 min: an unidentified dimer compound at 644.329 Daltons, and some inositol derivative at 345.152 Daltons. As seen with the feruylcholine, there is a possibility of two possible isomers, either 3,6-di-O-acetyl-1,2:4,5-di-O-isopropylidene-allo-inositol or 3,4-di-O-acetyl-1,2:5,6-di-O-isopropylidene-L-chiro-inositol of which both can be found in Fabaceae.[606] The peak at 7.448 min is also unidentified due to a high number of different classes coinciding with the molecular mass and chemical formula.

Three compounds were seen at 7.994 min, with no linkages to anything seen within the Fabaceae family. 4N-benzoylcytidine was seen at 8.418 min, with the chemical formula of $C_{16}H_{17}N_3O_6$, a natural substrate of uridine-cytidine kinase 1/2 and has been seen in Fabaceae.[607] However, a second chemical formula, $C_{21}H_{17}NO_4$, was also seen, and was identified as 5-O-diethyl-methyl-8,8,9-trimethoxy-5-methylbenz[cd]isoindolo[2,1-a]indol-1(8H)-one; a nitrogen-containing benzopyrrole. This compound can also be seen co-eluting at 8.975 min. Both could be novel compounds found in *S. brachypetala*. Also seen at 8.975 min, the compound 8,9-dehydrotheaspirone was identified, and has been seen the *Vigna* species of the family Fabaceae (**Figure 4-25**).[608]

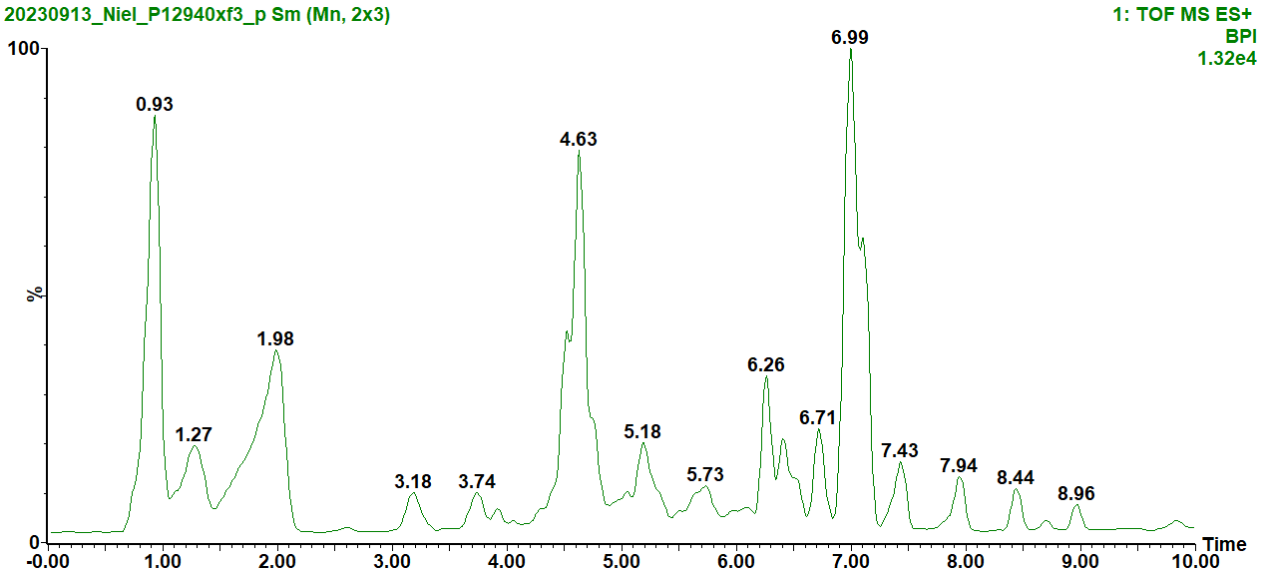

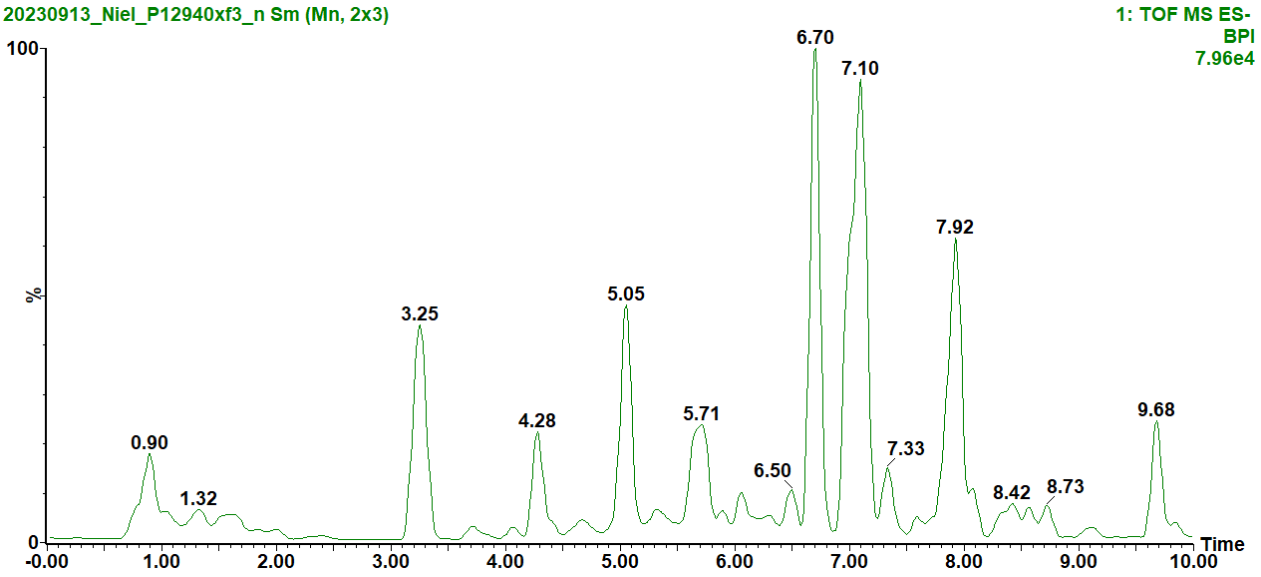

Figure 4-24: **Electrospray ionisation chromatograms in both positive (+) and negative (-) mode for *S. brachypetala* fraction 3.**

Table 4-13: Peaks identified in the chromatographs for *Schotia brachypetala* fraction 3.

Retention time (min)	m/z	M (Da) Experimental	Ion	Chemical formula	M (Da) Theoretical	UV
1.271	281.117	281.109	M+H	$C_{10}H_{19}NO_8$	281.28	258
1.995	281.119	281.112	M+H	$C_{10}H_{19}NO_8$	281.28	258
4.513	171.102	170.094	M+H	$C_9H_{14}O_3$	170.205	N/D
6.25	280.154	279.146	M+H	$C_{12}H_{21}NO_4$		N/D
6.393	169.123	168.115	M+H	$C_{10}H_{16}O_2$		N/D
6.714	225.11	224.102	M+H	$C_{12}H_{16}O_4$		N/D
7.002	197.117	196.109	M+H	$C_{11}H_{16}O_3$		~ 220
7.107	323.168	322.160	M+H	N/D		N/D
	645.337	644.329	2M+H	$C_{22}H_{52}N_4O_{17}$		
7.107	345.152	344.144	M+H	$C_{16}H_{24}O_8$		N/D
7.448	183.101	182.094	M+H	$C_{10}H_{14}O_3$		N/D
	205.083	183.094	M+Na			
7.944	415.163	414.155	M+H	$C_{19}H_{26}O_{10}$		N/D
8.418	348.121	347.11374	M+H	$C_{16}H_{17}N_3O_6$		N/D
				$C_{21}H_{17}NO_4$		
8.975	207.138	206.13062	M+H	$C_{13}H_{18}O_2$		N/D
	348.122	347.113	M+H	$C_{21}H_{17}NO_4$		N/D

Da: Dalton, M: molecular mass; m/z: experimental mass without ion amendment; UV: ultraviolet absorption.

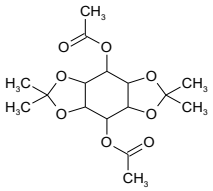

3,6-Di-O-acetyl-1,2:4,5-di-O-isopropylidene-allo-inositol

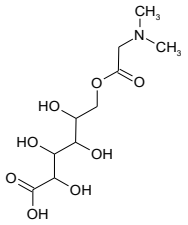

Pangamic acid

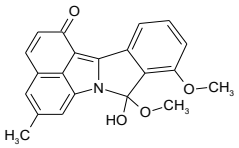

5-O-diethyl-methyl-8,8,9-trimethoxy-5-methylbenz[cd]isoindolo[2,1-a]indol-1(8H)-one;

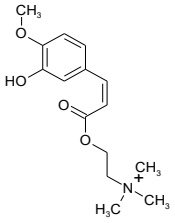

Feroylcholine

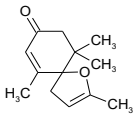

8,9-Dehydrotheaspirone

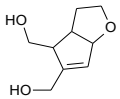

Ningpogenin

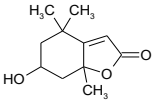

Loliolide

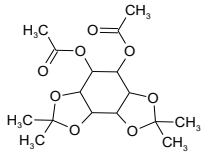

3,4-Di-O-acetyl-1,2:5,6-di-O-isopropylidene-L-chiro-inositol

Figure 4-25: Compounds and their associated chemical structures identified from chromatographs of *Schotia brachypetala* fraction 3. Figure is self-generated.

Fraction 4 presented with a multitude of unidentifiable compounds, with the peaks at 6.13, 6.218, 6.745 and 6.858 min being identified as a broad unspecified benzofuran or flavonoid **(Table 4-14)**. Whilst there are many flavonoids found within *Schotia* and specifically *S. brachypetala*, without any further elucidation it is improbable to get a positive identification.[548] The peak at 4.39 min (145.05 Daltons) is seen a derivative of the biperidine alkaloid scaffold. Whilst the compound at 260.122 Daltons is a glucose derivative, specifically the 2,3-O-isopropylidine-6-deoxyglucose. Either megastigmane or a derivative thereof is identified at 6.496 mins, with it being found within Fabaceae in the *Retama* genus **(Figures 4-26, 4-27)**.[609]

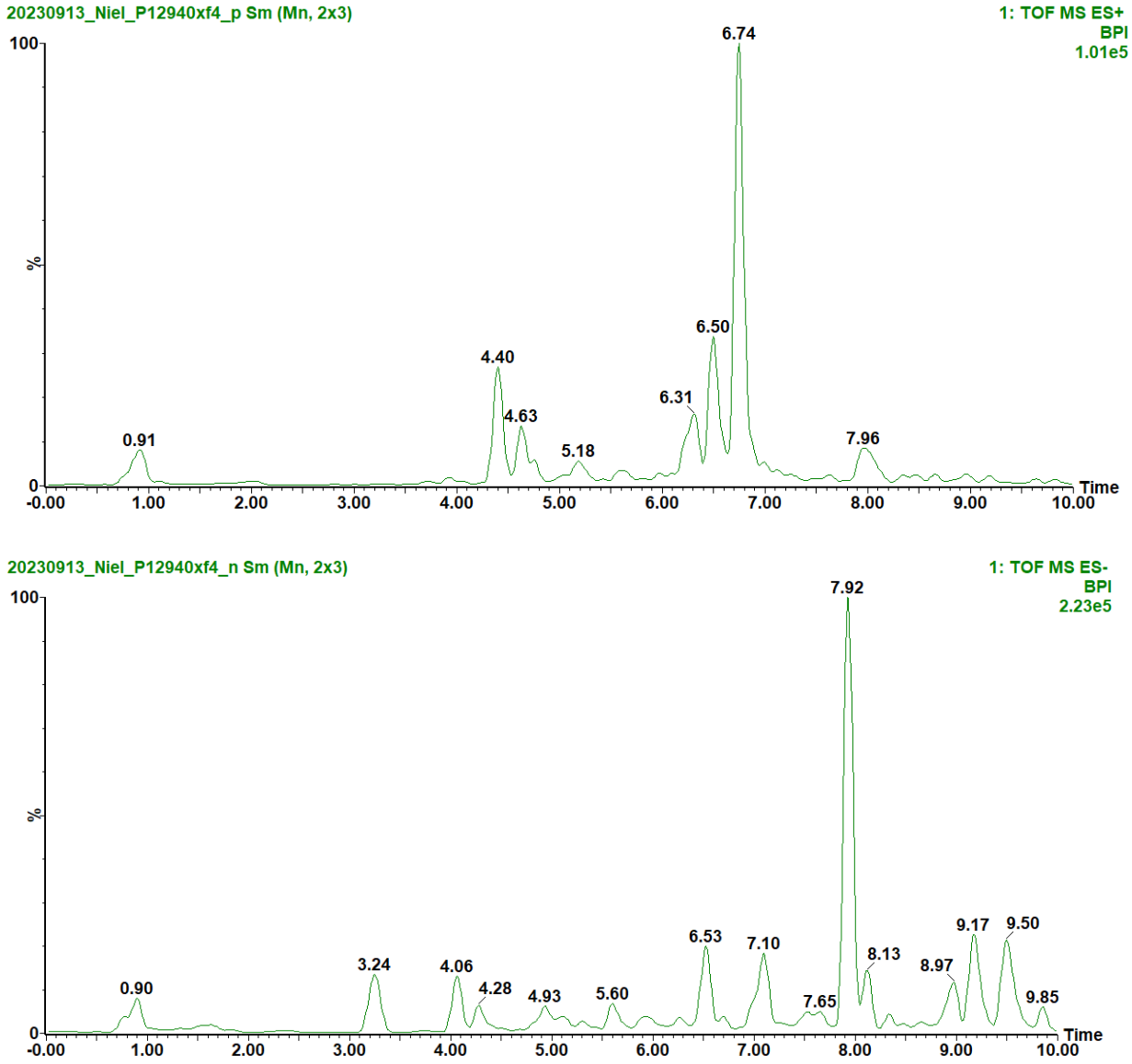

Figure 4-26: **Electrospray ionisation chromatograms in both positive (+) and negative (-) mode for *Schotia brachypetala* fraction 4.**

Table 4-14: Peaks identified in the chromatographs for *Schotia brachypetala* fraction 4.

Retention time (min)	m/z	M (Da) Experimental	Ion	Chemical formula	M (Da) Theoretical	UV
4.39	146.06	145.052	M+H	C_9H_7NO		N/D
	261.13	260.122	M+H	N/D		N/D
6.13	197.188	196.1099	M+H	$C_{11}H_{14}O_3$		N/D
6.218	195.10	194.09	M+H	$C_{11}H_{14}O_3$		N/D
6.496	227.164	226.1566	M+H	$C_{13}H_{22}O_3$		N/D
6.754	197.117	196.1099	M+H	$C_{11}H_{16}O_3$		N/D
6.858	169.122	168.114	M+H	$C_{10}H_{16}O_2$		N/D

Da: Dalton, M: molecular mass; m/z: experimental mass without ion amendment; UV: ultraviolet absorption.

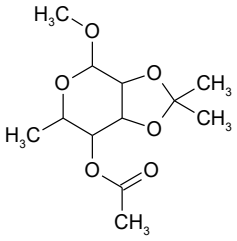

2,3-O-isopropylidene-6-deoxyglucose

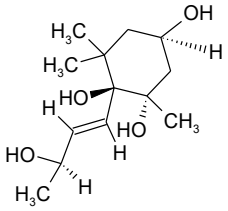

Megastigmane

Figure 4-27: Compounds and their associated chemical structures identified from chromatographs of *Schotia brachypetala* fraction 4. Figure is self-generated.

4.3.2 In vitro assays

The interaction between 6-OHDA-induced cytotoxicity and the cytoprotective mechanisms of the fractions involves a complex network of lipid peroxides, ROS, mitochondrial integrity, and GSH, all of which contribute to ferroptotic cell death. These were investigated as per the methods described in section 4.2.

4.3.2.1 Lipid peroxides

The 6-OHDA molecule increases lipid peroxide levels in various experiments. In rats, 6-OHDA increased TBARS progressively over 48 h when introduced extrastriatally,[610] and increased MDA concentrations by 0.361 nmol/mg protein in the corpus striatum of 6-OHDA-lesioned albino rats.[611] In the SH-SY5Y cell line, an increase in TBARS after exposure to 100 µM (20% increase[299], 60% increase[612]), 60 µM (8 nmol TBARS/mg protein increase),[613] and 50 µM (7.1 nmol TBARS/mg protein increase) 6-OHDA was noted.[612] Based on the mechanism of the assay, the fractions have two places where the effect of the proposed lipid peroxidase inhibition could take place, either in the original production of the OH● or in the induced LOO● production.[580]

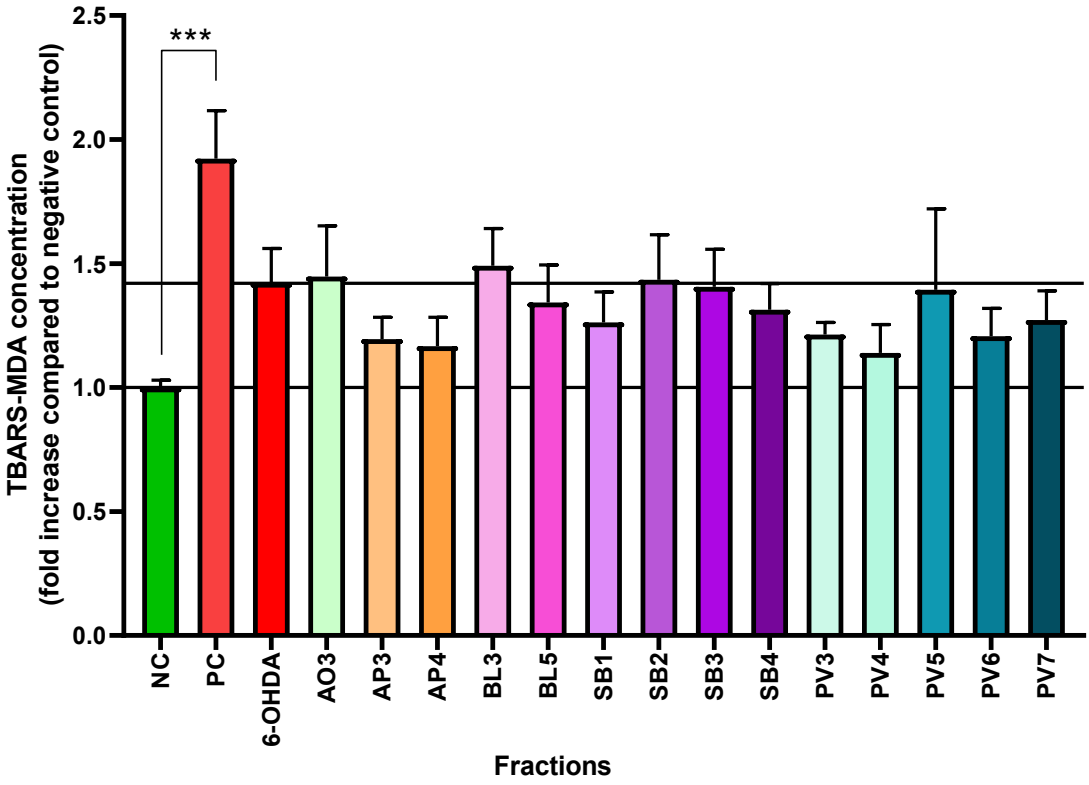

Figure 4-28: **Graph indicating the effect of selected plant fractions on the TBARS-MDA conjugate concentrations as fold increase compared to negative control (NC) ± SEM after 48 h exposure (n = 8). 6-OHDA (35 µM), positive control (PC; 500 µM, potassium persulphate), negative control (NC, FCS supplemented media, 10%), *A. oppositifolia* F3 (AO3), *A. procumbens* F3 (AP3), *A. procumbens* F4 (AP4), *B. latifolia* F3 (BL3), *B. latifolia* F5 (BL5), *S. brachypetala* F1 (SB1), *S. brachypetala* F2 (SB2), S. *brachypetala* F3 (SB3), *S. brachypetala* F4 (SB4), *P. virgata* F3 (PV3), *P. virgata* F4 (PV4), *P. virgata* F5 (PV5), *P. virgata* F6 (PV6), *P. virgata* F7 (PV7).**

Table 4-15: TBARS-MDA conjugate concentration shown as fold increase compared to negative control (NC) ± SEM after 48 h exposure (n = 8).

Control/plant fraction	MDA fold-change ± SEM	Change from 6-OHDA
Negative control	1.00 ± 0.03	N/A
Positive control	1.92 ± 0.19	N/A
6-OHDA	1.42 ± 0.14	N/A
A. oppositifolia F3	1.45 ± 0.20	-0.03
A. procumbens F3	1.20 ± 0.09	0.23
A. procumbens F4	1.17 ± 0.12	0.26

B. latifolia F3	1.49 ± 0.15	-0.07
B. latifolia F5	1.34 ± 0.15	0.08
S. brachypetala F1	1.26 ± 0.12	0.16
S. brachypetala F2	1.43 ± 0.18	-0.01
S. brachypetala F3	1.41 ± 0.15	0.02
S. brachypetala F4	1.31 ± 0.11	0.11
P. virgata F3	1.21 ± 0.05	0.21
P. virgata F4	1.14 ± 0.12	0.28
P. virgata F5	1.39 ± 0.33	0.03
P. virgata F6	1.21 ± 0.11	0.22
P. virgata F7	1.27 ± 0.12	0.15

6-OHDA: 6-hydroxydopamine; 35 µM; PC (positive control): potassium persulphate, 500 µM; MDA: malondialdehyde.

A. oppositifolia F3, *B. latifolia* F3 and *S. brachypetala* F2 did not reduce TBARS-MDA concentration after 48 h (0.025-, 0.068- and 0.011-fold increase), it shows the fractions, and associated phytochemicals are not able to reduce the production of lipid peroxides after 48 h. The hydrophilic nature of the fractions skews the compounds to a more hydrophilic nature, as seen in the large reduction of ROS species **(Table 4-16)** from these fractions. For optimal reduction in lipid peroxides, the compounds should be able to incorporate into the membrane, and thus a more lipophilic fraction (or compound) could have more beneficial physicochemical properties.[614] Reaction rates of lipid bilayer incorporation have been seen to be longer for hydrophilic antioxidants.[615] This is because of the penetration of the hydrophilic compound is less than the penetration of a more lipid soluble compound.[616] The initiation of LOO● is self-propagating, thus in a system where there are LOO● present, more LOO● will form due to the interaction with molecular oxygen.[617] Thus, one can propose that these fractions focus more on the reduction of ROS, rather than reduction on the self-propagation of LOO●. Ratiometrically, LOO● does form various arrangements,[618] with both *cis-cis* and *trans-cis*, as well cyclic forms with intramolecular bond conformations being formed, and these compounds could be reducing one or the other more due to stereospecificity of the compounds. A secondary mechanism behind the non-reduction could be seen in the agonistic interactions of lipoxygenases within the cells, where an increase in the induction of lipoxygenases could lead to an increase in LOO● species formed.[619]

A. oppositifolia crude extract has been reported to increase lipid peroxidation albeit non-significantly at all concentrations tested (1, 3.2, 10, 32 and 100 µg/mL, between 1 and 1.27-fold). With the phytochemical compound of 3-*O*-caffeoyl-muco-quinic acid being identified,[620] however, such lipid peroxidation generation was not observed in the study.

B. latifolia F3 was found to contain no known antioxidant compounds. The lack of larger molecular weight compounds with known antioxidant scaffolds, might explain the lack of reduction in TBARS-

MDA. Fraction 5 presented with several flavones and flavonoids (Table 4-5), including luteolin-7-sophoroside a known antioxidant which contains the flavone scaffold.[621] Luteolin has been reported to reduce radical-induced damage to lipids, DNA and protein.[622, 623] Fraction 5 also presented with a higher FRAP antioxidant value, when compared to F3 (101.67 ± 3.5 and 38.65 ± 4.49 µmol $FeSO_4$ equivalence/g extract, respectively), suggesting that it possesses an increased ability for single electron transfer mechanism than F3.[624] The presence of multiple hydroxylation in the identified methoxylated flavones within F5, supports the antioxidant activity.[625, 626] Whilst a small decrease was seen, F5 did induce a significant reduction at the concentration tested. The delocalisation of the electrons in the catechol ring and subsequent removal of a hydrogen ion is the proposed mechanism for lipid peroxide scrubbing **(Figure 4-29).**[627]

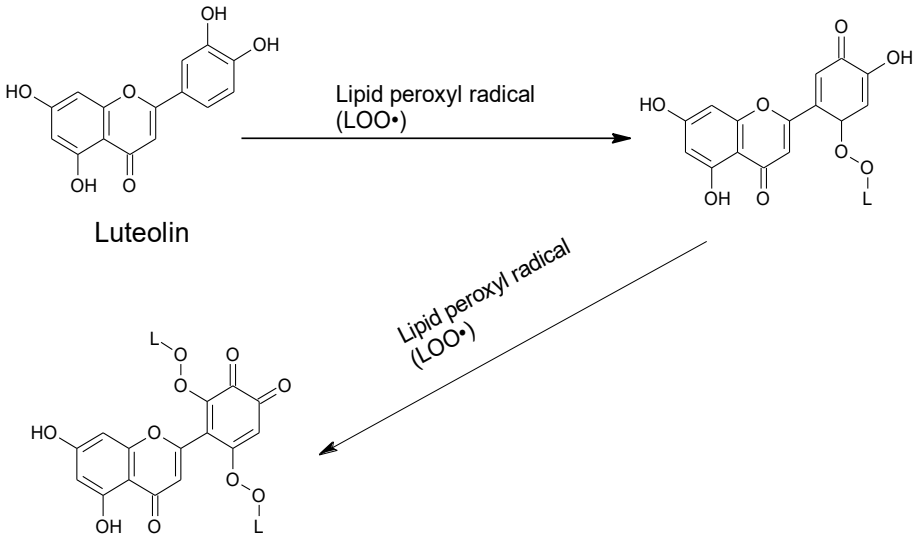

Figure 4-29: Proposed mechanism for lipid peroxyl scrubbing in the presence of multi-hydroxylated flavones (luteolin). Figure is self-generated.

Luteolin, as well as other flavanols such as fisetin and quercetin, possess lipoxygenase inhibition properties, harking to the catechol moiety within the substituent ring.[628] While lipoxygenases are not instrumental to promote ferroptosis, the role they play is in the continuous pool of LOO●, as overexpression of lipoxygenases has been seen to sensitise cells to ferroptosis.[629] Fractions 3 and 4 of *A. procumbens* reduced TBARS-MDA (0.228 and 0.257-fold, respectively) and ROS **(Table 4-16)**, so their phytochemical constituents are most likely reducing the OH●, thus reducing the initiation process to produce LOO●.

S. brachypetala F1, F3 and F4 presented with a decrease in TBARS-MDA with 0.161, 0.017, 0.109-fold, respectively. The fractions also had low FRAP values with F2, F3 and F4 only presenting with 1.02 ± 1.23, 5.35 ± 2.61 and 10.40 ± 2.26 µmol $FeSO_4$ equivalence/g extract, respectively. *S. brachypetala* crude fractions (water and methanol extractions) did show positive

correlations in reducing the OH● and lipid peroxides at 10 µg/mL at ~60% and ~90% scavenging, respectively.[630] The low antioxidant activity could be due to the removal of some polyphenolic compounds throughout the extraction and fractionation process, or the remaining phytochemicals not being active on this specific pathway. A different extraction method or solvent system may be required to ensure the full potential of this extraction.

P. virgata reduced TBARS-MDA levels by 0.21-, 0.28-, 0.22- and 0.15-fold, for F3, F4, F6 and F7, respectively. Fraction 4 decreased the TBARS-MDA the most of all fractions, which may be linked to the identified coumarin and isocoumarin derivatives which are able to reduce lipid peroxides.[631] Although no antioxidative studies have been reported for *P. virgata*, other species within the same genus has presented with lipid peroxide reduction.[632, 633] Fractions 5 to 7 all presents with xanthones as the main phytochemical class, with the change in activity between the fractions explained by ratiometric differences of the associated phytochemicals which can affect the reducing potential.

Xanthones, together with flavones, have potent antioxidative effects.[634] Substituents on the xanthone scaffold have a large effect on the activity, as seen with tetra- and trihydroxy xanthones being more potent antioxidants as compared to dihydroxy xanthones. Within the dihydroxy scaffold, a catechol ring is seen as key substituents.[635] The proposed mechanism of action is where the OH● is scrubbed by hydroxyl groups to reduce TBARS-MDA formation via OH● (**Figure 4-30**).[636]

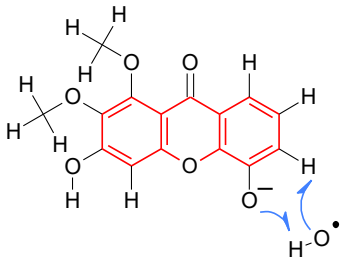

3,5-dihydroxy-1,2-dimethoxyxanthone

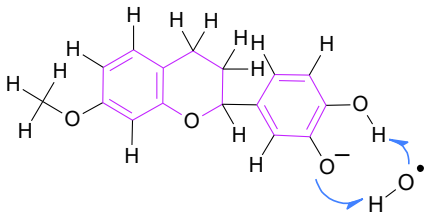

3',4'-dihydroxy-7-methoxyflavan

Figure 4-30: **Schematic representation of the proposed mechanism for scrubbing of hydroxyl radical (OH●) by means of hydrogen bonding (blue) as done by xanthone (red scaffold) and flavones (purple scaffold) identified out of *Polygala virgata*. Image self-generated.**

4.3.2.2 Reactive oxygen species

The generation of ROS by 6-OHDA is a well-established mechanism studied using the SH-SY5Y neuroblastoma cell line.[611] Various studies have demonstrated ROS generation induced by 6-OHDA, as measured by H_2-DCF-DA. With 6-OHDA increasing ROS at 23.4 µM (~200% increase after 48 h[488]), 50 µM (1.5-fold after 24 h,[637]), and 100 µM (5-fold increase after 24 h,[638] and 200 RFU/mg protein increase[639]).

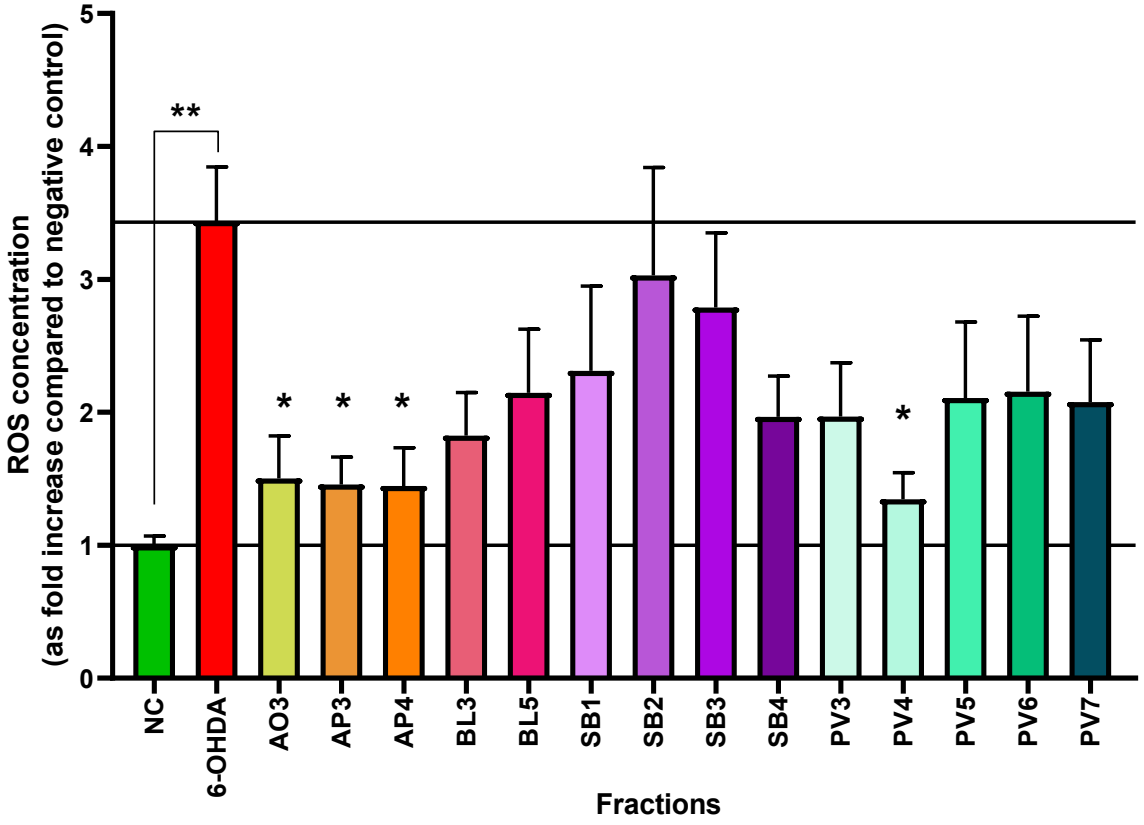

Figure 4-31: **Graph representing the effect of selected plant fractions on reactive oxygen species (ROS) concentration as fold increase compared to negative control (NC) ± SEM after 48 h exposure (n = 9). 6-OHDA (70 µM), positive control (PC; 500 µM, potassium persulphate), negative control (NC, 10%, FCS-supplemented media); *A. oppositifolia* F3 (AO3), *A. procumbens* F3 (AP3), *A. procumbens* F4 (AP4), *B. latifolia* F3 (BL3), *B. latifolia* F5 (BL5), *S. brachypetala* F1 (SB1), *S. brachypetala* F2 (SB2), S. *brachypetala* F3 (SB3), *S. brachypetala* F4 (SB4), *P. virgata* F3 (PV3), *P. virgata* F4 (PV4), *P. virgata* F5 (PV5), *P. virgata* F6 (PV6), *P. virgata* F7 (PV7).**

Significance shown is against 6-OHDA, with * p < 0.05, ** p < 0.005. Self-generated.

Table 4-16: Reactive oxygen species concentration shown as fold increase compared to negative control (NC) ± SEM after 48 h exposure (n = 9). 6-OHDA: 6-hydroxydopamine, 70 µM.

Control/plant fraction	ROS (as fold increase against NC) ± SEM	ROS Change from 6-OHDA
Negative control	1.00 ± 0.070	N/A
Positive control (potassium persulphate)	3.81 ± 0.76	N/A
6-OHDA**	3.44± 0.41	N/A
A. oppositifolia F3*	1.50 ± 0.32*	1.94
A. procumbens F3*	1.46 ± 0.21*	1.98
A. procumbens F4*	1.45 ± 0.29*	1.99
B. latifolia F3	1.83 ± 0.32	1.61
B. latifolia F5	2.15 ± 0.48	1.29
S. brachypetala F1	2.31 ± 0.64	1.12
S. brachypetala F2	3.03 ± 0.81	0.41
S. brachypetala F3	2.79 ± 0.56	0.65
S. brachypetala F4	1.97 ± 0.31	1.47
P. virgata F3	1.97 ± 0.40	1.47
P. virgata F4*	1.35 ± 0.20*	2.09
P. virgata F5	2.11 ± 0.57	1.33
P. virgata F6	2.16 ± 0.57	1.28
P. virgata F7	2.08 ± 0.47	1.36

Significance shown is against 6-OHDA, with * p < 0.05, ** p < 0.005

Like the TBARS assay, *P. virgata* F4 resulted in a significant reduction in intracellular ROS concentration (2.09-fold p < 0.05). This was also the case for *A. oppositifolia* F3, and F3 and 4 of *A. procumbens*. This suggests a stronger affinity for intracellular ROS compared to the other fractions tested. Fractions 3 and 4 of *A. procumbens* contain the same compound, with the catechol (3,4-dihydroxy) substitution, most likely contributing to the stabilisation and neutralisation of the radical.[640] When radicals are stabilised, they become less reactive to cells and cell organelles [641] This compound could explain the co-current reduction seen in both fractions (**Figure 4-31**). The reduction in ROS is also associated with the reduction in TBARS-MDA (**Table 4-13**). Fraction 4 of A. procumbens exhibited a FRAP value of 134.15 µmol $FeSO_4$/g extract, demonstrating its capacity for single electron transfer antioxidant activity. This activity is associated with the stabilisation of the radical electron (**Figure 4-32**).

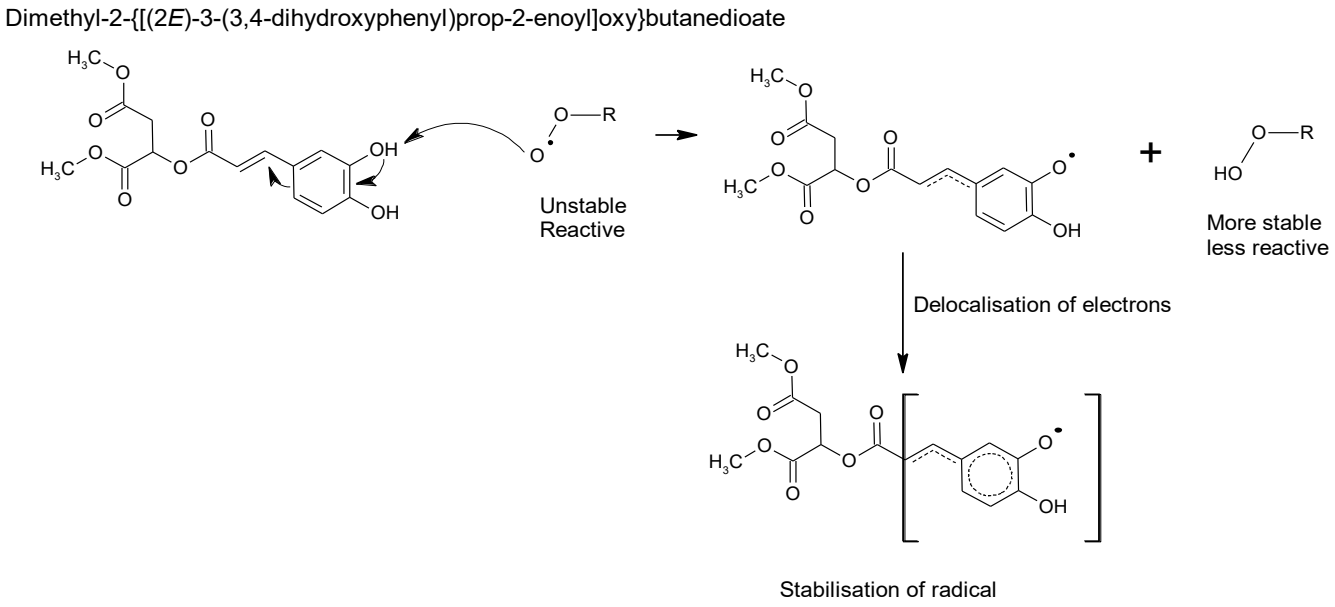

Figure 4-32: Schematic representation of the stabilisation of radicals through delocalisation on the catechol substituent of the co-eluting compounds in both *Aptosimum procumbens* fractions 3 and 4. Figure is self-generated.

Crude ethanol and acetone *A. oppositifolia* extracts also reduced 6-OHDA induced ROS significantly ($p < 0.01$), by ~190% at 0.5 µg/mL,[488] this is similar to the reduction seen in this study at 10 µg/mL (1.94-fold or 194.3%). Antioxidant activity was also seen in MeOH, acetone and chloroform crude extracts of *A. oppositifolia* (0.25 to 1 mg/mL).[642] A reduction in non-induced ROS species (i.e. ROS generated in normal cell metabolism) in HepG2 cells was reported for a water extraction of the plant (1 to 100 µg/mL, with 10 µg/mL reducing ROS by 0.08-fold).[620] With the prevalent identification of hydroxycinnamic acids within F3 of *A. oppositifolia*, it can be postulated that there exists a mixture of water soluble polyphenolic acids (**Figure 4-33**). These acids showcase an affinity more towards water-soluble radicals,[643] rather than lipid radicals. The TBARS assay results for F3 showed a non-reactive response in the reduction of lipid radicals. The FRAP value of F3 (255.08 ± 14.00 µmol $FeSO_4$ equivalence/g extract) also showcases a bigger affinity towards single electron transfer mechanism**,** as it showed the highest antioxidant value of all the fractions selected **(Table 3-7).**

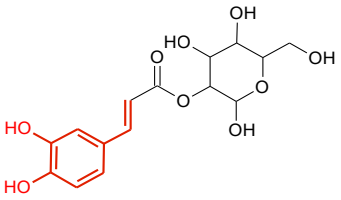

2-*O*-caffeoylglucose

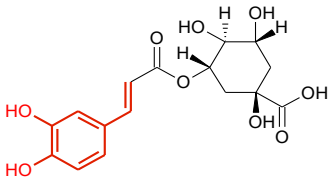

1-O-trans-caffeoyl-β-D-allopyranoside

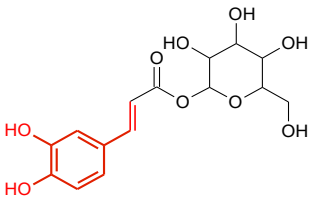

3-O-caffeoyl-muco-quinic acid

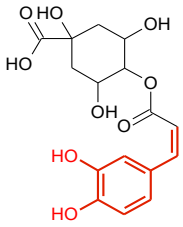

4-(3,4-dihydroxycinnamoyl)quinic acid

Figure 4-33: Chemical structures of phenolic compounds identified in *Acokanthera oppositifolia* fraction 3 with the catechol substituent indicated (in red).

Fraction 3 and 5 of *B. latifolia* reduced intracellular ROS by 1.61- and 1.29-fold respectively. The amount of reduction seen for F5 is not corroborated by the findings of luteolin and luteolin derivatives (at 50 µg/mL) in other studies, where the derivatives reduced ROS to a greater extent.[644] Fraction 5 also presented with a better FRAP antioxidant value, when compared to F3, but with the ROS reductions seen, it appears that the concentration of luteolin within F5 is not enough to reduce the water-soluble ROS generated by 6-OHDA. Additionally, the various flavones identified in F5, although multi-hydroxylated, lacked substitutions at the 2', 3', or 4' positions (**Figure 4-34**). The latter are associated with enhanced ROS reduction activity in acellular systems.[645] Currently, no data could be found on other *Bulbine* species being tested on the SH-SY5Y cell line.

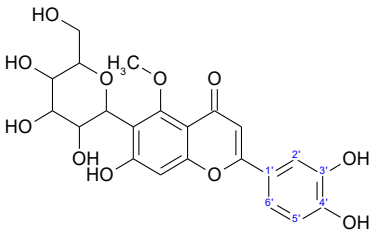

6-C-β-D-Glucopyranosyl-5-methoxy-3',4',7-trihydroxyflavone

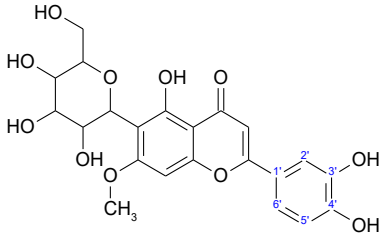

6-C-β-D-Glucopyranosyl-3',4',5-trihydroxy-7-methoxyflavone

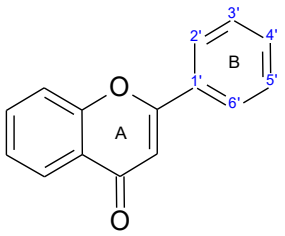

Flavone structure

Figure 4-34: Schematic representation of the chemical structures of the hydroxylated substituents of the compounds found in *Bulbine latifolia* fraction 5, where increased activity will be seen in 2',3',4'-trihydroxyflavones, but all identified compounds are seen to be derivatives of either 3',4',5'-trihydroxyflavones or 4',5,7-trihydroxyflavones. Image self-generated.

Fractions 1 to 4 of *S. brachypetala* reduced ROS by 1.12, 0.40-, 0.65-, and 1.47-fold. Even though the fractions did not contain strong FRAP activity, F4 of *S. brachypetala* is comparable to *B. latifolia* F3 in cellular ROS reduction but presented with a FRAP value almost four times as strong. This suggests that, although the FRAP assay did not demonstrate strong acellular activity, F4 exhibits greater antioxidant potency in vitro, implying the involvement of a different antioxidant mechanism than that assessed by the FRAP assay. S. brachypetala stem and bark extracts have been found to contain ~303.91 mg tannic acid/g plant material.[546] Crude water extracts of S. brachypetala leaves displayed high levels of flavonoids, including multiple quercetin and luteolin derivatives. However, these flavonoids were not detected in the sample used in this study, potentially due to losses during fractionation or variations introduced by the extraction solvents used.[548] This shows that locational and seasonal differences make a difference in activity elucidated.

P. virgata F4 reduced intracellular ROS levels significantly ($p < 0.05$) and by the largest margin (2.09-fold). Fractions 3, 5, 6 and 7 all had comparable reductions of 1.47-, 1.33-, 1.28-, 1.36-fold respectively with the only difference in these fractions being the ratios between the identified compounds. Fraction 4 was found to contain the coumarin derivatives, haworforbin B and saccharonol A. Coumarins with hydroxyl groups in the ortho position on ring A demonstrate high levels of ROS scavenging, as has been observed for catechol moieties earlier.[646] Haworforbin B

present with only one hydroxyl substituent, while saccharonol A has two hydroxyl groups, albeit in *meta* configuration (**Figure 4-35**). These structural changes may account for the strong ROS reduction noted for F4, as the conformations of these compounds could facilitate the induction or activation of antioxidant enzymes.[646] Even though the same coumarins were elucidated in F7, the concentration or ratio thereof could have been lower, thereby explaining the difference in activity noted.

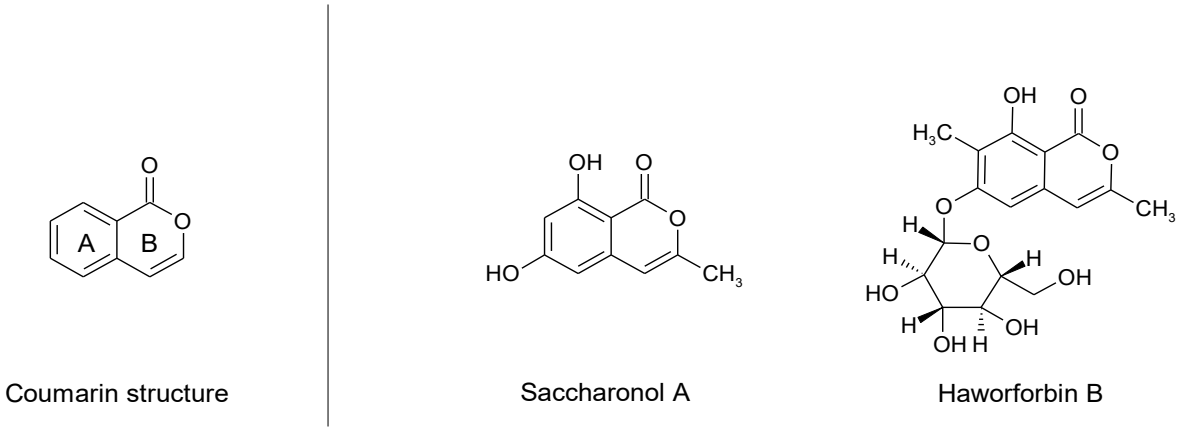

Figure 4-35: Chemical structures of the compounds identified from fraction 4 of *Polygala virgata* and the comparison to the base structure of coumarins.

Multiple xanthones were identified in F5 to 7, all of which contain a privileged scaffold.[647] This is from the ability of xanthones to form both zwitterionic bonds and various isomeric forms to produce multiple high affinity bindings to a large array of protein structures. These protein structures range from antioxidant enzymes,[648] MAO-B,[649] and tyrosinase inhibition.[650] This molecular and enzymatic promiscuity could prove difficult to understand, as there are many antagonistic or synergistic interactions possible between the impact and metabolism of ROS. This could explain the change in ROS seen between F4 and the rest of the *P. virgata* fractions.

4.3.2.3 Mitochondrial integrity

Mitochondrial membrane integrity and potential are affected by 6-OHDA as soon as 2 h after incubation, with 50 µM causing a 20% loss in ΔΨm after 24 h.[651] and at 23.5 µM, there is a 35% loss in $\Delta\Psi_m$ after 48h in the SH-SY5Y cell line.[488] At 23.5 µM, a 35% loss in ΔΨm was observed after 48 h of incubation. Additionally, the presence of 6-OHDA has been shown to increase the loss of Cyt c from the ETC, further inhibiting ΔΨm. It is known that 6-OHDA reversibly inhibits COM I (NADH dehydrogenase) and Cyt c in the electron transport chain.[652] Literature also suggests a reduction in total ATP production after cells are exposed to 6-OHDA, indicating a loss of ΔΨm.[653]

The generation of ROS via autooxidation and metabolism of 6-OHDA leads to direct cellular damage and activation of death signalling pathways.[31] This reduction in respiration and ATP production is attributed to a loss of ΔΨm (depolarisation), where the membrane of the mitochondria becomes more positive charged and there is loss in the proton movement across the inner membrane.[115] The affinity to Com I could be greater for some of the compounds compared to 6-OHDA, indicating a possible removal of 6-OHDA from the active site of Com I.[654] Studies using H_2O_2 as a cytotoxin have reported an increase in mitochondrial mass after exposure, eluding to the cell producing more mitochondria in an attempt to keep producing the energy needed for normal cell respiration.[655]

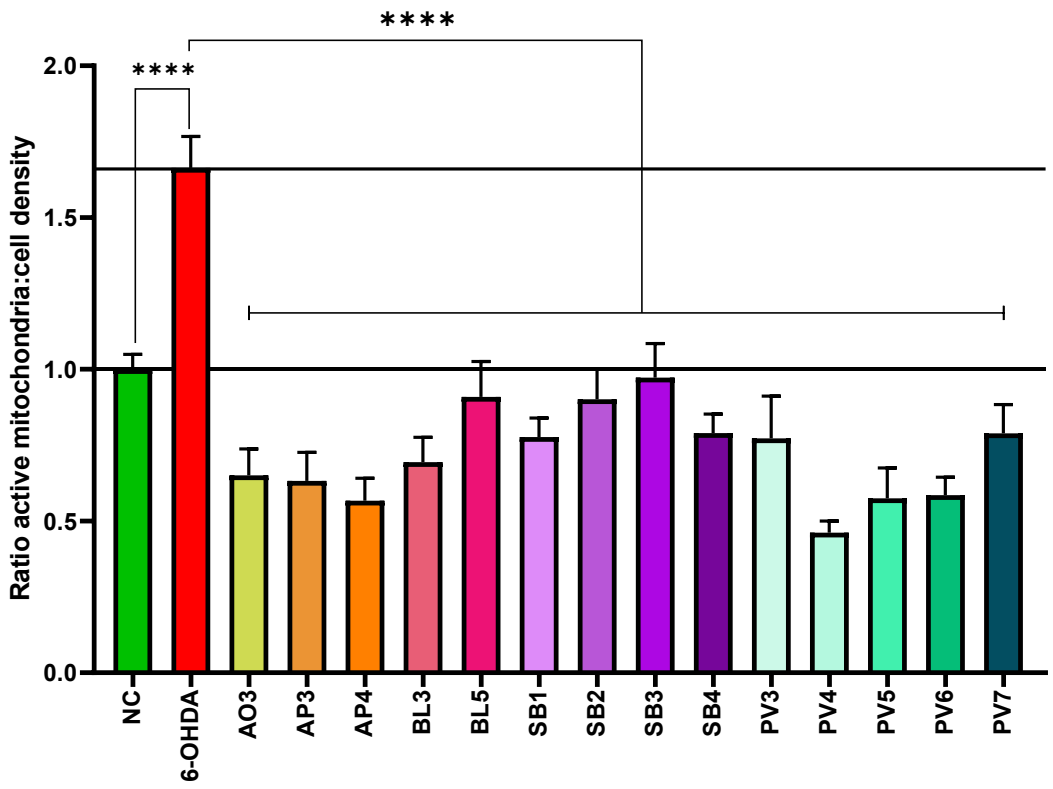

Figure 4-36: Graph representing the ratio of active mitochondria to cell density as fold increase compared to negative control (NC) ± SEM after 48 h exposure (n = 9). 6-OHDA (70 µM;), positive control (PC; 500 µM, potassium persulphate), negative control (NC; 10%, FCS supplemented media). Significance shown is against 6-OHDA, with **** $p < 0.001$. *A. oppositifolia* F3 (AO3), *A. procumbens* F3 (AP3), *A. procumbens* F4 (AP4), *B. latifolia* F3 (BL3), *B. latifolia* F5 (BL5), *S. brachypetala* F1 (SB1), *S. brachypetala* F2 (SB2), S. *brachypetala* F3 (SB3), *S. brachypetala* F4 (SB4), *P. virgata* F3 (PV3), *P. virgata* F4 (PV4), *P. virgata* F5 (PV5), *P. virgata* F6 (PV6), *P. virgata* F7 (PV7). Self-generated from data collected.

Table 4-17: Ratio of active mitochondria to cell density as fold increase compared to negative control (NC) ± SEM after 48 h exposure (n = 9). 6-OHDA: 6-hydroxydopamine, 70 µM.

Control/plant fraction	Ratio of active mitochondria to cell density as fold increase as compared to negative control (NC) ± SEM	Difference to negative control
Negative control	1.00 ± 0.05	N/A
6-OHDA	1.66± 0.10	0.66
A. oppositifolia F3****	0.65 ± 0.09	0.35
A. procumbens F3****	0.63 ± 0.10	0.37
A. procumbens F4****	0.57 ± 0.08	0.43
B. latifolia F3****	0.69 ± 0.08	0.31
B. latifolia F5****	0.91 ± 0.12	0.09
S. brachypetala F1****	0.78 ± 0.06	0.22
S. brachypetala F2****	0.90 ± 0.10	0.10
S. brachypetala F3****	0.98 ± 0.11	0.03
S. brachypetala F4****	0.79 ± 0.06	0.21
P. virgata F3****	0.77 ± 0.14	0.23
P. virgata F4****	0.46 ± 0.04	0.54
P. virgata F5****	0.58 ± 0.10	0.43
P. virgata F6****	0.59 ± 0.06	0.41
P. virgata F7****	0.79 ± 0.10	0.21

Significance relative 6-OHDA, **** $p < 0.0001$

All fractions showed a significant ($p < 0.001$) reduction of the ratio of active mitochondria to cell density (**Figure 4-36, Table 4-17**). Although fractions resulted in an increased in cell density, actively respirating mitochondria did not increase proportionally, e.g. *P. virgata* F4 – F6, and *A. procumbens* F3 and F4. The decrease in healthy mitochondria, despite the increase in cell density, suggests that the compounds are mitigating the effects of 6-OHDA on the cells without enhancing the number of mitochondria. The effect may also be attributed to a reduction in the inhibition of ATP synthase, which implies that the available mitochondria are still able to produce ATP.[656] These fractions may thus be inducing hyperpolarisation of the membrane. For example, *B. latifolia* F5 and *S. brachypetala* F3 resulted in an increase in active mitochondria as the cell density increased, normalising the ratio closer to that of the negative control. The β-carboline scaffold, identified in F1 of *S. brachypetala* has neuroprotective properties, since it led to an increase in dopamine secretion in dopaminergic cells in rat midbrains, and increased the respiration rate of Com V of the ETC. The latter may explain the normalisation seen in the mitochondrial assay.[657]

The change in the proton movement can affect the pH of the inner membrane, resulting in some voltage gated ion-channels altering transport characteristics.[658] It may thus be postulated that the

compounds in *P.* virgata F4 – F6, *A.* procumbens F3 and F4 could be affecting the ion-gated channels, resulting in a hyperpolarised state resulting in the inner mitochondrial membrane being more negatively charged. This could be due to the compounds not influencing the inhibition of Com I due to 6-OHDA (thus inhibiting the entry of new protons), or the compounds are altering the pH within the membrane.

4.3.2.4 Glutathione depletion

It has been suggested that 6-OHDA can increase GSH levels over a 24-h period, however a decrease in endpoint GSH levels has been observed in the SH-SY5Y cell line after 48 h of exposure to 6-OHDA.[488, 651] As 6-OHDA induces oxidation, the cells initially respond by increasing GSH levels to counteract the oxidative products of 6-OHDA exposure. However, as the cells begin to die, less GSH becomes available.[31] Evidence shows an increase in glutathione disulfide (GSSH) concentration, which skews the GSSH/GSH ratio in favour of oxidation products.[659]

Typically accounting for ~15% of cytoplasmic glutathione, GSSG is often considered just a byproduct of GSH metabolism.[660] However, under conditions of severe ROS or RNS exposure, the oxidation of GSH to GSSG may contribute significantly to its depletion and could play a critical role in apoptosis induced by cytotoxic agents.[661] Since GSH synthesis is ATP dependant,[662] the reduction of ATP levels should not be overlooked, though this falls outside the scope of this study

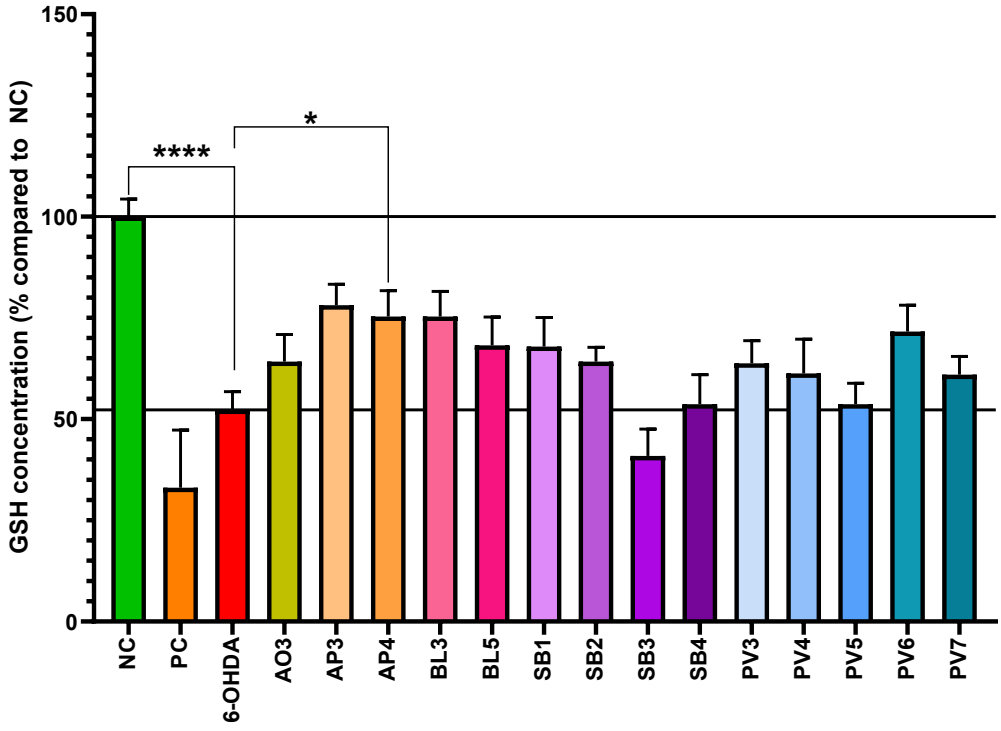

Figure 4-37: **Graph representing the glutathione (GSH) concentration as percentage compared to negative control (NC) ± SEM after 48 h exposure (n = 9). 6-OHDA (6-hydroxydopamine, 70 µM;), positive control (PC; n-ethylmaleimide 10 µM), negative control (NC; 10% FCS supplemented media). Significance shown is against 6-OHDA, with * p < 0.05, **** p < 0.0001. *A. oppositifolia* F3 (AO3), *A. procumbens* F3 (AP3), *A. procumbens* F4 (AP4), *B. latifolia* F3 (BL3), *B. latifolia* F5 (BL5), *S. brachypetala* F1 (SB1), *S. brachypetala* F2 (SB2), S*. brachypetala* F3 (SB3), *S. brachypetala* F4 (SB4), *P. virgata* F3 (PV3), *P. virgata* F4 (PV4), *P. virgata* F5 (PV5), *P. virgata* F6 (PV6), *P. virgata* F7 (PV7). Self-generated from data collected.**

Table 4-18: Glutathione (GSH) concentration as percentage compared to negative control (NC) ± SEM after 48 h exposure (n = 9). 6-OHDA (6-hydroxydopamine, 70 µM;), positive control (PC; n-ethylmaleimide 10 µM), negative control (NC, FCS supplemented media, 10%).

Control/plant fraction	Glutathione (GSH) concentration as percentage ± SEM	Change from 6-OHDA
Negative control	100.00 ± 4.35	N/A
Positive control (n-ethylmaleimide)	33.09 ± 14.18	N/A
6-OHDA	52.35 ± 4.45	N/A
A. oppositifolia F3	64.18 ± 6.69	11.83
A. procumbens F3	78.14 ± 5.16	25.79
A. procumbens F4*	75.33 ± 6.40	22.98
B. latifolia F3	75.31 ± 6.22	22.96
B. latifolia F5	68.23 ± 7.01	15.88
S. brachypetala F1	67.94 ± 7.13	15.59
S. brachypetala F2	64.18 ± 3.57	11.83
S. brachypetala F3	40.89 ± 6.66	-11.46
S. brachypetala F4	53.68 ± 7.28	1.33
P. virgata F3	63.75 ± 5.64	11.4
P. virgata F4	61.27 ± 8.46	8.92
P. virgata F5	53.69 ± 5.18	1.34
P. virgata F6	71.60 ± 6.51	19.25
P. virgata F7	61.01 ± 4.46	8.66

Significance relative to 6-OHDA, * $p < 0.05$.
N/A: not applicable

S. brachypetala F3 decreased the GSH concentration, whereas *S. brachypetala* F4 and *P. virgata* F5 did not alter the GSH level. The reduction in GSH concentration in *S. brachypetala* F3 could be due to interference in the antiporter system, which inhibited the influx of GSH into the cell,[663] or the inhibition of glutathione-disulphate reductase (GSR),[664] which reduces the conversion of GSSH back into GSH, or through conjugation with GSH itself over the 48 h.[665]

A. procumbens F3 increased GSH level with the biggest margin, with an increase of 25.79% when compared to 6-OHDA. *A. procumbens* F3 is followed by *A. procumbens* F4 (22.98% increase, $p < 0.05$), *B. latifolia* fraction 3 (22.96% increase) and *P. virgata* F6 (19.25% increase). Flavonoids and polyphenols have been reported to increase the expression of genes associated with GSH production,[666] however no information pertaining to *A. procumbens*, *B. latifolia*, *S. brachypetala* or *P. virgata* extracts is known

Both methanol and acetone crude extracts of *A. oppositifolia* have previously been studied using the 6-OHDA PD model. A reduction (~50% at 0.5 µg/mL) in GSH after 24 h exposure to 6-OHD

was reported.[488] Contrary, in the present study, after 48 h exposure, such an effect was not observed.

From the *in vitro* data it is suggested that these fractions and their associated compounds may offer protection through multiple mechanisms. While a semi-purified extract shows minimal cytotoxicity and some activity based on ferroptosis markers, the potential for synergy and possible antagonism between the compounds in the plant extract cannot be ruled out.[667]

While extensive purification and *in vitro* studies are tedious and costly, the identified compounds can be investigated *in silico* to determine whether they exhibit affinity for anti-ferroptotic targets.

Table 4-19: A summary of the results obtained in the mechanistic in vitro assays.

Control/plant fraction	TBARS-MDA concentration as fold increase as compared to negative control ± SEM	TBARS-MDA change from 6-OHDA	ROS as fold increase against negative control ± SEM	ROS change from 6-OHDA	Ratio active mitochondria to cell density as fold increase as compared to negative control (NC) ± SEM	Ratio active mitochondria to cell density difference to negative control	Glutathione (GSH) concentration as percentage GSH ± SEM	GSH concentration change from 6-OHDA
Negative control	1.00 ± 0.03	N/A	1.00 ± 0.07	N/A	1.00 ± 0.05	N/A	100.00 ± 4.35	N/A
6-OHDA	1.42 ± 0.14	N/A	3.44 ± 0.41	N/A	1.66 ± 0.10	0.66	52.35 ± 4.45	N/A
A. oppositifolia F3	1.45 ± 0.20	-0.025	1.50 ± 0.32	1.94	0.65 ± 0.09	0.35	64.18 ± 6.69	11.83
A. procumbens F3	1.19 ± 0.09	0.228	1.46 ± 0.21	1.98	0.63 ± 0.10	0.37	78.14 ± 5.16	25.79
A. procumbens F4	1.16 ± 0.12	0.257	1.45 ± 0.29	1.99	0.57 ± 0.08	0.43	75.33 ± 6.40	22.98
B. latifolia F3	1.49 ± 0.15	-0.068	1.83 ± 0.32	1.61	0.70 ± 0.08	0.31	75.31 ± 6.22	22.96
B. latifolia F5	1.34 ± 0.15	0.08	2.15 ± 0.48	1.30	0.91 ± 0.12	0.09	68.23 ± 7.01	15.88
S. brachypetala F1	1.26 ± 0.12	0.161	2.31 ± 0.64	1.13	0.78 ± 0.06	0.22	67.94 ± 7.13	15.59
S. brachypetala F2	1.43 ± 0.18	-0.011	3.03 ± 0.81	0.41	0.90 ± 0.10	0.10	64.18 ± 3.57	11.83
S. brachypetala F3	1.41 ± 0.15	0.017	2.79 ± 0.56	0.65	0.97 ± 0.11	0.03	40.89 ± 6.66	-11.46
S. brachypetala F4	1.31 ± 0.11	0.109	1.97 ± 0.31	1.47	0.79 ± 0.06	0.21	53.68 ± 7.28	1.33
P. virgata F3	1.21 ± 0.05	0.209	1.97 ± 0.40	1.47	0.77 ± 0.14	0.23	63.75 ± 5.64	11.4
P. virgata F4	1.14 ± 0.12	0.284	1.35 ± 0.20	2.10	0.47 ± 0.04	0.54	61.27 ± 8.46	8.92
P. virgata F5	1.39 ± 0.33	0.029	2.11 ± 0.57	1.33	0.58 ± 0.10	0.43	53.69 ± 5.18	1.34
P. virgata F6	1.21 ± 0.11	0.216	2.16 ± 0.57	1.28	0.59 ± 0.06	0.41	71.60 ± 6.51	19.25
P. virgata F7	1.27 ± 0.12	0.151	2.08 ± 0.47	1.36	0.79 ± 0.10	0.21	61.01 ± 4.46	8.66

CHAPTER 5: *IN SILICO* MOLECULAR MODELLING AND DETERMINATIONS

5.1 Determination of physicochemical properties

The search for compounds targeting the CNS is a lengthy and complex process due to the unique challenges posed by the CNS. Key factors include the BBB, which restricts drug entry, the intricate neuronal network, and the delicate balance required to avoid disrupting normal brain function. Developing CNS drugs necessitates an understanding of the molecular mechanisms underlying CNS diseases, precise targeting to minimise off-target effects, and robust testing to ensure efficacy and safety. However, recent advancements in *in silico* methods for identifying compounds with favourable physicochemical properties have significantly reduced the time required to discover and investigate potential drug candidates. The structure of drugs not only influences its target specificity but also its pharmacokinetic profile, both of which are critical in establishing the biological behaviour of the compound.[668] Therefore, i*n silico* investigations have been conducted in the current study to identify potential targets for the identified anti-ferroptotic compounds, gain insights into intracellular drug mechanisms, and predict molecular interactions.

The pharmacokinetic parameters of a drug are influenced by several factors including the biological sex[669] and age[670] of a patient, as well as the route of administration and dosage regimen.[671] For compounds predominately administered via the oral route (e.g., syrups, tablets, capsules), absorption becomes a critical determinant of therapeutic efficacy. This process is significantly influenced by the physicochemical properties of the compound. Key properties include solubility, which affects dissolution in gastrointestinal fluids; hydrophobicity, which determines membrane permeability; ionisation potential, which influences charge and solubility at physiological pH; diffusivity, which impacts transport across biological membranes; and hydrogen bonding potential, which can affect both solubility and binding interactions.[672-675]

When identifying drugs for CNS conditions, additional challenges arise due to the necessity of crossing the BBB. The BBB selectively restricts the passage of substances into the brain, permitting only those with specific physicochemical characteristics, such as high lipophilicity and low molecular weight, while actively effluxing other substances via transport proteins.[676]

In silico methods have become essential for identifying compounds capable of crossing the BBB and targeting the CNS. Successfully crossing the BBB requires considerations beyond standard pharmacokinetic properties to ensure compounds reach the CNS intact and exert their therapeutic effects. Key parameters in these analyses include molecular weight (MW < 450 Da), lipophilicity

(LogP between 2–5), topological polar surface area (TPSA < 90 Å²), intestinal permeability (LogD < 3), hydrogen bond donors (HBD ≤ 3), and ionisation state (pKa indicating a positive charge at pH 7–8, which is close to physiological pH).[677-679] However, it is important to note that these parameters are primarily based on passive diffusion mechanisms and may not account for the influence of tight junctions, active transport, or protein interactions, thus warranting further exploration *in silico*.[680]

5.1.1 Absorption, distribution, metabolism, excretion, and toxicity properties

The term “ADME-Tox” refers to the absorption (movement of molecules over the intestinal wall), distribution (amount of molecules in the bodily fluids), metabolism (how the molecules are changed in the body by the liver and kidneys), excretion (how the molecule is removed from the body), and toxicity (negative effects) of a drug candidate, forming the foundation of its pharmacokinetic profile.[681] I*n silico* ADME-Tox prediction tools can assess key parameters such as a drug candidate’s ability to permeate cell membranes, bind to plasma proteins, and cross the BBB.[682] These factors play a crucial role in determining the pharmacodynamic properties of the drug candidate, ultimately influencing its therapeutic efficacy and safety in the body.[683] A significant challenge in drug development is the high failure rate during clinical trials, often due to adverse effects and toxicity, which pose risks to patient safety and result in substantial costs for the pharmaceutical industry.[684] *In silico* methods, including ADME-Tox and drug-likeness predictions, play a crucial role in identifying new targets and compounds with reported biological activity, helping to mitigate these risks in the early stages of drug discovery.[685] Understanding and optimising ADMET characteristics is essential in drug development to ensure that the compound can reach its target site, exert the desired effect, and be safely eliminated from the body ultimately increasing the likelihood of clinical success.[686]

5.1.2 Molecular docking

Molecular docking is a computational method used to determine and evaluate the intra- and intermolecular interactions between a specific compound (ligand) and a target protein, such as a receptor or enzyme. By simulating how the compound fits and binds within the protein's binding (active) site, this method predicts the formation of the ligand-receptor complex. These interactions, unique to each ligand, can be analysed to identify pharmacophoric features key structural elements responsible for the compound's binding activity and to expand on structure-activity relationships (SAR), enabling the design of compounds with optimised binding properties.[687] Widely employed in drug discovery, molecular docking is invaluable for screening large libraries of compounds, significantly reducing time and resources by prioritizing candidates with favourable

binding properties. It also provides insight into the molecular basis of drug-receptor interactions, identifying critical residues within the active site that contribute to binding. The strength of ligand-protein interactions is quantified by a docking score, where a lower score typically indicates a stronger binding affinity as seen in kcal/mol. [688,689]

5.2 Method

5.2.1 Absorption, distribution, metabolism, excretion, and toxicity prediction

The SwissADME online platform, developed by the Swiss Institute for Bioinformatics was used to determine the physicochemical parameters of compounds identified through mass spectrometry.[690] SwissADME is a free online tool that evaluates drug-likeness by calculating various physicochemical properties. The molecular structures of the identified compound were uploaded on to the SMILES interface. The system uses several open-source software solutions to derive a set of results which was presented in a tabulated format. Basic properties like MW, molecular refractivity, TPSA (the surface area of all polar atoms) were calculated using OpenBabel (version 2.3.0). For the LogP descriptor, which represents the partition coefficient between n-octanol and water (Log Po/w), SwissADME employed multiple methods based on five fragmentation models i.e. XLOGP3, WLOGP, MLOGP (a linear relationship of molecular descriptors), and iLOGP (a free energy calculation based on solvation). SwissADME combined these calculations into a consensus LogP (cLogP) value, providing a more robust and accurate depiction of the LogP parameter.[690-696]

SwissADME employed two topological methods to determine solubility i.e., the estimated solubility (ESOL)[697] model and linear relationships identified by previous studies.[698] These models provide a reliable assessment of the solubility of the compound, which is crucial for its pharmacokinetic profile and its overall effectiveness in reaching the target tissues. The ESOL model is a Quantitative Structure-Property Relationship (QSPR) model that predicts aqueous solubility (log S) based on a linear relationship with five molecular parameters: molecular weight (MW), number of rotatable bonds, fraction of aromatic heavy atoms, and Daylight's CLOGP as a lipophilicity descriptor. However, due to the limited availability of CLOGP, the SwissADME implementation of ESOL substitutes this descriptor with XLOGP3 in its linear equation for predicting log S.[697] The models in SwissADME predict log S values, which are subsequently converted to solubility values expressed in mol/L and mg/mL. Based on these values, a qualitative classification of solubility is provided according to the following log S scale: highly soluble (>0), very soluble (0 to −2), soluble (−2 to −4), moderately soluble (−4 to −6), poorly soluble (−6 to −10), and insoluble (<−10). The

relationship between LogP and TPSA forms the basis for assessing gastrointestinal absorption (GIa) and blood-brain barrier permeation (BBBp).[699]

5.2.2 Molecular docking

5.2.2.1 Protein preparation

The three-dimensional (3D) X-ray crystal structure of the proteins involved in ferroptosis was accessed from the RCSB Protein Data Bank (PDB) (**Table 5-1**). For docking studies, protein structures that either contained co-crystallised ligands within the active site or had known active site residues were selected. Protein preparation was performed using the Protein Preparation wizard in Maestro, a tool designed for refining protein structures before docking simulations.[700] In this step, water molecules were removed, bond orders were assigned, and all hydrogen atoms were added. Additionally, bonds to metal ions were deleted with the formal charge in the metal and neighbouring atoms adjusted at a specified distance. Thereafter the protonation state for the residues in the workspace were adjusted to reflect physiological conditions (pH 7.4) and minimise structural errors. The final step in the protein preparation process involved a restrained minimisation using the OPLS-2005 forcefield which helped reduce steric clashes and optimise the protein's geometry while maintaining its overall conformation.

5.2.2.2 Ligand preparation

Ligand preparation was initiated by constructing the two-dimensional (2D) structure of each compound using the SMILES conversion on Chem Draw Ultra 10.0. (**Tables 5-2 – 5.6**) The 2D structures were saved in .sdf format and converted to 3D structures using the same software. The SMILES conversion ensured the correct initial molecular structure, including proper chirality. The aim was to generate a low-energy 3D structure for each input, which accurately reflected the proposed molecular geometry. Further ligand refinement was conducted using the LigPrep module in Maestro. In this step, chirality was preserved from the 3D structure, and the original ionisation states of the ligands were maintained. Tautomers were generated during this process, replacing any existing conformers to ensure that different possible forms of the ligand were considered. The conformational space was explored using the Monte Carlo method, a robust algorithm for finding the global minimum by testing a wide range of possible conformations. The search involved exploring all rotatable single bonds to account for the flexibility of the ligand. This exploration continued until the global energy minimum was identified multiple times, confirming the most stable conformation. Finally, the OPLS_2005 force field was applied during the energy minimisation step, ensuring accurate structural refinement based on the least square minimisation approach. This

methodology ensured that the ligand was prepared with the lowest energy, best conformer, and appropriate molecular properties for subsequent molecular docking studies.

5.2.2.3 Active site determination and receptor grid generation

To determine the potential binding sites on the target protein(s), a grid-based cavity prediction algorithm was used. Using the Glide docking model, grids were generated to evaluate the binding interactions between the ligand and the protein's active sites. These grids were created using the Receptor Grid Generation module in Glide, following standard procedures (OPLS_2005 forcefield minimisation, sampling the orientation of waters, optimising hydrogen bonds to pH set to 7.4), to define the receptor's active site. The grid generation process involved mapping the electrostatic and geometric properties of the receptor to provide an accurate docking environment. The grid defined the shape and electrostatics of the receptor, allowing for the precise placement of ligands within the protein's active site. Additionally, constraints were incorporated into the grid files, ensuring that critical interactions (such as hydrogen bonds with specific residues) were included during docking. Multiple fields were used to represent the receptor's properties, progressively enhancing the accuracy of ligand scoring. This included factors like steric and electrostatic complementarity, which are essential for determining the favourable binding poses of the ligand. As a result, the Glide model facilitated a comprehensive search for optimal ligand-receptor interactions, supporting drug discovery efforts by predicting the strength and mode of binding between molecules and their target proteins. This process was used to generate the receptor grid, into which the identified compounds were docked.

5.2.2.4 Pharmacophore determination

Pharmacophore models were developed using Maestro to map the spatial arrangement of essential molecular features critical for effective target binding. These models are invaluable in drug discovery, as they highlight the key functional groups such as hydrogen bond donors and acceptors, hydrophobic regions, aromatic rings, and charged groups that are crucial for ligand-target interactions. By aligning these features across a series of active ligands, the models provide insights into the structural requirements for activity, aiding in the rational design of new compounds. This approach not only facilitates the identification of potential drug candidates but also supports the optimisation of lead compounds by ensuring their structural compatibility with the target binding site.[701] In pharmacophore model development, each ligand structure is depicted as a set of points in 3D space, corresponding to specific chemical features that may enable non-covalent interactions with the target receptor. These pharmacophore sites are defined by their type, spatial position, and, where relevant, their directionality. Following widely accepted theories

of ligand-receptor interactions, Phase includes six predefined pharmacophore feature types: hydrogen bond acceptor, hydrogen bond donor, hydrophobic group, negatively ionizable group, positively ionizable group, and aromatic ring.[701] In this study, the chosen groups were linked towards the known interactions of the ligand in the active site.

5.2.2.5 Molecular docking

Molecular docking was performed by selecting a ligand molecule that was excluded from the grid generation, with the van der Waals radius scaling set to 1.00. The ligand was then docked into the receptor using the docking functionality in extra precision (XP) mode. This mode enabled the prediction of the most feasible orientation of the ligand within the binding pocket, which was determined by assessing the ligand's interaction with the receptor. The strength of the ligand-receptor interaction in this orientation was quantified using a scoring function, providing a numerical value that reflects the affinity and stability of the binding. This scoring function helped identify the most favourable binding poses and interactions, aiding in understanding how the ligand might exert its effect on the target protein. The amino acids are abbreviated as follows: alanine (ALA), arginine (ARG), asparagine (ASN), aspartic acid (ASP), cysteine (CYS), glutamine (GLN), glutamic acid (GLU), glycine (GLY), histidine (HIS), isoleucine (ILE), leucine (LEU), lysine (LYS), methionine (MET), phenylalanine (PHE), proline (PRO), serine (SER), threonine (THR), tryptophan (TRP), tyrosine (TYR), and valine (VAL).

5.2.2.6 Targets for docking

Structure-based analysis (molecular docking) leverages the protein structure of targets such as enzymes or receptors, to explore interactions with ligands.[702] While there are many targets encoded in the human genome, enzymes and G-protein-coupled receptors are the most commonly targeted, accounting for 47% and 30% of known drugs, respectively.[368] Identifying suitable targets for a specific disease requires a thorough understanding of its pathophysiology to pinpoint key molecules influencing disease progression. In the case of ferroptosis and PD, several critical targets involved in disease progression have been identified, offering potential pathways for therapeutic intervention, as summarised in **Table 5-1**. [703]

Table 5-1: Targets identified for molecular docking, with the PDB codes, and the roles these targets have in the pathophysiology of ferroptosis or Parkinson's disease (PD).

Target (receptor)	*PDB ID*	*Function within ferroptosis*
Dopamine 1 receptor	7JVQ (with apomorphine)	D1 receptors regulate neuronal growth and development, mediate some behavioural responses, and modulate dopamine receptor D2-mediated events.[704] Used as second line treatments in PD.
Dopamine 2 receptor	6CM4	D2 receptors are used in synaptic plasticity as well as treatment in PD to reduce off-peak dyskinesia [704]
GPx4	2OBI	LOOH is combated by GPx4, that reduces LOOH to lipid alcohols, and it is the only member of the glutathione peroxidase family that is capable for reducing LOOH, that makes it essential in the lipid oxidase pathway as well as ferroptosis [253, 254]. It uses GSH as a co-factor, which is synthesised from cysteine and glutamate together with glycine [705].
Xc- system	7P9V	Controls the concentrations of both glutamate and cysteine, both needed for GSH production [705].

5.3 Results and discussion

5.3.1 Absorption, distribution, metabolism, excretion, and toxicity prediction

5.3.1.1 Compounds identified in *Acokanthera oppositifolia*

Compounds identified from F3 of *A. oppositifolia* exhibited high polarity as evidenced by their TPSA score of > 90 Å^2 and a cLogP value of < 0, which suggests that they are unlikely to permeate the BBB **(Table 5-2).** Despite their relatively high solubility, this does not necessarily translate to theoretical BBB permeability. The elevated TPSA may be attributed to the presence of hydroxyl groups on the compounds, which could be reduced by either eliminating or substituting them with

halogens in future investigations. These halogens may also decrease the number of hydrogen bond donors, potentially improving availability for the identified compounds.[706] However, the lack of BBBp does not entirely rule out the therapeutic potential of these compounds, as interactions with transporters are not considered in this evaluation.[707] All compounds demonstrated high solubility, which is consistent with literature;[708] however, as the solubility reduced with the increase in methanol concentration, it is possible that these compounds were isolated in fraction 3.

Table 5-2: Physicochemical determinations for the compounds identified in fraction 3 of *Acokanthera oppositifolia*.

Compound	MW	TPSA	CLogP	ESOL Class	GIa	BBBp
2-*o*-caffeoylglucose	342.3	156.91	-0.87	Very soluble	Low	No
1-*o*-*trans*-caffeoyl-β-d-allopyranoside	342.3	156.91	-0.98	Very soluble	Low	No
3-*o*-caffeoyl-muco-quinic acid	354.31	164.75	-0.36	Very soluble	Low	No
4-(3,4-dihydroxycinnamoyl)quinic acid	354.31	164.75	-0.37	Very soluble	Low	No

BBBp: Blood brain barrier permeation; CLogP: consensus LogP; ESOL: estimated solubility; GIa: gastrointestinal absorption; MW: molecular weight, TPSA: topological surface area

5.3.1.2 Compounds identified in *Aptosimum procumbens*

Compounds identified from both F3 and F4 of *A. procumbens* did not exhibit BBBp **(Table 5-3)**. However, one from F3 (4 (dimethyl 2- [(2e)-3-(3,4-dihydroxyphenyl)prop-2-enoyl]oxy-butanedioate) and both compounds from F4 (dimethyl 2- [(2e)-3-(3,4-dihydroxyphenyl)prop-2-enoyl]oxy-butanedioate and hastatoside) showed a high GIa, suggesting a potentially higher blood concentration, assuming they are not extensively metabolised before reaching the bloodstream. However, hastatoside, isolated from F4 had a high MW, which exceeds the ideal limit of 450 Da, and breaches the upper limit of TPSA. All compounds identified were soluble in water.

Table 5-3: Physicochemical determinations for the compounds identified in fraction 3 and 4 of *Aptosimum procumbens*.

Compound	MW	TPSA	CLogP	ESOL Class	GIa	BBBp
Fraction 3						
Gouwenoside a	406.38	175.37	-2.16	Very soluble	Low	No
5-deoxypulchelloside i	406.38	175.37	-2.06	Very soluble	Low	No
Dimethyl 2- [(2e)-3-(3,4-dihydroxyphenyl)prop-2-enoyl]oxy}butanedioate	324.28	119.36	1.17	Soluble	High	No
Fraction 4						
Dimethyl 2- [(2e)-3-(3,4-dihydroxyphenyl)prop-2-enoyl]oxy-butanedioate	324.28	119.36	1.17	Soluble	High	No

Hastatoside	572.6	201.67	1.17	Soluble	High	No

BBBp: Blood brain barrier permeation; CLogP: consensus LogP; ESOL: estimated solubility; GIa: gastrointestinal absorption; MW: molecular weight, TPSA: topological surface area

5.3.1.3 Compounds identified in *Bulbine latifolia*

Two compounds (N-lauryldiethanolamine and 2-amino-1,3-hexadecanediol) identified from F3 of *B. latifolia* exhibited both BBBp, and a high GIa. This is likely due to their favourable CLogP values, which suggest optimal lipophilicity, which is a crucial determinant of a compound's ability to traverse a lipid-rich BBB via passive diffusion. The flavonoids identified in F5 exhibited high TPSA values, which, along with a low CLogP. High TPSA suggests increased polarity and hydrogen bonding potential, which limit a molecule's ability to permeate the BBB **(Table 5-4)**. The presence of sugar moieties (glycosides) in these flavonoids contributes significantly to their high TPSA, as sugars are highly polar and expand the molecule's overall surface area. Removing these sugar moieties could decrease both the TPSA and MW, improving the likelihood of BBBp.

Table 5-4: Physicochemical determinations for the compounds identified in fraction 3 and 5 of *Bulbine latifolia*

Compound	MW	TPSA	CLogP	ESOL class	GIa	BBBp
Fraction 3						
Patulin	154.12	55.76	0	Very soluble	High	No
Longianone	154.12	52.6	0.14	Very soluble	High	No
6-(3-hydroxypropyl)-4-methoxy-2h-pyran-2-one	184.19	59.67	0.99	Very soluble	High	No
N-lauryldiethanolamine	273.45	43.7	3.65	Soluble	High	Yes
2-amino-1,3-hexadecanediol	273.45	66.48	3.7	Soluble	High	Yes
Fraction 5						
Luteolin 7-sophoroside	610.52	269.43	-1.49	Soluble	Low	No
6-c-β-d-glucopyranosyl-5-methoxy-3',4',7-trihydroxyflavone	462.41	190.28	-0.17	Soluble	Low	No
6-c-β-d-glucopyranosyl-3',4',5-trihydroxy-7-methoxyflavone	462.41	190.28	-0.02	Soluble	Low	No
6-c-β-d-glucopyranosyl-4',5,7-trihydroxy-3'-methoxyflavone	462.41	190.28	0.04	Soluble	Low	No
6-c-α-d-glucopyranosyl-4',5,7-trihydroxy-3'-methoxyflavone	462.41	190.28	0.04	Soluble	Low	No
1,8-di-o-β-d-glucopyranoside derivative of 2-decene-4,6-diyne-1,8-diol	488.48	198.76	-1.68	Very soluble	Low	No

BBBp: Blood brain barrier permeation; CLogP: consensus LogP; ESOL: estimated solubility; GIa: gastrointestinal absorption; MW: molecular weight, TPSA: topological surface area

5.3.1.4 Compounds identified in *Polygala virgata*

The compounds with flavan scaffold (F4 – F7) have been highlighted for their potential to cross the BBB, which is attributed to their physicochemical properties, particularly their lower TPSA compared to xanthone structures. The calculated CLogP values of these compounds, which range between 0 and 3 **(Table 5-5)**, further support their favourable balance between solubility in aqueous environments and permeability through lipid membranes. These properties position flavan scaffolds as promising candidates for CNS-targeted drug development. Minor differences have been observed in the substitution patterns on the rings, which can significantly affect a compound's pharmacokinetic properties, including its solubility, stability, and interactions with the target protein or receptor. The compounds identified in *P. virgata* may differ from those represented in this analysis due to overlapping MW and UV values. However, the core scaffold offers significant potential for structural modifications through various substituents. The results obtained in the current study suggests that F5 – F7 may be the most promising due to the potential BBBp of the isoflavans.

Table 5-5: Physicochemical determinations for the compounds identified in fraction 3 – 7* of *Polygala virgata.*

Compound*	MW	TPSA	CLogP	ESOL class	Gla	BBBp
Fraction 3						
6-*O* -(4-hydroxy-3-methoxy-*e*-cinnamoyl)	518.47	225.06	-1.8	Very soluble	Low	No
3'-*O*-(4-hydroxy-3-methoxy-*e*-cinnamoyl)	518.47	225.06	-1.7	Very soluble	Low	No
1'-*O*-(4-hydroxy-3-methoxy-e-cinnamoyl)	518.47	225.06	-1.77	Very soluble	Low	No
Fraction 4						
2-[[6-hydroxy-8-(4-hydroxy-3-methoxyphenyl)-6,7-bis(hydroxymethyl)-1,3-dimethoxy-7,8-dihydro-5h-naphthalen-2-yl]oxy]-6-(hydroxymethyl)oxane-3,4,5-triol	568.57	207.99	-0.23	Soluble	Low	No
6-o-β-d-glucopyranoside-6,8-dihydroxy-3,7-dimethylisocoumarin	368.34	149.82	0.31	Soluble	Low	No
6-o-(4-o-methyl-β-d-glucopyranoside)-6,8-dihydroxy-3-methylisocoumarin	368.34	138.82	0.36	Soluble	Low	No
Fraction 5						
6,8-dihydroxy-3,7-dimethyl-1h-2-benzopyran-1-one (6-o-β-d-glucopyranoside derivative)	368.34	149.82	0.31	Soluble	Low	No
7-hydroxy-6-(2-hydroxyethyl)-2h-1-benzopyran-2-one (2'-o-β-d-glucopyranoside derivative)	368.34	149.82	-0.22	Very soluble	Low	No
1,2,8-trihydroxy-5-methoxy-3-methylxanthone	288.25	100.13	2.13	Soluble	High	No
3,5-dihydroxy-1,2-dimethoxyxanthone	288.25	89.13	1.93	Soluble	High	No
1,5-dihydroxy-2,3-dimethoxyxanthone	288.25	89.13	2.06	Soluble	High	No
3,7-dihydroxy-1,2-dimethoxyxanthone	288.25	89.13	1.91	Soluble	High	No
1,5-dihydroxy-2,7-dimethoxyxanthone	288.25	89.13	2.08	Soluble	High	No
1,5-dihydroxy-2,3-dimethoxyxanthone	288.25	89.13	2.06	Soluble	High	No
1,3-dihydroxy-2,4,7-trimethoxyxanthone	318.28	98.36	2.09	Soluble	High	No
3,8-dihydroxy-1,2,7-trimethoxyxanthone	318.28	98.36	2.07	Soluble	High	No
7,8-dihydroxy-1,2,3-trimethoxyxanthone	318.28	98.36	2.1	Soluble	High	No
1,8-dihydroxy-2,3,5-trimethoxyxanthone	318.28	98.36	2.13	Soluble	High	No
4',7-dihydroxy-3'-methoxyflavan	272.3	58.92	2.64	Soluble	High	Yes
3',4'-dihydroxy-7-methoxyflavan	272.3	58.92	2.65	Soluble	High	Yes

2',7-dihydroxy-4'-methoxyisoflavan	272.3	58.92	2.56	Soluble	High	Yes
2',4'-dihydroxy-7-methoxyisoflavan	272.3	58.92	2.56	Soluble	High	Yes
Fraction 6						
3,6-dihydroxy-1,2,7-trimethoxyxanthone	318.28	98.36	1.96	Soluble	High	No
3,8-dihydroxy-1,2,6-trimethoxyxanthone	318.28	98.36	2.11	Soluble	High	No
1,3-dihydroxy-2,4,7-trimethoxyxanthone	318.28	98.36	2.09	Soluble	High	No
1,8-dihydroxy-2,3,5-trimethoxyxanthone	318.28	98.36	2.13	Soluble	High	No
2',3',4,4'-tetrahydroxy-6,7-methylenedioxyisoflavan	318.28	108.61	1.3	Soluble	High	No
2,3-dihydro-2-(2-hydroxy-3,5-dimethoxyphenyl)benzofuran	272.3	47.92	2.76	Soluble	High	Yes
4',7-dihydroxy-3'-methoxyflavan	272.3	58.92	2.64	Soluble	High	Yes
3',4'-dihydroxy-7-methoxyflavan	272.3	58.92	2.65	Soluble	High	Yes

*Fraction 7 presented with the same compounds as fractions 5 and 6.

BBBp: Blood brain barrier permeation; CLogP: consensus LogP; ESOL: estimated solubility; GIa: gastrointestinal absorption; MW: molecular weight, TPSA: topological surface area.

5.3.1.5 Compounds identified in *Schotia brachypetala*

Some of the compounds identified from *S. brachypetala* F1 – F3 exhibited BBBp, among which 8,9-dehydrotheaspirone emerges as a novel scaffold with BBB permeability. This compound was found in black tea and responsible for its characteristic odour, demonstrating its potential for crossing the BBB.[709, 710] The meroterpenoid structure of this compound, similar to conidione (isolated from *Aplidium conicum* tunicate), suggests that it could have unique properties (such as a low TPSA) conducive to BBBp. Meroterpenoids (scaffold of 8,9-dehydrotheaspirone) have been shown to display a wide range of biological activities, and their structural characteristics may allow them to interact favourably with the BBB, either by their lipophilicity or through specific transport mechanisms.[711] However, several compounds are theoretically unable to cross the BBB due to high TPSA and CLogP values. Despite this, they show potential by demonstrating excellent GIa.

Table 5-6: Physicochemical determinations for the compounds identified in fraction 1 - 4 of *Schotia brachypetala.*

Compounds	MW	TPSA	CLogP	ESOL Class	GIa	BBBp
Fraction 1						
1-(3-propylphenyl)-β-carboline	286.37	28.68	4.64	Moderately soluble	High	Yes
Isocyalexin a	172.18	25.02	1.37	Soluble	High	Yes
Fraction 2						
2-amino-5-hydroxy-1,4-naphthoquinone	189.17	80.39	0.74	Soluble	High	No
1-nonylamine	143.27	26.02	2.76	Soluble	High	Yes
Fraction 3						
Ningpogenin	170.21	49.69	0.33	Very soluble	High	No
Pangamic acid	281.26	147.76	-2.4	Highly soluble	Low	No
Isoferuloylcholine/feruloylcholine	280.34	55.76	0.04	Soluble	High	Yes
Loliolide	196.24	46.53	1.53	Very soluble	High	Yes
3,6-di-o-acetyl-1,2:4,5-di-o-isopropylidene-allo-inositol	344.36	89.52	1.1	Soluble	High	No
3,4-di-o-acetyl-1,2:5,6-di-o-isopropylidene-l-chiro-inositol	344.36	89.52	1.12	Soluble	High	No
4n-benzoylcytidine	347.32	133.91	-0.42	Soluble	Low	No
8,8,9-trimethoxy-5-methylbenz[cd]isoindolo[2,1-a]indol-1(8h)-one; 5-o-de-me	347.36	60.69	3.1	Moderately soluble	High	Yes
8,9-dehydrotheaspirone	206.28	26.3	2.53	Soluble	High	Yes
Fraction 4						
4-methoxy-2,2,6-trimethyltetrahydro-4h-[1,3]dioxolo[4,5-c]pyran-7-yl acetate	260.28	63.22	0.97	Very soluble	High	No

BBBp: Blood brain barrier permeation; CLogP: consensus LogP; ESOL: estimated solubility; GIa: gastrointestinal absorption; MW: molecular weight, TPSA: topological surface area

5.3.2 Docking results and discussion

The molecular docking results are represented using a docking score (g-score) as well as a ligand interaction plot. These ligand interaction plots visually depict the various interactions between the compound and the active site of the protein, such as ionic bonds (salt bridges), hydrogen bonding (a hydrogen-oxygen dipole) or a pi-pi stacking interactions (stabilisation of delocalised electron clouds in cyclic systems).[712]

5.3.2.1 Dopamine 1 receptor

The DA-R1 receptor (PDB ID: 7JVQ) is co-crystallised with apomorphine, a well-established agonist, within its active site (**Figure 5-1**). The pharmacophore model of apomorphine was extrapolated based on its structural features (**Figure 5-2**) and interactions with key residues in the active site (**Figure 5-2**). Apomorphine form hydrogen bonds with both ASN 292 and SER 198, pi-pi interactions with PHE 289 and a salt bridge with ASP 103. Molecular docking analysis revealed that the top five (6-C-β-D-glucopyranosyl-3',4',5-trihydroxy-7-methoxyflavone, 3'-O-(4-hydroxy-3-methoxy-E-cinnamoyl), 6-c-β-d-glucopyranosyl-3',4',5-trihydroxy-7-methoxyflavone, 6-c-α-d-glucopyranosyl-4',5,7-trihydroxy-3'-methoxyflavone and 3,6-dihydroxy-1,2,7-trimethoxyxanthone) exhibited docking scores (g-scores) ranging from -11.529 to -8.029 kcal/mol whilst apomorphine presented with a g-score of –10.969 kcal/mol. Among the screened compounds, 6-C-β-D-glucopyranosyl-3',4',5-trihydroxy-7-methoxyflavone from fraction 3 of *B. latifolia* demonstrated the highest binding affinity at -11.529 kcal/mol **(Figure 5-3 A).**

The compound, 6-C-β-D-glucopyranosyl-3',4',5-trihydroxy-7-methoxyflavone demonstrated specific interactions within the active pocket of the DA-1R receptor. Hydrogen bonds were formed between the hydroxyl groups on the tetrahydropyran ring and SER 310, ASP 187 and CYS 186. Additional hydrogen bonds were observed between the catechol ring and SER 198 and SER 202, along with pi-pi stacking interactions between the chromene ring and the aromatic residues, PHE 289, and PHE 288 **(Figure 5-3 A).** The compound's interactions with SER 198 and PHE289 aligned with key binding interactions of apomorphine in the active site. However, despite exhibiting a higher binding affinity than apomorphine, the compound does not meet all the criteria outlined in the pharmacophore model of apomorphine, with a missing nitrogen group and one of the hydroxyl groups **(Figure 5-3 B**). Therefore, it is possible that 6-C-β-D-glucopyranosyl-3',4',5-trihydroxy-7-methoxyflavone may not produce the same effects as apomorphine, potentially acting as a non-agonist. The compound's ring structure aligns with the pharmacophore model, particularly due to the stabilisation provided by the pi-pi electron stacking interaction observed between PHE 289 and the catechol ring. However, this does not guarantee identical functional activity, as the compound may not fully mimic the agonist behaviour of apomorphine.

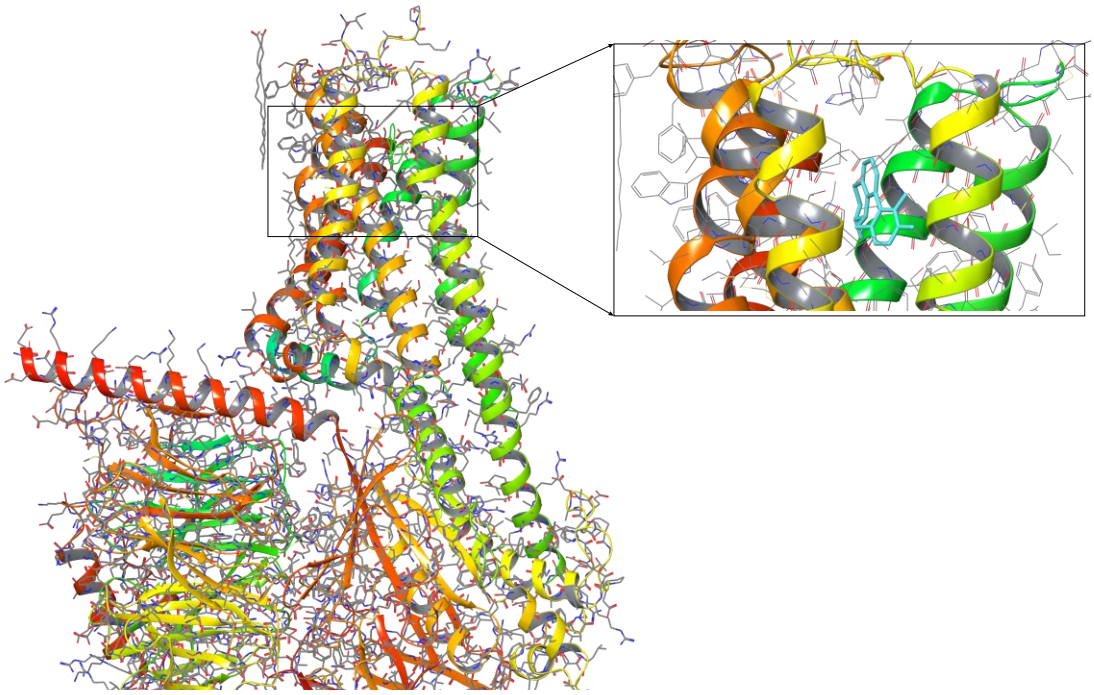

Figure 5-1: Apomorphine (teal) co-crystallised in the dopamine-1 receptor (PDB ID: 7JVQ).

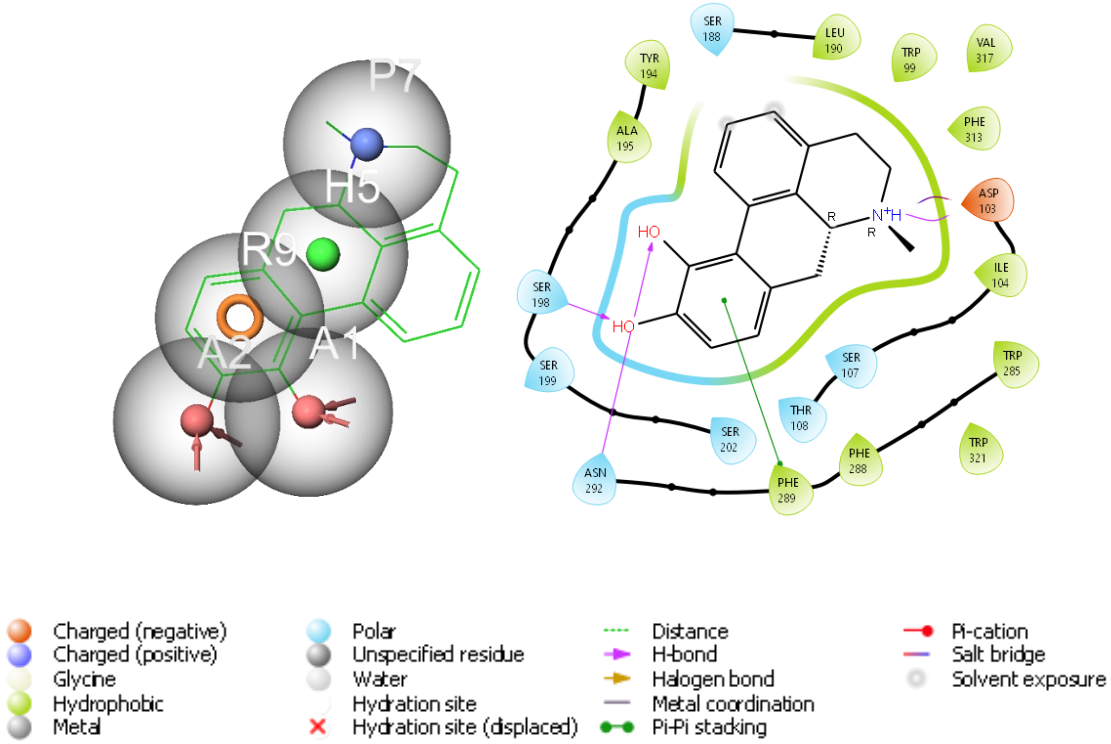

Figure 5-2: Apomorphine structure (green) with the pharmacophoric model (red dots [A1, A2]: hydrogens, orange ring [R9]: benzene ring; green dot [H5]: ring, blue dot [P7]: nitrogen) (left). B) Ligand plot showing apomorphine (black) bound to dopamine-1 (PDB ID: X). Purple line indicates hydrogen bonding, and green line indicate pi-pi stacking interactions (right).

A

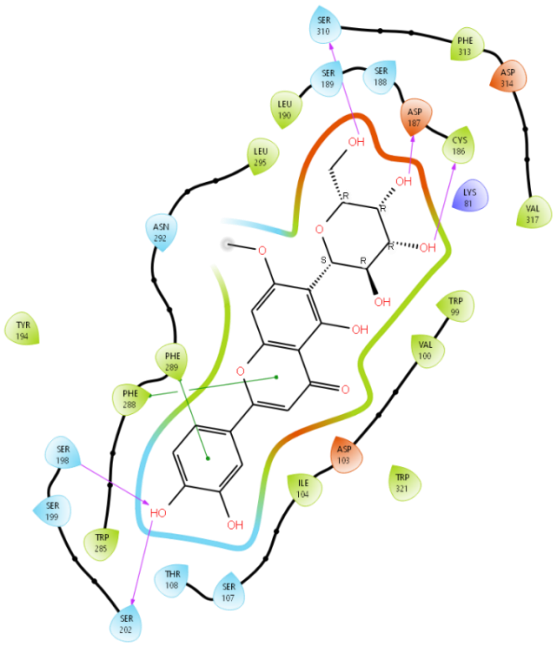

B

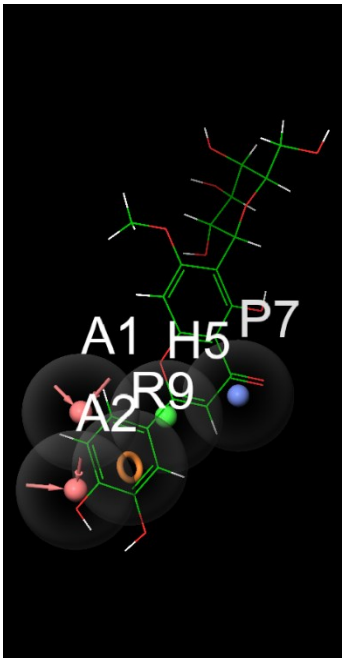

Figure 5-3: **A) 2D interaction model of *Bulbine latifolia* fraction 3 compound, 6-C-β-D-glucopyranosyl-3',4',5-trihydroxy-7-methoxyflavone docked into the active site of dopamine-1 with amino acid bindings. Purple line indicates hydrogen bonding, and green line indicate pi-pi stacking interactions B) Structure of 6-C-β-D-glucopyranosyl-3',4',5-trihydroxy-7-methoxyflavone overlayed with pharmacophoric model of apomorphine.**

The compound with the second highest binding affinity (-10.314 kcal/mol) was observed to be 3'-O-(4-hydroxy-3-methoxy-E-cinnamoyl) identified from *P. virgata* fraction 3. The compound formed hydrogen bonds with the hydroxyl groups of tetrahydropyran and interacted with SER310, SER188, and ASP137. A secondary hydrogen bond can be seen between the hydroxyl group on the tetrahydrofuran ring and ASP 137. As well as with CYS 186 **(Figure 5-4 A)**. The compounds do not fit into the pharmacophoric model of apomorphine **(Figure 5-4 B**); thus, the mechanism of action could be impacted. However, the g-score is marginally close to apomorphine (–10.969 kcal/mol) indicating that interactions might be possible with the compound.

A B

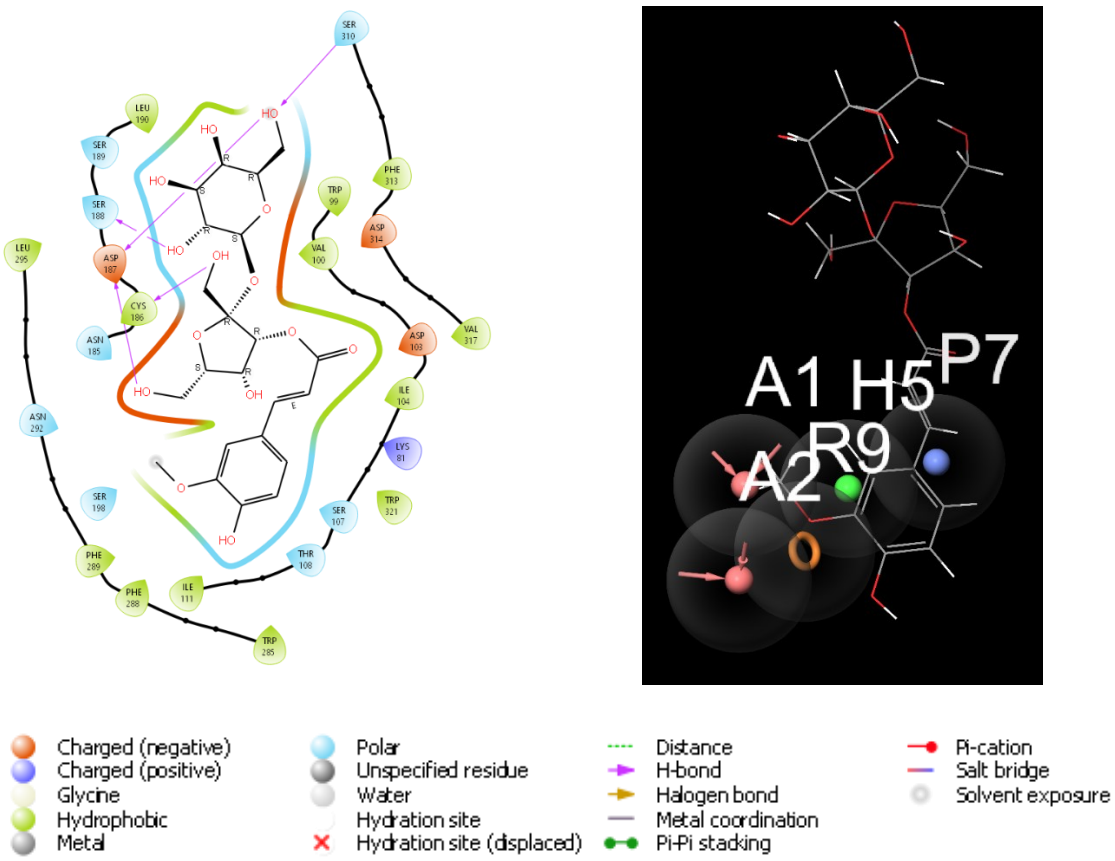

Figure 5-4: A) 2D interaction model of *Polygala virgata* fraction 3 compound, 3'-O-(4-hydroxy-3-methoxy-E-cinnamoyl), docked into the active site of dopamine-1 with amino acid bindings. Purple line indicates hydrogen bonding, and green line indicate pi-pi stacking interactions. B) Structure of 3'-O-(4-hydroxy-3-methoxy-E-cinnamoyl), overlayed with pharmacophoric model of apomorphine.

5.3.2.2 Dopamine 2 receptor

The DA-2R has a co-crystallised ligand, risperidone (PDB ID: 6CM4, **Figure 5-5**), which is a known dopaminergic antagonist that binds within the receptors active site.[713] This structure was selected for analysis because the crystal structures involving bromocriptine, a known PD treatment and dopamine agonist contained mutated residues on the protein structure. These mutations are not representative of the typical receptor configurations found in the midbrain, making the risperidone-bound DA-2R structure a more suitable model for the study.[713] The mechanism of the G-protein in DA-2R, which involves the inhibition of adenylyl cyclase, and the activation of K^+ channels, suggests a response distinct from that of DA-1R.[714] The benzoisoxazole ring of risperidone displayed pi-pi electron stacking interactions with PHE 390 and TRP 386, anchoring the molecule within the active site **(Figure 5-6)**. Parts of the risperidone molecule are solvated (specifically the quinazoline ring), highlighting the importance of these two residues (PHE 390 and TRP 386) in receptor activity, as they are holding the compound in place. Dopamine, as the endogenous ligand,

activates its target through interactions with ASP 114, SER 193, and SER 197, which are also associated with agonistic effects (not shown).[715]

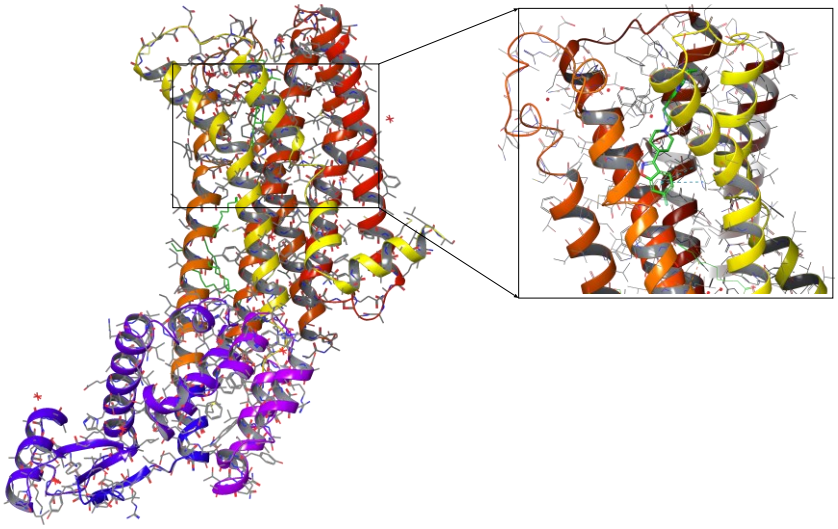

Figure 5-5: The crystal structure of dopamine-2 receptor (DA-2R), with risperidone (green) co-crystallised in the active site (PDB ID: 6CM4).

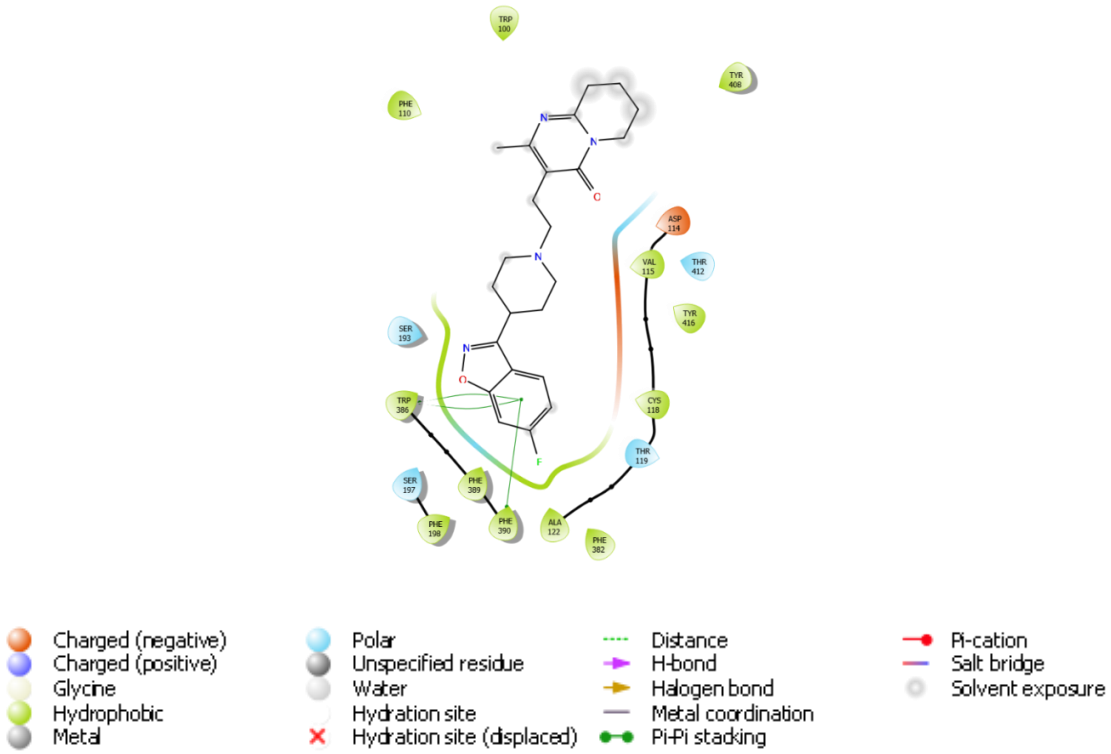

Figure 5-6: Risperidone (black) forms interactions with amino acid residues in the dopamine-2 receptor (PDB ID: 6CM4). The green line indicates pi-pi stacking interactions.

The compound, 1-*O*-trans-caffeoyl-β-d-allopyranoside isolated from fraction 3 of *A. oppositifolia* showed a docking score of -8.42 kcal/mol. This may be attributed to its interactions with PHE390

and TRP386 (**Figure 5-7**), which involved pi-pi stacking between the catechol ring of the compound and the aromatic ring structures of these residues **(Figure 5-8)**. The catechol ring is also present in the molecular structure of dopamine, which may enhance the compound's activity due to structural similarities with the endogenous ligand. This pi-pi stacking interactions stabilise the ligand within the active site; further supported by a hydrogen bond between the heterocyclic oxygen in the sugar moiety and water molecule. The water molecule assists in forming a hydrogen bond between the compound and HIS 393. The triad of ASP 114, SER 193 and SER 197[715], known to be activated with dopamine does not appear to be involved in the binding of 1-*O*-trans-caffeoyl-β-d-allopyranoside.

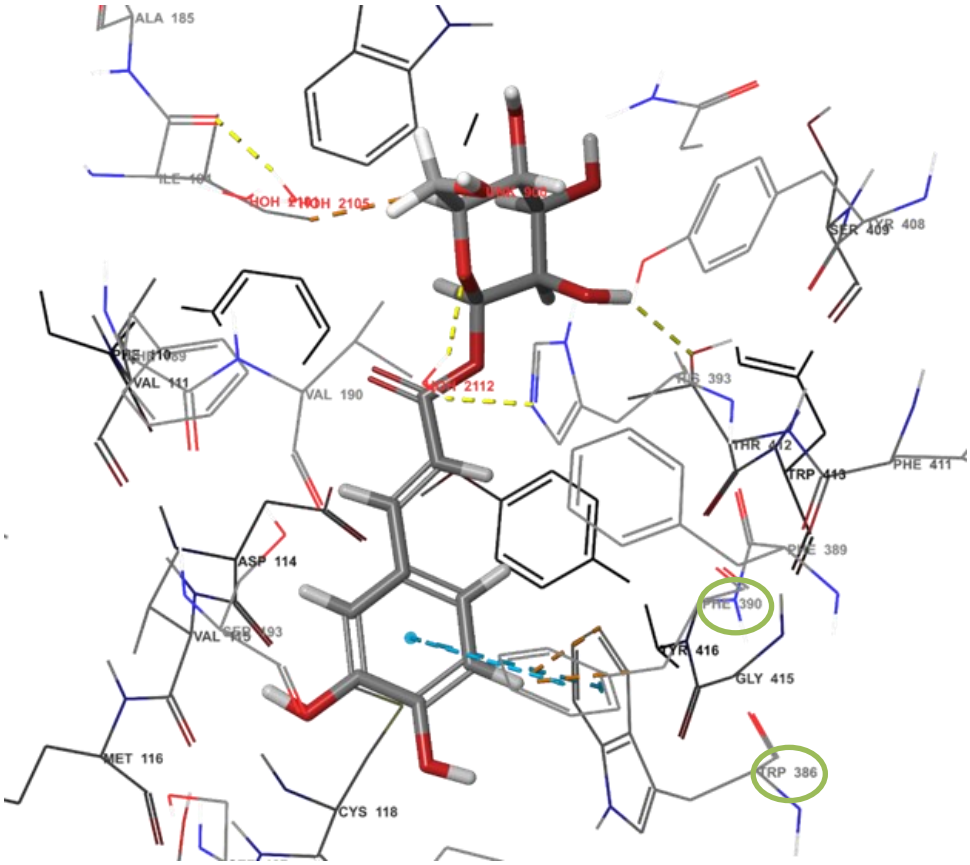

Figure 5-7: A 3D representation of 1-*O*-trans-caffeoyl-β-d-allopyranoside isolated from *Acokanthera oppositifolia* fraction 3 interacting with both TRP 386 and PHE 390 within the active site of the dopamine-2 receptor (PDB ID: 6CM4).

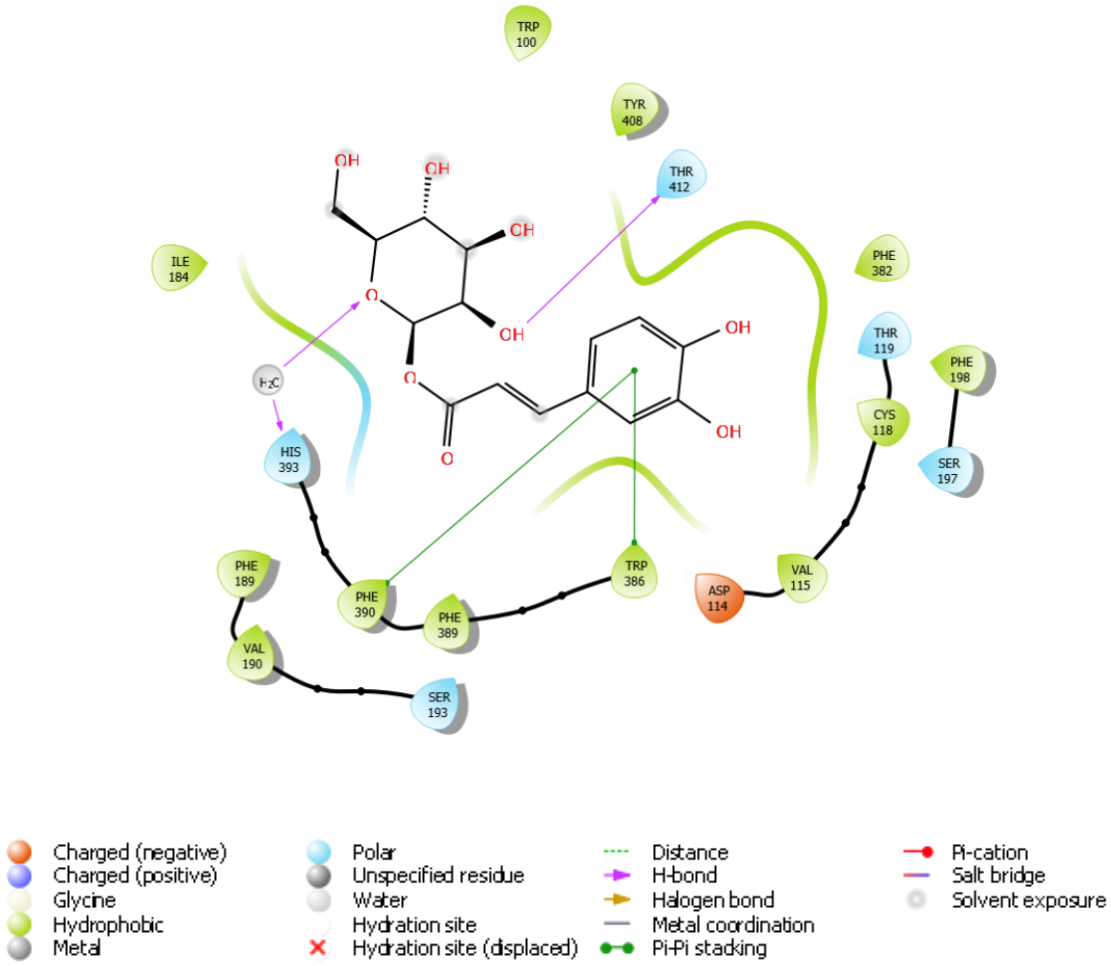

Figure 5-8: A 2D interaction diagram of 1-*O*-trans-caffeoyl-β-d-allopyranoside, isolated from *Acokanthera oppositifolia* fraction 3, displaying interactions with residues TRP 386 and PHE 390. The same interactions are seen with risperidone. An additional hydrogen bond is seen between THR 412. Purple line indicates hydrogen bonding, and green line indicate pi-pi stacking interactions.

The second compound, 2-*O*-caffeoyl glucose, also identified from *A. oppositifolia* F3, showed a binding affinity of -7.80 kcal/mol. While the compound does not interact with residues TRP 386 and PHE 390 as seen with risperidone, pi-pi electron stacking interactions can be seen between the catechol ring of the ligand and TRP 100. Hydrogen bonds can be seen between GLU 95 and LEU 94 and the hydroxyl groups on the sugar moiety **(Figure 5-9, Figure 5-10)**. [715] This suggests that while the compound occupies the receptor, it does not interact with the residues involved in risperidone binding or the agonistic triad (ASP114, SER193, and SER197) that dopamine engages with. A part of the catechol ring is solvated in this conformation, possibly reducing the effectiveness the catechol moiety can have on the receptor.

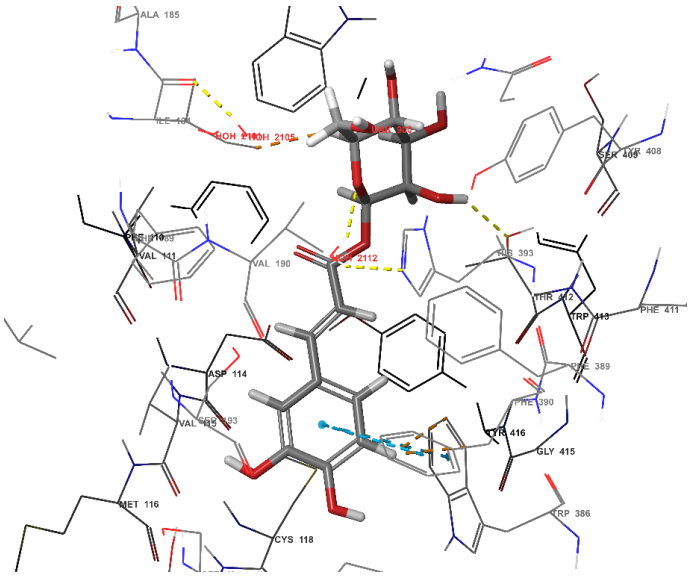

Figure 5-9: A 3D representation of 2-*O* -caffeoyl glucose isolated from *Acokanthera oppositifolia* fraction 3 showing different interactions than TRP 386 and PHE 390 within the active site of the dopamine-2 receptor (PDB ID: 6CM4).

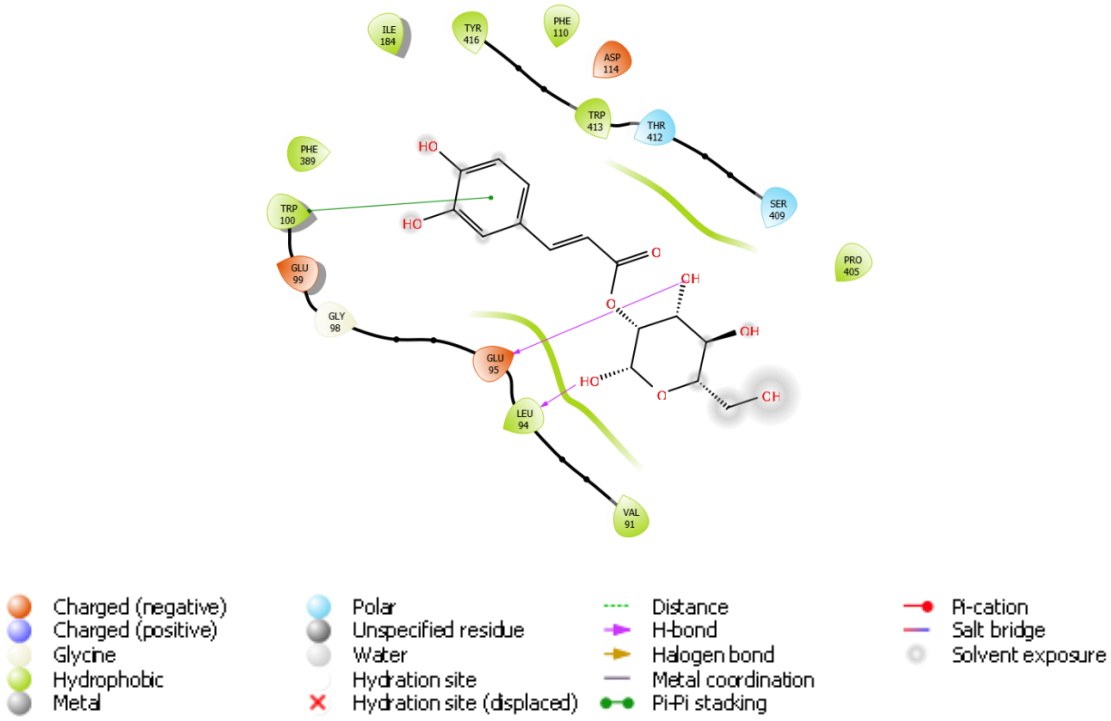

Figure 5-10: A 2D interaction diagram of 2-*O* -caffeoyl glucose isolated from *Acokanthera oppositifolia* fraction 3 indicating no interactions with residues TRP 386 and PHE 390 as seen in risperidone. However, there are hydrogen bond seen between the compound and LEU 94 and GLU 95, and pi-pi stacking seen with TRP 100. Purple line indicates hydrogen bonding, and green line indicate pi-pi stacking interactions.

5.3.2.3 Glutathione peroxidase 4: active catalytic site

The active site of GPx4, known as a catalytic triad, consists of the residues TRP 136, GLN 81 and CYS 46 **(Figure 5-11)**.[716, 717] The surficial nature of this binding pocket distinguishes GPx4 from other enzymes in the GPx family, enabling it to reduce larger molecules such as lipid peroxides to lipid alcohols.[253, 718] The affinity of compounds to this site may be used to determine if the compounds interfere with the reduction of lipid peroxides, or the utilisation of intracellular GSH.

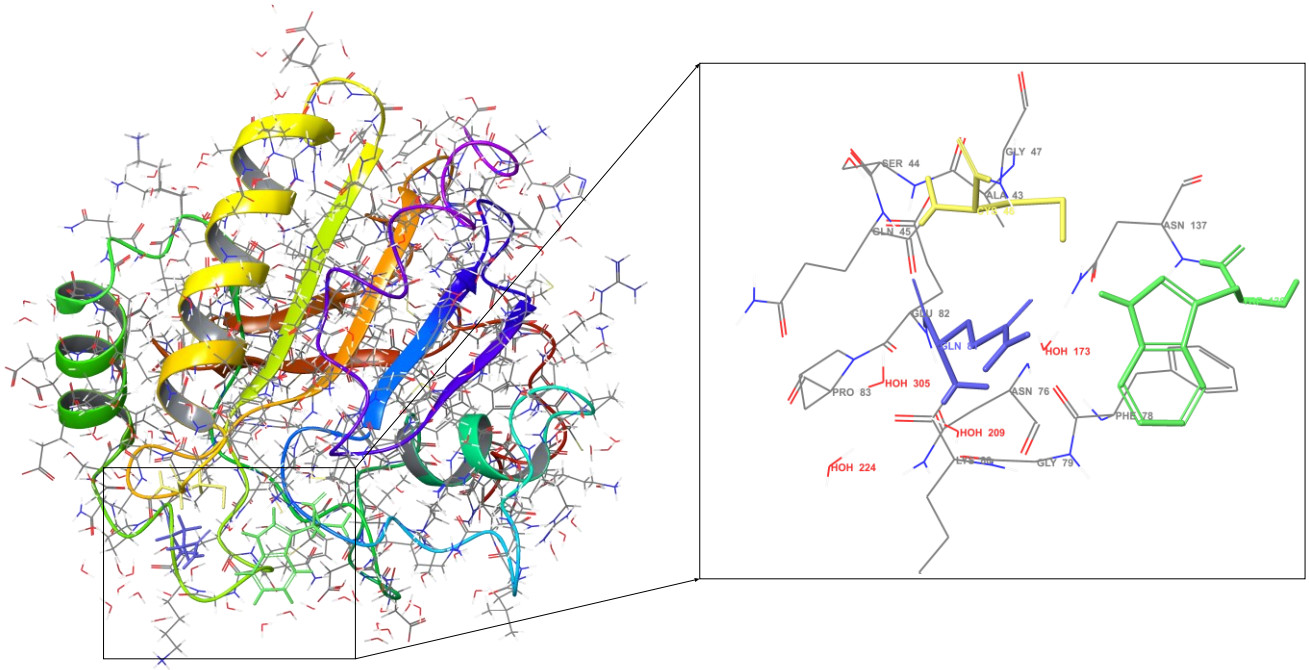

Figure 5-11: Protein structure of glutathione peroxidase 4 (GPx4. PDB ID: 3OBI) with the identified catalytic triad (GLN 81: blue, CYS 46: yellow, TRP 136: green) within the active site.

The compound with the highest affinity for the GPx4 active site, identified from *A. oppositifolia* F3, was 3-O-caffeoyl-muco-quinic acid, with a binding affinity of -4.73 kcal/mol. The ketone oxygen of the compound forms hydrogen bonds with the catalytic triad residues GLN 81, TRP 136, and CYS 46. **(Figure 5-12, Figure 5-13)**. Additionally, a salt bridge interaction with LYS 48 can be observed, which may be attributed to the ionised state of the carboxylic acid at a pH of 7.4 ± 1. This may impact the membrane permeability of the compound, as ionised molecules typically exhibit reduced permeability[719] It remains unclear whether active transport mechanisms exist for compounds of this nature.

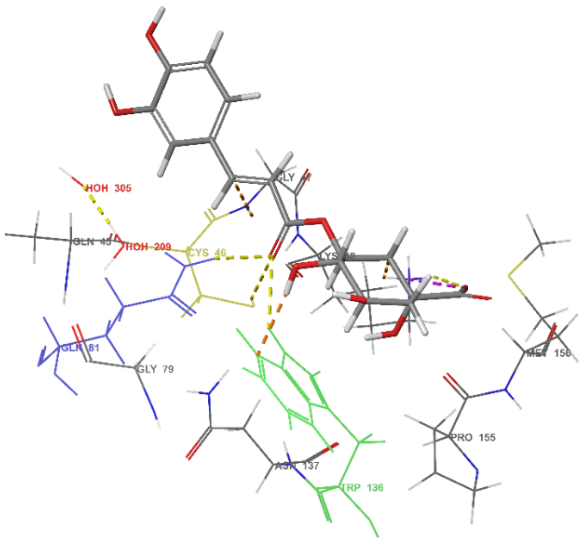

Figure 5-12: A 3D representation of 3-*O*-caffeoyl-muco-quinic acid identified from *Acokanthera oppositifolia* fraction 3 interacting with the catalytic triad (GLN 81: blue, CYS 46: yellow, TRP 136: green) of the glutathione peroxidase 4 active site.

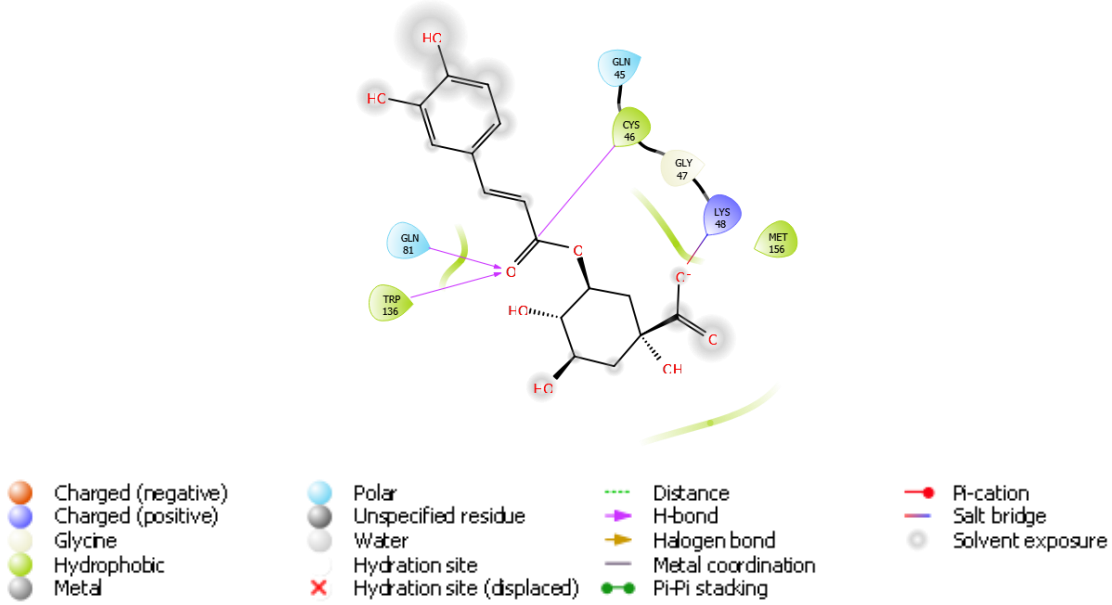

Figure 5-13: A 2D interaction diagram of 3-*O*-caffeoyl-muco-quinic acid identified from *Acokanthera oppositifolia* fraction 3 interacting with the catalytic triad (GLN 81, CYS 46, TRP 136) of the glutathione peroxidase 4 active site (PDB ID: 3OBI). Purple line indicates hydrogen bonding, and green line indicate pi-pi interactions.

The compound 3,5-dihydroxy-1,2-dimethoxyxanthone, identified from F5 - F7 of *P. virgata*, presents with a binding affinity of -4.03 kcal/mol. The compound forms hydrogen bonds with two

key residues of the catalytic triad, CYS 46 and GLY 47, and is further stabilised by pi-pi electron stacking interactions with TRP 136, involving the phenol and furano rings of the xanthone scaffold (**Figure 5-14, Figure 5-15**). However, the compact nature of the xanthone scaffold may have limited its ability to interact with GLN 81. Unlike the longer structure of 3-O-caffeoyl-muco-quinic acid, the smaller size of the compound prevents it from interacting with other regions in the binding pocket.

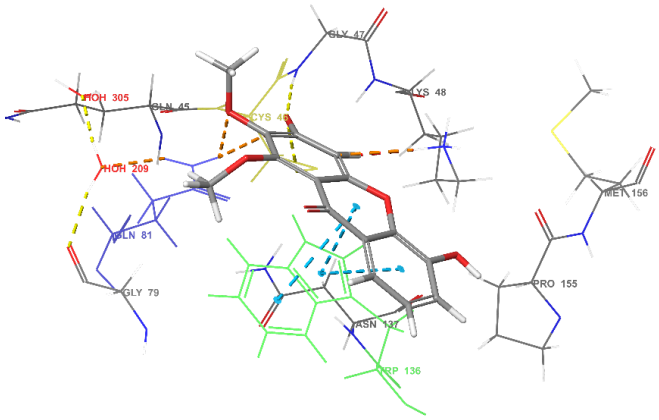

Figure 5-14: A 3D representation of 3,5-dihydroxy-1,2-dimethoxyxanthone identified from *Polygala virgata* fractions 5 and 7 interacting with two of the three residues in the catalytic triad (CYS 46: yellow, TRP 136: green) of the glutathione peroxidase 4 active site (PDB ID: 3OBI).

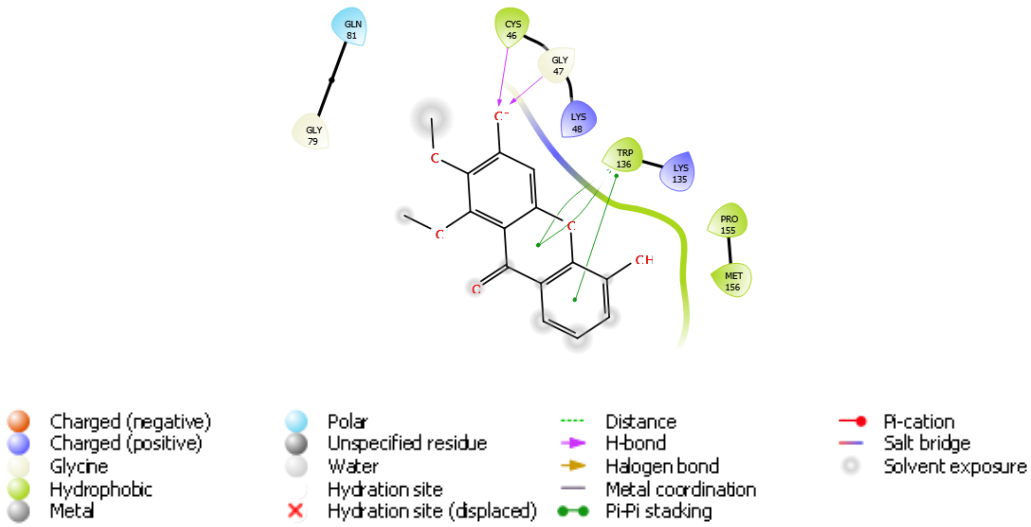

Figure 5-15: A 2D interaction diagram of 3,5-dihydroxy-1,2-dimethoxyxanthone identified from *Polygala virgata* fractions 5 and 7 interacting with two of the three residues in the catalytic triad (CYS 46, TRP 136) of the glutathione peroxidase 4 active site (PDB ID: 3OBI). An additional hydrogen bond is seen between GLY 47 Purple line indicates hydrogen bonding, and green line indicate pi-pi stacking interactions.

5.3.2.4 Glutathione peroxidase 4: allosteric binding site

In addition to the catalytic triad, GPx4 also features an allosteric binding site near CYS 66 (**Figure 5-16).** This site is of particular interest because it offers the potential for covalent bonding with inhibitors, due to the sulphur atom in cysteine.[720] Studies have shown that this allosteric site can regenerate the enzyme *in vitro*.[283] The thiol group on CYS 66 may function as a reductant within the catalytic triad, especially when there is insufficient GSH available. This suggests that targeting the allosteric site could provide a strategy for modulating GPx4 activity under specific conditions, especially in scenarios where GSH levels are low.[283]

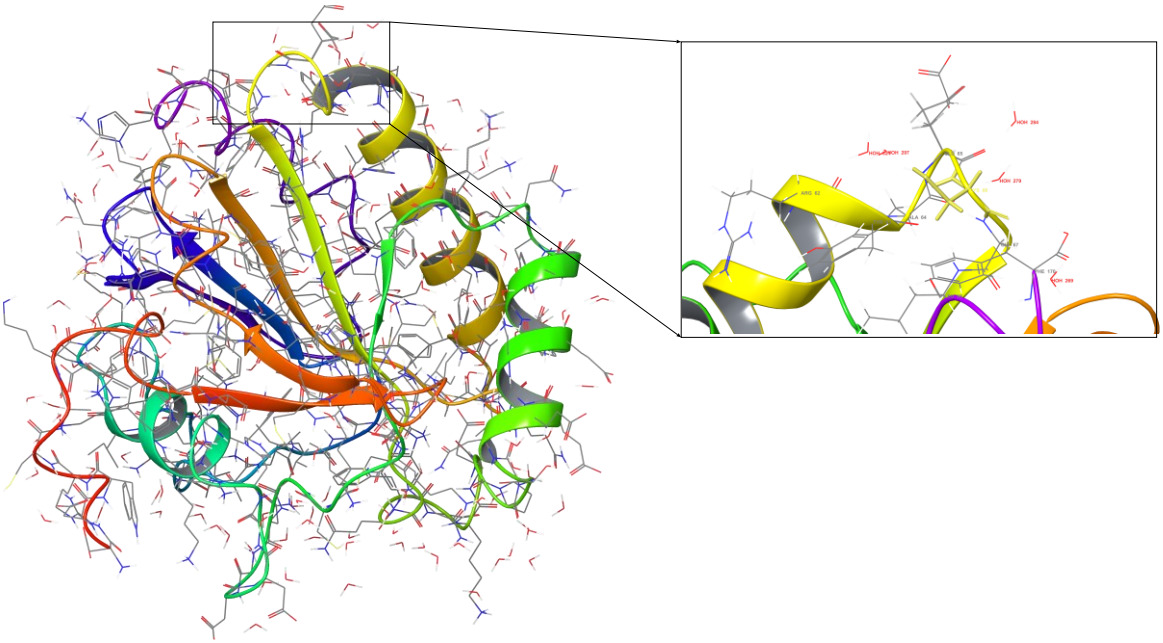

Figure 5-16: Glutathione peroxidase 4 (GPx4, PDB ID: 3OBI) with CYS 66 (yellow) identified as the zone in which an allosteric binding site resides.

The compound with the highest affinity for the allosteric binding site of GPx4, identified from *P. virgata* F3 was determined to be 1'-O-(4-hydroxy-3-methoxy-e-cinnamoyl), with a g-score of -6.384 kcal/mol. Although it does not interact directly with CYS 66, it spreads across the allosteric site, establishing hydrogen bond interactions with GLN 34 through water molecules (**Figure 5-17, Figure 5-18**). Its multi-hydroxylated structure enhances water solubility, and the enzyme's solvated cytoplasmic environment likely facilitates the compound's positioning over the allosteric site. This strategic coverage of the CYS 66 allosteric site may prevent GPx4 from engaging in its catalytic triad, particularly under low GSH conditions, such as during ferroptosis. Additionally, the compound lacks functional groups capable of forming covalent bonds, suggesting a non-covalent mechanism of action. This implies that its modulation of GPx4 activity occurs through allosteric regulation rather than direct inhibition.

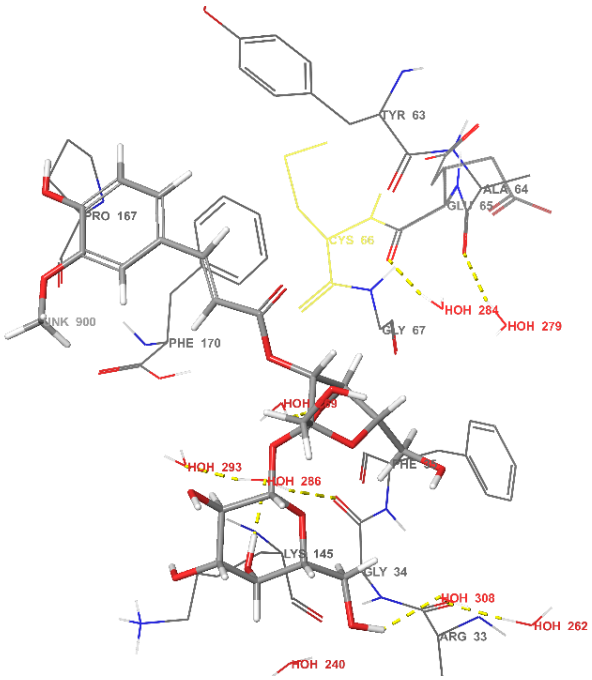

Figure 5-17: A 3D representation of 1'-*O*-(4-hydroxy-3-methoxy-*e*-cinnamoyl) identified from *Polygala virgata* fraction 3 in the allosteric binding site of glutathione peroxidase 4 (GPx4, PDB ID: 3OBI) surrounding CYS 66 (Yellow).

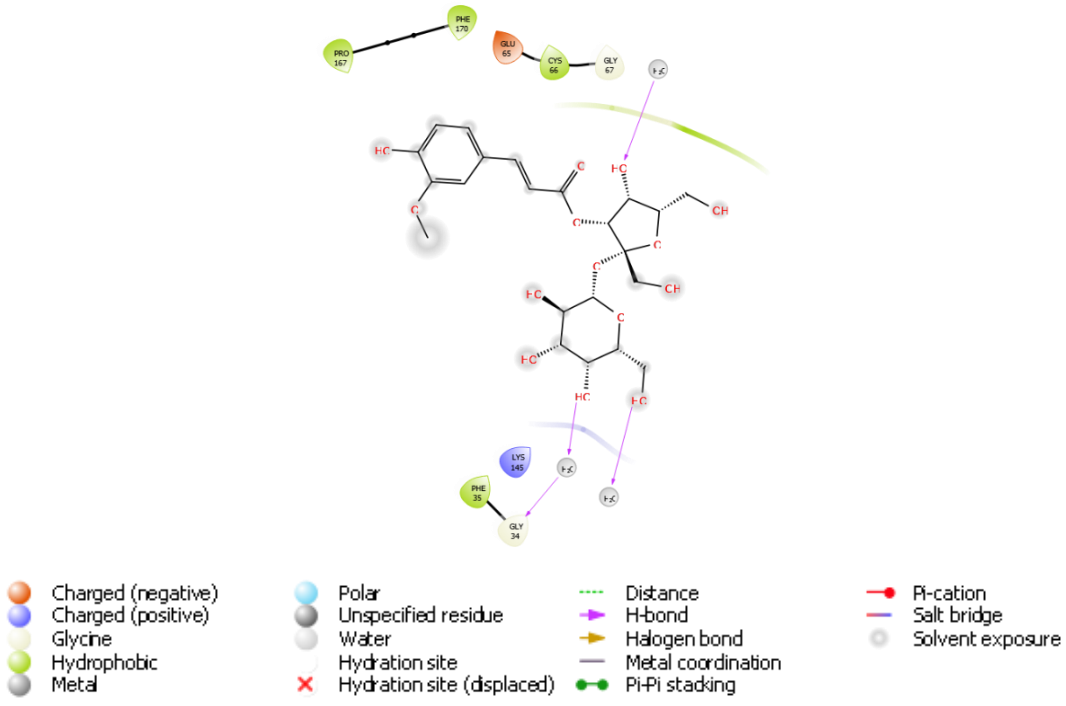

Figure 5-18: A 2D interaction diagram of 1'-*O*-(4-hydroxy-3-methoxy-*e*-cinnamoyl) identified from *Polygala virgata* fraction 3 in the allosteric binding site of glutathione peroxidase 4 (GPx4, PDB ID: 3OBI) surrounding CYS 66. Purple line indicates hydrogen bonding, and green line indicate pi-pi stacking interactions.

The compound with the second-best binding affinity is 3'-O-(4-hydroxy-3-methoxy-E-cinnamoyl), identified in *P. virgata* F3 (-4.929 kcal/mol). This compound formed two hydrogen bond interactions with CYS 66, originating from the hydroxyl groups on its sugar moiety, potentially contributing to protective effects on the enzyme in a low GSH environment (**Figure 5-19, Figure 5-20**). Additionally, two other hydrogen bond interactions can be observed between PHE 170 and GLU 65, involving hydroxyl groups on the tetrahydrofuran ring. The hydroxy and methoxy-substituted benzene ring extends outside the binding site, with a hydrogen bond interaction between one of the methoxy hydrogen atoms and CYS 66 (**Figure 5-19**). The structural similarity to 1'-O-(4-hydroxy-3-methoxy-E-cinnamoyl) suggests that the furan and heterocyclic rings could serve as viable scaffolds for allosteric binding.

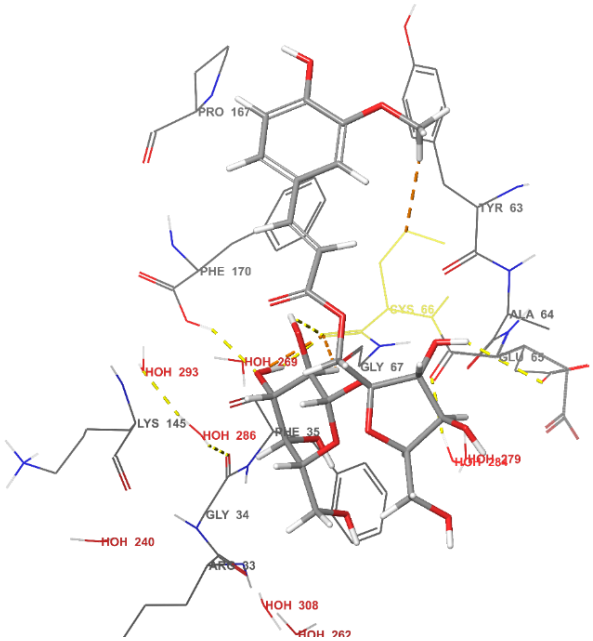

Figure 5-19: **A** 3D representation of 3'-*O*-(4-hydroxy-3-methoxy-*e*-cinnamoyl) identified from *Polygala virgata* fraction 3 in the allosteric binding site of glutathione peroxidase 4 (GPx4, PDB ID: 3OBI) surrounding CYS 66 (yellow).

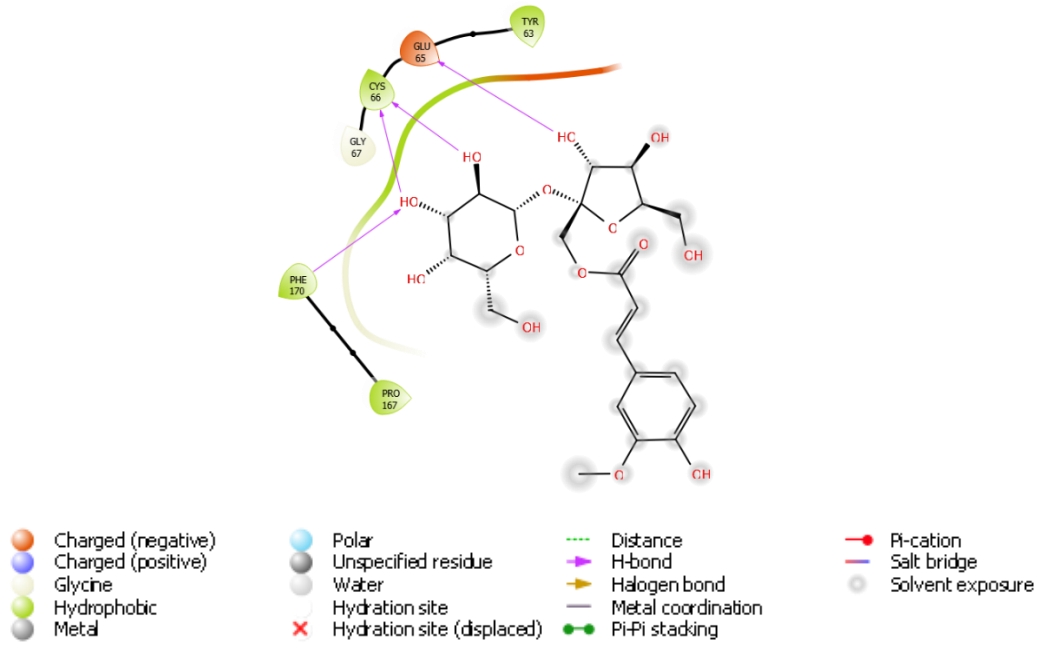

Figure 5-20: A 2D interaction diagram of 3'-*O*-(4-hydroxy-3-methoxy-*e*-cinnamoyl) identified from *Polygala virgata* fraction 3 in the allosteric binding site of glutathione peroxidase 4 (GPx4, PDB ID: 3OBI) surrounding CYS 66. Additional hydrogen bonds are seen between PHE 170 and GLU 65. Purple line indicates pi-pi stacking interactions.

5.3.2.5 Xc^- system (cysteine/glutamate antiporter)

Using a 1:1 counter-transport of glutamate, the antiporter system xc^- imports the oxidized form of the amino acid cysteine into the cells via sodium-independent and chloride-dependant transport.[721] Evidence suggests the xc^- system is highly inducible with both oxygen[722] and certain electrophiles[723] inducing the system to increase cysteine transport and glutamate removal. The transporter takes on an inward open conformation, and a sizable aqueous channel connects it to the central binding site to the membrane's cytoplasmic side **(Figure 5-21)**.[724] This channel is opened by glutamate binding to LYS 198, TYR 244 and ARG 396 forming the active site **(Figure 5-21)**.[725] This channel and active site form a positively charged environment to facilitate the movement of glutamate in favour for cysteine across the membrane (PDB ID: 7P9V).[726]

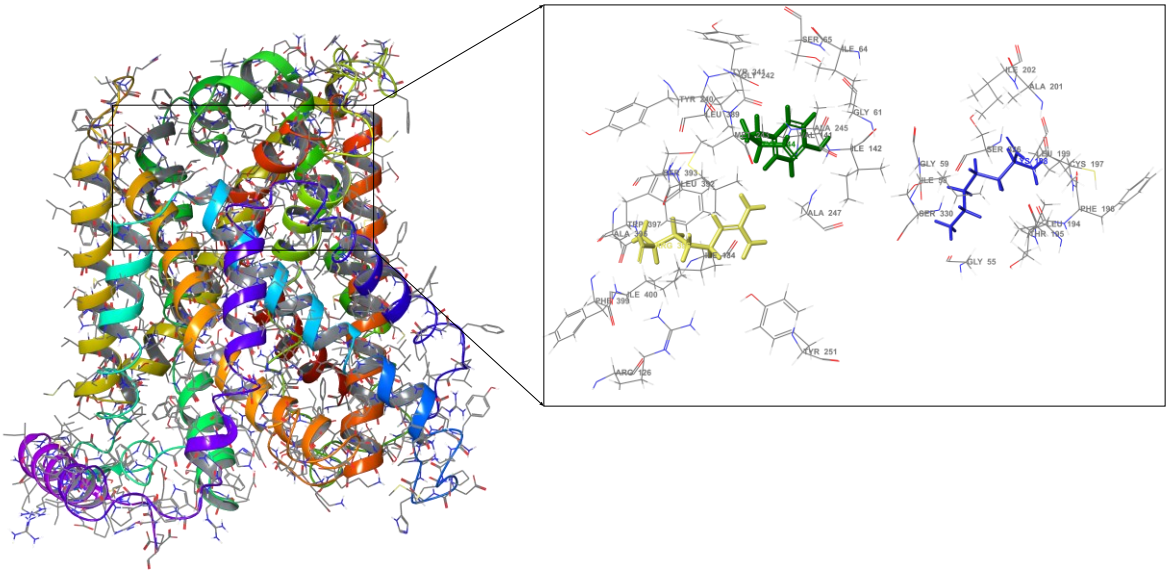

Figure 5-21: Membrane bound protein structure (PDB ID: 7P9V) of the xc- system with the active site residues of LYS 198 (blue), TYR 244 (green) and ARG 396 (yellow) expanded.

The compound, 6-c-β-d-glucopyranosyl-3',4',5-trihydroxy-7-methoxyflavone identified from *B. latifolia* F5 presents with a binding affinity of -9.181 kcal/mol. Hydrogen bond interactions with SER 330 and GLY 55 stabilises the compound within the binding pocket, and there is van der Waal's interaction with TYR 251 **(Figure 5-22)**. The hydrophilic nature of the compound aids in keeping the compound within the charged active site, but it does not have interact with LYS 198, TYR 244 or ARG 396 **(Figure 5-23).**

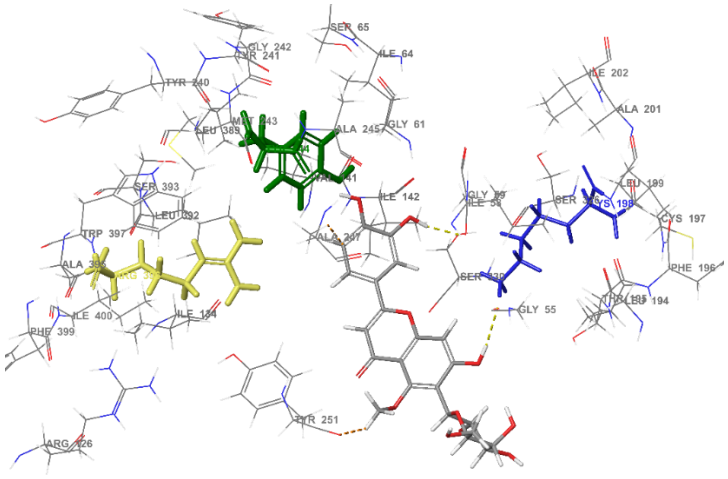

Figure 5-22: A 3D representation of 6-c-β-d-glucopyranosyl-3',4',5-trihydroxy-7-methoxyflavone, identified from *Bulbine latifolia* fraction 5 in the xc- system active pocket (PDB ID: 7P9V) with residues LYS 198 (blue), TYR 244 (green) and ARG 396 (yellow).

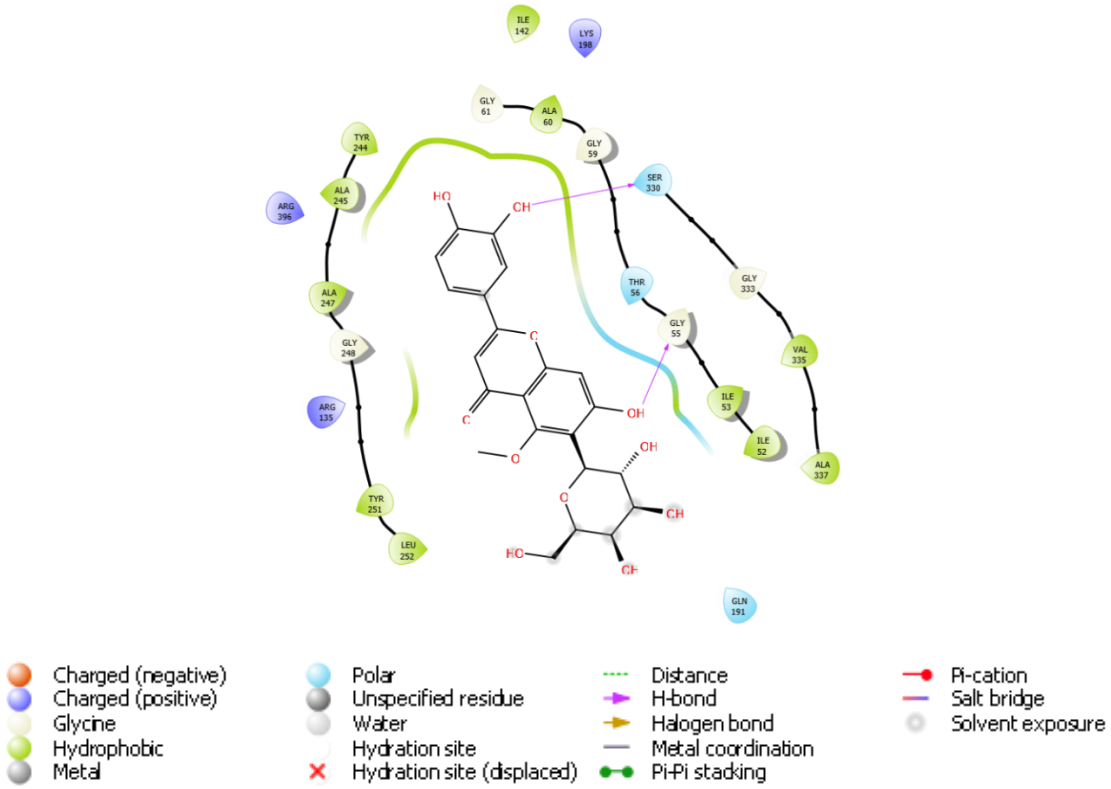

Figure 5-23: A 2D interaction diagram of 6-c-β-d-glucopyranosyl-3',4',5-trihydroxy-7-methoxyflavone, identified from *Bulbine latifolia* fraction 5 in the xc^- system active pocket (PDB ID: 7P9V). There are hydrogen bonds between GLY 59 and SER 338. Purple line indicates hydrogen bonding, and green line indicate pi-pi stacking interactions.

The compound, 3-*O*-caffeoyl-muco-quinic acid identified from *A. oppositifolia* F3 presents with a binding affinity of -8.859 kcal/mol. A hydrogen bond interaction can be seen between the hydrogen of the carboxylic acid and ARG 396 **(Figure 5-24, Figure 5-25)**. Additionally, a hydrogen bond has been formed between the hydroxyl group in the sugar moiety and ARG 135, stabilising the compound closer to the active residue with another hydrogen bond, ARG 396. The ionised nature of the compound allows it to interact favourably with the hydrophilic pocket of the xc^- system, as it can form dipoles between the amino acids and the hydroxyl groups of the compound. The catechol moiety remains solvated and positioned outside the range of the active residues. Binding of 3-*O*-caffeoyl-muco-quinic acid to ARG 396 may be sufficient to induce the xc^- system; however, additional *in vitro* data is required to confirm whether this effect is achievable with this class of phytochemicals.

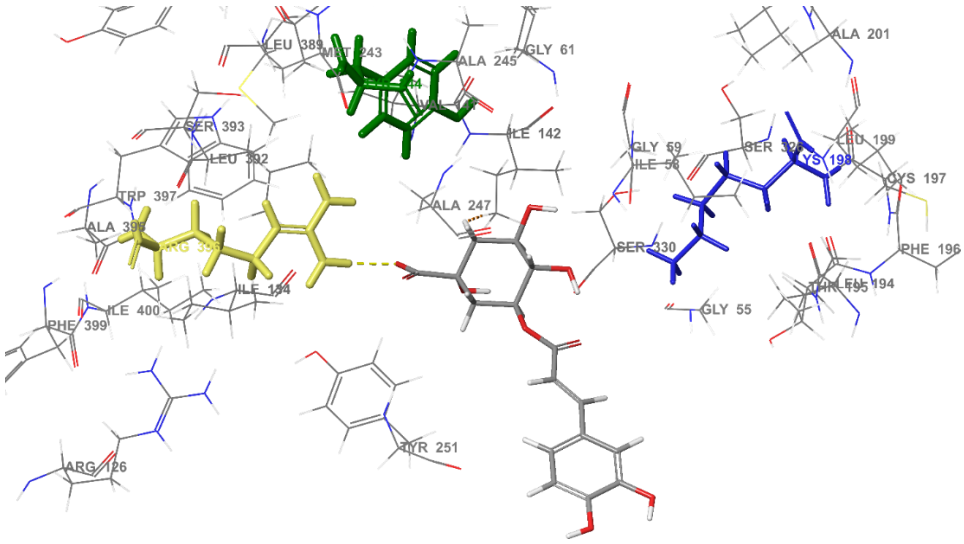

Figure 5-24: A 3D representation of 3-*O*-caffeoyl-muco-quinic acid identified from *Acokanthera oppositifolia* fraction 3 in the xc⁻ system active pocket (PDB ID: 7P9V) with residues LYS 198 (blue), TYR 244 (green) and ARG 396 (yellow).

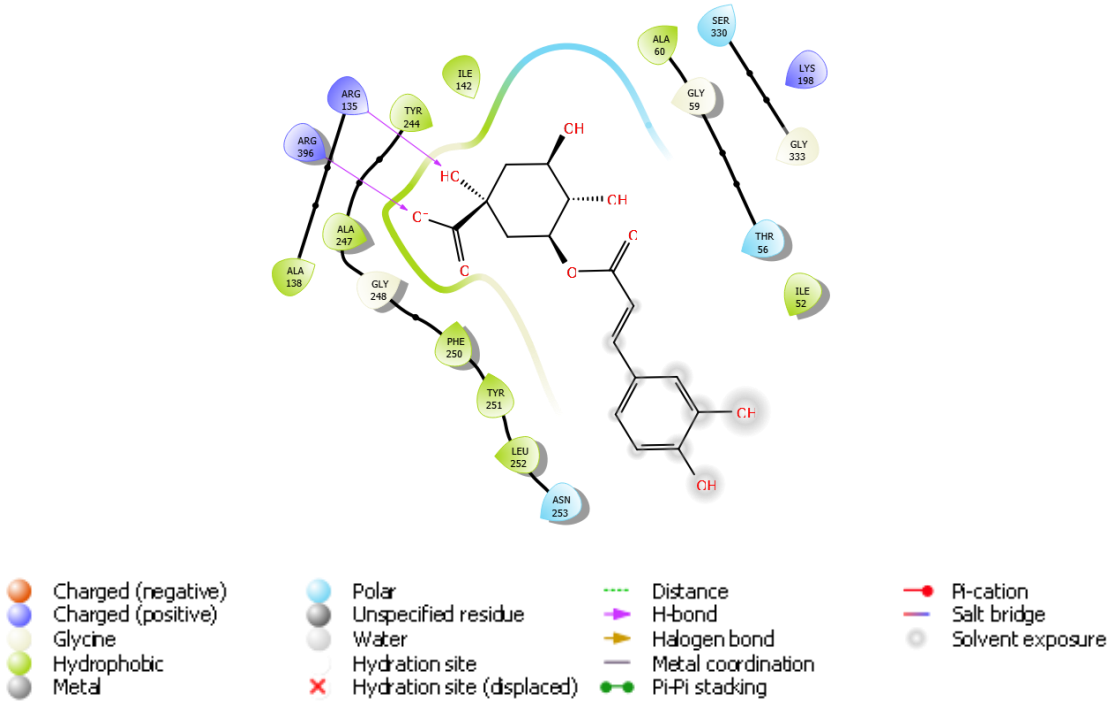

Figure 5-25: A 2D interaction diagram of 3-*O*-caffeoyl-muco-quinic acid identified from *Acokanthera oppositifolia* fraction 3 in the xc⁻ system active pocket (PDB ID: 7P9V). Two hydrogen bonds are seen between ARG 396 and ARG 135. Purple line indicates hydrogen bonding.

None of the high-affinity compounds were predicted to be permeable to the BBB. However, their potential utility should not be dismissed, as the docking scores alone does not account for the effects of transporters that may facilitate their passage. Furthermore, these compounds can still exist and exert their effects within the cell model, as the BBB is not represented in this experimental system. Therefore, the observed affinities may translate into measurable activity within the cellular context.

These *in silico* determinations provide a foundation for focused drug-target studies, particularly on the cytoprotective mechanisms of these plants and compounds. Targets such as GPx4 and the xc- system have the potential to be disease-modifying in conditions like ferroptosis, where their downstream effects could complement existing PD treatments. By preventing further degeneration of dopaminergic neurons, interactions with these targets may enhance the therapeutic efficacy of current PD medications.

CHAPTER 6: CONCLUSION

6.1 Disease modification via a multitarget approach

Parkinson's disease encompasses a wide range of cellular abnormalities throughout its prodromal and advanced stages, emphasizing the need for a multi-target therapeutic strategy. This study highlights the involvement of key redox regulators in ferroptosis as a potential therapeutic target to mitigate cell death caused by ROS generation, GSH depletion, mitochondrial dysfunction, and the subsequent accumulation of lipid peroxides. In this study plant extracts and their fractions with CNS activity, were investigated to harness the multi-target potential of herbal medicines. By investigating the intricate mechanisms underlying ferroptosis, this study provided valuable insights into potential strategies for disease modification. In the context of the models used, no studies have detailed the precise cascade of events leading to cell death induced by 6-OHDA, nor identified a definitive initial step in ROS generation and subsequent cell death. Therefore, the results should be interpreted as an interplay of multiple factors contributing to the mechanisms of cell protection exhibited by each plant fraction.

By investigating plant fractions with known CNS activity, the study uniquely leveraged the multi-target affinities inherent in herbal medicines .From the 24 plant species studied, a total of 192 fractions (seven fractions per plant along with the crude extract) were produced and screened for cytotoxicity and cytoprotection. Among these, only 15 fractions demonstrated significant cytoprotective effects against 6-OHDA exposure. Acellular chelation activity revealed that none of the 192 fractions exhibited notable chelation activity, with the highest chelation activity observed being 15% for *D. sylvatica*. Antioxidant activity, as measured using the FRAP assay, had results which corresponded with those of the cytoprotective effects. Fraction 3 of *A. oppositifolia* demonstrated no inherent cytotoxicity at 10 µg/mL in SHSY5Y cells suggesting that it does not present with detrimental effects to cell density. However, the fraction reduced 6-OHDA-induced cytotoxicity, while also modulating redox status. Furthermore, the fraction decreased ROS, which may be attributed to caffeoylquinic acids stabilising radicals via resonance structuring, as supported by its high FRAP activity. No chelation activity was observed, suggesting that the fractions do not inhibit ROS formation via the Fenton reaction. Instead, they appear to target water-soluble ROS, as indicated by unchanged TBARS-MDA levels. The increase in GSH levels suggests either GPx4 inhibition or conjugation with GSH, with docking studies supporting GPx4 inhibition due to the high affinity of 3-*O*-caffeoyl-muco-quinic acid for its active site. These protective effects likely arise from the fraction’s ability to scrub ROS and stabilise ΔΨm, promoting healthy respiration. Despite these advantages, the phytochemicals identified in the fraction were ineffective against lipid peroxidation, which limits their potential as therapeutic agents for CNS

diseases like PD where lipid peroxidation plays a crucial role. However, compounds such as 2-O-caffeoylglucose and 1-O-trans-caffeoyl-β-d-allopyranoside exhibit strong binding affinities for the DA-2R, presenting opportunities as scaffolds for receptor-targeted drugs. Structural modifications, such as substituting hydroxyl groups with halogens, could enhance BBBp and GIa. However, the current fraction and its phytochemicals require further optimisation to become viable treatment options for CNS diseases.

Fractions 3 and 4 of *A. procumbens* demonstrated minimal inherent cytotoxicity, suggesting that they do not adversely affect cell viability. Following 6-OHDA exposure, both fractions notably reduced ROS and TBARS-MDA levels, which correlated with the increased cell density noted. These findings highlight their protective effects against oxidative stress and lipid peroxidation. The reductions in oxidative markers observed are likely due to a dual mechanism: scavenging ROS that initiate lipid peroxidation and directly neutralising lipid peroxides to halt propagation reactions. While F4 demonstrated greater antioxidant potential than F3, these differences were not fully evident in the *in vitro* assays, suggesting a limited effect under the experimental conditions. The catechol-containing compound, dimethyl 2-[(2E)-3-(3,4-dihydroxyphenyl)prop-2-enoyl]oxy-butanedioate, present in both fractions, is likely a key contributor to their antioxidant activity. Its radical-stabilising and lipid peroxidation-inhibiting properties significantly enhance the fractions' overall effectiveness. Furthermore, both fractions increased GSH levels, potentially influencing lipid metabolism through GPx4 activity, where GSH serves as a co-factor. This increase in GSH may result from enhanced cysteine uptake via the antiporter system or an improved oxidised/reduced GSH ratio mediated by GSR. Molecular docking studies, however, did not reveal strong binding affinities for GPx4 or other ferroptosis-related targets. Despite this, the fractions demonstrated activity across all assays, suggesting broad antioxidant capabilities. Although not the fractions with the highest cytoprotective activity, their multifaceted activity, and mechanisms position *A. procumbens* as a promising candidate for further studies into ferroptosis-related pathways.

Fractions 3 and 5 of *B. latifolia* demonstrated reductions in ROS, with F5 exhibiting greater antioxidant potential compared to F3. These reductions did not however extend to lipid peroxides, as F3 showed no significant effect on lipid peroxidation caused by 6-OHDA. Fraction 3 increased GSH levels, likely due to enhanced GSH synthesis rather than GPx4 activity, as no corresponding reduction in lipid peroxides was observed. Fraction 5 stabilised mitochondrial ΔΨm, suggesting that its cytoprotective effects are related to mitigating mitochondrial dysfunction caused by 6-OHDA. The compound 6-C-β-d-glucopyranosyl-3',4',5-trihydroxy-7-methoxyflavone, identified in F5, exhibited strong affinity for the Xc^- system, potentially influencing cysteine transport and contributing to it increasing GSH However, the glycated nature of compounds in F5 limits their

BBB permeability. Modifications such as removing sugar moieties to reduce molecular size or substituting hydroxyl groups to improve lipophilicity could enhance absorption profiles and therapeutic potential. These flavonoid scaffolds present a promising foundation for further optimisation.

Fractions 3 to 7 of *P. virgata* exhibited no iron chelation but effectively reduced 6-OHDA-induced oxidative stress. Fraction 4 was the most effective in reducing ROS and TBARS-MDA levels, though this did not coincide with the greatest increase in GSH. All fractions improved cell density following 6-OHDA pre-treatment, with F6 showing the highest increase in cell density. This suggests that F6 exerts its cytoprotective effects through the scavenging of lipid peroxides and reduction of ROS, supported by its observed increase in GSH levels. Fraction 6 did not normalise the ratio of mitochondria to cell density, indicating that it may stabilise the remaining mitochondria rather than restore mitochondria. The compounds identified within the fractions, including derivatives of chromones, coumarins, and benzo-pyran-4-one, likely contribute to the observed activity. However, several glycated and sucrose-bound forms, as well as unidentified compounds, are also present, and further purification is required to determine their precise roles. The increase in cell density, coupled with the absence of unpolarised mitochondria, suggests the possibility of mitochondrial hyperpolarisation. The reduction in cytoplasmic ROS may help stabilise the $\Delta\Psi m$, potentially mitigating further inhibition of Com I by 6-OHDA or associated ROS. Fractions from *P. virgata* demonstrated a broad spectrum of activities, with ratiometric differences in the identified compounds observed between F5 to 7. Further elucidation and evaluation of these fractions, particularly in combination, may reveal synergistic effects. Furthermore, the presence of BBBp compounds in F5 to F7 highlights their potential as promising candidates for further exploration as treatments for PD, particularly due to their multi-target activity.

Fraction 3 from *S. brachypetala* was the only fraction to decrease GSH concentrations following 6-OHDA exposure, which corresponded to its low activity in reducing TBARS-MDA levels. In contrast, F2 increased GSH levels, but also showed an increase in TBARS-MDA after 48 h. This suggests that the constituents in F2 may inhibit GPx4, preventing the conversion of lipid peroxides into lipid alcohols. Fraction 2 also demonstrated the smallest reduction in ROS of all samples tested, indicating that the cytoprotective effects of these fractions are likely linked to stabilising $\Delta\Psi m$. Both F2 and F3 normalised the ratio of mitochondria to cell density compared to the negative control, further supporting this hypothesis. Although no compounds from these fractions displayed high affinities in the molecular docking studies, several BBBp compounds were identified, warranting further investigation. Among these, 8,9-dehydrotheasporine emerges as a novel scaffold with potential for development.

Although each plant and its respective fractions exhibited a broad spectrum of activity, fractionation has demonstrated a stronger affinity for specific role-players (**Figure 6-1**). For instance, *S. brachypetala* F1 and 2 showed a greater affinity for stabilising ΔΨm; however, these fractions did not exhibit a similar effect on ROS. The effect of *P. virgata* F4 on ROS was also more pronounced than for the other fractions of the plant. This effect also carried over into the reduction of TBARS. No single plant demonstrated the highest activity across all assays; however, *A. procumbens* displayed more consistent performance and was the most effective at increasing GSH levels. While the extent to which ferroptosis mitigation contributes to the cytoprotective activity of these fractions remains unclear, this study offers a foundation for further molecular investigations to clarify the protective mechanisms involved.

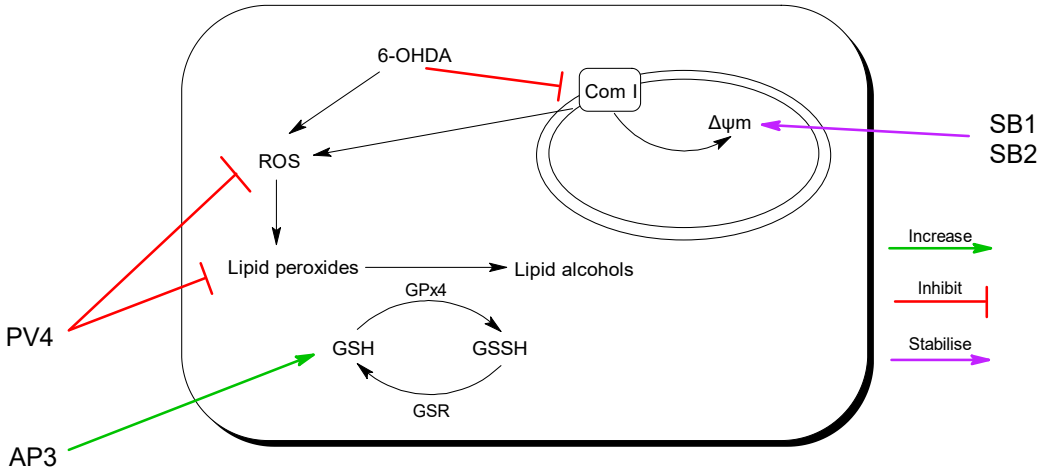

Figure 6-1: **Graphic summary of the selected fraction's mechanistic activity against *in vitro* targets of ferroptosis. ΔΨm: mitochondrial membrane potential, 6-OHDA: 6-hydroxydopamine, Com I: complex I, GPx4: glutathione peroxidase-4, GSH/GSSH: glutathione reduced/oxidised, GSR: glutathione reductase, ROS: reactive oxygen species, AP3: *Aptosimum procumbens* F3, PV4: *Polygala virgata* F4, SB2/SB3: *Schotia brachypetala* F2 and F3.**

In conclusion, plant-derived fractions have demonstrated potential as multi-target therapeutic candidates for PD, particularly by targeting ferroptosis, a critical cell death mechanism in the disease's progression. The results demonstrate that certain plant fractions, especially those with known CNS activity, can modulate key aspects of ferroptosis, including ROS generation, GSH depletion, and mitochondrial dysfunction, offering a promising approach for disease modification. While some fractions, such as those from *A. oppositifolia*, *A. procumbens*, and *P. virgata*, showed significant reductions in ROS and lipid peroxidation, and stabilisation of mitochondrial function, the ability to mitigate lipid peroxidation whilst having BBBp remains a challenge. These findings underscore the complexity of ferroptosis and the need to further optimise identified bioactive

phytochemicals. Structural modifications aimed at improving BBBp and enhancing the efficacy of these fractions are warranted.. In this project, the candidate spearheaded the screening of plant extracts to identify potential neuroprotective agents against PD through a holistic rather than a target-specific approach. While many researchers concentrate on individual compounds with known activities such as MAO-B inhibition, ROS scrubbing, and antioxidant properties, this study uniquely focused on whole plant fractions. Recognizing that neurodegeneration is a multifactorial disease with interplaying pathologies, the candidate designed and optimized cell-based assays to assess the efficacy of plant-derived compounds on dopaminergic neuron viability, ensuring that the complex interactions among various disease aspects were not overlooked.

The candidate further integrated chromatographic and spectrometric techniques to isolate and characterize active constituents, correlating these data with observed biological activities to propose plausible mechanisms of action. In addition to plant identification and phytochemical elucidation, both in vitro and in silico methods were employed to gain a comprehensive perspective on the multifaceted activities observed. By elucidating these complex interactions and establishing a robust methodology, the candidate not only underscored the potential synergy of plant extracts and phytochemicals as multitarget effectors but also paved the way for lead optimization and combinatorial therapies in the treatment of PD. Collaborative efforts with research colleagues further refined experimental protocols and ensured statistical robustness, significantly advancing the understanding of plant-based interventions for neurodegenerative disorders.

6.2 Limitations and recommendations

The use of a cell model will always be associated with limitations, and in this case the SH-SY5Y cell line is no different. *In vitro* models lack the barriers that these compounds need to traverse to be concentrated enough at the location, in this case for PD, in the midbrain.[727] They are also not representative of a mature neuron with pure dopaminergic expression.[728] For a more representative model, the cells could be matured using retinoic acid to provide a differentiation in response as compared to the immature cell line.[729]

The use of plant extracts has long been a cornerstone of phytochemical research; however, the unique fractionation system employed in this study affected comparability, as many published results obtained used crude extracts. The use of a crude fractions does impede the release and solubility of compounds, but is more representative of ethnomedicinal use.[730] The phytochemical mixture in a crude fraction is also difficult to identify, thus from a drug discovery approach, it makes it difficult to assign certain activity to one or two specific compounds. A single-point concentration

is useful for initial screening, but testing a range of concentrations per fraction is necessary to determine a more precise concentration that yields a significant effect.

The subsequent fractionation and identification as performed in this study, did provide a more specific approach to phytochemical activity elucidation. It is recommended to isolate the current fractions of *P. virgata* and *A. procumbens*, seeing as they did present with the highest activity across all *in vitro* assays. These plants' compounds also do present with a large chemical base of scaffold generation and expansion, especially if small molecules disease modifying drugs are to be investigated**.** For the elucidated compounds, the use of *in silico* throughput has proven to dissuade the use of the compounds due to low absorption and BBBp, however, with no information on the interaction of these compounds at the BBB or the associated transporters, this may be misleading until more research is done.

The combination of selected plants and neurodegenerative diseases, particularly in the 6-OHDA SH-SY5Y model, is underrepresented in literature. The plants were chosen based on their ethnomedicinal use for CNS conditions, and for *A. villicaulis, C. molle, G. physocarpus, J. abyssinicum, P. virgata,* and *V. myriantha*, this study provides the first evidence of their potential use in CNS models and 6-OHDA-induced neurodegenerative diseases. While these plants have undergone antioxidant activity determination, their promising acellular results did not translate effectively in biological systems, and a further exploration is needed in both 3D-cultures and animal studies. Antioxidant studies are essential for understanding the activity linked to ethnomedicinal uses, but concurrent research into ROS reduction is needed to ensure that the observed activity reflects the behaviour of phytochemicals in a biological context. The same applies to iron chelation, as no biological model of iron metabolism within the SH-SY5Y 6-OHDA model was developed in this study. Thus, further exploration of these plants in an iron-rich environment, such as in ferroptosis, is recommended.

APPENDIX I – RESEARCH ETHICS APPROVAL

UNIVERSITEIT VAN PRETORIA
UNIVERSITY OF PRETORIA
YUNIBESITHI YA PRETORIA

Faculty of Health Sciences

Institution: The Research Ethics Committee, Faculty Health Sciences, University of Pretoria complies with ICH-GCP guidelines and has US Federal wide Assurance.
- FWA 00002567, Approved dd 18 March 2022 and Expires 18 March 2027.
- IORG #: IORG0001762 OMB No. 0990-0279 Approved for use through June 30, 2025 and Expires 07/28/2026.

Faculty of Health Sciences **Research Ethics Committee**

14 August 2024

Approval Certificate
Annual Renewal

Dear Mr AD de Beer,

Ethics Reference No.: 443/2021 – Line 3
Title: Anti-ferroptotic properties of isolates from traditional South African medicinal plants in a 6-hydroxydopamine-induced SH-SY5Y cytotoxicity model

The **Annual Renewal** as supported by documents received between 2024-07-30 and 2024-08-13 for your research, was approved by the Faculty of Health Sciences Research Ethics Committee on 2024-08-13 as resolved by its quorate meeting.

Please note the following about your ethics approval:

- Renewal of ethics approval is valid for 1 year, subsequent annual renewal will become due on 2025-08-14.
- The Research Ethics Committee (REC) must monitor your research continuously. To this end, you must submit as may be applicable for your kind of research:
  a) annual reports;
  b) reports requested *ad hoc* by the REC;
  c) all visitation and audit reports by a regulatory body (e.g. the HPCSA, FDA, SAHPRA) within 10 days of receiving one;
  d) all routine monitoring reports compiled by the Clinical Research Associate or Site Manager within 10 days of receiving one.
- The REC may select your research study for an audit or a site visitation by the REC.
- The REC may require that you make amendments and take corrective actions.
- The REC may suspend or withdraw approval.
- Please remember to use your protocol number (443/2021) on any documents or correspondence with the Research Ethics Committee regarding your research.

Ethics approval is subject to the following:

- The ethics approval is conditional on the research being conducted as stipulated by the details of all documents submitted to the Committee. In the event that a further need arises to change who the investigators are, the methods or any other aspect, such changes must be submitted as an Amendment for approval by the Committee.

We wish you the best with your research.

Yours sincerely

On behalf of the FHS REC, Dr R Sommers
MBChB, MMed (Int), MPharmMed, PhD
Deputy Chairperson *of the Faculty of Health Sciences Research Ethics Committee, University of Pretoria*

The Faculty of Health Sciences Research Ethics Committee complies with the SA National Act 61 of 2003 as it pertains to health research and the United States Code of Federal Regulations Title 45 and 46. This committee abides by the ethical norms and principles for research, established by the Declaration of Helsinki, the South African Medical Research Council Guidelines as well as the Guidelines for Ethical Research: Principles Structures and Processes, Second Edition 2015 (Department of Health).

Research Ethics Committee
Room 4-60, Level 4, Tswelopele Building
University of Pretoria, Private Bag X323
Gezina 0031, South Africa
Tel +27 (0)12 356 3084
Email: deepeka.behari@up.ac.za
www.up.ac.za

Fakulteit Gesondheidswetenskappe
Lefapha la Disaense tša Maphelo

REFERENCES

1. Shahbaz M, Shafiullah M, Mahalik MK. The dynamics of financial development, globalisation, economic growth and life expectancy in sub-Saharan Africa. Aust. Econ. Pap. 2019; 58(4):444-79.

2. Mishra S. Does modern medicine increase life-expectancy: Quest for the Moon Rabbit? Indian Heart J. 2016; 68(1):19-27. doi:10.1016/j.ihj.2016.01.003

3. Martins IJ. Increased Risk for Obesity and Diabetes with Neurodegeneration in Developing Countries. Mol Genet Genom Med. 2014; s1(01) doi:10.4172/1747-0862.S1-001

4. Teguo MT, Kuate-Tegueu C, Dartigues JF, Cesari M. Frailty in sub-Saharan Africa. Lancet. 2015; 385(9983):2151. doi:10.1016/S0140-6736(15)61021-2

5. PopulationPyramid.net [Internet]. Population pyramids of the world from 1950 to 2100. 2019 [updated 2021-04-24; cited 2021 2021-04-24]. Available from: https://www.populationpyramid.net/sub-saharan-africa/2025/.

6. Abdulganiyu S, Tijjani M. Healthcare Expenditure and Life Expectancy in Africa: A Panel Study. SAJSSE. 2021:1-9.

7. Cenini G, Lloret A, Cascella R. Oxidative Stress in Neurodegenerative Diseases: From a Mitochondrial Point of View. Oxid Med Cell Longev. 2019; 2019:2105607. doi:10.1155/2019/2105607

8. Dorsey ER, Bloem BR. The Parkinson Pandemic-A Call to Action. JAMA Neurol. 2018; 75(1):9-10. doi:10.1001/jamaneurol.2017.3299

9. Feigin VL, Nichols E, Alam T, Bannick MS, Beghi E, Blake N, et al. Global, regional, and national burden of neurological disorders, 1990–2016: a systematic analysis for the Global Burden of Disease Study 2016. Lancet Neurol. 2019; 18(5):459-80.

10. Lampropoulos IC, Malli F, Sinani O, Gourgoulianis KI, Xiromerisiou G. Worldwide trends in mortality related to Parkinson's disease in the period of 1994-2019: Analysis of vital registration data from the WHO Mortality Database. Front Neurol. 2022; 13:956440. doi:10.3389/fneur.2022.956440

11. Callixte KT, Clet TB, Jacques D, Faustin Y, Francois DJ, Maturin TT. The pattern of neurological diseases in elderly people in outpatient consultations in Sub-Saharan Africa. BMC Res Notes. 2015; 8(1):159. doi:10.1186/s13104-015-1116-x

12. Paraiso MN, Guerchet M, Saizonou J, Cowppli-Bony P, Mouanga AM, Nubukpo P, et al. Prevalence of dementia among elderly people living in Cotonou, an urban area of Benin (West Africa). NEEPD3. 2011; 36(4):245-51. doi:10.1159/000328255

13. Guerchet M, Mbelesso P, Ndamba-Bandzouzi B, Pilleron S, Desormais I, Lacroix P, et al. Epidemiology of dementia in Central Africa (EPIDEMCA): protocol for a multicentre population-based study in rural and urban areas of the Central African Republic and the Republic of Congo. Springerplus. 2014; 3(1):338. doi:10.1186/2193-1801-3-338

14. Kuate-Tegueu C, Waffo-Teguo P, Simo N, Tabue-Teguo M. Promote a new paradigm to prevent neurodegenerative disease in sub-Saharan Africa. Pan Afr Med J. 2020; 36:138. doi:10.11604/pamj.2020.36.138.21881

15. Kovacs GG. Concepts and classification of neurodegenerative diseases. Handbook of clinical neurology: Elsevier; 2018. p. 301-7.

16. Frank-Cannon TC, Alto LT, McAlpine FE, Tansey MG. Does neuroinflammation fan the flame in neurodegenerative diseases? Mol Neurodegener. 2009; 4(1):47. doi:10.1186/1750-1326-4-47

17. Balestrino R, Schapira A. Parkinson disease. Eur J Neurol. 2020; 27(1):27-42.

18. Hirsch L, Jette N, Frolkis A, Steeves T, Pringsheim T. The Incidence of Parkinson's Disease: A Systematic Review and Meta-Analysis. NEEPD3. 2016; 46(4):292-300. doi:10.1159/000445751

19. World Health Organization. WHO traditional medicine strategy: 2014-2023: World Health Organization; 2013.

20. World Health Organization. Neurological disorders: public health challenges: World Health Organization; 2006.

21. Kumar R, Pal R. India achieves WHO recommended doctor population ratio: A call for paradigm shift in public health discourse! J Family Med Prim Care. 2018; 7(5):841-4. doi:10.4103/jfmpc.jfmpc_218_18

22. AlDakheel A, Kalia LV, Lang AE. Pathogenesis-targeted, disease-modifying therapies in Parkinson disease. Neurotherapeutics. 2014; 11(1):6-23. doi:10.1007/s13311-013-0218-1

23. Azevedo MJ. The state of health system (s) in Africa: challenges and opportunities. Historical perspectives on the state of health and health systems in Africa, volume II: the modern era. 2017:1-73.

24. WHO. Atlas: country resources for neurological disorders – 2nd ed. Geneva: World Health Organization. 2017:6-70.

25. Alexander GE. Biology of Parkinson's disease: pathogenesis and pathophysiology of a multisystem neurodegenerative disorder. Dialogues Clin Neurosci. 2004; 6(3):259-80. doi:10.31887/DCNS.2004.6.3/galexander

26. Lewitt PA. Levodopa for the treatment of Parkinson's disease. N Engl J Med. 2008; 359(23):2468-76. doi:10.1056/NEJMct0800326

27. Mucklow JC. Martindale: the complete drug reference. Br. J. Clin. Pharmacol. 2000; 49(6):613.

28. Lee ES, Chen H, King J, Charlton C. The role of 3-*O*-methyldopa in the side effects of L-dopa. Neurochem Res. 2008; 33(3):401-11. doi:10.1007/s11064-007-9442-6

29. Nord M, Zsigmond P, Kullman A, Arstrand K, Dizdar N. The effect of peripheral enzyme inhibitors on levodopa concentrations in blood and CSF. Mov Disord. 2010; 25(3):363-7. doi:10.1002/mds.22613

30. Standaert DG, Roberson ED. Treatment of Central Nervous System Degenerative Disorders. In: Brunton LL, Chabner BA, Knollmann BC, editors. Goodman & Gilman's: The Pharmacological Basis of Therapeutics, 12e. New York, NY: McGraw-Hill Education; 2015.

31. Tirmenstein MA, Hu CX, Scicchitano MS, Narayanan PK, McFarland DC, Thomas HC, et al. Effects of 6-hydroxydopamine on mitochondrial function and glutathione status in SH-SY5Y human neuroblastoma cells. Toxicol In Vitro. 2005; 19(4):471-9. doi:10.1016/j.tiv.2005.01.006

32. Perez CA, Tong Y, Guo M. Iron Chelators as Potential Therapeutic Agents for Parkinson's Disease. Curr Bioact Compd. 2008; 4(3):150-8. doi:10.2174/157340708786305952

33. Brooks DJ. Dopamine agonists: their role in the treatment of Parkinson's disease. J Neurol Neurosurg Psychiatry. 2000; 68(6):685-9. doi:10.1136/jnnp.68.6.685

34. Mandel S, Weinreb O, Amit T, Youdim MB. Mechanism of neuroprotective action of the anti-Parkinson drug rasagiline and its derivatives. Brain Res Brain Res Rev. 2005; 48(2):379-87. doi:10.1016/j.brainresrev.2004.12.027

35. Mestre T, Ferreira JJ. Pharmacotherapy in Parkinson's disease: case studies. Ther Adv Neurol Disord. 2010; 3(2):117-26. doi:10.1177/1756285609352366

36. Huse DM, Schulman K, Orsini L, Castelli-Haley J, Kennedy S, Lenhart G. Burden of illness in Parkinson's disease. Mov Disord. 2005; 20(11):1449-54. doi:10.1002/mds.20609

37. Jimenez-Jimenez FJ, Lopez-Alvarez J, Sanchez-Chapado M, Montero E, Miquel J, Sierra A, et al. Retroperitoneal fibrosis in a patient with Parkinson's disease treated with pergolide. Clin Neuropharmacol. 1995; 18(3):277-9. doi:10.1097/00002826-199506000-00009

38. Renoux C, Dell'Aniello S, Brophy JM, Suissa S. Dopamine agonist use and the risk of heart failure. Pharmacoepidemiol Drug Saf. 2012; 21(1):34-41. doi:10.1002/pds.2267

39. Ustione A, Piston DW, Harris PE. Minireview: Dopaminergic regulation of insulin secretion from the pancreatic islet. Mol Endocrinol. 2013; 27(8):1198-207. doi:10.1210/me.2013-1083

40. Lang AE, Espay AJ. Disease Modification in Parkinson's Disease: Current Approaches, Challenges, and Future Considerations. Mov Disord. 2018; 33(5):660-77. doi:10.1002/mds.27360

41. Mokgobi MG. Towards integration of traditional healing and western healing: Is this a remote possibility? Afr J Phys Health Educ Recreat Dance. 2013; 2013(Suppl 1):47-57.

42. Chavunduka EL [Internet]. Christianity, african religion and african medicine. Globethics.com: World Council of Churches; 1999 [cited 2021 29/04/2021]. Available from: http://wcc-coe.org/wcc/what/interreligious/cd33-02.html.

43. Mahomoodally MF. Traditional medicines in Africa: an appraisal of ten potent african medicinal plants. Evid Based Complement Alternat Med. 2013; 2013:617459. doi:10.1155/2013/617459

44. Krah E. 'Money spoils the medicine': Gift-exchange in practices of traditional healing in northern Ghana. 2014.

45. World Health Organization. Sixty-second world health assembly, Geneva, 18-22 May 2009: resolutions and decisions, annexes. 2009. p. 96.

46. Suroowan S, Mahomoodally F. Complementary and alternative medicine use among Mauritian women. Complement Ther Clin Pract. 2013; 19(1):36-43. doi:10.1016/j.ctcp.2012.07.002

47. Haimanot RT. Parkinson's disease in Ethiopia: a prospective study of 70 patients. East Afr Med J. 1985; 62(8):571-9.

48. Sofowora A. Medicinal plants and traditional medicine in Africa. Karthala; 1996.

49. Jegede AS. The Yoruba cultural construction of health and illness. NJAS. 2002; 11(3):14.

50. Fabricant DS, Farnsworth NR. The value of plants used in traditional medicine for drug discovery. Environ Health Perspect. 2001; 109 Suppl 1(Suppl 1):69-75. doi:10.1289/ehp.01109s169

51. Saedder EA, Brock B, Nielsen LP, Bonnerup DK, Lisby M. Classification of drugs with different risk profiles. Dan Med J. 2015; 62(8):A5118.

52. Krippner R, Staples J. Suspected allergy to artemether-lumefantrine treatment of malaria. J Travel Med. 2003; 10(5):303-5. doi:10.2310/7060.2003.2744

53. Amoateng P, Quansah E, Karikari TK, Asase A, Osei-Safo D, Kukuia KKE, et al. Medicinal Plants Used in the Treatment of Mental and Neurological Disorders in Ghana. Evid Based Complement Alternat Med. 2018; 2018:8590381. doi:10.1155/2018/8590381

54. Mothibe ME, Sibanda M. African traditional medicine: South African perspective. J. Tradit. Complement. Med. 2019:1-27.

55. White P. The concept of diseases and health care in African traditional religion in Ghana. HTS: Theological Studies. 2015; 71(3):1-7.

56. Mokgobi MG. Understanding traditional African healing. Afr J Phys Health Educ Recreat Dance. 2014; 20(Suppl 2):24-34.

57. Silverman RB, Holladay MW. The organic chemistry of drug design and drug action: Academic press; 2014.

58. Steinmetz KL, Spack EG. The basics of preclinical drug development for neurodegenerative disease indications. BMC Neurol. 2009; 9 (Suppl 1):S2. doi:10.1186/1471-2377-9-S1-S2

59. Curry S, Brown R. The target product profile as a planning tool in drug discovery research. Business Briefing: PharmaTech. 2003; 2003:67-71.

60. Wiesner J. Challenges of safety evaluation. J Ethnopharmacol. 2014; 158 Pt B:467-70. doi:10.1016/j.jep.2014.08.013

61. Hou Y, Dan X, Babbar M, Wei Y, Hasselbalch SG, Croteau DL, et al. Ageing as a risk factor for neurodegenerative disease. Nat Rev Neurol. 2019; 15(10):565-81. doi:10.1038/s41582-019-0244-7

62. de Lau LM, Breteler MM. Epidemiology of Parkinson's disease. Lancet Neurol. 2006; 5(6):525-35. doi:10.1016/S1474-4422(06)70471-9

63. Feigin VL, Abajobir AA, Abate KH, Abd-Allah F, Abdulle AM, Abera SF, et al. Global, regional, and national burden of neurological disorders during 1990–2015: a systematic analysis for the Global Burden of Disease Study 2015. Lancet Neurol. 2017; 16(11):877-97.

64. Rocca WA. The burden of Parkinson's disease: a worldwide perspective. Lancet Neurol. 2018; 17(11):928-9. doi:10.1016/S1474-4422(18)30355-7

65. Lopez-Otin C, Blasco MA, Partridge L, Serrano M, Kroemer G. The hallmarks of aging. Cell. 2013; 153(6):1194-217. doi:10.1016/j.cell.2013.05.039

66. Chow HM, Herrup K. Genomic integrity and the ageing brain. Nat Rev Neurosci. 2015; 16(11):672-84. doi:10.1038/nrn4020

67. Lopez-Otin C, Blasco MA, Partridge L, Serrano M, Kroemer G. Hallmarks of aging: An expanding universe. Cell. 2023; 186(2):243-78. doi:10.1016/j.cell.2022.11.001

68. Baker DJ, Wijshake T, Tchkonia T, LeBrasseur NK, Childs BG, Van De Sluis B, et al. Clearance of p16 Ink4a-positive senescent cells delays ageing-associated disorders. Nature. 2011; 479(7372):232-6.

69. Rando TA, Chang HY. Aging, rejuvenation, and epigenetic reprogramming: resetting the aging clock. Cell. 2012; 148(1-2):46-57. doi:10.1016/j.cell.2012.01.003

70. Cacabelos R. Parkinson's Disease: From Pathogenesis to Pharmacogenomics. Int J Mol Sci. 2017; 18(3):551. doi:10.3390/ijms18030551

71. Dickson DW. Neuropathology of Parkinson disease. Parkinsonism Relat Disord. 2018; 46 Suppl 1(Suppl 1):S30-S3. doi:10.1016/j.parkreldis.2017.07.033

72. Kouli A, Torsney KM, Kuan W-L. Parkinson's disease: etiology, neuropathology, and pathogenesis. Exon Publications. 2018:3-26.

73. Ma SY, Roytta M, Rinne JO, Collan Y, Rinne UK. Correlation between neuromorphometry in the substantia nigra and clinical features in Parkinson's disease using disector counts. J Neurol Sci. 1997; 151(1):83-7. doi:10.1016/s0022-510x(97)00100-7

74. Giguere N, Burke Nanni S, Trudeau LE. On Cell Loss and Selective Vulnerability of Neuronal Populations in Parkinson's Disease. Front Neurol. 2018; 9:455. doi:10.3389/fneur.2018.00455

75. Meiser J, Weindl D, Hiller K. Complexity of dopamine metabolism. Cell Commun Signal. 2013; 11(1):34. doi:10.1186/1478-811X-11-34

76. Mishra A, Singh S, Shukla S. Physiological and Functional Basis of Dopamine Receptors and Their Role in Neurogenesis: Possible Implication for Parkinson's disease. J Exp Neurosci. 2018; 12:1179069518779829. doi:10.1177/1179069518779829

77. De Keyser J, Claeys A, De Backer JP, Ebinger G, Roels F, Vauquelin G. Autoradiographic localization of D1 and D2 dopamine receptors in the human brain. Neurosci Lett. 1988; 91(2):142-7. doi:10.1016/0304-3940(88)90758-6

78. Ha CM, Park D, Han JK, Jang JI, Park JY, Hwang EM, et al. Calcyon forms a novel ternary complex with dopamine D1 receptor through PSD-95 protein and plays a role in dopamine receptor internalization. J Biol Chem. 2012; 287(38):31813-22. doi:10.1074/jbc.M112.370601

79. Lacey MG, Mercuri NB, North RA. Dopamine acts on D2 receptors to increase potassium conductance in neurones of the rat substantia nigra zona compacta. J Physiol. 1987; 392(1):397-416. doi:10.1113/jphysiol.1987.sp016787

80. Nishi A, Snyder GL, Nairn AC, Greengard P. Role of calcineurin and protein phosphatase-2A in the regulation of DARPP-32 dephosphorylation in neostriatal neurons. J Neurochem. 1999; 72(5):2015-21. doi:10.1046/j.1471-4159.1999.0722015.x

81. Jaber M, Robinson SW, Missale C, Caron MG. Dopamine receptors and brain function. Neuropharmacology. 1996; 35(11):1503-19. doi:10.1016/s0028-3908(96)00100-1

82. Blandini F, Nappi G, Tassorelli C, Martignoni E. Functional changes of the basal ganglia circuitry in Parkinson's disease. Prog Neurobiol. 2000; 62(1):63-88. doi:10.1016/s0301-0082(99)00067-2

83. Zhai S, Tanimura A, Graves SM, Shen W, Surmeier DJ. Striatal synapses, circuits, and Parkinson's disease. Curr Opin Neurobiol. 2018; 48:9-16. doi:10.1016/j.conb.2017.08.004

84. Crossman AR. Functional anatomy of movement disorders. J Anat. 2000; 196 (Pt 4)(Pt 4):519-25. doi:10.1046/j.1469-7580.2000.19640519.x

85. Kita H, Kitai ST. Glutamate decarboxylase immunoreactive neurons in rat neostriatum: their morphological types and populations. Brain Res. 1988; 447(2):346-52. doi:10.1016/0006-8993(88)91138-9

86. Beckstead RM. Complementary mosaic distributions of thalamic and nigral axons in the caudate nucleus of the cat: double anterograde labeling combining autoradiography and wheat germ-HRP histochemistry. Brain Res. 1985; 335(1):153-9. doi:10.1016/0006-8993(85)90287-2

87. Parent A, Hazrati L-N. Functional anatomy of the basal ganglia. II. The place of subthalamic nucleus and external pallidium in basal ganglia circuitry. Brain Res. Rev. 1995; 20(1):128-54.

88. Kawaguchi Y, Wilson CJ, Augood SJ, Emson PC. Striatal interneurones: chemical, physiological and morphological characterization. Trends Neurosci. 1995; 18(12):527-35. doi:10.1016/0166-2236(95)98374-8

89. Wisden W, Laurie DJ, Monyer H, Seeburg PH. The distribution of 13 GABAA receptor subunit mRNAs in the rat brain. I. Telencephalon, diencephalon, mesencephalon. J Neurosci. 1992; 12(3):1040-62. doi:10.1523/JNEUROSCI.12-03-01040.1992

90. Fonnum F, Gottesfeld Z, Grofova I. Distribution of glutamate decarboxylase, choline acetyl-transferase and aromatic amino acid decarboxylase in the basal ganglia of normal and operated rats. Evidence for striatopallidal, striatoentopeduncular and striatonigral GABAergic fibres. Brain Res. 1978; 143(1):125-38. doi:10.1016/0006-8993(78)90756-4

91. Hauber W. Involvement of basal ganglia transmitter systems in movement initiation. Prog Neurobiol. 1998; 56(5):507-40. doi:10.1016/s0301-0082(98)00041-0

92. Oertel WH, Mugnaini E. Immunocytochemical studies of GABAergic neurons in rat basal ganglia and their relations to other neuronal systems. Neurosci Lett. 1984; 47(3):233-8. doi:10.1016/0304-3940(84)90519-6

93. Smith Y, Parent A. Neurons of the subthalamic nucleus in primates display glutamate but not GABA immunoreactivity. Brain Res. 1988; 453(1-2):353-6. doi:10.1016/0006-8993(88)90177-1

94. DeLong MR. Primate models of movement disorders of basal ganglia origin. Trends Neurosci. 1990; 13(7):281-5. doi:10.1016/0166-2236(90)90110-v

95. Alexander GE, Crutcher MD. Functional architecture of basal ganglia circuits: neural substrates of parallel processing. Trends Neurosci. 1990; 13(7):266-71. doi:10.1016/0166-2236(90)90107-l

96. McGregor MM, Nelson AB. Circuit Mechanisms of Parkinson's Disease. Neuron. 2019; 101(6):1042-56. doi:10.1016/j.neuron.2019.03.004

97. Alexander GE, Crutcher MD. Functional architecture of basal ganglia circuits: neural substrates of parallel processing. Trends Neurosci. 1990; 13(7):266-71. doi:10.1016/0166-2236(90)90107-l

98. Deng YP, Lei WL, Reiner A. Differential perikaryal localization in rats of D1 and D2 dopamine receptors on striatal projection neuron types identified by retrograde labeling. J Chem Neuroanat. 2006; 32(2-4):101-16. doi:10.1016/j.jchemneu.2006.07.001

99. Herve D, Rogard M, Levi-Strauss M. Molecular analysis of the multiple Golf alpha subunit mRNAs in the rat brain. Brain Res Mol Brain Res. 1995; 32(1):125-34. doi:10.1016/0169-328x(95)00070-9

100. Christensen M, Norr SE, Gether U, Rickhag M. Direct-Pathway Spiny Projection Neuron Inhibition Evokes Transient Circuit Imbalance Manifested as Rotational Behavior. Neuroscience. 2021; 453:32-42. doi:10.1016/j.neuroscience.2020.11.035

101. Bolam JP, Hanley JJ, Booth PA, Bevan MD. Synaptic organisation of the basal ganglia. J Anat. 2000; 196 (Pt 4)(Pt 4):527-42. doi:10.1046/j.1469-7580.2000.19640527.x

102. DeLong MR. Primate models of movement disorders of basal ganglia origin. Trends Neurosci. 1990; 13(7):281-5. doi:10.1016/0166-2236(90)90110-v

103. Baldereschi M, Di Carlo A, Vanni P, Ghetti A, Carbonin P, Amaducci L, et al. Lifestyle-related risk factors for Parkinson's disease: a population-based study. Acta Neurol Scand. 2003; 108(4):239-44. doi:10.1034/j.1600-0404.2003.00128.x

104. Pont-Sunyer C, Hotter A, Gaig C, Seppi K, Compta Y, Katzenschlager R, et al. The Onset of Nonmotor Symptoms in Parkinson's disease (The ONSET PD Study). Movement Disorders. 2015; 30(2):229-37.

105. Katzenschlager R, Head J, Schrag A, Ben-Shlomo Y, Evans A, Lees AJ, et al. Fourteen-year final report of the randomized PDRG-UK trial comparing three initial treatments in PD. Neurology. 2008; 71(7):474-80. doi:10.1212/01.wnl.0000310812.43352.66

106. Khoo TK, Yarnall AJ, Duncan GW, Coleman S, O'Brien JT, Brooks DJ, et al. The spectrum of nonmotor symptoms in early Parkinson disease. Neurology. 2013; 80(3):276-81. doi:10.1212/WNL.0b013e31827deb74

107. Deftereos SN, Dodou E, Andronis C, Persidis A. From depression to neurodegeneration and heart failure: re-examining the potential of MAO inhibitors. Expert Rev Clin Pharmacol. 2012; 5(4):413-25. doi:10.1586/ecp.12.29

108. Duchen MR. Mitochondria and calcium: from cell signalling to cell death. J Physiol. 2000; 529 Pt 1(Pt 1):57-68. doi:10.1111/j.1469-7793.2000.00057.x

109. Wallace DC. A mitochondrial paradigm of metabolic and degenerative diseases, aging, and cancer: a dawn for evolutionary medicine. Annu Rev Genet. 2005; 39:359-407. doi:10.1146/annurev.genet.39.110304.095751

110. Guo R, Zong S, Wu M, Gu J, Yang M. Architecture of Human Mitochondrial Respiratory Megacomplex I(2)III(2)IV(2). Cell. 2017; 170(6):1247-57 e12. doi:10.1016/j.cell.2017.07.050

111. Andersson SG, Zomorodipour A, Andersson JO, Sicheritz-Ponten T, Alsmark UC, Podowski RM, et al. The genome sequence of Rickettsia prowazekii and the origin of mitochondria. Nature. 1998; 396(6707):133-40. doi:10.1038/24094

112. Ahmad M, Wolberg A, Kahwaji CI. Biochemistry, electron transport chain. 2018;

113. Pallotti F, Bergamini C, Lamperti C, Fato R. The Roles of Coenzyme Q in Disease: Direct and Indirect Involvement in Cellular Functions. Int J Mol Sci. 2021; 23(1):128. doi:10.3390/ijms23010128

114. Kalpage HA, Wan J, Morse PT, Zurek MP, Turner AA, Khobeir A, et al. Cytochrome c phosphorylation: Control of mitochondrial electron transport chain flux and apoptosis. Int J Biochem Cell Biol. 2020; 121:105704. doi:10.1016/j.biocel.2020.105704

115. Labajova A, Vojtiskova A, Krivakova P, Kofranek J, Drahota Z, Houstek J. Evaluation of mitochondrial membrane potential using a computerized device with a tetraphenylphosphonium-selective electrode. Anal Biochem. 2006; 353(1):37-42. doi:10.1016/j.ab.2006.03.032

116. Mitchell P. Chemiosmotic coupling in oxidative and photosynthetic phosphorylation. Biol Rev Camb Philos Soc. 1966; 41(3):445-502. doi:10.1111/j.1469-185x.1966.tb01501.x

117. Zamzami N, Marchetti P, Castedo M, Decaudin D, Macho A, Hirsch T, et al. Sequential reduction of mitochondrial transmembrane potential and generation of reactive oxygen species in early programmed cell death. J Exp Med. 1995; 182(2):367-77. doi:10.1084/jem.182.2.367

118. Zorova LD, Popkov VA, Plotnikov EY, Silachev DN, Pevzner IB, Jankauskas SS, et al. Mitochondrial membrane potential. Anal Biochem. 2018; 552:50-9. doi:10.1016/j.ab.2017.07.009

119. Izyumov DS, Avetisyan AV, Pletjushkina OY, Sakharov DV, Wirtz KW, Chernyak BV, et al. “Wages of fear”: transient threefold decrease in intracellular ATP level imposes apoptosis. Biochimica et Biophysica Acta (BBA)-Bioenergetics. 2004; 1658(1-2):141-7.

120. Giacomello M, Pyakurel A, Glytsou C, Scorrano L. The cell biology of mitochondrial membrane dynamics. Nat Rev Mol Cell Biol. 2020; 21(4):204-24. doi:10.1038/s41580-020-0210-7

121. Ataullakhanov FI, Vitvitsky VM. What determines the intracellular ATP concentration. Biosci Rep. 2002; 22(5-6):501-11. doi:10.1023/a:1022069718709

122. Lencina AM, Franza T, Sullivan MJ, Ulett GC, Ipe DS, Gaudu P, et al. Type 2 NADH Dehydrogenase Is the Only Point of Entry for Electrons into the *Streptococcus agalactiae* Respiratory Chain and Is a Potential Drug Target. mBio. 2018; 9(4):10.1128/mbio. 01034-18. doi:10.1128/mBio.01034-18

123. Brand MD. Mitochondrial generation of superoxide and hydrogen peroxide as the source of mitochondrial redox signaling. Free Radic Biol Med. 2016; 100:14-31. doi:10.1016/j.freeradbiomed.2016.04.001

124. Chen C, Turnbull DM, Reeve AK. Mitochondrial Dysfunction in Parkinson's Disease-Cause or Consequence? Biology (Basel). 2019; 8(2):38. doi:10.3390/biology8020038

125. Cohen G, Farooqui R, Kesler N. Parkinson disease: a new link between monoamine oxidase and mitochondrial electron flow. Proc Natl Acad Sci U S A. 1997; 94(10):4890-4. doi:10.1073/pnas.94.10.4890

126. Reczek CR, Chandel NS. ROS-dependent signal transduction. Curr Opin Cell Biol. 2015; 33:8-13. doi:10.1016/j.ceb.2014.09.010

127. Schieber M, Chandel NS. ROS function in redox signaling and oxidative stress. Curr Biol. 2014; 24(10):R453-62. doi:10.1016/j.cub.2014.03.034

128. Orrenius S, Gogvadze V, Zhivotovsky B. Mitochondrial oxidative stress: implications for cell death. Annu Rev Pharmacol Toxicol. 2007; 47:143-83. doi:10.1146/annurev.pharmtox.47.120505.105122

129. Korshunov SS, Skulachev VP, Starkov AA. High protonic potential actuates a mechanism of production of reactive oxygen species in mitochondria. FEBS Lett. 1997; 416(1):15-8. doi:10.1016/s0014-5793(97)01159-9

130. Wojtczak L, Teplova VV, Bogucka K, Czyz A, Makowska A, Wieckowski MR, et al. Effect of glucose and deoxyglucose on the redistribution of calcium in ehrlich ascites tumour and Zajdela hepatoma cells and its consequences for mitochondrial energetics. Further arguments for the role of Ca(2+) in the mechanism of the crabtree effect. Eur J Biochem. 1999; 263(2):495-501. doi:10.1046/j.1432-1327.1999.00522.x

131. Langston JW, Ballard P, Tetrud JW, Irwin I. Chronic Parkinsonism in humans due to a product of meperidine-analog synthesis. Science. 1983; 219(4587):979-80. doi:10.1126/science.6823561

132. Glover V, Gibb C, Sandler M. The role of MAO in MPTP toxicity -- a review. J Neural Transm Suppl. 1986; 20:65-76.

133. Langston JW, Ballard Jr PA. Parkinson's disease in a chemist working with l-methyl-4-phenyl-l, 2, 5, 6-tetrahydropyridine. N Engl J Med. 1983; 309(5)

134. Schapira AH, Cooper JM, Dexter D, Jenner P, Clark JB, Marsden CD. Mitochondrial complex I deficiency in Parkinson's disease. Lancet. 1989; 1(8649):1269. doi:10.1016/s0140-6736(89)92366-0

135. Heikkila RE, Nicklas WJ, Vyas I, Duvoisin RC. Dopaminergic toxicity of rotenone and the 1-methyl-4-phenylpyridinium ion after their stereotaxic administration to rats: implication for the mechanism of 1-methyl-4-phenyl-1,2,3,6-tetrahydropyridine toxicity. Neurosci Lett. 1985; 62(3):389-94. doi:10.1016/0304-3940(85)90580-4

136. Fato R, Bergamini C, Bortolus M, Maniero AL, Leoni S, Ohnishi T, et al. Differential effects of mitochondrial Complex I inhibitors on production of reactive oxygen species. Biochim Biophys Acta. 2009; 1787(5):384-92. doi:10.1016/j.bbabio.2008.11.003

137. Greenamyre JT, Sherer TB, Betarbet R, Panov AV. Complex I and Parkinson's disease. IUBMB Life. 2001; 52(3-5):135-41. doi:10.1080/15216540152845939

138. Fukui H, Moraes CT. Mechanisms of formation and accumulation of mitochondrial DNA deletions in aging neurons. Hum Mol Genet. 2009; 18(6):1028-36. doi:10.1093/hmg/ddn437

139. Hirsch EC, Jenner P, Przedborski S. Pathogenesis of Parkinson's disease. Mov Disord. 2013; 28(1):24-30. doi:10.1002/mds.25032

140. Bender A, Krishnan KJ, Morris CM, Taylor GA, Reeve AK, Perry RH, et al. High levels of mitochondrial DNA deletions in substantia nigra neurons in aging and Parkinson disease. Nat Genet. 2006; 38(5):515-7. doi:10.1038/ng1769

141. Manczak M, Anekonda TS, Henson E, Park BS, Quinn J, Reddy PH. Mitochondria are a direct site of Aβ accumulation in Alzheimer's disease neurons: implications for free radical generation and oxidative damage in disease progression. Human molecular genetics. 2006; 15(9):1437-49.

142. Ozawa T. Mitochondrial genome mutation in cell death and aging. J Bioenerg Biomembr. 1999; 31(4):377-90. doi:10.1023/a:1005479920097

143. Elmore S. Apoptosis: a review of programmed cell death. Toxicol Pathol. 2007; 35(4):495-516. doi:10.1080/01926230701320337

144. Zhang C, Rissman RA, Feng J. Characterization of ATP alternations in an Alzheimer's disease transgenic mouse model. J Alzheimers Dis. 2015; 44(2):375-8. doi:10.3233/JAD-141890

145. Grimm A, Friedland K, Eckert A. Mitochondrial dysfunction: the missing link between aging and sporadic Alzheimer's disease. Biogerontology. 2016; 17(2):281-96. doi:10.1007/s10522-015-9618-4

146. Reeve AK, Krishnan KJ, Turnbull D. Mitochondrial DNA mutations in disease, aging, and neurodegeneration. Ann N Y Acad Sci. 2008; 1147(1):21-9. doi:10.1196/annals.1427.016

147. Dimauro S, Davidzon G. Mitochondrial DNA and disease. Ann Med. 2005; 37(3):222-32. doi:10.1080/07853890510007368

148. Trifunovic A, Larsson NG. Mitochondrial dysfunction as a cause of ageing. J Intern Med. 2008; 263(2):167-78. doi:10.1111/j.1365-2796.2007.01905.x

149. Dizdaroglu M. Oxidative damage to DNA in mammalian chromatin. Mutat Res. 1992; 275(3-6):331-42. doi:10.1016/0921-8734(92)90036-o

150. Breen AP, Murphy JA. Reactions of oxyl radicals with DNA. Free Radic Biol Med. 1995; 18(6):1033-77. doi:10.1016/0891-5849(94)00209-3

151. Chance B, Sies H, Boveris A. Hydroperoxide metabolism in mammalian organs. Physiol Rev. 1979; 59(3):527-605. doi:10.1152/physrev.1979.59.3.527

152. Kraytsberg Y, Kudryavtseva E, McKee AC, Geula C, Kowall NW, Khrapko K. Mitochondrial DNA deletions are abundant and cause functional impairment in aged human substantia nigra neurons. Nat Genet. 2006; 38(5):518-20. doi:10.1038/ng1778

153. Hoeijmakers JH. DNA damage, aging, and cancer. N Engl J Med. 2009; 361(15):1475-85. doi:10.1056/NEJMra0804615

154. Lewerenz J, Maher P. Control of redox state and redox signaling by neural antioxidant systems. Antioxid Redox Signal. 2011; 14(8):1449-65. doi:10.1089/ars.2010.3600

155. Gough DR, Cotter TG. Hydrogen peroxide: a Jekyll and Hyde signalling molecule. Cell Death Dis. 2011; 2(10):e213. doi:10.1038/cddis.2011.96

156. Fridovich I. Superoxide anion radical (O2-.), superoxide dismutases, and related matters. JBC. 1997; 272(30):18515-7.

157. Lee KH, Cha M, Lee BH. Neuroprotective Effect of Antioxidants in the Brain. Int J Mol Sci. 2020; 21(19):7152. doi:10.3390/ijms21197152

158. Zhan CD, Sindhu RK, Pang J, Ehdaie A, Vaziri ND. Superoxide dismutase, catalase and glutathione peroxidase in the spontaneously hypertensive rat kidney: effect of antioxidant-rich diet. J Hypertens. 2004; 22(10):2025-33. doi:10.1097/00004872-200410000-00027

159. Hunt CR, Sim JE, Sullivan SJ, Featherstone T, Golden W, Von Kapp-Herr C, et al. Genomic instability and catalase gene amplification induced by chronic exposure to oxidative stress. Cancer Res. 1998; 58(17):3986-92.

160. Terlecky SR, Koepke JI, Walton PA. Peroxisomes and aging. Biochim Biophys Acta. 2006; 1763(12):1749-54. doi:10.1016/j.bbamcr.2006.08.017

161. Arthur J. The glutathione peroxidases. Cellular and Molecular Life Sciences CMLS. 2001; 57:1825-35.

162. Nimse SB, Pal D. Free radicals, natural antioxidants, and their reaction mechanisms. RSC advances. 2015; 5(35):27986-8006.

163. Lobo V, Patil A, Phatak A, Chandra N. Free radicals, antioxidants and functional foods: Impact on human health. Pharmacogn Rev. 2010; 4(8):118-26. doi:10.4103/0973-7847.70902

164. Yin H, Xu L, Porter NA. Free radical lipid peroxidation: mechanisms and analysis. Chem Rev. 2011; 111(10):5944-72. doi:10.1021/cr200084z

165. Trist BG, Hare DJ, Double KL. Oxidative stress in the aging substantia nigra and the etiology of Parkinson's disease. Aging Cell. 2019; 18(6):e13031. doi:10.1111/acel.13031

166. Pizzino G, Irrera N, Cucinotta M, Pallio G, Mannino F, Arcoraci V, et al. Oxidative Stress: Harms and Benefits for Human Health. Oxid Med Cell Longev. 2017; 2017:8416763. doi:10.1155/2017/8416763

167. Zecca L, Shima T, Stroppolo A, Goj C, Battiston GA, Gerbasi R, et al. Interaction of neuromelanin and iron in substantia nigra and other areas of human brain. Neuroscience. 1996; 73(2):407-15. doi:10.1016/0306-4522(96)00047-4

168. Shulman JM, De Jager PL, Feany MB. Parkinson's disease: genetics and pathogenesis. Annu Rev Pathol. 2011; 6(1):193-222. doi:10.1146/annurev-pathol-011110-130242

169. Blum D, Torch S, Lambeng N, Nissou M, Benabid AL, Sadoul R, et al. Molecular pathways involved in the neurotoxicity of 6-OHDA, dopamine and MPTP: contribution to the apoptotic theory in Parkinson's disease. Prog Neurobiol. 2001; 65(2):135-72. doi:10.1016/s0301-0082(01)00003-x

170. Mythri RB, Venkateshappa C, Harish G, Mahadevan A, Muthane UB, Yasha TC, et al. Evaluation of markers of oxidative stress, antioxidant function and astrocytic proliferation in the striatum and frontal cortex of Parkinson's disease brains. Neurochem Res. 2011; 36(8):1452-63. doi:10.1007/s11064-011-0471-9

171. Sian J, Dexter DT, Lees AJ, Daniel S, Agid Y, Javoy-Agid F, et al. Alterations in glutathione levels in Parkinson's disease and other neurodegenerative disorders affecting basal ganglia. Ann Neurol. 1994; 36(3):348-55. doi:10.1002/ana.410360305

172. Ludtmann MHR, Angelova PR, Horrocks MH, Choi ML, Rodrigues M, Baev AY, et al. alpha-synuclein oligomers interact with ATP synthase and open the permeability transition pore in Parkinson's disease. Nat Commun. 2018; 9(1):2293. doi:10.1038/s41467-018-04422-2

173. Gandhi S, Abramov AY. Mechanism of oxidative stress in neurodegeneration. Oxid Med Cell Longev. 2012; 2012(1):428010. doi:10.1155/2012/428010

174. Berlett BS, Stadtman ER. Protein oxidation in aging, disease, and oxidative stress. J Biol Chem. 1997; 272(33):20313-6. doi:10.1074/jbc.272.33.20313

175. Venderova K, Park DS. Programmed cell death in Parkinson's disease. Cold Spring Harb Perspect Med. 2012; 2(8):a009365. doi:10.1101/cshperspect.a009365

176. Halliwell B, Gutteridge JM. Free radicals in biology and medicine: Oxford university press, USA; 2015.

177. Mukherji S, Singh S. Reaction mechanism in organic chemistry: Macmillan; 1984.

178. Genestra M. Oxyl radicals, redox-sensitive signalling cascades and antioxidants. Cell Signal. 2007; 19(9):1807-19. doi:10.1016/j.cellsig.2007.04.009

179. Neta P, Huie RE, Ross AB. Rate constants for reactions of peroxyl radicals in fluid solutions. JPCRD. 1990; 19(2):413-513.

180. Fomenko DE, Koc A, Agisheva N, Jacobsen M, Kaya A, Malinouski M, et al. Thiol peroxidases mediate specific genome-wide regulation of gene expression in response to hydrogen peroxide. Proc Natl Acad Sci USA. 2011; 108(7):2729-34. doi:10.1073/pnas.1010721108

181. Sena LA, Chandel NS. Physiological roles of mitochondrial reactive oxygen species. Mol Cell. 2012; 48(2):158-67. doi:10.1016/j.molcel.2012.09.025

182. Kehrer JP. The Haber-Weiss reaction and mechanisms of toxicity. Toxicology. 2000; 149(1):43-50. doi:10.1016/s0300-483x(00)00231-6

183. Koppenol WH. The centennial of the Fenton reaction. Free Radic Biol Med. 1993; 15(6):645-51. doi:10.1016/0891-5849(93)90168-t

184. Steenken S. Addition–elimination paths in electron-transfer reactions between radicals and molecules. Oxidation of organic molecules by the OH radical. Journal of the Chemical Society, Faraday Transactions 1: Physical Chemistry in Condensed Phases. 1987; 83(1):113-24.

185. Chawla LS, Beers-Mulroy B, Tidmarsh GF. Therapeutic Opportunities for Hepcidin in Acute Care Medicine. Crit Care Clin. 2019; 35(2):357-74. doi:10.1016/j.ccc.2018.11.014

186. Liochev SI. The Mechanism of" fenton-like" Reactions and Their Importance For Biological Systems A Biologist's View. MIBs. 1999; 36:1-40.

187. Buxton GV, Greenstock CL, Helman WP, Ross AB. Critical Review of rate constants for reactions of hydrated electrons, hydrogen atoms and hydroxyl radicals (· OH/· O− in Aqueous Solution. Journal of physical and chemical reference data. 1988; 17(2):513-886.

188. Juan CA, Perez de la Lastra JM, Plou FJ, Perez-Lebena E. The Chemistry of Reactive Oxygen Species (ROS) Revisited: Outlining Their Role in Biological Macromolecules (DNA, Lipids and Proteins) and Induced Pathologies. Int J Mol Sci. 2021; 22(9):4642. doi:10.3390/ijms22094642

189. Sulzer D, Bogulavsky J, Larsen KE, Behr G, Karatekin E, Kleinman MH, et al. Neuromelanin biosynthesis is driven by excess cytosolic catecholamines not accumulated by synaptic vesicles. Proc Natl Acad Sci USA. 2000; 97(22):11869-74. doi:10.1073/pnas.97.22.11869

190. Polymeropoulos MH, Lavedan C, Leroy E, Ide SE, Dehejia A, Dutra A, et al. Mutation in the alpha-synuclein gene identified in families with Parkinson's disease. Science. 1997; 276(5321):2045-7. doi:10.1126/science.276.5321.2045

191. Burre J, Sharma M, Tsetsenis T, Buchman V, Etherton MR, Sudhof TC. Alpha-synuclein promotes SNARE-complex assembly in vivo and in vitro. Science. 2010; 329(5999):1663-7. doi:10.1126/science.1195227

192. Grenier K, Kontogiannea M, Fon EA. Short mitochondrial ARF triggers Parkin/PINK1-dependent mitophagy. J Biol Chem. 2014; 289(43):29519-30. doi:10.1074/jbc.M114.607150

193. Gosavi N, Lee HJ, Lee JS, Patel S, Lee SJ. Golgi fragmentation occurs in the cells with prefibrillar alpha-synuclein aggregates and precedes the formation of fibrillar inclusion. J Biol Chem. 2002; 277(50):48984-92. doi:10.1074/jbc.M208194200

194. Guardia-Laguarta C, Area-Gomez E, Rub C, Liu Y, Magrane J, Becker D, et al. alpha-Synuclein is localized to mitochondria-associated ER membranes. J Neurosci. 2014; 34(1):249-59. doi:10.1523/JNEUROSCI.2507-13.2014

195. Tabner BJ, El-Agnaf OM, German MJ, Fullwood NJ, Allsop D. Protein aggregation, metals and oxidative stress in neurodegenerative diseases. Biochem Soc Trans. 2005; 33(Pt 5):1082-6. doi:10.1042/BST20051082

196. Stadtman ER, Levine RL. Free radical-mediated oxidation of free amino acids and amino acid residues in proteins. Amino Acids. 2003; 25(3-4):207-18. doi:10.1007/s00726-003-0011-2

197. Garrison WM. Reaction mechanisms in the radiolysis of peptides, polypeptides, and proteins. Chem. Rev. 1987; 87(2):381-98.

198. Rodriguez M, Morales I, Rodriguez-Sabate C, Sanchez A, Castro R, Brito JM, et al. The degeneration and replacement of dopamine cells in Parkinson's disease: the role of aging. Front Neuroanat. 2014; 8(80):80. doi:10.3389/fnana.2014.00080

199. Napolitano A, Cesura AM, Da Prada M. The role of monoamine oxidase and catechol O-methyltransferase in dopaminergic neurotransmission. J Neural Transm Suppl. 1995; 45:35-45.

200. Myohanen TT, Schendzielorz N, Mannisto PT. Distribution of catechol-O-methyltransferase (COMT) proteins and enzymatic activities in wild-type and soluble COMT deficient mice. J Neurochem. 2010; 113(6):1632-43. doi:10.1111/j.1471-4159.2010.06723.x

201. Edmondson DE, Bhattacharyya AK, Walker MC. Spectral and kinetic studies of imine product formation in the oxidation of p-(N, N-dimethylamino) benzylamine analogs by monoamine oxidase B. Biochem. 1993; 32(19):5196-202.

202. Bach AW, Lan NC, Johnson DL, Abell CW, Bembenek ME, Kwan SW, et al. cDNA cloning of human liver monoamine oxidase A and B: molecular basis of differences in enzymatic properties. Proc Natl Acad Sci USA. 1988; 85(13):4934-8. doi:10.1073/pnas.85.13.4934

203. Binda C, Newton-Vinson P, Hubalek F, Edmondson DE, Mattevi A. Structure of human monoamine oxidase B, a drug target for the treatment of neurological disorders. Nat Struct Biol. 2002; 9(1):22-6. doi:10.1038/nsb732

204. Binda C, Li M, Hubalek F, Restelli N, Edmondson DE, Mattevi A. Insights into the mode of inhibition of human mitochondrial monoamine oxidase B from high-resolution crystal structures. Proc Natl Acad Sci U S A. 2003; 100(17):9750-5. doi:10.1073/pnas.1633804100

205. Plotegher N, Berti G, Ferrari E, Tessari I, Zanetti M, Lunelli L, et al. DOPAL derived alpha-synuclein oligomers impair synaptic vesicles physiological function. Sci Rep. 2017; 7(1):40699. doi:10.1038/srep40699

206. Qu L, Akbergenova Y, Hu Y, Schikorski T. Synapse-to-synapse variation in mean synaptic vesicle size and its relationship with synaptic morphology and function. J Comp Neurol. 2009; 514(4):343-52. doi:10.1002/cne.22007

207. Bonanomi D, Benfenati F, Valtorta F. Protein sorting in the synaptic vesicle life cycle. Prog Neurobiol. 2006; 80(4):177-217. doi:10.1016/j.pneurobio.2006.09.002

208. Bellani S, Sousa VL, Ronzitti G, Valtorta F, Meldolesi J, Chieregatti E. The regulation of synaptic function by alpha-synuclein. Commun Integr Biol. 2010; 3(2):106-9. doi:10.4161/cib.3.2.10964

209. Anderson DG, Mariappan SV, Buettner GR, Doorn JA. Oxidation of 3,4-dihydroxyphenylacetaldehyde, a toxic dopaminergic metabolite, to a semiquinone radical and an ortho-quinone. J Biol Chem. 2011; 286(30):26978-86. doi:10.1074/jbc.M111.249532

210. Palazzi L, Fongaro B, Leri M, Acquasaliente L, Stefani M, Bucciantini M, et al. Structural Features and Toxicity of alpha-Synuclein Oligomers Grown in the Presence of DOPAC. Int J Mol Sci. 2021; 22(11):6008. doi:10.3390/ijms22116008

211. Marchitti SA, Deitrich RA, Vasiliou V. Neurotoxicity and metabolism of the catecholamine-derived 3,4-dihydroxyphenylacetaldehyde and 3,4-dihydroxyphenylglycolaldehyde: the role of aldehyde dehydrogenase. Pharmacol Rev. 2007; 59(2):125-50. doi:10.1124/pr.59.2.1

212. Fitzmaurice AG, Rhodes SL, Cockburn M, Ritz B, Bronstein JM. Aldehyde dehydrogenase variation enhances effect of pesticides associated with Parkinson disease. Neurology. 2014; 82(5):419-26. doi:10.1212/WNL.0000000000000083

213. Rees JN, Florang VR, Eckert LL, Doorn JA. Protein reactivity of 3,4-dihydroxyphenylacetaldehyde, a toxic dopamine metabolite, is dependent on both the aldehyde and the catechol. Chem Res Toxicol. 2009; 22(7):1256-63. doi:10.1021/tx9000557

214. Fedorow H, Tribl F, Halliday G, Gerlach M, Riederer P, Double KL. Neuromelanin in human dopamine neurons: comparison with peripheral melanins and relevance to Parkinson's disease. Prog Neurobiol. 2005; 75(2):109-24. doi:10.1016/j.pneurobio.2005.02.001

215. Zecca L, Casella L, Albertini A, Bellei C, Zucca FA, Engelen M, et al. Neuromelanin can protect against iron-mediated oxidative damage in system modeling iron overload of brain aging and Parkinson's disease. J Neurochem. 2008; 106(4):1866-75. doi:10.1111/j.1471-4159.2008.05541.x

216. Zucca FA, Basso E, Cupaioli FA, Ferrari E, Sulzer D, Casella L, et al. Neuromelanin of the human substantia nigra: an update. Neurotox Res. 2014; 25(1):13-23. doi:10.1007/s12640-013-9435-y

217. Engelen M, Vanna R, Bellei C, Zucca FA, Wakamatsu K, Monzani E, et al. Neuromelanins of human brain have soluble and insoluble components with dolichols attached to the melanic structure. PLoS One. 2012; 7(11):e48490. doi:10.1371/journal.pone.0048490

218. Zucca FA, Vanna R, Cupaioli FA, Bellei C, De Palma A, Di Silvestre D, et al. Neuromelanin organelles are specialized autolysosomes that accumulate undegraded proteins and lipids in aging human brain and are likely involved in Parkinson's disease. NPJ Parkinsons Dis. 2018; 4(1):17. doi:10.1038/s41531-018-0050-8

219. Glinka Y, Gassen M, Youdim MB. Mechanism of 6-hydroxydopamine neurotoxicity. J Neural Transm Suppl. 1997; 50:55-66. doi:10.1007/978-3-7091-6842-4_7

220. Luthman J, Fredriksson A, Sundstrom E, Jonsson G, Archer T. Selective lesion of central dopamine or noradrenaline neuron systems in the neonatal rat: motor behavior and monoamine alterations at adult stage. Behav Brain Res. 1989; 33(3):267-77. doi:10.1016/s0166-4328(89)80121-4

221. Vareslija D, Tipton KF, Davey GP, McDonald AG. 6-Hydroxydopamine: a far from simple neurotoxin. J Neural Transm (Vienna). 2020; 127(2):213-30. doi:10.1007/s00702-019-02133-6

222. Dixon SJ, Lemberg KM, Lamprecht MR, Skouta R, Zaitsev EM, Gleason CE, et al. Ferroptosis: an iron-dependent form of nonapoptotic cell death. Cell. 2012; 149(5):1060-72. doi:10.1016/j.cell.2012.03.042

223. Ball N, Teo WP, Chandra S, Chapman J. Parkinson's Disease and the Environment. Front Neurol. 2019; 10:218. doi:10.3389/fneur.2019.00218

224. Lill CM. Genetics of Parkinson's disease. Mol Cell Probes. 2016; 30(6):386-96. doi:10.1016/j.mcp.2016.11.001

225. Igney FH, Krammer PH. Death and anti-death: tumour resistance to apoptosis. Nat Rev Cancer. 2002; 2(4):277-88. doi:10.1038/nrc776

226. Fiskum G, Starkov A, Polster BM, Chinopoulos C. Mitochondrial mechanisms of neural cell death and neuroprotective interventions in Parkinson's disease. Ann N Y Acad Sci. 2003; 991(1):111-9. doi:10.1111/j.1749-6632.2003.tb07469.x

227. Martinvalet D, Zhu P, Lieberman J. Granzyme A induces caspase-independent mitochondrial damage, a required first step for apoptosis. Immunity. 2005; 22(3):355-70. doi:10.1016/j.immuni.2005.02.004

228. Cohen JJ. Programmed cell death in the immune system. Adv. Immunol. Elsevier; 1991. p. 55-85.

229. Rai NK, Tripathi K, Sharma D, Shukla VK. Apoptosis: a basic physiologic process in wound healing. Int J Low Extrem Wounds. 2005; 4(3):138-44. doi:10.1177/1534734605280018

230. Nemes Z, Jr., Friis RR, Aeschlimann D, Saurer S, Paulsson M, Fesus L. Expression and activation of tissue transglutaminase in apoptotic cells of involuting rodent mammary tissue. Eur J Cell Biol. 1996; 70(2):125-33.

231. Wang L, Zeng X, Ye J, Chen X, Lin X. Diplatin, a novel water-soluble platinum complex, inhibits lung cancer growth via augmentation of Fas-mediated apoptosis. Eur J Pharmacol. 2020; 879:173128. doi:10.1016/j.ejphar.2020.173128

232. Thakor P, Subramanian RB, Thakkar SS, Ray A, Thakkar VR. Phytol induces ROS mediated apoptosis by induction of caspase 9 and 3 through activation of TRAIL, FAS and TNF receptors and inhibits tumor progression factor Glucose 6 phosphate dehydrogenase in lung carcinoma cell line (A549). Biomed Pharmacother. 2017; 92:491-500. doi:10.1016/j.biopha.2017.05.066

233. Bortner CD, Oldenburg NB, Cidlowski JA. The role of DNA fragmentation in apoptosis. Trends Cell Biol. 1995; 5(1):21-6. doi:10.1016/s0962-8924(00)88932-1

234. Zhang J, Shen Q, Ma Y, Liu L, Jia W, Chen L, et al. Calcium Homeostasis in Parkinson's Disease: From Pathology to Treatment. Neurosci Bull. 2022; 38(10):1267-70. doi:10.1007/s12264-022-00899-6

235. Subramaniam M, Althof D, Gispert S, Schwenk J, Auburger G, Kulik A, et al. Mutant alpha-synuclein enhances firing frequencies in dopamine substantia nigra neurons by oxidative impairment of A-type potassium channels. J Neurosci. 2014; 34(41):13586-99. doi:10.1523/JNEUROSCI.5069-13.2014

236. Jancovic J. Parkinson’s Disease: Clinical Features and diagnosis. JNNP. 2008; 79:368-76.

237. Green DR. Apoptotic pathways: ten minutes to dead. Cell. 2005; 121(5):671-4. doi:10.1016/j.cell.2005.05.019

238. Rivero-Rios P, Gomez-Suaga P, Fdez E, Hilfiker S. Upstream deregulation of calcium signaling in Parkinson's disease. Front Mol Neurosci. 2014; 7:53. doi:10.3389/fnmol.2014.00053

239. Ferreiro E, Oliveira CR, Pereira CMF. The release of calcium from the endoplasmic reticulum induced by amyloid-beta and prion peptides activates the mitochondrial apoptotic pathway. Neurobiol Dis. 2008; 30(3):331-42. doi:10.1016/j.nbd.2008.02.003

240. Orrenius S, Zhivotovsky B, Nicotera P. Regulation of cell death: the calcium-apoptosis link. Nat Rev Mol Cell Biol. 2003; 4(7):552-65. doi:10.1038/nrm1150

241. Duchen MR. Mitochondria, calcium-dependent neuronal death and neurodegenerative disease. Pflugers Arch. 2012; 464(1):111-21. doi:10.1007/s00424-012-1112-0

242. Michel PP, Hirsch EC, Hunot S. Understanding Dopaminergic Cell Death Pathways in Parkinson Disease. Neuron. 2016; 90(4):675-91. doi:10.1016/j.neuron.2016.03.038

243. Anglade P, Vyas S, Javoy-Agid F, Herrero MT, Michel PP, Marquez J, et al. Apoptosis and autophagy in nigral neurons of patients with Parkinson's disease. Histol Histopathol. 1997; 12(1):25-31.

244. Mochizuki H, Goto K, Mori H, Mizuno Y. Histochemical detection of apoptosis in Parkinson's disease. J Neurol Sci. 1996; 137(2):120-3. doi:10.1016/0022-510x(95)00336-z

245. Tatton NA, Maclean-Fraser A, Tatton WG, Perl DP, Olanow CW. A fluorescent double-labeling method to detect and confirm apoptotic nuclei in Parkinson's disease. Ann Neurol. 1998; 44(3 Suppl 1):S142-8. doi:10.1002/ana.410440721

246. Akao Y, Maruyama W, Yi H, Shamoto-Nagai M, Youdim MB, Naoi M. An anti-Parkinson's disease drug, N-propargyl-1(R)-aminoindan (rasagiline), enhances expression of anti-apoptotic bcl-2 in human dopaminergic SH-SY5Y cells. Neurosci Lett. 2002; 326(2):105-8. doi:10.1016/s0304-3940(02)00332-4

247. Iaccarino C, Crosio C, Vitale C, Sanna G, Carri MT, Barone P. Apoptotic mechanisms in mutant LRRK2-mediated cell death. Hum Mol Genet. 2007; 16(11):1319-26. doi:10.1093/hmg/ddm080

248. Dixon SJ, Stockwell BR. The role of iron and reactive oxygen species in cell death. Nat Chem Biol. 2014; 10(1):9-17. doi:10.1038/nchembio.1416

249. Wu Y, Zhang S, Gong X, Tam S, Xiao D, Liu S, et al. The epigenetic regulators and metabolic changes in ferroptosis-associated cancer progression. Mol Cancer. 2020; 19(1):39. doi:10.1186/s12943-020-01157-x

250. Yang WS, Kim KJ, Gaschler MM, Patel M, Shchepinov MS, Stockwell BR. Peroxidation of polyunsaturated fatty acids by lipoxygenases drives ferroptosis. Proc Natl Acad Sci U S A. 2016; 113(34):E4966-75. doi:10.1073/pnas.1603244113

251. Stockwell BR, Friedmann Angeli JP, Bayir H, Bush AI, Conrad M, Dixon SJ, et al. Ferroptosis: A Regulated Cell Death Nexus Linking Metabolism, Redox Biology, and Disease. Cell. 2017; 171(2):273-85. doi:10.1016/j.cell.2017.09.021

252. Seiler A, Schneider M, Forster H, Roth S, Wirth EK, Culmsee C, et al. Glutathione peroxidase 4 senses and translates oxidative stress into 12/15-lipoxygenase dependent- and AIF-mediated cell death. Cell Metab. 2008; 8(3):237-48. doi:10.1016/j.cmet.2008.07.005

253. Cozza G, Rossetto M, Bosello-Travain V, Maiorino M, Roveri A, Toppo S, et al. Glutathione peroxidase 4-catalyzed reduction of lipid hydroperoxides in membranes: The polar head of membrane phospholipids binds the enzyme and addresses the fatty acid hydroperoxide group toward the redox center. Free Radic Biol Med. 2017; 112:1-11. doi:10.1016/j.freeradbiomed.2017.07.010

254. Forcina GC, Dixon SJ. GPX4 at the Crossroads of Lipid Homeostasis and Ferroptosis. Proteomics. 2019; 19(18):e1800311. doi:10.1002/pmic.201800311

255. Isom AL, Barnes S, Wilson L, Kirk M, Coward L, Darley-Usmar V. Modification of Cytochrome c by 4-hydroxy- 2-nonenal: evidence for histidine, lysine, and arginine-aldehyde adducts. J Am Soc Mass Spectrom. 2004; 15(8):1136-47. doi:10.1016/j.jasms.2004.03.013

256. Huang C, Anderson M, Meister A, editors. The function of the light subunit of gamma-glutamylcysteine synthetase (rat-kidney). Faseb journal; 1993: Federation Amer Soc Exp Biol md 20814-3998.

257. Bannai S. Exchange of cystine and glutamate across plasma membrane of human fibroblasts. J Biol Chem. 1986; 261(5):2256-63.

258. Meister A. Glutathione, metabolism and function via the gamma-glutamyl cycle. Life Sci. 1974; 15(2):177-90. doi:10.1016/0024-3205(74)90206-9

259. Muyderman H, Nilsson M, Sims NR. Highly selective and prolonged depletion of mitochondrial glutathione in astrocytes markedly increases sensitivity to peroxynitrite. J Neurosci. 2004; 24(37):8019-28. doi:10.1523/JNEUROSCI.1103-04.2004

260. Wullner U, Seyfried J, Groscurth P, Beinroth S, Winter S, Gleichmann M, et al. Glutathione depletion and neuronal cell death: the role of reactive oxygen intermediates and mitochondrial function. Brain Res. 1999; 826(1):53-62. doi:10.1016/s0006-8993(99)01228-7

261. Yang WS, Stockwell BR. Synthetic lethal screening identifies compounds activating iron-dependent, nonapoptotic cell death in oncogenic-RAS-harboring cancer cells. Chem Biol. 2008; 15(3):234-45. doi:10.1016/j.chembiol.2008.02.010

262. Imai H, Hirao F, Sakamoto T, Sekine K, Mizukura Y, Saito M, et al. Early embryonic lethality caused by targeted disruption of the mouse PHGPx gene. Biochem Biophys Res Commun. 2003; 305(2):278-86. doi:10.1016/s0006-291x(03)00734-4

263. Yant LJ, Ran Q, Rao L, Van Remmen H, Shibatani T, Belter JG, et al. The selenoprotein GPX4 is essential for mouse development and protects from radiation and oxidative damage insults. Free Radic Biol Med. 2003; 34(4):496-502. doi:10.1016/s0891-5849(02)01360-6

264. Cardoso BR, Hare DJ, Bush AI, Roberts BR. Glutathione peroxidase 4: a new player in neurodegeneration? Mol Psychiatry. 2017; 22(3):328-35. doi:10.1038/mp.2016.196

265. Joshi YB, Giannopoulos PF, Pratico D. The 12/15-lipoxygenase as an emerging therapeutic target for Alzheimer's disease. Trends Pharmacol Sci. 2015; 36(3):181-6. doi:10.1016/j.tips.2015.01.005

266. Deas E, Cremades N, Angelova PR, Ludtmann MH, Yao Z, Chen S, et al. Alpha-Synuclein Oligomers Interact with Metal Ions to Induce Oxidative Stress and Neuronal Death in Parkinson's Disease. Antioxid Redox Signal. 2016; 24(7):376-91. doi:10.1089/ars.2015.6343

267. Abeti R, Parkinson MH, Hargreaves IP, Angelova PR, Sandi C, Pook MA, et al. 'Mitochondrial energy imbalance and lipid peroxidation cause cell death in Friedreich's ataxia'. Cell Death Dis. 2016; 7(5):e2237. doi:10.1038/cddis.2016.111

268. Paul BD, Sbodio JI, Xu R, Vandiver MS, Cha JY, Snowman AM, et al. Cystathionine gamma-lyase deficiency mediates neurodegeneration in Huntington's disease. Nature. 2014; 509(7498):96-100. doi:10.1038/nature13136

269. Bazinet RP, Laye S. Polyunsaturated fatty acids and their metabolites in brain function and disease. Nat Rev Neurosci. 2014; 15(12):771-85. doi:10.1038/nrn3820

270. Wagner BA, Buettner GR, Burns CP. Free radical-mediated lipid peroxidation in cells: oxidizability is a function of cell lipid bis-allylic hydrogen content. Biochem. 1994; 33(15):4449-53. doi:10.1021/bi00181a003

271. Seiler A, Schneider M, Förster H, Roth S, Wirth EK, Culmsee C, et al. Glutathione peroxidase 4 senses and translates oxidative stress into 12/15-lipoxygenase dependent-and AIF-mediated cell death. Cell Metab. 2008; 8(3):237-48.

272. Li Y, Maher P, Schubert D. A role for 12-lipoxygenase in nerve cell death caused by glutathione depletion. Neuron. 1997; 19(2):453-63. doi:10.1016/s0896-6273(00)80953-8

273. Ayala A, Munoz MF, Arguelles S. Lipid peroxidation: production, metabolism, and signaling mechanisms of malondialdehyde and 4-hydroxy-2-nonenal. Oxid Med Cell Longev. 2014; 2014:360438. doi:10.1155/2014/360438

274. Vatsyayan R, Lelsani PC, Chaudhary P, Kumar S, Awasthi S, Awasthi YC. The expression and function of vascular endothelial growth factor in retinal pigment epithelial (RPE) cells is regulated by 4-hydroxynonenal (HNE) and glutathione S-transferase A4-4. Biochem Biophys Res Commun. 2012; 417(1):346-51. doi:10.1016/j.bbrc.2011.11.113

275. Chandra A, Srivastava SK. A synthesis of 4-hydroxy-2-trans-nonenal and 4-(3H) 4-hydroxy-2-trans-nonenal. Lipids. 1997; 32(7):779-82. doi:10.1007/s11745-997-0100-6

276. Siems W, Grune T. Intracellular metabolism of 4-hydroxynonenal. Mol Aspects Med. 2003; 24(4-5):167-75. doi:10.1016/s0098-2997(03)00011-6

277. Jenner P. Oxidative stress in Parkinson's disease. Ann Neurol. 2003; 53 Suppl 3(S3):S26-36; discussion S-8. doi:10.1002/ana.10483

278. Mattson MP. Roles of the lipid peroxidation product 4-hydroxynonenal in obesity, the metabolic syndrome, and associated vascular and neurodegenerative disorders. Exp Gerontol. 2009; 44(10):625-33. doi:10.1016/j.exger.2009.07.003

279. Zheng J, Conrad M. The Metabolic Underpinnings of Ferroptosis. Cell Metab. 2020; 32(6):920-37. doi:10.1016/j.cmet.2020.10.011

280. Brigelius-Flohe R, Flohe L. Regulatory Phenomena in the Glutathione Peroxidase Superfamily. Antioxid Redox Signal. 2020; 33(7):498-516. doi:10.1089/ars.2019.7905

281. Weaver K, Skouta R. The Selenoprotein Glutathione Peroxidase 4: From Molecular Mechanisms to Novel Therapeutic Opportunities. Biomed. 2022; 10(4):891. doi:10.3390/biomedicines10040891

282. Brigelius-Flohe R, Maiorino M. Glutathione peroxidases. Biochim Biophys Acta. 2013; 1830(5):3289-303. doi:10.1016/j.bbagen.2012.11.020

283. Liu H, Forouhar F, Lin AJ, Wang Q, Polychronidou V, Soni RK, et al. Small-molecule allosteric inhibitors of GPX4. Cell Chem Biol. 2022; 29(12):1680-93 e9. doi:10.1016/j.chembiol.2022.11.003

284. Xie Y, Kang R, Klionsky DJ, Tang D. GPX4 in cell death, autophagy, and disease. Autophagy. 2023; 19(10):2621-38. doi:10.1080/15548627.2023.2218764

285. Behnisch-Cornwell S, Bandaru SSM, Napierkowski M, Wolff L, Zubair M, Urbainsky C, et al. Pentathiepins: A Novel Class of Glutathione Peroxidase 1 Inhibitors that Induce Oxidative Stress,

Loss of Mitochondrial Membrane Potential and Apoptosis in Human Cancer Cells. ChemMedChem. 2020; 15(16):1515-28. doi:10.1002/cmdc.202000160

286. Liu J, Nussinov R. Allostery: An Overview of Its History, Concepts, Methods, and Applications. PLoS Comput Biol. 2016; 12(6):e1004966. doi:10.1371/journal.pcbi.1004966

287. Dexter DT, Wells FR, Lees AJ, Agid F, Agid Y, Jenner P, et al. Increased nigral iron content and alterations in other metal ions occurring in brain in Parkinson's disease. J Neurochem. 1989; 52(6):1830-6. doi:10.1111/j.1471-4159.1989.tb07264.x

288. Martin WR, Wieler M, Gee M. Midbrain iron content in early Parkinson disease: a potential biomarker of disease status. Neurology. 2008; 70(16 Pt 2):1411-7. doi:10.1212/01.wnl.0000286384.31050.b5

289. Duce JA, Wong BX, Durham H, Devedjian JC, Smith DP, Devos D. Post translational changes to alpha-synuclein control iron and dopamine trafficking; a concept for neuron vulnerability in Parkinson's disease. Mol Neurodegener. 2017; 12(1):45. doi:10.1186/s13024-017-0186-8

290. Baksi S, Tripathi AK, Singh N. Alpha-synuclein modulates retinal iron homeostasis by facilitating the uptake of transferrin-bound iron: Implications for visual manifestations of Parkinson's disease. Free Radic Biol Med. 2016; 97:292-306. doi:10.1016/j.freeradbiomed.2016.06.025

291. Devos D, Moreau C, Devedjian JC, Kluza J, Petrault M, Laloux C, et al. Targeting chelatable iron as a therapeutic modality in Parkinson's disease. Antioxid Redox Signal. 2014; 21(2):195-210. doi:10.1089/ars.2013.5593

292. Levi S, Corsi B, Bosisio M, Invernizzi R, Volz A, Sanford D, et al. A human mitochondrial ferritin encoded by an intronless gene. J Biol Chem. 2001; 276(27):24437-40. doi:10.1074/jbc.C100141200

293. Santambrogio P, Biasiotto G, Sanvito F, Olivieri S, Arosio P, Levi S. Mitochondrial ferritin expression in adult mouse tissues. J Histochem Cytochem. 2007; 55(11):1129-37. doi:10.1369/jhc.7A7273.2007

294. Arosio P, Levi S. Ferritin, iron homeostasis, and oxidative damage. Free Radic Biol Med. 2002; 33(4):457-63. doi:10.1016/s0891-5849(02)00842-0

295. Abboud S, Haile DJ. A novel mammalian iron-regulated protein involved in intracellular iron metabolism. J Biol Chem. 2000; 275(26):19906-12. doi:10.1074/jbc.M000713200

296. David S, Jhelum P, Ryan F, Jeong SY, Kroner A. Dysregulation of Iron Homeostasis in the Central Nervous System and the Role of Ferroptosis in Neurodegenerative Disorders. Antioxid Redox Signal. 2022; 37(1-3):150-70. doi:10.1089/ars.2021.0218

297. Crichton RR, Boelaert JR. Inorganic biochemistry of iron metabolism: from molecular mechanisms to clinical consequences: John Wiley & Sons; 2001.

298. Jameson GN, Jameson RF, Linert W. New insights into iron release from ferritin: direct observation of the neurotoxin 6-hydroxydopamine entering ferritin and reaching redox equilibrium with the iron core. Org Biomol Chem. 2004; 2(16):2346-51. doi:10.1039/B408044K

299. Shi ZH, Nie G, Duan XL, Rouault T, Wu WS, Ning B, et al. Neuroprotective mechanism of mitochondrial ferritin on 6-hydroxydopamine-induced dopaminergic cell damage: implication for neuroprotection in Parkinson's disease. Antioxid Redox Signal. 2010; 13(6):783-96. doi:10.1089/ars.2009.3018

300. Richter D, Bartig D, Muhlack S, Hartelt E, Scherbaum R, Katsanos AH, et al. Dynamics of Parkinson's Disease Multimodal Complex Treatment in Germany from 2010(-)2016: Patient Characteristics, Access to Treatment, and Formation of Regional Centers. Cells. 2019; 8(2):151. doi:10.3390/cells8020151

301. Stoker TB, Barker RA. Recent developments in the treatment of Parkinson's Disease. F1000 Res. 2020; 9 doi:10.12688/f1000research.25634.1

302. Connolly BS, Lang AE. Pharmacological treatment of Parkinson disease: a review. JAMA. 2014; 311(16):1670-83. doi:10.1001/jama.2014.3654

303. Chondrogiorgi M, Tatsioni A, Reichmann H, Konitsiotis S. Dopamine agonist monotherapy in Parkinson's disease and potential risk factors for dyskinesia: a meta-analysis of levodopa-controlled trials. Eur J Neurol. 2014; 21(3):433-40. doi:10.1111/ene.12318

304. Hornykiewicz O. L-DOPA: from a biologically inactive amino acid to a successful therapeutic agent. Amino Acids. 2002; 23(1-3):65-70. doi:10.1007/s00726-001-0111-9

305. Astarloa R, Mena MA, Sanchez V, de la Vega L, de Yebenes JG. Clinical and pharmacokinetic effects of a diet rich in insoluble fiber on Parkinson's disease. Clin Neuropharmacol. 1992; 15(5):375-80. doi:10.1097/00002826-199210000-00004

306. Contin M, Riva R, Albani F, Baruzzi A. Pharmacokinetic optimisation in the treatment of Parkinson's disease. Clin Pharmacokinet. 1996; 30(6):463-81. doi:10.2165/00003088-199630060-00004

307. MacDonald A, Singh RH, Rocha JC, van Spronsen FJ. Optimising amino acid absorption: essential to improve nitrogen balance and metabolic control in phenylketonuria. Nutr Res Rev. 2019; 32(1):70-8. doi:10.1017/S0954422418000173

308. Contin M, Riva R, Martinelli P, Procaccianti G, Cortelli P, Avoni P, et al. Response to a standard oral levodopa test in parkinsonian patients with and without motor fluctuations. Clin Neuropharmacol. 1990; 13(1):19-28. doi:10.1097/00002826-199002000-00002

309. Contin M, Riva R, Martinelli P, Albani F, Baruzzi A. Effect of age on the pharmacokinetics of oral levodopa in patients with Parkinson's disease. Eur J Clin Pharmacol. 1991; 41(5):463-6. doi:10.1007/BF00626370

310. Patel AB, Jimenez-Shahed J. Profile of inhaled levodopa and its potential in the treatment of Parkinson's disease: evidence to date. Neuropsychiatr Dis Treat. 2018; 14:2955-64. doi:10.2147/NDT.S147633

311. Nutt JG, Woodward WR, Gancher ST, Merrick D. 3-*O*-methyldopa and the response to levodopa in Parkinson's disease. Ann Neurol. 1987; 21(6):584-8. doi:10.1002/ana.410210610

312. Vidgren J, Svensson LA, Liljas A. Crystal structure of catechol-*O*-methyltransferase. Nature. 1994; 368(6469):354-8. doi:10.1038/368354a0

313. Rivera-Calimlim L, Tandon D, Anderson F, Joynt R. The clinical picture and plasma levodopa metabolite profile of parkinsonian nonresponders. Treatment with levodopa and decarboxylase inhibitor. Arch Neurol. 1977; 34(4):228-32. doi:10.1001/archneur.1977.00500160042007

314. Jatana N, Apoorva N, Malik S, Sharma A, Latha N. Inhibitors of catechol-O-methyltransferase in the treatment of neurological disorders. Cent Nerv Syst Agents Med Chem. 2013; 13(3):166-94. doi:10.2174/18715249136661401091133 41

315. Muller T. Catechol-*O*-methyltransferase inhibitors in Parkinson's disease. Drugs. 2015; 75(2):157-74. doi:10.1007/s40265-014-0343-0

316. Tohgi H, Abe T, Kikuchi T, Takahashi S, Nozaki Y. The significance of 3-*O*-methyldopa concentrations in the cerebrospinal fluid in the pathogenesis of wearing-off phenomenon in Parkinson's disease. Neurosci Lett. 1991; 132(1):19-22. doi:10.1016/0304-3940(91)90422-p

317. Kiss LE, Soares-da-Silva P. Medicinal chemistry of catechol-*O*-methyltransferase (COMT) inhibitors and their therapeutic utility. J Med Chem. 2014; 57(21):8692-717. doi:10.1021/jm500572b

318. Lotta T, Vidgren J, Tilgmann C, Ulmanen I, Melen K, Julkunen I, et al. Kinetics of human soluble and membrane-bound catechol-*O*-methyltransferase: a revised mechanism and description of the thermolabile variant of the enzyme. Biochem. 1995; 34(13):4202-10. doi:10.1021/bi00013a008

319. Lyytinen J, Kaakkola S, Ahtila S, Tuomainen P, Teravainen H. Simultaneous MAO-B and COMT inhibition in L-Dopa-treated patients with Parkinson's disease. Mov Disord. 1997; 12(4):497-505. doi:10.1002/mds.870120404

320. Ries V, Selzer R, Eichhorn T, Oertel WH, Eggert K, German Tolcapone Study G. Replacing a dopamine agonist by the COMT-inhibitor tolcapone as an adjunct to L-dopa in the treatment of Parkinson's disease: a randomized, multicenter, open-label, parallel-group study. Clin Neuropharmacol. 2010; 33(3):142-50. doi:10.1097/WNF.0b013e3181d99d6f

321. Robakis D, Fahn S. Defining the Role of the Monoamine Oxidase-B Inhibitors for Parkinson's Disease. CNS Drugs. 2015; 29(6):433-41. doi:10.1007/s40263-015-0249-8

322. Wierenga RK, de Jong RJ, Kalk KH, Hol WG, Drenth J. Crystal structure of p-hydroxybenzoate hydroxylase. J Mol Biol. 1979; 131(1):55-73. doi:10.1016/0022-2836(79)90301-2

323. Johnston JP. Some observations upon a new inhibitor of monoamine oxidase in brain tissue. Biochem Pharmacol. 1968; 17(7):1285-97. doi:10.1016/0006-2952(68)90066-x

324. Westlund KN, Denney RM, Rose RM, Abell CW. Localization of distinct monoamine oxidase A and monoamine oxidase B cell populations in human brainstem. Neuroscience. 1988; 25(2):439-56. doi:10.1016/0306-4522(88)90250-3

325. Collins G, Sandler M, Williams E, Youdim MBH. Multiple Forms of Human Brain Monoamine Oxidase. Nature 1970; 225:817–20.

326. Youdim MB, Maruyama W, Naoi M. Neuropharmacological, neuroprotective and amyloid precursor processing properties of selective MAO-B inhibitor antiparkinsonian drug, rasagiline. Drugs Today (Barc). 2005; 41(6):369-91. doi:10.1358/dot.2005.41.6.893613

327. Yamada M, Yasuhara H. Clinical pharmacology of MAO inhibitors: safety and future. Neurotoxicology. 2004; 25(1-2):215-21. doi:10.1016/S0161-813X(03)00097-4

328. Edmondson DE, Mattevi A, Binda C, Li M, Hubalek F. Structure and mechanism of monoamine oxidase. Curr Med Chem. 2004; 11(15):1983-93. doi:10.2174/0929867043364784

329. Berman SB, Hastings TG. Dopamine oxidation alters mitochondrial respiration and induces permeability transition in brain mitochondria: implications for Parkinson's disease. J Neurochem. 1999; 73(3):1127-37. doi:10.1046/j.1471-4159.1999.0731127.x

330. Anastassova N, Aluani D, Hristova-Avakumova N, Tzankova V, Kondeva-Burdina M, Rangelov M, et al. Study on the Neuroprotective, Radical-Scavenging and MAO-B Inhibiting Properties of New Benzimidazole Arylhydrazones as Potential Multi-Target Drugs for the

Treatment of Parkinson's Disease. Antioxidants (Basel). 2022; 11(5):884. doi:10.3390/antiox11050884

331. Mandel S, Weinreb O, Amit T, Youdim MB. Mechanism of neuroprotective action of the anti-Parkinson drug rasagiline and its derivatives. Brain Res. Rev. 2005; 48(2):379-87.

332. Maruyama W, Akao Y, Carrillo MC, Kitani K, Youdium MB, Naoi M. Neuroprotection by propargylamines in Parkinson's disease: suppression of apoptosis and induction of prosurvival genes. Neurotoxicol Teratol. 2002; 24(5):675-82. doi:10.1016/s0892-0362(02)00221-0

333. Carrillo MC, Minami C, Kitani K, Maruyama W, Ohashi K, Yamamoto T, et al. Enhancing effect of rasagiline on superoxide dismutase and catalase activities in the dopaminergic system in the rat. Life Sci. 2000; 67(5):577-85. doi:10.1016/s0024-3205(00)00643-3

334. Kitani K, Kanai S, Ivy GO, Carrillo MC. Pharmacological modifications of endogenous antioxidant enzymes with special reference to the effects of deprenyl: a possible antioxidant strategy. Mech Ageing Dev. 1999; 111(2-3):211-21. doi:10.1016/s0047-6374(99)00065-2

335. Youdim MB, Bakhle YS. Monoamine oxidase: isoforms and inhibitors in Parkinson's disease and depressive illness. Br J Pharmacol. 2006; 147 Suppl 1(Suppl 1):S287-96. doi:10.1038/sj.bjp.0706464

336. Fernandez HH, Chen JJ. Monoamine oxidase-B inhibition in the treatment of Parkinson's disease. Pharmacotherapy. 2007; 27(12 Pt 2):174S-85S. doi:10.1592/phco.27.12part2.174S

337. Moore JJ, Saadabadi A. Selegiline. 2023 Aug 17. In: StatPearls [Internet]. Treasure Island (FL): StatPearls Publishing; 2024 Jan–. PMID: 30252350

338. Volz HP, Gleiter CH. Monoamine oxidase inhibitors. A perspective on their use in the elderly. Drugs Aging. 1998; 13(5):341-55. doi:10.2165/00002512-199813050-00002

339. Henriot S, Kuhn C, Kettler R, Da Prada M. Lazabemide (Ro 19-6327), a reversible and highly sensitive MAO-B inhibitor: preclinical and clinical findings. Amine Oxidases: Function and Dysfunction: Springer; 1994. p. 321-5.

340. Caccia C, Maj R, Calabresi M, Maestroni S, Faravelli L, Curatolo L, et al. Safinamide: from molecular targets to a new anti-Parkinson drug. Neurology. 2006; 67(7 Suppl 2):S18-23. doi:10.1212/wnl.67.7_suppl_2.s18

341. Stowe R, Ives N, Clarke C, Ferreira J, Hawker RJ, Shah L, et al. Dopamine agonist therapy in early Parkinson's disease. 2008.

342. García DS, Mora JP, Sevilla FE, Ruiz PG, Ceberio JI, Bojarski JK, et al. Dopamine agonist therapy in Parkinson's disease: Spanish expert consensus on its use in different clinical situations. Neurología (English Edition). 2023;

343. Katzung BG, Masters SB, Trevor AJ. Basic and Clinical Pharmacology (LANGE Basic Science): McGraw-Hill Education; 2012.

344. Shulman LM. Parkinson's Disease: The Proper Use of Dopamine Receptor Agonists. Curr Treat Options Neurol. 1999; 1(1):14-20. doi:10.1007/s11940-999-0028-2

345. Olanow CW, Watts RL, Koller WC. An algorithm (decision tree) for the management of Parkinson's disease (2001): treatment guidelines. Neurology. 2001; 56(11 Suppl 5):S1-S88. doi:10.1212/wnl.56.suppl_5.s1

346. Davie CA. A review of Parkinson's disease. Br Med Bull. 2008; 86(1):109-27. doi:10.1093/bmb/ldn013

347. Mucklow J. Martindale: the complete drug reference. Br. J. Clin. Pharmacol. 2000; 49(6):613-.

348. Blanchet P, Bedard PJ, Britton DR, Kebabian JW. Differential effect of selective D-1 and D-2 dopamine receptor agonists on levodopa-induced dyskinesia in 1-methyl-4-phenyl-1,2,3,6-tetrahydropyridine- exposed monkeys. J Pharmacol Exp Ther. 1993; 267(1):275-9.

349. Brooks D. Dopamine agonists: their role in the treatment of Parkinson's disease. BMJ Publishing Group Ltd; 2000.

350. Hubble JP. Pre-clinical studies of pramipexole: clinical relevance. Eur J Neurol. 2000; 7 Suppl 1:15-20. doi:10.1046/j.1468-1331.2000.0070s1015.x

351. Rascol O, Brooks DJ, Brunt ER, Korczyn AD, Poewe WH, Stocchi F. Ropinirole in the treatment of early Parkinson's disease: a 6-month interim report of a 5-year levodopa-controlled study. 056 Study Group. Mov Disord. 1998; 13(1):39-45. doi:10.1002/mds.870130111

352. Schapira AH. Neuroprotection and dopamine agonists. Neurology. 2002; 58(suppl 1):S9-S18.

353. Pankevich DE, Altevogt BM, Dunlop J, Gage FH, Hyman SE. Improving and accelerating drug development for nervous system disorders. Neuron. 2014; 84(3):546-53. doi:10.1016/j.neuron.2014.10.007

354. Sadybekov AV, Katritch V. Computational approaches streamlining drug discovery. Nature. 2023; 616(7958):673-85. doi:10.1038/s41586-023-05905-z

355. Mohan SB, Dinda S, Kumar RB, Panda J. Computational approaches for drug design and discovery process. Journal of Current Pharma Research. 2012; 2(3):600.

356. Shaker B, Ahmad S, Lee J, Jung C, Na D. In silico methods and tools for drug discovery. Comput Biol Med. 2021; 137:104851. doi:10.1016/j.compbiomed.2021.104851

357. Tropsha A. Best Practices for QSAR Model Development, Validation, and Exploitation. Mol Inform. 2010; 29(6-7):476-88. doi:10.1002/minf.201000061

358. Verma J, Khedkar VM, Coutinho EC. 3D-QSAR in drug design--a review. Curr Top Med Chem. 2010; 10(1):95-115. doi:10.2174/156802610790232260

359. Wang W, Kim MT, Sedykh A, Zhu H. Developing Enhanced Blood-Brain Barrier Permeability Models: Integrating External Bio-Assay Data in QSAR Modeling. Pharm Res. 2015; 32(9):3055-65. doi:10.1007/s11095-015-1687-1

360. Nascimento AC, Prudencio RB, Costa IG. A multiple kernel learning algorithm for drug-target interaction prediction. BMC Bioinformatics. 2016; 17:46. doi:10.1186/s12859-016-0890-3

361. Schyman P, Liu R, Desai V, Wallqvist A. vNN Web Server for ADMET Predictions. Front Pharmacol. 2017; 8:889. doi:10.3389/fphar.2017.00889

362. Liu R, Tawa G, Wallqvist A. Locally weighted learning methods for predicting dose-dependent toxicity with application to the human maximum recommended daily dose. Chem Res Toxicol. 2012; 25(10):2216-26. doi:10.1021/tx300279f

363. Paul SM, Mytelka DS, Dunwiddie CT, Persinger CC, Munos BH, Lindborg SR, et al. How to improve R&D productivity: the pharmaceutical industry's grand challenge. Nat Rev Drug Discov. 2010; 9(3):203-14. doi:10.1038/nrd3078

364. Di L, Kerns EH. Drug-like properties: concepts, structure design and methods from ADME to toxicity optimization: Academic press; 2015.

365. Jones AW. Early drug discovery and the rise of pharmaceutical chemistry. Drug Test Anal. 2011; 3(6):337-44. doi:10.1002/dta.301

366. Duarte CD, Barreiro EJ, Fraga CA. Privileged structures: a useful concept for the rational design of new lead drug candidates. Mini Rev Med Chem. 2007; 7(11):1108-19. doi:10.2174/138955707782331722

367. Mahapatra AD, Bhowmik P, Banerjee A, Das A, Ojha D, Chattopadhyay D. Ethnomedicinal wisdom: an approach for antiviral drug development. New look to phytomedicine: Elsevier; 2019. p. 35-61.

368. Singh S, Malik BK, Sharma DK. Molecular drug targets and structure based drug design: A holistic approach. Bioinformation. 2006; 1(8):314-20. doi:10.6026/97320630001314

369. Solecki RS. Shanidar IV, a Neanderthal flower burial in northern Iraq. Science. 1975; 190(4217):880-1.

370. Ma SS. The I Ching and the psyche-body connection. J Anal Psychol. 2005; 50(2):237-50. doi:10.1111/j.0021-8774.2005.00526.x

371. de Medeiros PM, Santos Pinto BL, do Nascimento VT. Can organoleptic properties explain the differential use of medicinal plants? Evidence from Northeastern Brazil. J Ethnopharmacol. 2015; 159:43-8. doi:10.1016/j.jep.2014.11.001

372. Salim AA, Chin Y-W, Kinghorn AD. Drug discovery from plants. Bioactive molecules and medicinal plants: Springer; 2008. p. 1-24.

373. Kunzelman J, Durako MJ, Kenworthy W, Stapleton A, Wright JL. Irradiance-induced changes in the photobiology of Halophila johnsonii. Marine Biology. 2005; 148(2):241-50.

374. Yarnell E, Abascal K. Dilemmas of traditional botanical research. HerbalGram. 2002;

375. Schmidt B, Ribnicky DM, Poulev A, Logendra S, Cefalu WT, Raskin I. A natural history of botanical therapeutics. Metabolism. 2008; 57(7 Suppl 1):S3-9. doi:10.1016/j.metabol.2008.03.001

376. Calixto JB. The role of natural products in modern drug discovery. An Acad Bras Cienc. 2019; 91 Suppl 3:e20190105. doi:10.1590/0001-3765201920190105

377. Smith T, Majid F, Eckl V, Reynolds CM. Herbal supplement sales in US increase by record-breaking 17.3% in 2020. HerbalGram. 2021; 131:52-65.

378. Egbuna C, Mukherjee M, Rao GN, Gido LJFJ, Tijjani H. Introduction to phytochemistry. Phytochemistry: Apple Academic Press; 2018. p. 3-36.

379. Dafni A, Bock B. Medicinal plants of the Bible-revisited. J Ethnobiol Ethnomed. 2019; 15(1):57. doi:10.1186/s13002-019-0338-8

380. Teall EK. Medicine and doctoring in ancient Mesopotamia. GVJH. 2014; 3(1):2.

381. Newman DJ, Cragg GM, Snader KM. The influence of natural products upon drug discovery. Nat Prod Rep. 2000; 17(3):215-34. doi:10.1039/a902202c

382. Jacoby DB, Youngson RM. Encyclopedia of family health: Marshall Cavendish; 2004.

383. Achan J, Talisuna AO, Erhart A, Yeka A, Tibenderana JK, Baliraine FN, et al. Quinine, an old anti-malarial drug in a modern world: role in the treatment of malaria. Malar J. 2011; 10(1):144. doi:10.1186/1475-2875-10-144

384. Kumar V, Veeranjaneyulu A. Herbs for Diabetes and Neurological Disease Management: Research and Advancements: CRC Press; 2018.

385. World Health Organization. National policy on traditional medicine and regulation of herbal medicines: Report of a WHO global survey: World Health Organization; 2005.

386. World Health Organization. International Regulatory Cooperation for Herbal Medicines (IRCH). Pubmed| Crossref| O thers. 2014;

387. Stierle A, Strobel G, Stierle D. Taxol and taxane production by *Taxomyces andreanae*, an endophytic fungus of Pacific yew. Science. 1993; 260(5105):214-6. doi:10.1126/science.8097061

388. Lachance H, Wetzel S, Kumar K, Waldmann H. Charting, navigating, and populating natural product chemical space for drug discovery. J Med Chem. 2012; 55(13):5989-6001. doi:10.1021/jm300288g

389. Enke CG, Nagels LJ. Undetected components in natural mixtures: how many? What concentrations? Do they account for chemical noise? What is needed to detect them? Anal. Chem. 2011; 83(7):2539-46.

390. Qiu F, Cai G, Jaki BU, Lankin DC, Franzblau SG, Pauli GF. Quantitative purity-activity relationships of natural products: the case of anti-tuberculosis active triterpenes from Oplopanax horridus. J Nat Prod. 2013; 76(3):413-9. doi:10.1021/np3007809

391. Balunas MJ, Kinghorn AD. Drug discovery from medicinal plants. Life Sci. 2005; 78(5):431-41. doi:10.1016/j.lfs.2005.09.012

392. Ma Z, Li S, Zhang M, Jiang S, Xiao Y. Light intensity affects growth, photosynthetic capability, and total flavonoid accumulation of Anoectochilus plants. HortScience. 2010; 45(6):863-7.

393. Naczk M, Shahidi F. Phenolics in cereals, fruits and vegetables: occurrence, extraction and analysis. J Pharm Biomed Anal. 2006; 41(5):1523-42. doi:10.1016/j.jpba.2006.04.002

394. Ncube B, Van Staden J. Tilting Plant Metabolism for Improved Metabolite Biosynthesis and Enhanced Human Benefit. Molecules. 2015; 20(7):12698-731. doi:10.3390/molecules200712698

395. Awuchi CG. Plants, phytochemicals, and natural practices in complementary and alternative system of medicine for treatment of central nervous system disorders. Int. J. Food Prop. 2023; 26(1):1190-213.

396. Reichman WE. Current pharmacologic options for patients with Alzheimer's disease. Ann Gen Hosp Psychiatry. 2003; 2(1):1. doi:10.1186/1475-2832-2-1

397. Enogieru AB, Omoruyi SI, Hiss DC, Ekpo OE. Potential antiparkinsonian agents derived from South African medicinal plants. J. Herb. Med. 2018; 13:1-7.

398. Nielsen ND, Sandager M, Stafford GI, van Staden J, Jager AK. Screening of indigenous plants from South Africa for affinity to the serotonin reuptake transport protein. J Ethnopharmacol. 2004; 94(1):159-63. doi:10.1016/j.jep.2004.05.013

399. Pedersen ME, Szewczyk B, Stachowicz K, Wieronska J, Andersen J, Stafford GI, et al. Effects of South African traditional medicine in animal models for depression. J Ethnopharmacol. 2008; 119(3):542-8. doi:10.1016/j.jep.2008.08.030

400. Stafford GI, Pedersen ME, van Staden J, Jager AK. Review on plants with CNS-effects used in traditional South African medicine against mental diseases. J Ethnopharmacol. 2008; 119(3):513-37. doi:10.1016/j.jep.2008.08.010

401. Gribkoff VK, Kaczmarek LK. The need for new approaches in CNS drug discovery: Why drugs have failed, and what can be done to improve outcomes. Neuropharmacology. 2017; 120:11-9. doi:10.1016/j.neuropharm.2016.03.021

402. World Health Organisation. WHO guidelines on good agricultural and collection practices [GACP] for medicinal plants: World Health Organization; 2003.

403. Sobeickie, JF. A preliminary inventory of plants used for psychoactive purposes in southern African healing traditions. Transactions of the Royal Society of South Africa. 2002; 57(1-2):1-24.

404. Stafford GI, Jager AK, van Staden J. Activity of traditional South African sedative and potentially CNS-acting plants in the GABA-benzodiazepine receptor assay. J Ethnopharmacol. 2005; 100(1-2):210-5. doi:10.1016/j.jep.2005.04.004

405. Van Wyk B-E, Gericke N. People's plants: A guide to useful plants of Southern Africa: Briza publications; 2000.

406. Gomes NG, Campos MG, Orfao JM, Ribeiro CA. Plants with neurobiological activity as potential targets for drug discovery. Prog Neuropsychopharmacol Biol Psychiatry. 2009; 33(8):1372-89. doi:10.1016/j.pnpbp.2009.07.033

407. Gadaga LL, Tagwireyi D, Dzangare J, Nhachi CF. Acute oral toxicity and neurobehavioural toxicological effects of hydroethanolic extract of *Boophone disticha* in rats. Hum Exp Toxicol. 2011; 30(8):972-80. doi:10.1177/0960327110384524

408. Mwamatope B, Tembo D, Chikowe I, Kampira E, Nyirenda C. Total phenolic contents and antioxidant activity of *Senna singueana*, *Melia azedarach*, *Moringa oleifera* and *Lannea discolor* herbal plants. Scientific African. 2020; 9:e00481.

409. Hutchings A. Zulu medicinal plants: An inventory: University of Natal press; 1996.

410. Masondo NA, Stafford GI, Aremu AO, Makunga NP. Acetylcholinesterase inhibitors from southern African plants: An overview of ethnobotanical, pharmacological potential and phytochemical research including and beyond Alzheimer's disease treatment. South African Journal of Botany. 2019; 120:39-64.

411. Kalita P. An overview on *Mangifera indica*: Importance and its various pharmacological action. PharmaTutor. 2014; 2(12):72-6.

412. Lopez-Rios L, Wiebe JC, Vega-Morales T, Gericke N. Central nervous system activities of extract *Mangifera indica* L. J Ethnopharmacol. 2020; 260:112996. doi:10.1016/j.jep.2020.112996

413. Suroowan S, Pynee K, Mahomoodally M. A comprehensive review of ethnopharmacologically important medicinal plant species from Mauritius. S. Afr. J. Bot. 2019; 122:189-213.

414. Samoisy AK, Mahomoodally MF. Ethnopharmacological analysis of medicinal plants used against non-communicable diseases in Rodrigues Island, Indian Ocean. J Ethnopharmacol. 2015; 173:20-38. doi:10.1016/j.jep.2015.06.036

415. Stafford GI, Pedersen ME, van Staden J, Jäger AK. Review on plants with CNS-effects used in traditional South African medicine against mental diseases. J. Ethnopharmaco. 2008; 119(3):513-37.

416. McGaw LJ, Lall N, Hlokwe TM, Michel AL, Meyer JJM, Eloff JN. The Herbalist Handbook. Natur Africa, 1990. Biological & pharmaceutical bulletin. 2008; 31(7):1429-33.

417. Van Wyk BE. The potential of South African plants in the development of new medicinal products. S. Afr. J. Bot. 2011; 77(4):812-29.

418. Watt JM, Breyer-Brandwijk MG. The Medicinal and Poisonous Plants of Southern and Eastern Africa being an Account of their Medicinal and other Uses, Chemical Composition, Pharmacological Effects and Toxicology in Man and Animal. The Medicinal and Poisonous Plants of Southern and Eastern Africa being an Account of their Medicinal and other Uses, Chemical Composition, Pharmacological Effects and Toxicology in Man and Animal. 1962; (Edn 2)

419. Afolayan A. Extracts from the shoots of *Arctotis arctotoides* inhibit the growth of bacteria and fungi. Pharm. Biol. 2003; 41(1):22-5.

420. Long C. Swaziland's flora: siSwati names and uses. Swaziland National Trust Commission: Mbambane, Swaziland. 2005;

421. Moroole MA, Materechera SA, Mbeng WO, Aremu AO. Medicinal plants used for contraception in South Africa: A review. J Ethnopharmacol. 2019; 235:19-27. doi:10.1016/j.jep.2019.02.002

422. Gelfland M, Mavi S, Drummond RB, Ndemera B. The traditional medical practitioner in Zimbabwe: his principles of practice and pharmacopoeia: Mambo Press; 1985.

423. Burkill HM. The Useful Plants of West Tropical Africa, Families SZ Addenda. Royal Botanic Gardens, Kew, Richmond, United Kingdom. 2000; 5:686.

424. Amabeoku GJ, Green I, Kabatende J. Anticonvulsant activity of *Cotyledon orbiculata* L. (Crassulaceae) leaf extract in mice. J Ethnopharmacol. 2007; 112(1):101-7. doi:10.1016/j.jep.2007.02.016

425. Maroyi A. A review of botany, medicinal uses, phytochemistry and biological activities of *Cotyledon orbiculata*. Int. J. Pharm. Sci. Res. 2019; 11(10):3491-6.

426. Beinart W, Beinart R. 'From Elephant's Foot… to Cortisone': Boots Pure Drug Company and *Dioscorea sylvatica* in South Africa, c. 1950–1963. S. Afr. Hist. J. 2019; 71(4):644-75.

427. Mintsa Mi Nzue AP. Use and conservation status of medicinal plants in the Cape Peninsula, Western Cape Province of South Africa [thesis]. Stellenbosch: University of Stellenbosch; 2009.

428. Philander LA. An ethnobotany of Western Cape Rasta bush medicine. J Ethnopharmacol. 2011; 138(2):578-94.

429. Maria M R, Maria Cristina D, Bucar I, Luís C. Medicinal plants used to treat neurological disorders in West Africa: a case study with Guinea-Bissau flora. Am. J. Plant Sci. 2012; 2012

430. De Wet H, Ngubane S. Traditional herbal remedies used by women in a rural community in northern Maputaland (South Africa) for the treatment of gynaecology and obstetric complaints. S. Afr. J. Bot. 2014; 94:129-39.

431. Hutchings A, van Staden J. Plants used for stress-related ailments in traditional Zulu, Xhosa and Sotho medicine. Part 1: Plants used for headaches. J Ethnopharmacol. 1994; 43(2):89-124. doi:10.1016/0378-8741(94)90008-6

432. Maroyi A. Traditional usage, phytochemistry and pharmacology of *Croton sylvaticus* Hochst. ex C. Krauss. Asian Pac J Trop Med. 2017; 10(5):423-9. doi:10.1016/j.apjtm.2017.05.002

433. Palmer E, Pitman N. Trees of South Africa, Vol. 2. Balkema, Cape Town. 1973;

434. Gapuz MCD, Besagas RL. Phytochemical profiles and antioxidant activities of leaf extracts of Euphorbia species. JBES. 2018; 12(4):59-65.

435. Mogale MMP, Raimondo D, VanWyk B-E. The ethnobotany of Central Sekhukhuneland, South Africa. S. Afr. J. Bot. 2019; 122:90-119.

436. Bienvenu E, Amabeoku GJ, Eagles PK, Scott G, Springfield EP. Anticonvulsant activity of aqueous extract of *Leonotis leonurus*. PYTOEY. 2002; 9(3):217-23. doi:10.1078/0944-7113-00103

437. El-Ansari MA, Aboutabl EA, Farrag ARH, Sharaf M, Hawas UW, Soliman GM, et al. Phytochemical and pharmacological studies on *Leonotis leonurus*. Pharm. Biol. 2009; 47(9):894-902.

438. Cakilcioglu U, Khatun S, Turkoglu I, Hayta S. Ethnopharmacological survey of medicinal plants in Maden (Elazig-Turkey). J Ethnopharmacol. 2011; 137(1):469-86. doi:10.1016/j.jep.2011.05.046

439. Eissa TA, Palomino OM, Carretero ME, Gomez-Serranillos MP. Ethnopharmacological study of medicinal plants used in the treatment of CNS disorders in Sinai Peninsula, Egypt. J Ethnopharmacol. 2014; 151(1):317-32. doi:10.1016/j.jep.2013.10.041

440. Amabeoku GJ, Erasmus SJ, Ojewole JA, Mukinda JT. Antipyretic and antinociceptive properties of *Mentha longifolia* Huds. (Lamiaceae) leaf aqueous extract in rats and mice. Methods Find Exp Clin Pharmacol. 2009; 31(10):645-9. doi:10.1358/mf.2009.31.10.1441861

441. Bussmann RW, Gilbreath GG, Solio J, Lutura M, Lutuluo R, Kunguru K, et al. Plant use of the Maasai of Sekenani Valley, Maasai Mara, Kenya. J Ethnobiol Ethnomed. 2006; 2:22. doi:10.1186/1746-4269-2-22

442. Bashir A, Hamburger M, Msonthi J, Hostettmann K. Isoflavones and Xanthones from the Roots of *Polygala virgata*. Planta Med. 1991; 57(S 2):A112-A.

443. Peredery O, Persinger MA. Herbal treatment following post-seizure induction in rat by lithium pilocarpine: *Scutellaria lateriflora* (Skullcap), *Gelsemium sempervirens* (Gelsemium) and *Datura stramonium* (Jimson Weed) may prevent development of spontaneous seizures. Phytother Res. 2004; 18(9):700-5. doi:10.1002/ptr.1511

444. Dessanges JF. A history of nebulization. J Aerosol Med. 2001; 14(1):65-71. doi:10.1089/08942680152007918

445. Rajbhandari K. Ethnobotany of Nepal Kathmandu. ESON. 2001;

446. Pretorius E, Marx J. *Datura stramonium* in asthma treatment and possible effects on prenatal development. Environ Toxicol Pharmacol. 2006; 21(3):331-7. doi:10.1016/j.etap.2005.10.006

447. Soni P, Siddiqui AA, Dwivedi J, Soni V. Pharmacological properties of *Datura stramonium* L. as a potential medicinal tree: an overview. Asian Pac J Trop Biomed. 2012; 2(12):1002-8. doi:10.1016/S2221-1691(13)60014-3

448. Nagashayana N, Sankarankutty P, Nampoothiri MR, Mohan PK, Mohanakumar KP. Association of L-DOPA with recovery following Ayurveda medication in Parkinson's disease. J Neurol Sci. 2000; 176(2):124-7. doi:10.1016/s0022-510x(00)00329-4

449. Kumar S, Tewari A, Dwivedi R. The use of aphrodisiacs in medival India. Nagarjun. 1980; 23:170-4.

450. Saleem S, Muhammad G, Hussain MA, Altaf M, Bukhari SNA. *Withania somnifera* L.: Insights into the phytochemical profile, therapeutic potential, clinical trials, and future prospective. Iran J Basic Med Sci. 2020; 23(12):1501-26. doi:10.22038/IJBMS.2020.44254.10378

451. Paranjpe P. Indian medicinal plants: forgotten healers: a guide to ayurvedic herbal medicine with identity, habitat, botany, photochemistry, ayurvedic properties, formulations & clinical usage: Chaukhamba Sanskrit Pratishthan; 2001.

452. Kuboyama T, Tohda C, Komatsu K. Neuritic regeneration and synaptic reconstruction induced by withanolide A. Br J Pharmacol. 2005; 144(7):961-71. doi:10.1038/sj.bjp.0706122

453. Dzoyem JP, Eloff JN. Anti-inflammatory, anticholinesterase and antioxidant activity of leaf extracts of twelve plants used traditionally to alleviate pain and inflammation in South Africa. J Ethnopharmacol. 2015; 160:194-201. doi:10.1016/j.jep.2014.11.034

454. Gelfand M. The traditional medical practitioner in Zimbabwe: his principles of practice and pharmacopoeia: Mambo Press; 1985.

455. York T. An ethnopharmacological study of plants used for treating respiratory infections in rural Maputaland [disstertation]. University of Zululand; 2012.

456. Altemimi A, Lakhssassi N, Baharlouei A, Watson DG, Lightfoot DA. Phytochemicals: Extraction, Isolation, and Identification of Bioactive Compounds from Plant Extracts. Plants (Basel). 2017; 6(4):42. doi:10.3390/plants6040042

457. Ingle KP, Deshmukh AG, Padole DA, Dudhare MS, Moharil MP, Khelurkar VC. Phytochemicals: Extraction methods, identification and detection of bioactive compounds from plant extracts. J Pharmacogn Phytochem. 2017; 6(1):32-6.

458. Mishra K, Ojha H, Chaudhury NK. Estimation of antiradical properties of antioxidants using DPPH assay: A critical review and results. Food Chem. 2012; 130(4):1036-43.

459. Contreras-Guzmán ES, Strong III FC. Determination of tocopherols (vitamin E) by reduction of cupric ion. J. AOAC Int. 1982; 65(5):1215-21.

460. Blois MS. Antioxidant determinations by the use of a stable free radical. Nat. 1958; 181(4617):1199-200.

461. Marc F, Davin A, Deglene-Benbrahim L, Ferrand C, Baccaunaud M, Fritsch P. Studies of several analytical methods for antioxidant potential evaluation in food. Med Sci (Paris). 2004; 20(4):458-63. doi:10.1051/medsci/2004204458

462. Miller NJ, Rice-Evans C, Davies MJ, Gopinathan V, Milner A. A novel method for measuring antioxidant capacity and its application to monitoring the antioxidant status in premature neonates. Clin Sci (Lond). 1993; 84(4):407-12. doi:10.1042/cs0840407

463. Li D, Li B, Ma Y, Sun X, Lin Y, Meng X. Polyphenols, anthocyanins, and flavonoids contents and the antioxidant capacity of various cultivars of highbush and half-high blueberries. J. Food Compos. Anal. 2017; 62:84-93.

464. Benzie IF, Strain JJ. The ferric reducing ability of plasma (FRAP) as a measure of "antioxidant power": the FRAP assay. Anal. Biochem. 1996; 239(1):70-6.

465. Istifli ES, Hüsunet MT, Ila HB. Cell division, cytotoxicity, and the assays used in the detection of cytotoxicity. Cytotoxicity-Definition, Identification, and Cytotoxic Compounds. 2019; 1

466. Riss T, Niles A, Moravec R, Karassina N, Vidugiriene J. Cytotoxicity assays: in vitro methods to measure dead cells. Assay guidance manual [internet]. 2019;

467. Altshuler B. Modeling of dose-response relationships. Environ Health Perspect. 1981; 42:23-7. doi:10.1289/ehp.814223

468. de Visser S, Truebel H. The pharmaceutical research and development productivity crisis: can exploratory clinical studies be of any help? JACC: Basic to Transl. Sci. 2021. p. 239-45.

469. Ben-Arye E, Samuels N, Goldstein LH, Mutafoglu K, Omran S, Schiff E, et al. Potential risks associated with traditional herbal medicine use in cancer care: A study of Middle Eastern oncology health care professionals. Cancer. 2016; 122(4):598-610. doi:10.1002/cncr.29796

470. Ruben RL. Cell culture for testing anticancer compounds. Advances in cell culture: Elsevier; 1988. p. 161-97.

471. Commandeur JN, Vermeulen NP. Cytotoxicity and cytoprotective activities of natural compounds. The case of curcumin. Xenobiotica. 1996; 26(7):667-80. doi:10.3109/00498259609046741

472. Alberts B. Molecular biology of the cell: Garland science; 2017.

473. Vichai V, Kirtikara K. Sulforhodamine B colorimetric assay for cytotoxicity screening. Nat Protoc. 2006; 1(3):1112-6. doi:10.1038/nprot.2006.179

474. Voigt W. Sulforhodamine B assay and chemosensitivity: Springer; 2005.

475. Soikkeli A, Sempio C, Kaukonen AM, Urtti A, Hirvonen J, Yliperttula M. Feasibility evaluation of 3 automated cellular drug screening assays on a robotic workstation. J Biomol Screen. 2010; 15(1):30-41. doi:10.1177/1087057109352236

476. Marston A. Role of advances in chromatographic techniques in phytochemistry. Phytochemistry. 2007; 68(22-24):2786-98. doi:10.1016/j.phytochem.2007.08.004

477. Brown PR. High-performance liquid chromatography. Past developments, present status, and future trends. Anal. Chem. 1990; 62(19):995A-1008A.

478. Strober W. Trypan blue exclusion test of cell viability. Curr Protoc Immunol. 1997; 21(1):A. 3B. 1-A. 3B. 2.

479. Vichai V, Kirtikara K. Sulforhodamine B colorimetric assay for cytotoxicity screening. Nat. Protoc. 2006; 1(3):1112-6. doi:10.1038/nprot.2006.179

480. Grkovic T, Akee RK, Thornburg CC, Trinh SK, Britt JR, Harris MJ, et al. National Cancer Institute (NCI) Program for Natural Products Discovery: Rapid Isolation and Identification of Biologically Active Natural Products from the NCI Prefractionated Library. ACS Chem Biol. 2020; 15(4):1104-14. doi:10.1021/acschembio.0c00139

481. Wang L, Wang Y. 2,4,6-Tri(2'-pyridyl)-1,3,5-triazine for determination of iron(II), Iron(III), and total iron contents on human palms. J Forensic Sci. 2023; 68(4):1317-24. doi:10.1111/1556-4029.15271

482. Muller P. Glossary of terms used in physical organic chemistry (IUPAC Recommendations 1994). Pure Appl. Chem. 1994; 66(5):1077-184.

483. Andersen O. Principles and recent developments in chelation treatment of metal intoxication. Chem Rev. 1999; 99(9):2683-710. doi:10.1021/cr980453a

484. Ghous T, Rasheed A, Yasin KA, Nasim F-u-H. Exploring anti-acetylcholinesterase, antioxidant and metal chelating activities of extracts of *Moringa oleifera* L. for possible prevention and cure of Alzheimer's. Scientific Research and Essays. 2014; 9(11):523-7.

485. Gulcin İ, Alwasel SH. Metal ions, metal chelators and metal chelating assay as antioxidant method. Processes. 2022; 10(1):132.

486. Kangwa TS, Hiss DC, Hussein AA, Ekpo OE, Omoruyi SI. In vitro neuroprotective effects of B*oophone disticha, Brunsvigia bosmaniae and Strumaria truncata* extracts in SH-SY5Y cells. S. Afr. J. Bot. 2024; 166:512-24.

487. Lepule KH. Assessment of the effect of selected African plants on an in vitro model of Parkinson's disease [dissertation]. University of Pretoria; 2017.

488. Lepule KH, Cordier W, Steenkamp P, Nell M, Steenkamp V. The ability of three African herbal remedies to offer protection against an in vitro model of Parkinson's disease. S. Afr. J. Bot. 2019; 126:121-31.

489. Kawpoomhae K, Sukma M, Ngawhirunpat T, Opanasopit P, Sripattanaporn A. Antioxidant and neuroprotective effects of standardized extracts of *Mangifera indica* leaf. Thai J. Pharm. Sci. 2010; 34(1)

490. Thambiraj J, Paulsamy S, Sevukaperumal R. Evaluation of in vitro antioxidant activity in the traditional medicinal shrub of western districts of Tamilnadu, India, *Acalypha fruticosa* Forssk.(Euphorbiaceae). Asian Pac. J. Trop. Biomed. 2012; 2(1):S127-S30.

491. Adedapo AA, Jimoh FO, Afolayan AJ, Masika PJ. Antioxidant activities and phenolic contents of the methanol extracts of the stems of *Acokanthera oppositifolia* and *Adenia gummifera*. BMC Complement Altern Med. 2008; 8(1):54. doi:10.1186/1472-6882-8-54

492. Pezzani R, Rubin B, Redaelli M, Radu C, Barollo S, Cicala MV, et al. The antiproliferative effects of ouabain and everolimus on adrenocortical tumor cells. Endocr J. 2014; 61(1):41-53. doi:10.1507/endocrj.ej13-0225

493. Lees GJ, Lehmann A, Sandberg M, Hamberger A. The neurotoxicity of ouabain, a sodium-potassium ATPase inhibitor, in the rat hippocampus. Neurosci Lett. 1990; 120(2):159-62. doi:10.1016/0304-3940(90)90027-7

494. Fouche G, Cragg GM, Pillay P, Kolesnikova N, Maharaj VJ, Senabe J. In vitro anticancer screening of South African plants. J Ethnopharmacol. 2008; 119(3):455-61. doi:10.1016/j.jep.2008.07.005

495. Saeed MEM, Meyer M, Hussein A, Efferth T. Cytotoxicity of South-African medicinal plants towards sensitive and multidrug-resistant cancer cells. J Ethnopharmacol. 2016; 186:209-23. doi:10.1016/j.jep.2016.04.005

496. Cordier W, Steenkamp V. Evaluation of four assays to determine cytotoxicity of selected crude medicinal plant extracts in vitro. Br J Pharm Res. 2015; 7:16-21.

497. Van Heerden F, Viljoen A, Mohoto S, Jäger A. A phytochemical investigation of *Craterocapsa tarsodes*, a plant used for the treatment of epilepsy by the Northern Sotho people of South Africa. S. Afr. J. Bot. 2002; 68(1):77-9.

498. Afolayan A, Jimoh F, Sofidiya M, Koduru S, Lewu F. Medicinal Potential of the Root of *Arctotis arctotoides*. Pharm. Biol. 2007; 45(6):486-93.

499. Saleh-e-In MM, Van Staden J. Ethnobotany, phytochemistry and pharmacology of *Arctotis arctotoides* (Lf) O. Hoffm.: a review. J. Ethnopharmacol. 2018; 220:294-320.

500. Nair JJ, Van Staden J. Traditional usage, phytochemistry and pharmacology of the South African medicinal plant *Boophone disticha* (Lf) Herb.(Amaryllidaceae). J. Ethnopharmacol. 2014; 151(1):12-26.

501. Risa A, Risa J, Adsersen A, Stafford G, Van Staden J, Jäger A, et al. Acetylcholinesterase inhibitory activity of plants used as memory-enhancers in traditional South African medicine. S. Afr. J. Bot. 2004; 70(4):664-6.

502. Padayachee B, Odun-Ayo F, Reddy L. Apoptotic effect of *Bulbine natalensis* and *Chlorophytum comosum* in myelogenous Leukemia K562 cell line. Braz J Biol. 2021; 84:e251336. doi:10.1590/1519-6984.251336

503. Van Wyk BE, Heerden F, Van Oudtshoorn B. Poisonous plants of South Africa: Briza Publications; 2002.

504. Bae JY, Ali Z, Wang YH, Chittiboyina AG, Zaki AA, Viljoen AM, et al. Anthraquinone-Based Specialized Metabolites from Rhizomes of *Bulbine natalensis*. J Nat Prod. 2019; 82(7):1893-901. doi:10.1021/acs.jnatprod.9b00187

505. Ntshanka NM, Ejidike IP, Mthunzi FM, Moloto MJ, Mubiayi KP. Investigation into the phytochemical profile, antioxidant and antibacterial potentials of *Combretum molle* and A*cacia mearnsii* leaf parts. Biomed. Pharmacol. J. 2020; 13(4):1683-94.

506. Dawe A, Pierre S, Tsala DE, Habtemariam S. Phytochemical constituents of *Combretum* Loefl. (Combretaceae). Pharmaceutical Crops. 2013; 4:38-59.

507. Botha C. Potential Health Risks Posed by Plant-Derived Cumulative Neurotoxic Bufadienolides in South Africa. Molecules. 2016; 21(3):348. doi:10.3390/molecules21030348

508. Roux WC. The antioxidant properties of the methanol extract of *Cotyledon orbiculata* L. var *orbiculata* (Haw.) DC. Leaves [disstertation]. North-West University; 2012.

509. Ndunda B. Phytochemistry and bioactivity investigations of three Kenyan *Croton* species [thesis]. University of Nairobi; 2014.

510. Frum Y, Viljoen AM. In vitro 5-lipoxygenase and anti-oxidant activities of South African medicinal plants commonly used topically for skin diseases. Skin Pharmacol Physiol. 2006; 19(6):329-35. doi:10.1159/000095253

511. Aderogba MA, Ndhlala AR, Van Staden J. Acetylcholinesterase inhibitors from *Croton sylvaticus* ethyl acetate leaf extract and their mutagenic effects. Nat. Prod. Commun. 2013; 8(6):1934578X1300800628.

512. Ivancheva S, Nikolova M, Tsvetkova R. Pharmacological activities and biologically active compounds of Bulgarian medicinal plants. Phytochemistry: Advances in Research. 2006; 37661:87-103.

513. Berkov S, Zayed R, Doncheva T. Alkaloid patterns in some varieties of *Datura stramonium*. Fitoterapia. 2006; 77(3):179-82. doi:10.1016/j.fitote.2006.01.002

514. Gaire BP, Subedi L. A review on the pharmacological and toxicological aspects of *Datura stramonium* L. J Integr Med. 2013; 11(2):73-9. doi:10.3736/jintegrmed2013016

515. Vaza JS, Bhalerao A. Phytochemistry, medicinal values and pharmacological potential of *Datura stramonium* L. review. IJPDA. 2018:540-4.

516. Sreenivasa S, Vinay K, Mohan N. Phytochemical analysis, antibacterial and antioxidant activity of leaf extract of *Datura stramonium*. nt. J. Sci. Res. 2012; 1(2):83-6.

517. Cogne A-L. Phytochemical investigation of plants used in African traditional medicine: *Dioscorea sylvatica* (Dioscoreaceae), *Urginea altissima* (Liliaceae), *Jamesbrittenia fodina* and *Jamesbrittenia elegantissima* (Scrophulariaceae) [thesis]. Université de Lausanne, Faculté des sciences; 2002.

518. Saleem H, Zengin G, Locatelli M, Mollica A, Ahmad I, Mahomoodally FM, et al. In vitro biological propensities and chemical profiling of *Euphorbia milii* Des Moul (Euphorbiaceae): A novel source for bioactive agents. Ind. Crop. Prod. 2019; 130:9-15.

519. Chohan TA, Sarfraz M, Rehman K, Muhammad T, Ghori MU, Khan KM, et al. Phytochemical profiling, antioxidant and antiproliferation potential of *Euphorbia milii* var.: Experimental analysis and in-silico validation. Saudi J Biol Sci. 2020; 27(11):3025-34. doi:10.1016/j.sjbs.2020.08.003

520. Tauchen J, Doskocil I, Caffi C, Lulekal E, Marsik P, Havlik J, et al. In vitro antioxidant and anti-proliferative activity of Ethiopian medicinal plant extracts. Ind. Crop. Prod. 2015; 74:671-9.

521. Gallo FR, Palazzino G, Federici E, Iurilli R, Monache FD, Chifundera K, et al. Oligomeric secoiridoid glucosides from *Jasminum abyssinicum*. Phytochemistry. 2006; 67(5):504-10. doi:10.1016/j.phytochem.2005.11.007

522. Tadiwos Y, Nedi T, Engidawork E. Analgesic and anti-inflammatory activities of 80% methanol root extract of *Jasminum abyssinicum* Hochst. ex. Dc. (Oleaceae) in mice. J Ethnopharmacol. 2017; 202:281-9. doi:10.1016/j.jep.2017.02.036

523. Chakuma N, Chipurura B, Muchuweti M, Chitindingu K, Bhebhe M, Chagonda L. Total phenolic content, free radical scavenging and antioxidant potential of *Lannea discolor* (Sond.) Engl bark and root extracts. JBAPN. 2015; 5(1):71-7.

524. Mwamatope B, Tembo D, Kampira E, Maliwichi-Nyirenda C, Ndolo V. Seasonal Variation of Phytochemicals in Four Selected Medicinal Plants. Pharmacogn. Res. 2021; 13(4)

525. Kabongo-Kayoka PN, Eloff JN, Obi CL, McGaw LJ. Antimycobacterial Activity and Low Cytotoxicity of Leaf Extracts of Some African Anacardiaceae Tree Species. Phytother. Res. 2016; 30(12):2001-11. doi:10.1002/ptr.5706

526. Shikanga E, Combrinck S, Regnier T. South African *Lippia* herbal infusions: Total phenolic content, antioxidant and antibacterial activities. S. Afr. J. Bot. 2010; 76(3):567-71.

527. Katerere DR, Graziani G, Thembo KM, Nyazema NZ, Ritieni A. Antioxidant activity of some African medicinal and dietary leafy African vegetables. Afr. J. Biotechnol. 2012; 11(17):4103-8.

528. Maroyi A. *Lippia javanica* (Burm.f.) Spreng.: Traditional and Commercial Uses and Phytochemical and Pharmacological Significance in the African and Indian Subcontinent. Evid Based Complement Alternat Med. 2017; 2017:6746071. doi:10.1155/2017/6746071

529. Bhebhe M, Chipurura B, Muchuweti M. Determination and comparison of phenolic compound content and antioxidant activity of selected local Zimbabwean herbal teas with exotic *Aspalathus linearis*. S. Afr. J. Bot. 2015; 100:213-8.

530. Bhebhe M, Füller TN, Chipurura B, Muchuweti M. Effect of solvent type on total phenolic content and free radical scavenging activity of black tea and herbal infusions. Food Anal. Methods. 2016; 9:1060-7.

531. Ayuko TA, Njau RN, Cornelius W, Leah N, Ndiege IO. In vitro antiplasmodial activity and toxicity assessment of plant extracts used in traditional malaria therapy in the Lake Victoria Region. Mem Inst Oswaldo Cruz. 2009; 104(5):689-94. doi:10.1590/s0074-02762009000500004

532. Clarkson C, Maharaj VJ, Crouch NR, Grace OM, Pillay P, Matsabisa MG, et al. In vitro antiplasmodial activity of medicinal plants native to or naturalised in South Africa. J Ethnopharmacol. 2004; 92(2-3):177-91. doi:10.1016/j.jep.2004.02.011

533. Nsuala BN, Enslin G, Viljoen A. "Wild cannabis": A review of the traditional use and phytochemistry of *Leonotis leonurus.* J Ethnopharmacol. 2015; 174:520-39.

534. He F, Lindqvist C, Harding WW. Leonurenones A-C: Labdane diterpenes from *Leonotis leonurus*. Phytochemistry. 2012; 83:168-72. doi:10.1016/j.phytochem.2012.07.014

535. Ling LT, Yap S-A, Radhakrishnan AK, Subramaniam T, Cheng HM, Palanisamy UD. Standardised *Mangifera indica* extract is an ideal antioxidant. Food Chem. 2009; 113(4):1154-9.

536. Quintana SE, Salas S, Garcia-Zapateiro LA. Bioactive compounds of mango (*Mangifera indica*): a review of extraction technologies and chemical constituents. J Sci Food Agric. 2021; 101(15):6186-92. doi:10.1002/jsfa.11455

537. Sultana B, Hussain Z, Asif M, Munir A. Investigation on the antioxidant activity of leaves, peels, stems bark, and kernel of mango (*Mangifera indica* L.). J Food Sci. 2012; 77(8):C849-52. doi:10.1111/j.1750-3841.2012.02807.x

538. Er HM, Cheng EH, Radhakrishnan AK. Anti-proliferative and mutagenic activities of aqueous and methanol extracts of leaves from *Pereskia bleo* (Kunth) DC (Cactaceae). J Ethnopharmacol. 2007; 113(3):448-56. doi:10.1016/j.jep.2007.06.026

539. Gulluce M, Sahin F, Sokmen M, Ozer H, Daferera D, Sokmen A, et al. Antimicrobial and antioxidant properties of the essential oils and methanol extract from *Mentha longifolia* L. ssp. longifolia. Food Chem. 2007; 103(4):1449-56.

540. Motamed SM, Naghibi F. Antioxidant activity of some edible plants of the Turkmen Sahra region in northern Iran. Food Chem. 2010; 119(4):1637-42.

541. Fathi F, Oryan S, Rafieian-Kopael M, Eidi A. Neuroprotective effect of pretreatment with *Mentha longifolia* L. extract on brain ischemia in the rat stroke model. Arch. Biol. Sci. 2015; 67(4):1151-63.

542. Lopez V, Martin S, Gomez-Serranillos MP, Carretero ME, Jager AK, Calvo MI. Neuroprotective and neurochemical properties of mint extracts. Phytother Res. 2010; 24(6):869-74. doi:10.1002/ptr.3037

543. Magama S, Lieta M, Asita A. Antioxidant and free radical scavenging properties of four plant species used in traditional medicine in Lesotho. J. Med. Plant Res. 2013; 2(3):170-8.

544. Bashir A, Hamburger M, Msonthi JD, Hostettmann K. Isoflavones and xanthones from *Polygala virgata*. Phytochemistry. 1992; 31(1):309-11.

545. Donnelly D, Boland G. Isoflavonoids and neoflavonoids: naturally occurring O-heterocycles. Natural Product Reports. 1995; 12(3):321-38.

546. Adewusi EA, Moodley N, Steenkamp V. Antioxidant and acetylcholinesterase inhibitory activity of selected southern African medicinal plants. S. Afr. J. Bot. 2011; 77(3):638-44.

547. McGaw LJ, Jager AK, van Staden J. Isolation of antibacterial fatty acids from *Schotia brachypetala*. Fitoterapia. 2002; 73(5):431-3. doi:10.1016/s0367-326x(02)00120-x

548. Sobeh M, ElHawary E, Peixoto H, Labib RM, Handoussa H, Swilam N, et al. Identification of phenolic secondary metabolites from *Schotia brachypetala* Sond. (Fabaceae) and demonstration

of their antioxidant activities in *Caenorhabditis elegans*. PeerJ. 2016; 4:e2404. doi:10.7717/peerj.2404

549. Stafford G, Pedersen P, Jäger A, Van Staden J. Monoamine oxidase inhibition by southern African traditional medicinal plants. S. Afr. J. Bot. 2007; 73(3):384-90.

550. Thakur A, Chun YS, October N, Yang HO, Maharaj V. Potential of South African medicinal plants targeting the reduction of Abeta42 protein as a treatment of Alzheimer's disease. J Ethnopharmacol. 2019; 231:363-73. doi:10.1016/j.jep.2018.11.034

551. Mekuriaw E, Mengistu E, Erdedo A, Mamo H. In Vitro Antibacterial Activity, Preliminary Phytochemical Screening Profile, and In Vivo Toxicity of Seven Traditional Medicinal Plants in Ethiopia. TCIM. 2021:398-413.

552. Jayaprakasam B, Zhang Y, Seeram NP, Nair MG. Growth inhibition of human tumor cell lines by withanolides from *Withania somnifera* leaves. Life Sci. 2003; 74(1):125-32. doi:10.1016/j.lfs.2003.07.007

553. Ahmad M, Saleem S, Ahmad AS, Ansari MA, Yousuf S, Hoda MN, et al. Neuroprotective effects of *Withania somnifera* on 6-hydroxydopamine induced Parkinsonism in rats. Hum Exp Toxicol. 2005; 24(3):137-47. doi:10.1191/0960327105ht509oa

554. Saykally JN, Hatic H, Keeley KL, Jain SC, Ravindranath V, Citron BA. *Withania somnifera* Extract Protects Model Neurons from In Vitro Traumatic Injury. Cell Transplant. 2017; 26(7):1193-201. doi:10.1177/0963689717714320

555. Pandey A, Bani S, Dutt P, Kumar Satti N, Avtar Suri K, Nabi Qazi G. Multifunctional neuroprotective effect of Withanone, a compound from *Withania somnifera* roots in alleviating cognitive dysfunction. Cytokine. 2018; 102:211-21. doi:10.1016/j.cyto.2017.10.019

556. Maphanga VB, Skalicka-Wozniak K, Budzynska B, Enslin GM, Viljoen AM. Screening selected medicinal plants for potential anxiolytic activity using an in vivo zebrafish model. Psychopharmacology (Berl). 2020; 237(12):3641-52. doi:10.1007/s00213-020-05642-5

557. Fouché G, Senabe J, Khorombi E, Kolesnikoya N, Maharaj V, Nthambeleni R. High throughput screening of South African plants for anti-cancer properties [poster]. CSIR, 2008;

558. Vakele Y, Odun-Ayo F, Reddy L. In vitro antioxidant and cytotoxicity activities of selected indigenous South African medicinal plants. Afr Health Sci. 2022; 22(1):395-403. doi:10.4314/ahs.v22i1.48

559. Joshi T, Deepa PR, Sharma PK. Effect of Different Proportions of Phenolics on Antioxidant Potential: Pointers for Bioactive Synergy/Antagonism in Foods and Nutraceuticals. Proc Natl Acad Sci India Sect B Biol Sci. 2022; 92(4):939-46. doi:10.1007/s40011-022-01396-6

560. Plaza M, Pozzo T, Liu J, Gulshan Ara KZ, Turner C, Nordberg Karlsson E. Substituent effects on in vitro antioxidizing properties, stability, and solubility in flavonoids. J Agric Food Chem. 2014; 62(15):3321-33. doi:10.1021/jf405570u

561. Sannigrahi S, Kanti Mazuder U, Kumar Pal D, Parida S, Jain S. Antioxidant Potential of Crude Extract and Different Fractions of *Enhydra fluctuans* Lour. Iran J Pharm Res. 2010; 9(1):75-82.

562. Wojtunik-Kulesza KA. Approach to Optimization of FRAP Methodology for Studies Based on Selected Monoterpenes. Molecules. 2020; 25(22):5267. doi:10.3390/molecules25225267

563. Sun X, Sarteshnizi RA, Udenigwe CC. Recent advances in protein–polyphenol interactions focusing on structural properties related to antioxidant activities. Current Opinion in Food Science. 2022; 45:100840.

564. Oliviero T, Capuano E, Cammerer B, Fogliano V. Influence of roasting on the antioxidant activity and HMF formation of a cocoa bean model systems. J Agric Food Chem. 2009; 57(1):147-52. doi:10.1021/jf802250j

565. Egbujor MC, Olaniyan OT, Emeruwa CN, Saha S, Saso L, Tucci P. An insight into role of amino acids as antioxidants via NRF2 activation. Amino Acids. 2024; 56(1):23. doi:10.1007/s00726-024-03384-8

566. Phan MAT, Paterson J, Bucknall M, Arcot J. Interactions between phytochemicals from fruits and vegetables: Effects on bioactivities and bioavailability. Crit Rev Food Sci Nutr. 2018; 58(8):1310-29. doi:10.1080/10408398.2016.1254595

567. Costa M, Losada-Barreiro S, Paiva-Martins F, Bravo-Diaz C. Polyphenolic Antioxidants in Lipid Emulsions: Partitioning Effects and Interfacial Phenomena. Foods. 2021; 10(3):539. doi:10.3390/foods10030539

568. Marković Z. Study of the mechanisms of antioxidative action of different antioxidants. JSSCM. 2016; 10(1):135-50.

569. Porter NA. A perspective on free radical autoxidation: the physical organic chemistry of polyunsaturated fatty acid and sterol peroxidation. J Org Chem. 2013; 78(8):3511-24. doi:10.1021/jo4001433

570. Degirmenci I, Coote ML. Comparison of Thiyl, Alkoxyl, and Alkyl Radical Addition to Double Bonds: The Unusual Contrasting Behavior of Sulfur and Oxygen Radical Chemistry. J Phys Chem A. 2016; 120(10):1750-5. doi:10.1021/acs.jpca.6b00538

571. Farhan H, Rammal H, Hijazi A, Hamad H, Daher A, Reda M, et al. In vitro antioxidant activity of ethanolic and aqueous extracts from crude *Malva parviflora* L. grown in Lebanon. AJPCR. 2012; 5(3):234-8.

572. Ranjbaran P, Moradkhani S. Iron Chelating Activity of *Nepeta Crispa* Willd., an Endemic Plant in the West of Iran. Avicenna J Med Biochem. 2022; 10(1):65-70.

573. Zhao X, Wang X, Pang Y. Phytochemicals Targeting Ferroptosis: Therapeutic Opportunities and Prospects for Treating Breast Cancer. Pharmaceuticals (Basel). 2022; 15(11):1360. doi:10.3390/ph15111360

574. Atanasov AG, Waltenberger B, Pferschy-Wenzig EM, Linder T, Wawrosch C, Uhrin P, et al. Discovery and resupply of pharmacologically active plant-derived natural products: A review. Biotechnol Adv. 2015; 33(8):1582-614. doi:10.1016/j.biotechadv.2015.08.001

575. Koehn FE, Carter GT. The evolving role of natural products in drug discovery. Nat Rev Drug Discov. 2005; 4(3):206-20. doi:10.1038/nrd1657

576. Zhou B, Xiao JF, Tuli L, Ressom HW. LC-MS-based metabolomics. Mol Biosyst. 2012; 8(2):470-81. doi:10.1039/c1mb05350g

577. Murayama C, Kimura Y, Setou M. Imaging mass spectrometry: principle and application. Biophys Rev. 2009; 1(3):131. doi:10.1007/s12551-009-0015-6

578. Chassagne F, Cabanac G, Hubert G, David B, Marti G. The landscape of natural product diversity and their pharmacological relevance from a focus on the Dictionary of Natural Products®. Phytochem. Rev. 2019; 18:601-22.

579. Stern S, Potter T, Neun B. NCL method GTA-4; Hep G2 hepatocyte lipid peroxidation assay. Nanotechnology Characterization Laboratory, National Cancer Institute-Frederick. 2010;

580. De Leon JAD, Borges CR. Evaluation of oxidative stress in biological samples using the thiobarbituric acid reactive substances assay. JoVE. 2020; (159):e61122.

581. Ng NS, Ooi L. A Simple Microplate Assay for Reactive Oxygen Species Generation and Rapid Cellular Protein Normalization. Bio Protoc. 2021; 11(1):e3877. doi:10.21769/BioProtoc.3877

582. Rastogi A, Timme-Laragy AR. Using Monochlorobimane to Visualize Glutathione Utilization in the Developing Zebrafish (*Danio rerio*) Embryo. Curr Protoc. 2021; 1(2):e124. doi:10.1002/cpz1.24

583. Thabet AA, Ayoub IM, Youssef FS, Al-Sayed E, Efferth T, Singab ANB. Phytochemistry, structural diversity, biological activities and pharmacokinetics of iridoids isolated from various genera of the family Scrophulariaceae Juss. API. 2022; 2(3):100287.

584. Molahloe TS. Phytochemical and bioactivity investigations on *Aptosimum elongatum* Engl. Extracts [disstertation]. University of the Free State; 2019.

585. Yao T, Feng K, Xie M, Barros J, Tschaplinski TJ, Tuskan GA, et al. Phylogenetic Occurrence of the Phenylpropanoid Pathway and Lignin Biosynthesis in Plants. Front Plant Sci. 2021; 12:704697. doi:10.3389/fpls.2021.704697

586. Colegate SM, Molyneux RJ. Bioactive natural products: detection, isolation, and structural determination: CRC press; 2007.

587. Lykakis IN, Zaravinos IP, Raptis C, Stratakis M. Divergent synthesis of the co-isolated mycotoxins longianone, isopatulin, and (Z)-ascladiol via furan oxidation. J Org Chem. 2009; 74(16):6339-42. doi:10.1021/jo900855e

588. Odeyemi SW, Afolayan AJ. Identification of Antidiabetic Compounds from Polyphenolic-rich Fractions of *Bulbine abyssinica* A. Rich Leaves. Pharmacognosy Res. 2018; 10(1):72-80. doi:10.4103/pr.pr_55_17

589. Bezabih M, Abegaz BM. 4′-Demethylknipholone from aerial parts of *Bulbine capitata*. Phytochemistry. 1998; 48(6):1071-3.

590. Bodede O, Prinsloo G. Ethnobotany, phytochemistry and pharmacological significance of the genus *Bulbine* (Asphodelaceae). J Ethnopharmacol. 2020; 260:112986. doi:10.1016/j.jep.2020.112986

591. Bashir A, Hamburger M, Msonthi JD, Hostettmann K. Sinapic acid esters from *Polygala virgata*. Phytochemistry. 1993; 32(3):741-5. doi:10.1016/s0031-9422(00)95164-1

592. Ghosal S, Chauhan RP, Srivastava RS. Two new aryl naphthalide lignans from *Polygala chinensis*. Phytochemistry. 1974; 13(9):1933-6.

593. Silva DF, Alves CQ, Brandao HN, David JM, David JP, Silva RL, et al. Poligalen, a new coumarin from *Polygala boliviensis*, reduces the release of TNF and IL-6 independent of NF-kB downregulation. Fitoterapia. 2016; 113:139-43. doi:10.1016/j.fitote.2016.07.021

594. Tizziani T, Venzke D, Ruani AP, Marques LB, Prazeres PHDM, Souza-Fagundes EM, et al. Antitumor screening of crude extracts of ten medicinal plants of *Polygala* genus from Southern Brazil. J. Appl. Pharm. Sci. 2017; 7(10):079-83.

595. Lacaille-Dubois MA, Delaude C, Mitaine-Offer AC. A review on the phytopharmacological studies of the genus *Polygala*. J Ethnopharmacol. 2020; 249:112417. doi:10.1016/j.jep.2019.112417

596. Chabowska G, Barg E, Wojcicka A. Biological Activity of Naturally Derived Naphthyridines. Molecules. 2021; 26(14):4324. doi:10.3390/molecules26144324

597. Aly SH, Elissawy AM, Eldahshan OA, Elshanawany MA, Efferth T, Singab ANB. The pharmacology of the genus *Sophora* (Fabaceae): An updated review. PYTOEY. 2019; 64:153070. doi:10.1016/j.phymed.2019.153070

598. Wink M. Evolution of secondary metabolites in legumes (Fabaceae). S. Afr. J. Bot. 2013; 89:164-75.

599. Piasecka A, Jedrzejczak-Rey N, Bednarek P. Secondary metabolites in plant innate immunity: conserved function of divergent chemicals. New Phytol. 2015; 206(3):948-64. doi:10.1111/nph.13325

600. Bagni N, Tassoni A. Biosynthesis, oxidation and conjugation of aliphatic polyamines in higher plants. Amino Acids. 2001; 20(3):301-17. doi:10.1007/s007260170046

601. Boonen J, Bronselaer A, Nielandt J, Veryser L, De Tre G, De Spiegeleer B. Alkamid database: Chemistry, occurrence and functionality of plant N-alkylamides. J Ethnopharmacol. 2012; 142(3):563-90. doi:10.1016/j.jep.2012.05.038

602. Vadnere G, Patil A, Wagh S, Jain S. In vitro free radical scavenging and antioxidant activity of Cicer arietinum L.(Fabaceae). Int J PharmTech Res. 2012; 4(1):343-50.

603. El-Seedi HR, Taher EA, Sheikh BY, Anjum S, Saeed A, AlAjmi MF, et al. Hydroxycinnamic acids: Natural sources, biosynthesis, possible biological activities, and roles in Islamic medicine. Stud. Nat. Prod. Chem. 2018; 55:269-92.

604. Khalil AM, Sabry OM, El-Askary HI, El Zalabani SM, Fayek NM. Acylated polyphenolics of family Fabaceae: distribution, chemodiversity, and bioactivity, a comprehensive review. IJFST. 2023; 58(3):1028-36.

605. Rodriguez JL, Berrios P, Clavo ZM, Marin-Bravo M, Inostroza-Ruiz L, Ramos-Gonzalez M, et al. Chemical Characterization, Antioxidant Capacity and Anti-Oxidative Stress Potential of South American Fabaceae *Desmodium tortuosum*. Nutrients. 2023; 15(3):746. doi:10.3390/nu15030746

606. Siracusa L, Napoli E, Ruberto G. Novel Chemical and Biological Insights of Inositol Derivatives in Mediterranean Plants. Molecules. 2022; 27(5):1525. doi:10.3390/molecules27051525

607. Wishart DS, Guo A, Oler E, Wang F, Anjum A, Peters H, et al. HMDB 5.0: the Human Metabolome Database for 2022. Nucleic Acids Res. 2022; 50(D1):D622-D31. doi:10.1093/nar/gkab1062

608. Leu YL, Hwang TL, Kuo PC, Liou KP, Huang BS, Chen GF. Constituents from *Vigna vexillata* and their anti-inflammatory activity. Int J Mol Sci. 2012; 13(8):9754-68. doi:10.3390/ijms13089754

609. Ouissem Bensaid S, Carbone M, Palomba L, Bicha S, Bentamene A, Carannante A, et al. First Occurrence of Megastigmane Glucosides in a Plant of *Retama* Genus. Chem Biodivers. 2022; 19(11):e202200675. doi:10.1002/cbdv.202200675

610. Sanchez-Iglesias S, Rey P, Mendez-Alvarez E, Labandeira-Garcia JL, Soto-Otero R. Time-course of brain oxidative damage caused by intrastriatal administration of 6-hydroxydopamine in a rat model of Parkinson's disease. Neurochem Res. 2007; 32(1):99-105. doi:10.1007/s11064-006-9232-6

611. Kumar R, Agarwal AK, Seth PK. Free radical-generated neurotoxicity of 6-hydroxydopamine. J Neurochem. 1995; 64(4):1703-7. doi:10.1046/j.1471-4159.1995.64041703.x

612. Shi Z, Lu Z, Zhao Y, Wang Y, Zhao-Wilson X, Guan P, et al. Neuroprotective effects of aqueous extracts of *Uncaria tomentosa*: Insights from 6-OHDA induced cell damage and transgenic *Caenorhabditis elegans* model. Neurochem Int. 2013; 62(7):940-7. doi:10.1016/j.neuint.2013.03.001

613. Chang G-C, Kim H-C, Wie M-B. Neuroprotective effects of resveratrol on 6-hydroxydopamine-induced damage of SH-SY5Y cell line. Korean J Vet Res. 2014; 54(1):1-6.

614. Takahashi M, Tsuchiya J, Niki E, Urano S. Action of vitamin E as antioxidant in phospholipid liposomal membranes as studied by spin label technique. J Nutr Sci Vitaminol (Tokyo). 1988; 34(1):25-34. doi:10.3177/jnsv.34.25

615. Niki E, Noguchi N. Evaluation of antioxidant capacity. What capacity is being measured by which method? IUBMB Life. 2000; 50(4-5):323-9. doi:10.1080/713803736

616. Gotoh N, Noguchi N, Tsuchiya J, Morita K, Sakai H, Shimasaki H, et al. Inhibition of oxidation of low density lipoprotein by vitamin E and related compounds. Free Radic Res. 1996; 24(2):123-34. doi:10.3109/10715769609088008

617. Dix TA, Aikens J. Mechanisms and biological relevance of lipid peroxidation initiation. Chem Res Toxicol. 1993; 6(1):2-18. doi:10.1021/tx00031a001

618. Porter NA, Caldwell SE, Mills KA. Mechanisms of free radical oxidation of unsaturated lipids. Lipids. 1995; 30(4):277-90. doi:10.1007/BF02536034

619. Kuhn H, Banthiya S, van Leyen K. Mammalian lipoxygenases and their biological relevance. Biochim Biophys Acta. 2015; 1851(4):308-30. doi:10.1016/j.bbalip.2014.10.002

620. Cordier W, Steenkamp P, Steenkamp V. Cytostatic and cytotoxic effects of a hot water and methanol extract of *Acokanthera oppositifolia* in HepG2 hepatocarcinoma cells. J Ethnopharmacol. 2023; 314:116617. doi:10.1016/j.jep.2023.116617

621. Maestri D, Nepote V, Lamarque A, Zygadlo J. Natural products as antioxidants. Phytochem. 2006:105-35.

622. Robak J, Shridi F, Wolbis M, Krolikowska M. Screening of the influence of flavonoids on lipoxygenase and cyclooxygenase activity, as well as on nonenzymic lipid oxidation. Pol J Pharmacol Pharm. 1988; 40(5):451-8.

623. Brown JE, Rice-Evans CA. Luteolin-rich artichoke extract protects low density lipoprotein from oxidation in vitro. Free Radic Res. 1998; 29(3):247-55. doi:10.1080/10715769800300281

624. Li Z, Moalin M, Zhang M, Vervoort L, Hursel E, Mommers A, et al. The Flow of the Redox Energy in Quercetin during Its Antioxidant Activity in Water. Int J Mol Sci. 2020; 21(17):6015. doi:10.3390/ijms21176015

625. Prior RL, Wu X, Schaich K. Standardized methods for the determination of antioxidant capacity and phenolics in foods and dietary supplements. J Agric Food Chem. 2005; 53(10):4290-302. doi:10.1021/jf0502698

626. Valgimigli L. Lipid Peroxidation and Antioxidant Protection. Biomolecules. 2023; 13(9):1291. doi:10.3390/biom13091291

627. Heijnen CG, Haenen GR, Oostveen RM, Stalpers EM, Bast A. Protection of flavonoids against lipid peroxidation: the structure activity relationship revisited. Free Radic Res. 2002; 36(5):575-81. doi:10.1080/10715760290025951

628. Sroka Z, Sowa A, Dryś A. Inhibition of lipoxygenase and peroxidase reaction by some flavonols and flavones: the structure-activity relationship. Natural Product Communications. 2017; 12(11):1934578X1701201111.

629. Shah R, Shchepinov MS, Pratt DA. Resolving the Role of Lipoxygenases in the Initiation and Execution of Ferroptosis. ACS Cent Sci. 2018; 4(3):387-96. doi:10.1021/acscentsci.7b00589

630. Steenkamp V, Grimmer H, Semano M, Gulumian M. Antioxidant and genotoxic properties of South African herbal extracts. Mutat Res. 2005; 581(1-2):35-42. doi:10.1016/j.mrgentox.2004.10.009

631. Di Stasi LC. Coumarin Derivatives in Inflammatory Bowel Disease. Molecules. 2021; 26(2):422. doi:10.3390/molecules26020422

632. Venzke D, Carvalho FK, Ruani AP, Oliveira AS, Brighente I, Micke GA, et al. PAMPA permeability, acetylcholinesterase inhibition and antioxidant activity of pyranoisoflavones from *Polygala molluginifolia* (polygalaceae). J. Braz. Chem. Soc. 2013; 24:1991-7.

633. Chao X, Zhou J, Chen T, Liu W, Dong W, Qu Y, et al. Neuroprotective effect of osthole against acute ischemic stroke on middle cerebral ischemia occlusion in rats. Brain Res. 2010; 1363:206-11. doi:10.1016/j.brainres.2010.09.052

634. Panda SS, Chand M, Sakhuja R, Jain SC. Xanthones as potential antioxidants. Curr Med Chem. 2013; 20(36):4481-507. doi:10.2174/09298673113209990144

635. Santos CM, Freitas M, Ribeiro D, Gomes A, Silva AM, Cavaleiro JA, et al. 2,3-diarylxanthones as strong scavengers of reactive oxygen and nitrogen species: a structure-activity relationship study. Bioorg Med Chem. 2010; 18(18):6776-84. doi:10.1016/j.bmc.2010.07.044

636. Amorati R, Baschieri A, Cowden A, Valgimigli L. The Antioxidant Activity of Quercetin in Water Solution. Biomimetics (Basel). 2017; 2(3):9. doi:10.3390/biomimetics2030009

637. Jaisin Y, Ratanachamnong P, Kuanpradit C, Khumpum W, Suksamrarn S. Protective effects of gamma-mangostin on 6-OHDA-induced toxicity in SH-SY5Y cells. Neurosci Lett. 2018; 665:229-35. doi:10.1016/j.neulet.2017.11.059

638. Kim DW, Lee KT, Kwon J, Lee HJ, Lee D, Mar W. Neuroprotection against 6-OHDA-induced oxidative stress and apoptosis in SH-SY5Y cells by 5,7-Dihydroxychromone: Activation of the Nrf2/ARE pathway. Life Sci. 2015; 130:25-30. doi:10.1016/j.lfs.2015.02.026

639. Guo S, Bezard E, Zhao B. Protective effect of green tea polyphenols on the SH-SY5Y cells against 6-OHDA induced apoptosis through ROS-NO pathway. Free Radic Biol Med. 2005; 39(5):682-95. doi:10.1016/j.freeradbiomed.2005.04.022

640. Dziedzic SZ, Hudson BJ. Polyhydroxy chalcones and flavanones as antioxidants for edible oils. Food Chem. 1983; 12(3):205-12.

641. Mazzone G, Malaj N, Galano A, Russo N, Toscano M. Antioxidant properties of several coumarin–chalcone hybrids from theoretical insights. RSC Advances. 2015; 5(1):565-75.

642. Sharma P, Chaurasia S. Evaluation of total phenolic, flavonoid contents and antioxidant activity of *Acokanthera oppositifolia* and *Leucaena leucocephala*. Int J Pharmacogn Phytochem Res. 2015; 7:175-80.

643. Razzaghi-Asl N, Garrido J, Khazraei H, Borges F, Firuzi O. Antioxidant properties of hydroxycinnamic acids: a review of structure- activity relationships. Curr Med Chem. 2013; 20(36):4436-50. doi:10.2174/09298673113209990141

644. Kang KA, Piao MJ, Ryu YS, Hyun YJ, Park JE, Shilnikova K, et al. Luteolin induces apoptotic cell death via antioxidant activity in human colon cancer cells. Int J Oncol. 2017; 51(4):1169-78. doi:10.3892/ijo.2017.4091

645. Cotelle N, Bernier JL, Catteau JP, Pommery J, Wallet JC, Gaydou EM. Antioxidant properties of hydroxy-flavones. Free Radic Biol Med. 1996; 20(1):35-43. doi:10.1016/0891-5849(95)02014-4

646. Filipsky T, Riha M, Macakova K, Anzenbacherova E, Karlickova J, Mladenka P. Antioxidant effects of coumarins include direct radical scavenging, metal chelation and inhibition of ROS-producing enzymes. Curr Top Med Chem. 2015; 15(5):415-31. doi:10.2174/1568026615666150206152233

647. Evans BE, Rittle KE, Bock MG, DiPardo RM, Freidinger RM, Whitter WL, et al. Methods for drug discovery: development of potent, selective, orally effective cholecystokinin antagonists. J Med Chem. 1988; 31(12):2235-46. doi:10.1021/jm00120a002

648. Fernandas ER, Carvalho FD, Remião FG, Bastos ML, Pinto MM, Gottlieb OR. Hepatoprotective activity of xanthones and xanthonolignoids against tert-butylhydroperoxide-induced toxicity in isolated rat hepatocytes—comparison with silybin. Pharmaceutical research. 1995; 12:1756-60.

649. Gnerre C, Thull U, Gaillard P, Carrupt PA, Testa B, Fernandes E, et al. Natural and synthetic xanthones as monoamine oxidase inhibitors: biological assay and 3D-QSAR. Helv. Chim. Acta. 2001; 84(3):552-70.

650. Hashim NM, Rahmani M, Ee GCL, Sukari MA, Yahayu M, Amin MAM, et al. Antioxidant, antimicrobial and tyrosinase inhibitory activities of xanthones isolated from *Artocarpus obtusus* FM Jarrett. Molecules. 2012; 17(5):6071-82.

651. Tirmenstein MA, Hu CX, Scicchitano MS, Narayanan PK, McFarland DC, Thomas HC, et al. Effects of 6-hydroxydopamine on mitochondrial function and glutathione status in SH-SY5Y human neuroblastoma cells. Toxicology in Vitro. 2005; 19(4):471-9.

652. Glinka YY, Youdim MB. Inhibition of mitochondrial complexes I and IV by 6-hydroxydopamine. Eur J Pharmacol. 1995; 292(3-4):329-32. doi:10.1016/0926-6917(95)90040-3

653. Simoes RF, Oliveira PJ, Cunha-Oliveira T, Pereira FB. Evaluation of 6-Hydroxydopamine and Rotenone In Vitro Neurotoxicity on Differentiated SH-SY5Y Cells Using Applied Computational Statistics. Int J Mol Sci. 2022; 23(6):3009. doi:10.3390/ijms23063009

654. Hirst J, King MS, Pryde KR. The production of reactive oxygen species by complex I. Portland Press Ltd.; 2008.

655. Lee HC, Yin PH, Lu CY, Chi CW, Wei YH. Increase of mitochondria and mitochondrial DNA in response to oxidative stress in human cells. Biochem J. 2000; 348 Pt 2(Pt 2):425-32.

656. Iglesias-Gonzalez J, Sanchez-Iglesias S, Mendez-Alvarez E, Rose S, Hikima A, Jenner P, et al. Differential toxicity of 6-hydroxydopamine in SH-SY5Y human neuroblastoma cells and rat brain mitochondria: protective role of catalase and superoxide dismutase. Neurochem Res. 2012; 37(10):2150-60. doi:10.1007/s11064-012-0838-6

657. Wernicke C, Hellmann J, Zieba B, Kuter K, Ossowska K, Frenzel M, et al. 9-Methyl-beta-carboline has restorative effects in an animal model of Parkinson's disease. Pharmacol Rep. 2010; 62(1):35-53. doi:10.1016/s1734-1140(10)70241-3

658. Bernardi P. Mitochondrial transport of cations: channels, exchangers, and permeability transition. Physiol Rev. 1999; 79(4):1127-55. doi:10.1152/physrev.1999.79.4.1127

659. Griffith OW. Biologic and pharmacologic regulation of mammalian glutathione synthesis. Free Radic Biol Med. 1999; 27(9-10):922-35. doi:10.1016/s0891-5849(99)00176-8

660. Oda T, Sadakata N, Komatsu N, Muramatsu T. Specific Efflux of Glutathione from the Basolateral Membrance Domain in Polarized MDCK Cells during Ricin-Induced Apoptosis. J. Biochem. 1999; 126(4):715-21.

661. Mattson DM, Ahmad IM, Dayal D, Parsons AD, Aykin-Burns N, Li L, et al. Cisplatin combined with zidovudine enhances cytotoxicity and oxidative stress in human head and neck cancer cells via a thiol-dependent mechanism. Free Radic Biol Med. 2009; 46(2):232-7. doi:10.1016/j.freeradbiomed.2008.10.023

662. Meister A. On the discovery of glutathione. Trends Biochem Sci. 1988; 13(5):185-8. doi:10.1016/0968-0004(88)90148-x

663. Dixon SJ, Patel DN, Welsch M, Skouta R, Lee ED, Hayano M, et al. Pharmacological inhibition of cystine-glutamate exchange induces endoplasmic reticulum stress and ferroptosis. Elife. 2014; 3:e02523. doi:10.7554/eLife.02523

664. Zhao Y, Seefeldt T, Chen W, Wang X, Matthees D, Hu Y, et al. Effects of glutathione reductase inhibition on cellular thiol redox state and related systems. Arch Biochem Biophys. 2009; 485(1):56-62. doi:10.1016/j.abb.2009.03.001

665. Testa B, Kramer SD. The biochemistry of drug metabolism--an introduction: part 4. reactions of conjugation and their enzymes. Chem Biodivers. 2008; 5(11):2171-336. doi:10.1002/cbdv.200890199

666. Moskaug JO, Carlsen H, Myhrstad MC, Blomhoff R. Polyphenols and glutathione synthesis regulation. Am J Clin Nutr. 2005; 81(1 Suppl):277S-83S. doi:10.1093/ajcn/81.1.277S

667. Caesar LK, Cech NB. Synergy and antagonism in natural product extracts: when 1 + 1 does not equal 2. Nat Prod Rep. 2019; 36(6):869-88. doi:10.1039/c9np00011a

668. Wenlock MC, Barton P. In silico physicochemical parameter predictions. Mol Pharm. 2013; 10(4):1224-35. doi:10.1021/mp300537k

669. Soldin OP, Mattison DR. Sex differences in pharmacokinetics and pharmacodynamics. Clin Pharmacokinet. 2009; 48(3):143-57. doi:10.2165/00003088-200948030-00001

670. Mangoni AA, Jackson SH. Age-related changes in pharmacokinetics and pharmacodynamics: basic principles and practical applications. Br J Clin Pharmacol. 2004; 57(1):6-14. doi:10.1046/j.1365-2125.2003.02007.x

671. Benet LZ, Kroetz D, Sheiner L, Hardman J, Limbird L. Pharmacokinetics: the dynamics of drug absorption, distribution, metabolism, and elimination. Goodman and Gilman's the pharmacological basis of therapeutics. 1996; 3:e27.

672. Martinez MN, Amidon GL. A mechanistic approach to understanding the factors affecting drug absorption: a review of fundamentals. J Clin Pharmacol. 2002; 42(6):620-43. doi:10.1177/00970002042006005

673. Lawrence XY, Lipka E, Crison JR, Amidon GL. Transport approaches to the biopharmaceutical design of oral drug delivery systems: prediction of intestinal absorption. Advanced drug delivery reviews. 1996; 19(3):359-76.

674. Lobenberg R, Amidon GL. Modern bioavailability, bioequivalence and biopharmaceutics classification system. New scientific approaches to international regulatory standards. Eur J Pharm Biopharm. 2000; 50(1):3-12. doi:10.1016/s0939-6411(00)00091-6

675. Pardridge WM. Blood-brain barrier biology and methodology. J Neurovirol. 1999; 5(6):556-69. doi:10.3109/13550289909021285

676. Kadry H, Noorani B, Cucullo L. A blood-brain barrier overview on structure, function, impairment, and biomarkers of integrity. Fluids Barriers CNS. 2020; 17(1):69. doi:10.1186/s12987-020-00230-3

677. Wager TT, Hou X, Verhoest PR, Villalobos A. Moving beyond rules: the development of a central nervous system multiparameter optimization (CNS MPO) approach to enable alignment of druglike properties. ACS Chem Neurosci. 2010; 1(6):435-49. doi:10.1021/cn100008c

678. Hitchcock SA. Blood-brain barrier permeability considerations for CNS-targeted compound library design. Curr Opin Chem Biol. 2008; 12(3):318-23. doi:10.1016/j.cbpa.2008.03.019

679. Clark DE. In silico prediction of blood-brain barrier permeation. Drug Discov Today. 2003; 8(20):927-33. doi:10.1016/s1359-6446(03)02827-7

680. Mikitsh JL, Chacko AM. Pathways for small molecule delivery to the central nervous system across the blood-brain barrier. Perspect Medicin Chem. 2014; 6:11-24. doi:10.4137/PMC.S13384

681. Ekins S, Rose J. In silico ADME/Tox: the state of the art. J Mol Graph Model. 2002; 20(4):305-9. doi:10.1016/s1093-3263(01)00127-9

682. Wrighton S, Silber P. Screening studies for metabolism and toxicology. Scientific strategies for accelerated drug discovery. 1996:4.1-4.18.

683. Li H, Yap CW, Ung CY, Xue Y, Li ZR, Han LY, et al. Machine learning approaches for predicting compounds that interact with therapeutic and ADMET related proteins. J Pharm Sci. 2007; 96(11):2838-60. doi:10.1002/jps.20985

684. Sun D, Gao W, Hu H, Zhou S. Why 90% of clinical drug development fails and how to improve it? Acta Pharmaceutica Sinica B. 2022; 12(7):3049-62.

685. Gleeson MP, Modi S, Bender A, Robinson RL, Kirchmair J, Promkatkaew M, et al. The challenges involved in modeling toxicity data in silico: a review. Curr Pharm Des. 2012; 18(9):1266-91. doi:10.2174/138161212799436359

686. Doogue MP, Polasek TM. The ABCD of clinical pharmacokinetics. Sage Publications Sage UK: London, England; 2013. p. 5-7.

687. Jain AN. Virtual screening in lead discovery and optimization. Curr Opin Drug Discov Devel. 2004; 7(4):396-403.

688. Kitchen DB, Decornez H, Furr JR, Bajorath J. Docking and scoring in virtual screening for drug discovery: methods and applications. Nat Rev Drug Discov. 2004; 3(11):935-49. doi:10.1038/nrd1549

689. Das DR, Kumar D, Kumar P, Dash BP. Molecular docking and its application in search of antisickling agent from Carica papaya. J. Appl. Biol. Biotechnol. 2020; 8(01):105-16.

690. Daina A, Michielin O, Zoete V. SwissADME: a free web tool to evaluate pharmacokinetics, drug-likeness and medicinal chemistry friendliness of small molecules. Sci Rep. 2017; 7(1):42717. doi:10.1038/srep42717

691. Ertl P, Rohde B, Selzer P. Fast calculation of molecular polar surface area as a sum of fragment-based contributions and its application to the prediction of drug transport properties. J Med Chem. 2000; 43(20):3714-7. doi:10.1021/jm000942e

692. Cheng T, Zhao Y, Li X, Lin F, Xu Y, Zhang X, et al. Computation of octanol-water partition coefficients by guiding an additive model with knowledge. J Chem Inf Model. 2007; 47(6):2140-8. doi:10.1021/ci700257y

693. Wildman SA, Crippen GM. Prediction of physicochemical parameters by atomic contributions. J. Chem. Inf. Comput. 1999; 39(5):868-73.

694. Moriguchi I, Hirono S, Liu Q, NAKAGOME I, MATSUSHITA Y. Simple method of calculating octanol/water partition coefficient. Chem. Pharm. Bull. 1992; 40(1):127-30.

695. Moriguchi I, Hirono S, Nakagome I, Hirano H. Comparison of reliability of log P values for drugs calculated by several methods. Chem. Pharm. Bull. 1994; 42(4):976-8.

696. Daina A, Michielin O, Zoete V. iLOGP: a simple, robust, and efficient description of n-octanol/water partition coefficient for drug design using the GB/SA approach. J Chem Inf Model. 2014; 54(12):3284-301. doi:10.1021/ci500467k

697. Delaney JS. ESOL: estimating aqueous solubility directly from molecular structure. J Chem Inf Comput Sci. 2004; 44(3):1000-5. doi:10.1021/ci034243x

698. Ali J, Camilleri P, Brown MB, Hutt AJ, Kirton SB. Revisiting the general solubility equation: in silico prediction of aqueous solubility incorporating the effect of topographical polar surface area. J Chem Inf Model. 2012; 52(2):420-8. doi:10.1021/ci200387c

699. Daina A, Zoete V. A BOILED-Egg To Predict Gastrointestinal Absorption and Brain Penetration of Small Molecules. ChemMedChem. 2016; 11(11):1117-21. doi:10.1002/cmdc.201600182

700. Friesner RA, Banks JL, Murphy RB, Halgren TA, Klicic JJ, Mainz DT, et al. Glide: a new approach for rapid, accurate docking and scoring. 1. Method and assessment of docking accuracy. J Med Chem. 2004; 47(7):1739-49. doi:10.1021/jm0306430

701. Dixon SL, Smondyrev AM, Knoll EH, Rao SN, Shaw DE, Friesner RA. PHASE: a new engine for pharmacophore perception, 3D QSAR model development, and 3D database screening: 1. Methodology and preliminary results. J Comput Aided Mol Des. 2006; 20(10-11):647-71. doi:10.1007/s10822-006-9087-6

702. Hardy LW, Malikayil A. The impact of structure-guided drug design on clinical agents. Curr. Drug Discov. 2003; 3:15-20.

703. Hughes JP, Rees S, Kalindjian SB, Philpott KL. Principles of early drug discovery. Br J Pharmacol. 2011; 162(6):1239-49. doi:10.1111/j.1476-5381.2010.01127.x

704. Paul ML, Graybiel AM, David JC, Robertson HA. D1-like and D2-like dopamine receptors synergistically activate rotation and c-fos expression in the dopamine-depleted striatum in a rat model of Parkinson's disease. J Neurosci. 1992; 12(10):3729-42. doi:10.1523/JNEUROSCI.12-10-03729.1992

705. Eagle H. Nutrition needs of mammalian cells in tissue culture. Science. 1955; 122(3168):501-14. doi:10.1126/science.122.3168.501

706. Kenny PW. Hydrogen-Bond Donors in Drug Design. J Med Chem. 2022; 65(21):14261-75. doi:10.1021/acs.jmedchem.2c01147

707. Wu D, Chen Q, Chen X, Han F, Chen Z, Wang Y. The blood-brain barrier: structure, regulation, and drug delivery. Signal Transduct Target Ther. 2023; 8(1):217. doi:10.1038/s41392-023-01481-w

708. Huang Q, Hao X, Qiao L, Wu M, Shen G, Ma S. Measurement and thermodynamic functions of solid–liquid phase equilibrium of d-(−)-quinic acid in H2O, methanol, ethanol and (H2O+ methanol),(H2O+ ethanol) binary solvent mixtures. J. Chem. Thermodyn. 2016; 100:140-7.

709. Marx J. A new synthesis of theaspirone, an odiferous principle of tea. Tetrahedron. 1975; 31(10):1251-3.

710. Ina K, Sakato Y. Isolation and structure elucidation of theaspirone, a component of tea essential oil. Tetrahedron Lett. 1968; 9(23):2777-80. doi:10.1016/s0040-4039(00)89650-1

711. Garrido L, Zubía E, Ortega MJ, Salvá J. New Meroterpenoids from the Ascidian *Aplidium conicum*. J. Nat. Prod. 2002; 65(9):1328-31.

712. Mohanty M, Mohanty PS. Molecular docking in organic, inorganic, and hybrid systems: a tutorial review. Monatsh Chem. 2023; 154(7):1-25. doi:10.1007/s00706-023-03076-1

713. Wang S, Che T, Levit A, Shoichet BK, Wacker D, Roth BL. Structure of the D2 dopamine receptor bound to the atypical antipsychotic drug risperidone. Nature. 2018; 555(7695):269-73. doi:10.1038/nature25758

714. Bhatia A, Lenchner JR, Saadabadi A. Biochemistry, dopamine receptors. 2019;

715. Shi L, Javitch JA. The binding site of aminergic G protein-coupled receptors: the transmembrane segments and second extracellular loop. Annu Rev Pharmacol Toxicol. 2002; 42(1):437-67. doi:10.1146/annurev.pharmtox.42.091101.144224

716. Scheerer P, Borchert A, Krauss N, Wessner H, Gerth C, Hohne W, et al. Structural basis for catalytic activity and enzyme polymerization of phospholipid hydroperoxide glutathione peroxidase-4 (GPx4). Biochem. 2007; 46(31):9041-9. doi:10.1021/bi700840d

717. Labrecque CL, Fuglestad B. Electrostatic Drivers of GPx4 Interactions with Membrane, Lipids, and DNA. Biochem. 2021; 60(37):2761-72. doi:10.1021/acs.biochem.1c00492

718. Ursini F, Maiorino M. Lipid peroxidation and ferroptosis: The role of GSH and GPx4. Free Radic Biol Med. 2020; 152:175-85. doi:10.1016/j.freeradbiomed.2020.02.027

719. Cooper G, Adams K. The cell: a molecular approach: Oxford University Press; 2022.

720. Moosmayer D, Hilpmann A, Hoffmann J, Schnirch L, Zimmermann K, Badock V, et al. Crystal structures of the selenoprotein glutathione peroxidase 4 in its apo form and in complex with the covalently bound inhibitor ML162. Acta Crystallogr D Struct Biol. 2021; 77(Pt 2):237-48. doi:10.1107/S2059798320016125

721. Bannai S, Kitamura E. Role of proton dissociation in the transport of cystine and glutamate in human diploid fibroblasts in culture. J Biol Chem. 1981; 256(11):5770-2.

722. Bannai S, Sato H, Ishii T, Sugita Y. Induction of cystine transport activity in human fibroblasts by oxygen. J Biol Chem. 1989; 264(31):18480-4.

723. Bannai S. Induction of cystine and glutamate transport activity in human fibroblasts by diethyl maleate and other electrophilic agents. J Biol Chem. 1984; 259(4):2435-40.

724. Oda K, Lee Y, Wiriyasermkul P, Tanaka Y, Takemoto M, Yamashita K, et al. Consensus mutagenesis approach improves the thermal stability of system x(c) (-) transporter, xCT, and enables cryo-EM analyses. Protein Sci. 2020; 29(12):2398-407. doi:10.1002/pro.3966

725. Parker JL, Deme JC, Kolokouris D, Kuteyi G, Biggin PC, Lea SM, et al. Molecular basis for redox control by the human cystine/glutamate antiporter system xc(). Nat Commun. 2021; 12(1):7147. doi:10.1038/s41467-021-27414-1

726. Kandasamy P, Gyimesi G, Kanai Y, Hediger MA. Amino acid transporters revisited: New views in health and disease. Trends Biochem Sci. 2018; 43(10):752-89. doi:10.1016/j.tibs.2018.05.003

727. Naba A, Pearce OMT, Del Rosario A, Ma D, Ding H, Rajeeve V, et al. Characterization of the Extracellular Matrix of Normal and Diseased Tissues Using Proteomics. J Proteome Res. 2017; 16(8):3083-91. doi:10.1021/acs.jproteome.7b00191

728. Biedler JL, Helson L, Spengler BA. Morphology and growth, tumorigenicity, and cytogenetics of human neuroblastoma cells in continuous culture. Cancer Res. 1973; 33(11):2643-52.

729. Cuende J, Moreno S, Bolanos JP, Almeida A. Retinoic acid downregulates Rae1 leading to APC(Cdh1) activation and neuroblastoma SH-SY5Y differentiation. Oncogene. 2008; 27(23):3339-44. doi:10.1038/sj.onc.1210987

730. Abubakar AR, Haque M. Preparation of Medicinal Plants: Basic Extraction and Fractionation Procedures for Experimental Purposes. J Pharm Bioallied Sci. 2020; 12(1):1-10. doi:10.4103/jpbs.JPBS_175_19